UNIVERSITÀ
DEGLI STUDI
DI PADOVA

SEDE AMMINISTRATIVA

UNIVERSITÀ DEGLI STUDI DI PADOVA

DIPARTIMENTO DI SCIENZE CHIMICHE

CORSO DI DOTTORATO DI RICERCA IN: SCIENZE MOLECOLARI

CURRICOLO: SCIENZE CHIMICHE

CICLO XXX

MOLECULAR EVENTS WITHIN A CONFINED SPACE

Coordinatore: Ch.mo Prof. Leonard Prins

Supervisore: Ch.mo Prof. Cristiano Zonta

Dottorando : Carlo Bravin

Summary

The scope of this Ph.D. thesis deals with the synthesis of molecular cages based on tris(2-pyridylmethyl)amines (**TPMAs**) scaffold and characterized by the presence of metals having a non-saturated coordination sphere in the inner part of the system. The new molecular architectures were synthesized taking advantage of Dynamic Covalent Chemistry DCC, in particular imine condensation, on opportunely functionalized **TPMA** metal complexes. The main objective was to control the self-assembly of the **TPMA** metal complexes in order to obtain new functional systems. The cages obtained have allowed to describe several molecular events within a confined space.

In the Introduction chapter, after a brief overview of **TPMAs** synthesis and the coordination chemistry, the supramolecular applications of **TPMAs** complexes are reported. The latter is mainly focused on chirality sensing and recent supramolecular structures involving these ligands. A part of the survey is dedicated to the applications of **TPMAs** complexes as metal receptor and anion sensor and the capability of this ligand to coordinate the metal center in helical fashion which allowed the use of these ligands as molecular switches. Afterwards, this property is further analyzed toward the application of these metal complexes in the determination of enantiomeric excess (e.e) and other functions. In the last section, **TPMAs** are envisaged as capping agents to obtain several supramolecular structures.

In *Chapter 1* the synthesis of a novel supramolecular cage built from the self-assembly of **TPMA** zinc complexes through imine condensation chemistry is reported. The cage recognition properties over a variety of structurally related dicarboxylic acid guests, together with the kinetic study of the template assembly and disassembly, have been investigated in detail. This knowledge has been used to selectively modulate the rate of both assembly and disassembly processes. In particular, a novel disassembly method induced by strain release of the guest has been developed.

In *Chapter 2* is reported the extension of the cage series varying the structural parameter and the metal ion coordinated to the **TPMA** unit. These cages have been obtained through the self-assembly of modified tris(pyridylmethyl)amine complexes and different diamines have been chosen to vary their size and flexibility. The recognition properties of this cage series were characterized with a novel rapid method based on ESI-MS therefore the determination of binding profiles for linear saturated dicarboxylic acids within the cage series was studied. This methodology has allowed to gather how small changes in the

structure of the host and guest can contribute to the recognition events. Moreover, it was possible to study molecular systems which contains paramagnetic metals that are not suitable for classical binding constant determination by ^{1}H NMR.

In *Chapter 3* is discussed the synthesis of a novel chiral supramolecular cage and the capability of this structure to control the helicity of a perfluorinated carbon chain are reported. The helix configuration of the perfluoroalkyl chain was evaluated with a combination of theoretical calculations of the host-guest complex and the support of Vibrational Circular Dichroism (VCD) experiments

In *Chapter 4* a detailed study on homo and hetero co-encapuslation processes within a supramolecular cage is reported. In particular, the model case under study regards the possibility to have different p-substituted benzoic acid, within a supramolecular cage containing two metals. While electron-withdrawing EWG substituents are preferential guests, it has been possible to evaluate the conditions in which hetero co-encapuslation is favoured. This part of the study has been carried out in part at the University of Cambridge (UK) in the group of Prof. C.A. Hunter. In the Appendices are contained the experimental information related to each chapter.

Riassunto

Lo scopo di questa tesi di dottorato consiste nella sintesi di gabbie molecolari basate su tris(2-piridilmetil)ammine (**TPMAs**) e caratterizzate dalla presenza di metalli con centri di coordinazione non saturi nella parte interna del sistema. Le nuove architetture molecolari sono state sintetizzate traendo vantaggio della *Dynamic Covalent Chemistry* DCC, in particolare della reazione di condensazione imminica su complessi metallici di **TPMA** opportunamente funzionalizzati. Il principale obiettivo è stato il controllo del self-assembly dei complessi metallici di **TPMA** al fine di ottenere questi nuovi sistemi funzionali. Le gabbie ottenute hanno permesso di descrivere diversi eventi molecolari in uno spazio confinato.

Nel capitolo introduttivo dopo una rapida panoramica sulla sintesi e sulla coordinazione delle **TPMA** vengono riportate le loro applicazioni in chimica supramoleculare. Quest'ultime consistono principalmente in sensori per la chiralità e recenti strutture supramolecolari che coinvolgono questi leganti. Una parte dell'indagine è dedicata alle applicazioni dei complessi metallici di **TPMA** come recettori di metalli e sensori di anioni e alla loro capacità di coordinarsi a centri metallici in maniera elicoidale, questo ha permesso di utilizzare questi leganti come *switch* molecolari. Questa proprietà è stata poi analizzata per ulteriori applicazioni di questi complessi metallici come la determinazione dell'eccesso enantiomerico (e.e) e altre funzioni. Nell'ultima sezione le **TPMAs** vengono descritte come *capping agents* al fine di ottenere diverse strutture supramolecolari.

Nel primo capitolo viene riportata la sintesi di una nuova gabbia supramolecolare costitutita dal self-assembly di due complessi **TPMA** di zinco attraverso condensazione imminica. Le proprietà di riconoscimento molecolare della gabbia nei confronti di una serie di acidi dicarbossilici come *guests* sono state investigate in dettaglio, assieme allo studio cinetico del assemblaggio e disassemblaggio della struttura. Queste conoscenze hanno portato alla modulazione selettiva della velocità dei processi di *assembly* e *disassembly* ed in particolare è stato possibile programmare un nuovo metodo di *disassembly* basato sulla pressione esercitata dal *guest* all'interno della gabbia.

Nel Capitolo 2 viene descritta una serie di gabbie omologhe ottenute variando i parametri strutturali e il metallo coordinato all' unità **TPMA**. Queste gabbie sono state ottenute attraverso il *self-assembly* di complessi trispiridilmetilamminici opportunamente modificati e varie ammine, scelte al fine di variare la dimensione e la flessibilità della strutture finali.

Le proprietà di riconoscimento molecolare di questa serie di gabbie sono state investigate con metodo rapido e innovativo basato sull'analisi ESI-MS, in questo modo è stato

possibile determinare diversi profili di *binding* per una serie di acidi dicarbossilici saturi. Questa metodologia ha permesso di concludere che piccole variazioni strutturali delle gabbie molecolari in questione modificano le loro proprietà di riconoscimento molecolare.
È stato inoltre possibile studiare sistemi molecolari contenenti centri metallici paramagnetici che non risultano adatti per la determinazione delle costanti di binding via ^{1}H NMR.
Nel capitolo 3 viene descritta la sintesi di una gabbia supramolecolare chirale e la sua capacità di controllare l' elicità preferenziale in una catena perfluorurata inclusa nella cavità della struttura. La configurazione dell'elica della catena perfluoroalchilica è stata valuta con una combinazione di calcoli teorici del complesso *host-guest* e col supporto di esperimenti di dicroismo vibrazionale circolare (VCD).
Nel capitolo 4 viene affrontato uno studio dettagliato sull' omo ed etero co-incapsulazione in una gabbia supramolecolare. In particolare il modello in esame ha riguardato la possibilità di incapsulare acidi benzoici diversamente sostituiti in posizione para in una gabbia contente due metalli. I gruppi elettronattratori risultano essere *guest* preferenziali ed è stato possibile valutare le condizioni in cui l'etero co-incapsulazione viene favorita. Questo studio è stato condotto in parte presso l'Università di Cambridge (UK) nel gruppo del prof. C.A. Hunter.
Nelle appendici sono contenuti i dettagli sperimentali relativi ad ogni capitolo.

Declaration

- *Chapter 1* has been adapted with permission from Bravin, C., Badetti, E., Scaramuzzo, F. A., Licini, G., Zonta, C. *J. Am. Chem. Soc.* **2017**, *139*, 6456- 6460. "Copyright 2017 American Chemical Society."

- *Chapter 2* is submitted at *Chemistry-A European Journal.* Part of research (crystal structures determination) was carried out during a short term scientific mission (COST-STSM-CM1005-21531) at Department of Chemistry, University of Jyväskylä, (Finland) under the supervision of Prof. K. Rissanen.

- *Chapter 3* was carried out in collaboration with prof. Longhi and prof. Abbate at Department of Medicina Molecolare e Traslazionale, University of Brescia (Italy).

- *Chapter 4* was carried out during a visiting period at Department of Chemistry University of Cambridge (UK) under the supervision of Prof. C. A. Hunter.

Carlo Bravin, Padova 30-10-2017

Acknowledgments

Now that my Ph.D. is finishing, is time to thank all the people which have contributed to this amazing experience.

Firstly, I would like to thank my Ph.D. supervisor Prof. Cristiano Zonta for the continuous support during my Ph.D, the great opportunity to extend our research in an international context and the strong enthusiasm that he put in the development of this new supramolecular system. Beside the “official” gratitude, I thank prof. Cristiano Zonta as a scientific mentor and a close friend. Then, I would like to thank Prof. Giulia Licini for her suggestions and encouragement along my Ph.D.

My sincere thanks also goes to Prof Kari Rissanen (University of Jyväskylä (FI)) for giving me the opportunity to work in his group during my stay for the STSM within COST Action CM1005.

I would like to thank Prof. Christopher A. Hunter (University of Cambridge (UK)) for the great opportunity to work in his group, an international experience that have contributed in my career development and personal growth. I thank prof. Hunter for the helpful discussions and for the improvement of my critical spirit toward research. At the same time I would like to thank all the Hunter’s, Stefan, Yudì and in particular all the Italians: Maria, Giulia, Cristina, Ennio, Nicola and Luca. We had great moments together.

Moreover, I thank all the people that have worked in the group in Padova during these years and especially the guys of our building “Organica 170”. Special thanks goes to Dr. Paolo Zardi and Dr. Claudia Miceli for their help and kindness and for all the fun we had in the last four years with Rosalia, Emanule, Giulia, Irene, Davide and many others. Not least, all the students Riccardo, Donato, Andrea, Giulia, and all the bachelor students, which have helped me during the research.

I would like to thank all my colleagues on my “musical side” which I am grateful for the beautiful moments we had together. In particular, M° Marco Gerboni for his inspiring behaviour and as a mentor not only on the professional part.

A huge thank goes to my family: my mum Carmen, my dad Gigi, Federico and Davide and their families. They gave me a fundamental support in this part of my life and I am grateful for all the moments we spent together.

Last but not least, I thank Justyna to support me everyday with her smile and patience and I hope to realize our dreams together.

Carlo

Contents

Introduction

Tris(2-pyridylmethyl)amines as Emerging Scaffold in Supramolecular Chemistry

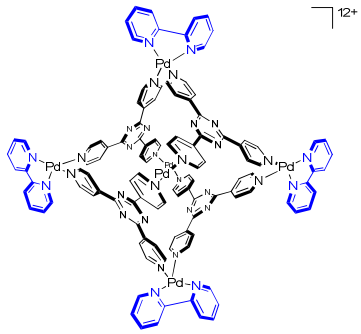

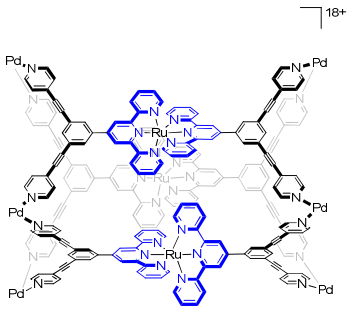

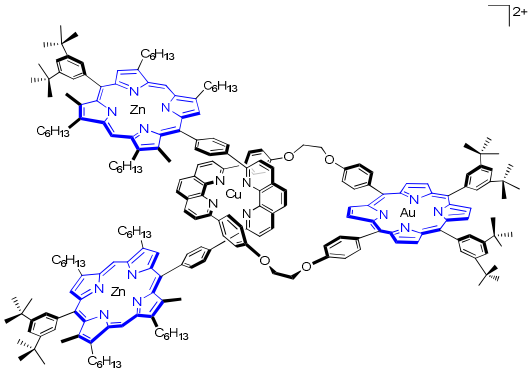

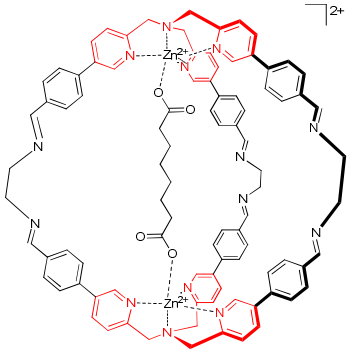

ABSTRACT tris(2-pyridylmethyl)amines (**TPMA**)s represents a series of ligands which are emerging in many branches of chemistry due to their ability to form stable and catalytically active metal complexes with a wide variety of metals and to assume a helical arrangement around the metal center. This two features make **TPMA** eligible for several supramolecular applications.

In this introduction, after a brief overview of the synthesis and the coordination chemistry, the supramolecular applications of **TPMAs** complexes are reported. A part of the survey is dedicated to the use of **TPMAs** complexes as metal receptor and anion sensor. In S 1.4.2 the capability of this ligand to coordinate the metal center in helical fashion allowing the use of these ligands as molecular switches is described. Afterwards, in S 1.4.3, this property is further analyzed reviewing the studies of Canary in the 90s toward the application of these metal complexes in the determination of enantiomeric excess (e.e). This seminal work, followed by the extensive research carried out by Anslyn, have increased the use of these ligands also to other applications. In the last section, S 1.4.4 **TPMAs** are envisaged as capping agents to obtain several supramolecular structures.

I.1 Introduction

In coordination chemistry, ligands are used to control the environment of the metal centers modulating the electronic and steric properties of the corresponding complexes, thus controlling metals functional properties. While a considerable number of ligands are present in literature, few of them are defined as *privileged* (e.g. BINOLs, BINAPs, Josiphos, Salens and Cinchona alkaloids).[1]

To a similar extent, some ligand classes and their relative metal complexes have found wide applications in supramolecular chemistry.[2] In other words, some classes of metal complexes have constituted the cornerstones for the development of supramolecular structures, active sites towards molecular recognition of specific functions and, to a minor extent, active catalytic sites within supramolecular architectures.[3] Among the large number of coordination compounds exploiting the above mentioned functions, nitrogen ligands containing metal complexes , and more in particular porphyrins and polypyridines, have been recurring motifs in several nano-architectures (Figure 1). The large variety of metals suitable for these ligands combined with the well-defined geometry of the resulting complexes, have contributed to make them “ligand of choice” for supramolecular architecture design since the early days of supramolecular chemistry.

While porphyrins, [4], bipyridines [5] and terpyridines [6] have been largely used in the development of supramolecular structures, more recently, tris(2-pyridylmethyl)amine (**TPMA**) ligands have emerged within the field due to their ability to form stable and catalytically active metal complexes with a wide variety of metals. In addition, due to their particular feature to assume a helical arrangement around the metal center, they have been extensively used in chirality recognition.

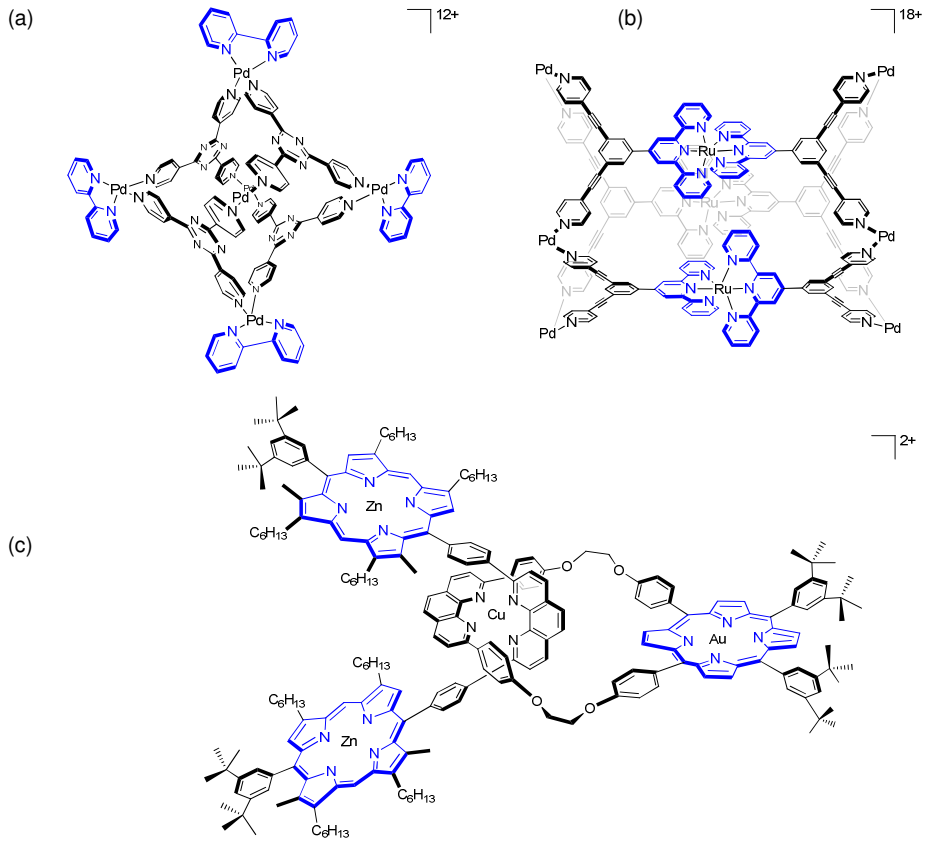

Figure 1 Supramolecular structures based on nitrogen ligands. a) M_6L_4-type coordination nanocage with 2,2'-bipyridine ancillary ligands cage,[5a] b) self-assembling metallosupramolecular cage based on cavitand–terpyridine subunit,[6] and c) porphyrin [2]rotaxanes.[4a]

Tris(2-pyridylmethyl)amines **TPMA**s are a general class of metal chelating ligands which consist in a central aliphatic nitrogen atom attached to three methyl-2-pyridyl arms. Beside the formation of stable complexes, the straightforward possibility to differently functionalize **TPMA**s skeletons gave rise to a large number of ligands and relative metal complexes. Furthermore, molecular functions have been added to modify steric, electronic and chiral properties of the ligands. As example, the **TPMA** skeleton can be modified with one (**BPQA**), two (**BQPA**), or three (**TMQA**) 2-quinolyl groups leading to different ligands which maintain similar coordination chemistry (Figure 2).

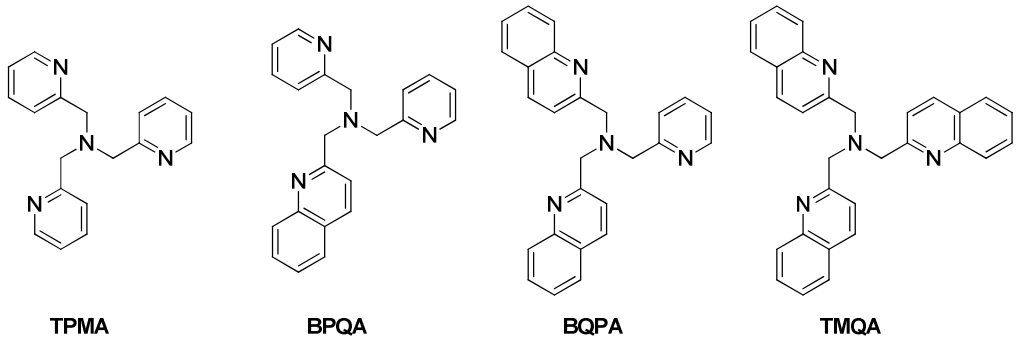

Figure 2. Tris(2-pyridylmethyl)amine **TPMA**, **BPQA**, **BQPA** and **TMQA** ligands.

It should be noted that while the application of **TPMA** based systems in molecular recognition is recent, **TPMA** complexes have a broad and successful story as catalysts for many different reactions. This is due to their ability to often leave one or two coordination sites unoccupied for reagents activation, mimicking enzyme and biological environment. Important applications in catalysis with **TPMA** metal complexes are oxidation with manganese,[7] iron,[8] rutenium,[9] copper[10], zinc, hydrolisis of phosphoric esters,[11], atom-transfer radical addition and polymerization with Cu(I)/Cu(II).[12] (Figure 3).

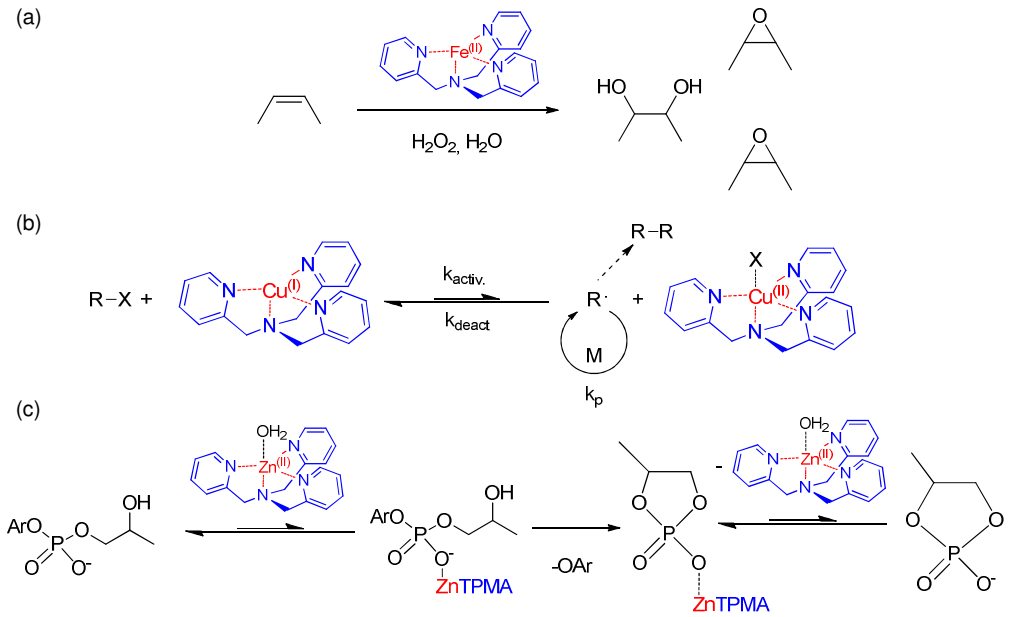

Figure 3. Example of a) catalytic oxidation reaction with iron **TPMA**[8a] b) Atom Transfer Radical Polimerization (ATRP) with copper **TPMA**[12b] and c) zinc hydrolysis of phosphodiester.[11c]

In this introduction, after a rapid overview of the synthesis and the coordination chemistry, the supramolecular applications of the **TPMA** complexes will be reported. The latter is mainly focus on chirality sensing and recent supramolecular structures involving **TPMA**. This description will open the opportunity to discuss some of the results reported by the group where the thesis has been carried out.

In the second part (S 1.4.1), a survey of the applications of **TPMA** complexes as metal receptor and anion sensor is presented. In section S 1.4.2 it is described the use of these ligands as molecular switches due to their particular feature to adopt a propeller-like arrangement around the coordinated metal. Afterwards, in S 1.4.3, this property is further analyzed reviewing the studies of Canary in the 90s toward the application of these metal complexes in the determination of enantiomeric excess (e.e). This seminal work, followed by the extensive research carried out by Anslyn, have increase the use of these ligands also to other functions. In the last

section, S 1.4.4 **TPMA** are envisaged as capping agents to obtain several supramolecular structures.

I.2 TPMA Synthesis

The first synthesis of **TPMA** dates back to Andregg and Wenk in 1967.[13] In their work the synthetic method was based on the alkylation of primary (pyridil)methylamine **1** with two equivalents of (chloromethyl)pyridine **2** in aqueous NaOH solution (Scheme 1a). The reaction, yielded a brown tris(2-pyridylmethyl)amine after recrystallization from water with total yield of 55%. Generally, alkylation methods remain the most common procedure for preparation of **TPMA** core, even though bromide are usually preferred than chloride, and ammonia is used as nitrogen source for the preparation of symmetric molecules. The functionalization by direct substitution of pyridine rings of the ligand is not suitable to prepare **TPMA** derivatives, as a consequence of the low reactivity of pyridines. To overcome this problem, previously functionalized pyridine precursors are used. More recently, the use of reductive amination of pyridine-carbaldehyde precursors with sodium triacetoxyborohydride has shown to be an interesting alternative method that could be used in the presence of sensitive groups (Scheme.1b).[14]

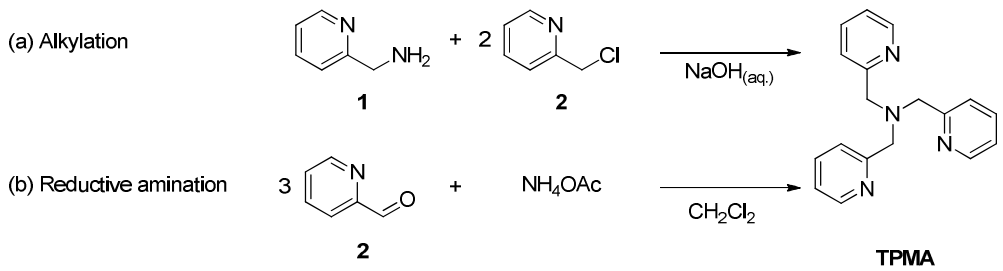

Scheme 1. tris(2-pyridylmethyl)amine **TPMA** main synthetic routes a) alkylation b) reductive amination

I.3 Complexes and their geometry

The first reported synthesis of a **TPMA** metal complex dates back to 1969 and it was a Ni(II) complex.[15] Since then, a large variety of metal complexes have been reported in literature. **TPMA**s can form tetra-dentate complexes, binding with three pyridyl nitrogens and the central tertiary amine a large variety of metals ranging from transition metals to lanthanide ions, as well as most of the Group 1 and Group 2 metals and some actinides.[16] According to a survey on the Cambridge Crystallographic Data Centre (CCSD) of November 2016, among over one thousand of structures containing **TPMA** and derivative ligands transition metal complexes, iron complexes accounts for one fourth of the entire series, followed by copper. Other widely used metals are Co, Zn, Ni, Ru and Mn (Figure 4).

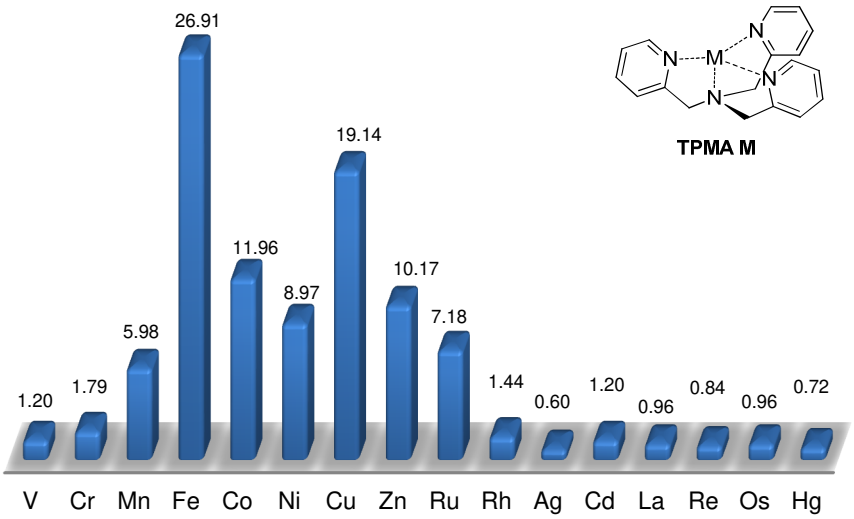

Figure 4 Percentage crystallographic structure distribution of **TPMA** transition metal complexes within the Cambridge Crystallographic Data Centre (CCDC) in 2016.

In general, **TPMA** metal complexes show a 1:1 metal to ligand stoichiometry. An exception is represented only by lower metal/ligand ratio in 1:2 $[M(TPMA)_2]^{n+}$ complexes, being formed by metal ions having radii greater than 0.9 Å such as Ca^{2+}.[17] Tetrahedral coordination is rarely observed because the bite angle of these

molecules is not wide enough to afford the binding of every coordination site around the metal ion. The most common geometry is trigonal bipyramidal (TBP), where **TPMA**s occupy one apical and the three equatorial positions around the metal center and the empty apical coordination site is taken by a solvent molecule or by another monodentate ligand (L). Octahedral complexes are less common than TBP,they have a general formula $[M(TPMA)X_2]^{n+}$ and they are formed predominantly by nichel and iron.[18] Another important exception is observed for d^8 metal ions, such as Pt^{2+} and Pd^{2+}, which tend to adopt a square planar geometry. [19] In this case, **TPMA** is forced to bind in a hypodentate fashion as a tridentate ligand in which one pyridine arm remains uncoordinated. Hypodentate coordination is also observed in some copper (I) complexes where tetrahedral geometry about the ion is preferred and one **TPMA** arm is displaced by a much more mobile ligand L (solvent molecule or anion) capable of positioning in a more favored way (Figure 5).[20]

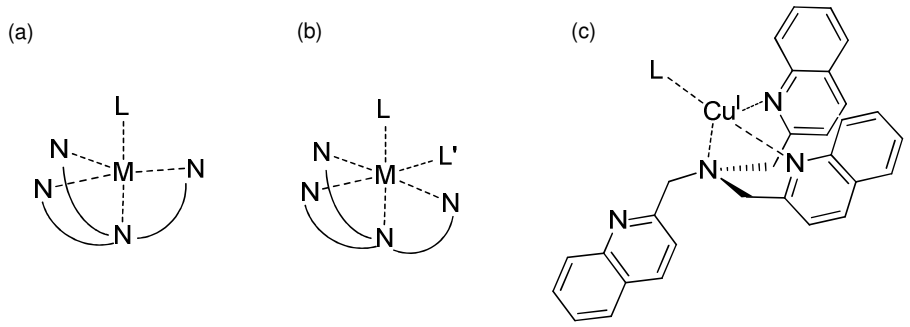

Figure 5 Common geometries in **TPMA** complexes. a) Trigonal bipyramidal TBP; b) octahedral and c) hypodentate fashion coordination of a **TPMA** in a Cu(I) complex.

As already mentioned, **TPMA** metal complexes are characterized by a propeller-like arrangement of the ligand around the metal. The ligand rapidly interconverts, at room temperature, between two enantiomeric forms, nominally Δ and Λ, differing for the handedness of the arms twist (Figure 6). The exploitation of this property is one of the key features that have promoted the use of **TPMA** ligands in supramolecular applications, besides their capability to coordinate several metal ions and the possibility to functionalize their scaffolds.

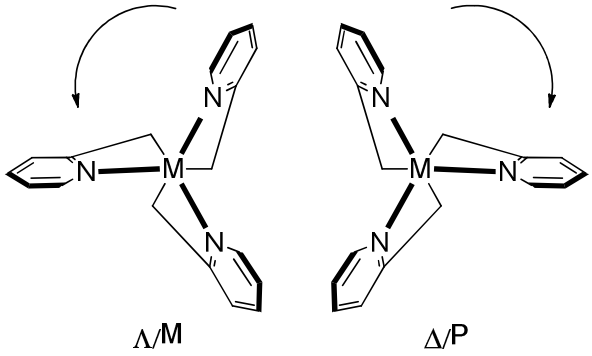

Figure 6. Λ (counterclockwise) and Δ (clockwise) conformation of **TPMA** ligands wrapped around a metal center.

I.4 Application of TMPA in Supramolecular Chemistry

In this part of the introduction, the attention will be focused on supramolecular application that have involved tris(pyridylmethyl)amine **TPMA** and its derivatives as building blocks for construction of: *i)* anion sensor-metal receptors *ii*) molecular switches, *iii)* supramolecular analytical assembly for detection of enantiomeric excess (e.e.) and *iv*) confined systems.

I.4.1 TPMA as anion sensor and metal receptor

I.4.1.1 Anion sensor

The capability of the metal centres to coordinate anions has been largely explored in **TPMA** complexes.[21] In particular, luminescence properties of **TPMA** lanthanide complexes can be used for anion sensing. Lanthanide complexes have attracted considerable attention as promising sensory materials, because of their unique coordination chemistry and intense luminescence with long excited-state lifetimes.[22] In this context, Tsukube has reported since 2002 a series of these complexes exhibiting anion-specific sensor function, and their anion selectivity and response sensitivity were modulated by a combination of lanthanide centre and **TPMA**.[23] As example, it was demonstrated that Eu^{3+} complex with ligand **3** acts as a luminescent receptor effective for NO_3^- anion, while corresponding Tb^{3+} complex exhibits Cl^- anion selectivity. The luminescence of the europium complex is enhanced 4.9 times in the presence of NO_3^- relative to other anions while the terbium complex results selective for Cl^-, with an enhancement of 5.4 times respect to the initial complex (Figure 7).

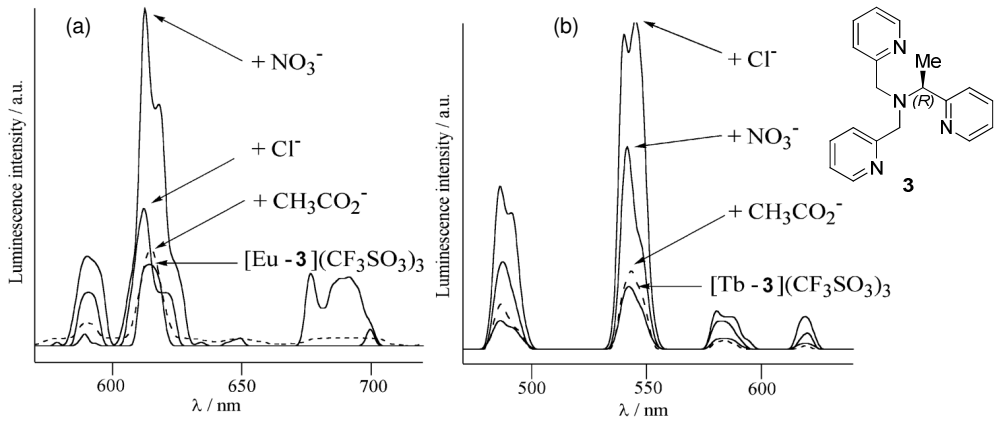

Figure 7 Luminescence spectral changes of (a) [Eu-**3**]$(CF_3SO_3)_3$ and (b) [Tb-**3**]$(CF_3SO_3)_3$ by the addition of NO_3^-, Cl^- and $CH_3CO_2^-$ anions in acetonitrile, excitation at 260 nm. Adapted from reference [22].

The outstanding features of the system can be explained in term of the effective arrangement of the three pyridine to act as effective photon antenna, and to the presence of several vacant sites of the lanthanide coordination sphere available for anion binding. The initial system was further developed removing one pyridine arm in favour of a hard amide oxygen. These mixed donor tripods formed more stable 1:1 complexes with $Eu(NO_3)_3$, $La(NO_3)_3$ and $Tb(NO_3)_3$ than the corresponding **TPMA,** allowing Cl^- anion-selective luminescence enhancement that was easily observed even by naked eye.[24]

Another modification involved the incorporation of a fluorescent quinolone as in **4 M**. This feature, combined with a stereo-controlled substituent in the tetradentate skeleton and the lanthanide metals, offered the possibility to perform multiple anion sensing combining fluorescence, luminescence, and circular dichroism spectra (Figure 8) [25]

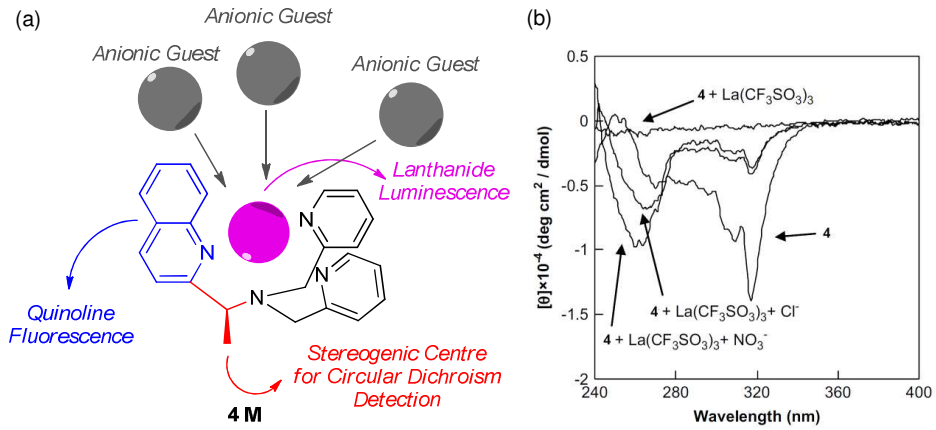

Figure 8. a) Tripodal ligand **4** for multiple anion sensing with lanthanide as metal center. b) CD anion sensing profiles of **4**-La^{3+} complex. Adapted from reference [25].

I.4.1.2 Metal receptor

The **TPMA**s ability to coordinate a wide variety of transition metal cations offered the possibility to use this ligand as metal receptor for Cd[26],Cu[27] and Zn.[28] In particular, the determination of zinc concentration and its imaging in brain tissues is of major interest due to the implication of this metal in brain diseases such as epilepsy, Alzheimer's, and Parkinson's diseases. The research has been mainly focused on the design of **TPMA** based ligands in order to: *i*) improve their sensitivity towards zinc, *ii*) increase the quantum yield to facilitate the fluorescence detection and *iii*) to enhance the solubility in organic and aqueous solvents.[29]

As example, fluorescent sensor **5** demonstrated femtomolar sensitivity for zinc ions with a 14-fold enhanced quantum yield upon chelation. In particular, it has also exhibited high selectivity over other physiological relevant divalent metals and in the presence of EDTA as competing ligand. This peculiar affinity was explained by the X-ray crystal structure of zinc complex which revealed that an acetic carboxylic group participates in metal coordination(Figure 9).[30]

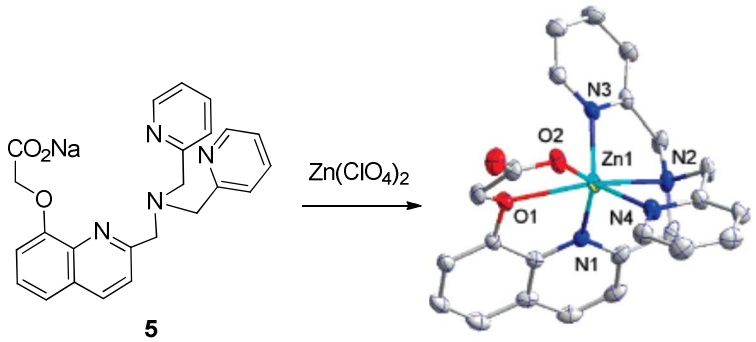

Figure 9. Coordination of Zn^{2+} to Ligand **5**. From the fluorescence emission spectra the fitting of the titration point data results to a 1:1 binding model to generate a log K_d = 15.35 ± 0.03. Adapted from reference [30].

While in molecule **5** is the quinolone moiety responsible for the fluorescence, Canary reported zinc fluorescent **TPMA**s. [31] Fluorescence properties of **6-8** zinc complexes could be explained by charge-transfer phenomena and possible contributions from a planarization of the pyridyl-trimethoxyphenyl groups in the excited state. As example in the case of ligand **7**, the fluorescence emission maximum showed a pronounced red shift of~80 nm (from 376 to 457 nm) which was enhanced by a factor of >100 when measured at 520 nm in the presence of zinc ions (Figure 10).

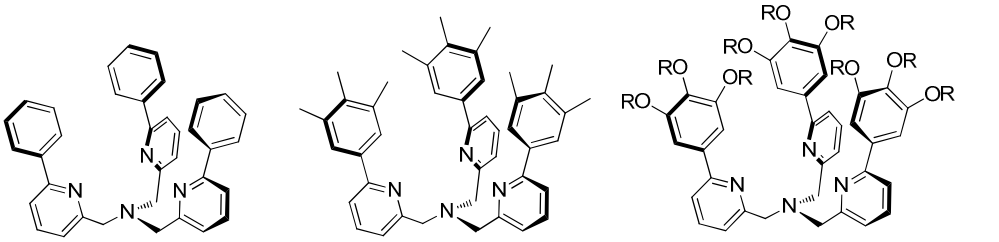

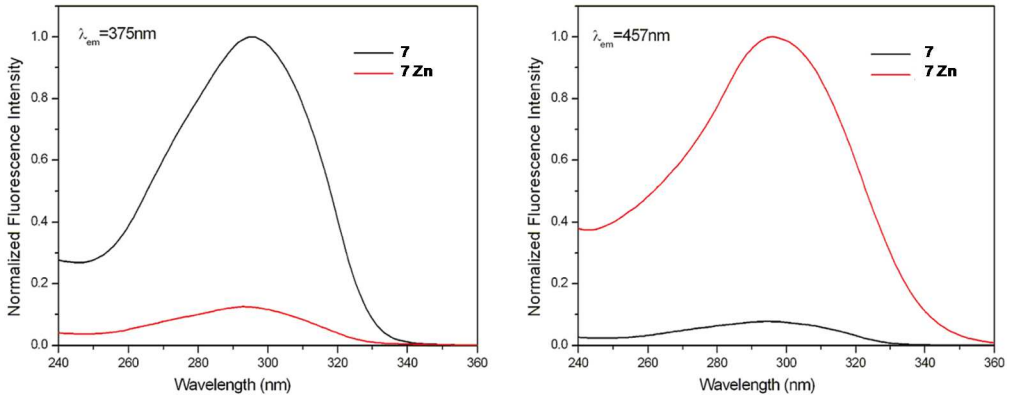

Figure 10. Excitation spectra of **7** and its zinc complex in CH_3CN, the emission wavelengths are 375 and 457 nm, respectively. Adapted from reference [31].

A remarkable example of the application of this system in imaging is represented by **BPQA** ligand **9** Figure (11).[32] This probe showed the possibility to exploit its functions under two-photon excitation detection. This technique is becoming widely used in biology because of low phototoxicity, good spatial resolution and negligible background fluorescence. The use of **9** as zinc detection probes was investigated, under two photon excitations, after introduction in HeLa cells. Ligand **9** showed a large red shift upon Zn^{2+} binding with 14-fold emission enhancement exhibiting high ion selectivity and sensitivity for Zn^{2+} in a neutral aqueous solution. The in vivo two-photon microscopy imaging experiments demonstrated that the new probes were cell permeable and could be used for imaging Zn^{2+} in living cells (Figure 11).

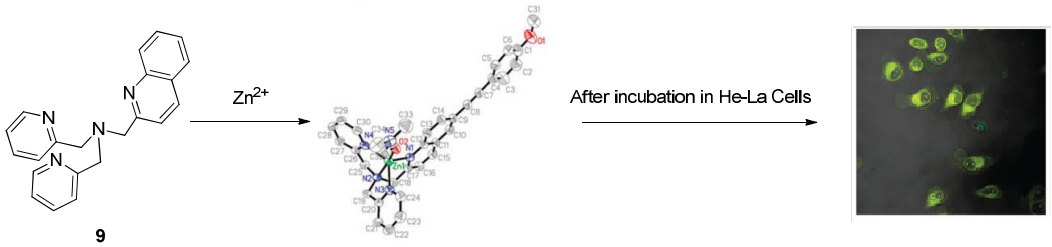

Figure 11. Tripodal ligand **X** and the coordination complex with Zn^{2+}. Imaging of the Zn^{2+} after incubation in HeLa cells. Adapted from reference [32a].

I.4.2 TPMA Molecular Switches

At the beginning of 90s, the interest on **TPMA** coordination chemistry was mainly related to copper and iron complexes capability to act as biomimetic oxygen activating species.[10b] In particular, how modification of **TPMA** units were influencing the electrochemistry of the complexes and their reactivity toward oxygen was deeply investigated.[33] Moreover, crystallographic data of the resulting complexes showed that **TPMA** ligands wrap around the metal center in a helical fashion. Initial hints came from the work of Karlin which reported the crystal structure of various copper **TPMA** complexes, showing a trigonal bipyramidal geometry in which a propeller-like C_3-symmetrical arms arrangements are diplayed.[34] The conformation of the complex rapidly interconverts, at room temperature, between two enantiomeric forms, nominally Δ and Λ, differing for the handedness of the arms twist (Figure.6). The mainstay of consecutive studies was to notice that the twist of **TPMA** ligand wrapped around a metal could be forced to show propeller helicity toward one single direction. This characteristic was initially achieved by placing a substituent on the methylene carbon of one **TPMA** arm.[35] The methyl group in the benzylic position adopt preferentially a pseudo axial conformation in anti position with respect to the proximal pyridine moiety **11**.

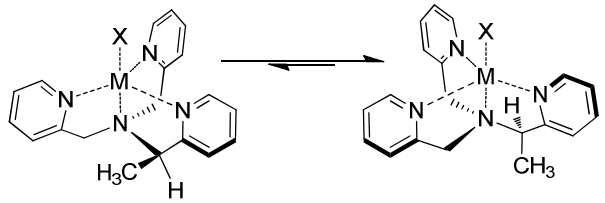

Figure 12. Chirally modified **TPMA** ligand with its relative conformational diasteromers in coordination with generic metal ion (M). On the right the favored **11** diastereoisomer.

This arrangement favours the formation of one diastereoisomer, thus a *S* stereocenter induce a P (right-handed) propeller-like twist, whereas a *R* stereocenter would induce the opposite one (Figure 12). The presence of a unique propeller like

conformation was confirmed both by the crystallographic structure of the racemic Zn(II) complex and by the CD spectra of the enantiopure complex. The versatility of this approach was demonstrated by extending this family of compounds to other metals such as Cd (II) and Cu(II), and to different substituents on the methylene position (i.e. methyl, phenyl).[36] Moreover, it was also possible to crystallize an optically pure complex and to correlate the absolute configuration of **TPMA** ligand around the metal to the molecular spectroscopic data.[37]

These preliminary studies were fundamental for the successive works on **TPMA** ligands, principally **TMQA** based molecular switches, published since 1998. A molecular switch is a simple molecular machine capable of reversibly interchange between two different stable states in response to external stimuli.[4d] The interest on these compounds increased in the past years because of two main features: their nano-size scale and their envisioned usage for optical displays, telecommunications, and most of all data storage.[38] For our purposes, we will focalize on chiroptical switches defined as molecules capable of changing their interaction with polarized light under an impulse. These systems are interesting because they can be easily followed by absorption spectroscopic methods such as circular dichroism (CD). Chiroptical switches have been already reported in an exhaustive and detailed review,[39] therefore our main focus will be on **TPMA** based switches.

The first application of **TPMA** ligands as molecular switches was performed by Canary group whose initial works date back to 1998.[40] In the system described, the operating mechanism is based on the redox process of the ionic couple Cu(I)/Cu(II). Switching abilities of ligands are modulated over the oxidation state of the metal center, for this reason these structures are defined as redox-driven. In general, systems that are considered redox-switch must fulfill some basic requirements: *i*) stability of the optically active forms, *ii*) chemical reversibility of the redox processes, *iii*) high sensitivity of the chiroptical response and *iv*) potential application in multimode switching.

In Canary systems, the difference between the two oxidation states of the metal complexes affects the coordination mode of the **TPMA** derivative, Cu(I) generally prefers tetrahedral environment while Cu(II) undergoes a TBP arrangement. As

example, Cu(II) **TMQA** complex with a chiral modified tris(quinolinmethyl)amine **12** displayed an intense exciton-coupled circular dichroism (ECCD) absorption in the CD spectrum due to the chromophores coupling of the most stable diastereoisomer present in solution. On the contrary, Cu(I) complex **13** showed a weak signal in the CD spectrum because the ligand undergoes to tetrahedral coordination, therefore no chromophore coupling and CD signal were present.

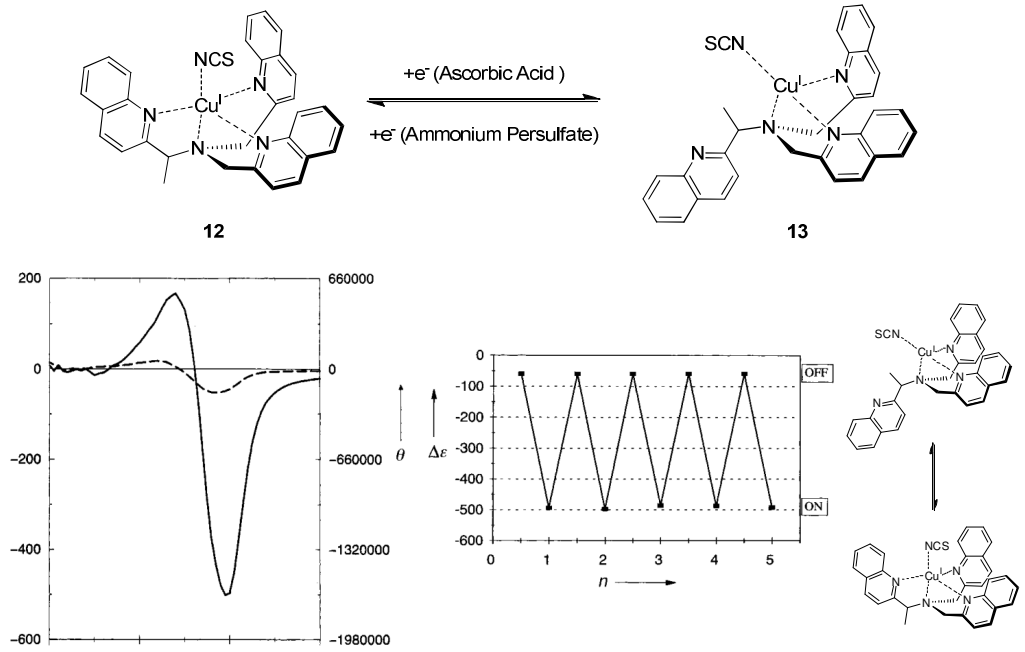

Figure 13 Cu(I) (dashed line) and Cu(II) (solid line) complexes CD spectra with a highlight on the intensity at 240nm in each redox cycle. Adapted from reference [40].

This capability to modify the coordination geometry of **TMQA** complexes, depending on the metal, was demonstrated by the redox process occurring between **12** and **13**. Chemical reduction of complex **12** was performed with sodium ascorbate while the oxidation of **13** to **12** was performed by addition of ammonium persulfate. The redox process was demonstrated to be reversible for several cycles (Figure 13).

This kind of molecular switch is called ON/OFF because it can reversibly interchange from a state with a peculiar spectroscopic property to a state in which the same property is totally lost.

In order to optimize the functionalities of the redox switch, a detailed study on the influence of the chromophores and a possible mechanism of interconversion was reported. In this system, copper was chosen as metal center because of its fast ligand exchange properties, potentially fast electron-transfer kinetics, stereoelectronic structure, corresponding sensitivity to coordinating anions and stability to the environment.

To envisage the mechanism of this transformation, Canary reported another example of ON/OFF switch which involved a **TPMA** derivative containing a piperidine moiety with two stereocenters (Figure 14).[41] In this example, the redox switch of the complex was able to control the chair conformation of the piperidine ring. In the Cu(II) state **15**, the higher-coordination number metal ion coordinated the three quinolines and the piperidine was forced to adopt a higher energy chair with two axial and one equatorial substituents. On the other hand, in the lower Cu(I) oxidation state **14**, the piperidine switched to a more stable cyclohexane chair conformation. This conformation was due to the tetrahedral geometry adopted by Cu(I) TPMA complexes, in which only two quinoline were coordinated to the metal center. Also in this case, while a strong CD signal was observed for Cu(II) complex, Cu(I) species did not give any signal. Differently from the above mentioned case, the rate of interconversion between the two states was slower as a consequence of the piperidine ring rigidity.

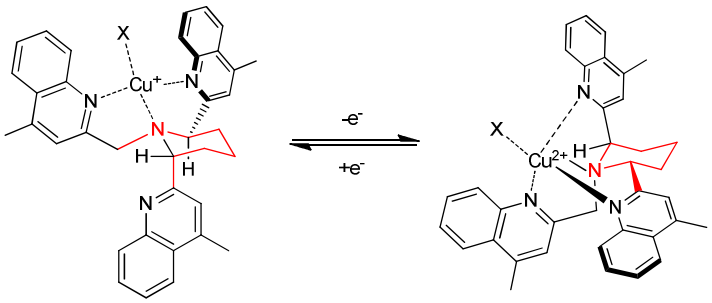

Figure 14. ON/OFF switch based on the piperidine modified **TQPA** (X=solvent molecule). Adapted from reference [41].

It is remarkable that an improvement on ON/OFF devices was obtained by a process in which the ligand is capable to invert its helicity, and so its CD sign, upon redox change. In this context, it was discovered an amino acid derivative based on methionine and a bis(quinolinemethyl)amine **16-17**.[42]

This ligand has three nitrogens as coordinating sites and the methionine can potentially coordinate with carboxylate or sulfide moiety (Figure 16). The methionine groups have different affinity for copper, depending on its oxidation state. With Cu(II) the carboxylate group binds the metal together with the three nitrogens and a solvent molecule **16**. The propeller's twist is dictated by the sulfide position, which has to be on the opposite side with respect to the ligand arms. When the metal is reduced to Cu(I), the carboxylate pivots away leaving a coordination site free for the more stable sulfide, allowing the tetrahedral geometry which is preferred by this cation because of its longer arm **17**. In this case, the carboxylate dictates the direction of the twist, which will be opposed to the previous one. The spectra intensities of the Cu(I) and Cu(II) are identical because there is no displacement of any quinoline arm (Figure 15).

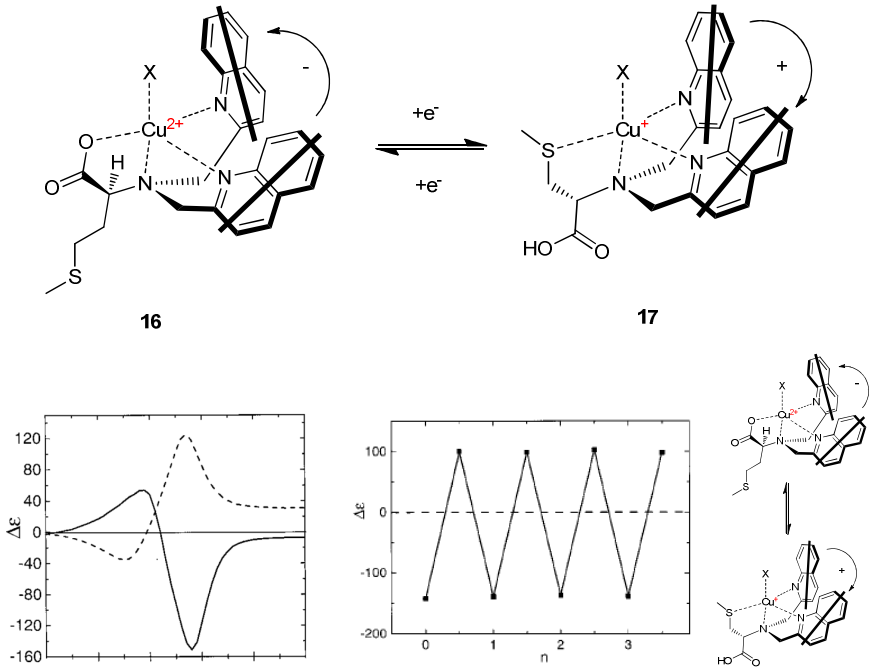

Figure 15. Description of Canary's +/- switch; complexes, their spectra (Cu(I) dashed line, Cu(II) solid line) and CD intensity at 239nm in each redox cycle. Adapted from reference [42].

I.4.3 Determination of Enantiomeric Excess

The knowledge developed in Canary studies paved the way for the development of molecular sensors based on **TPMA**. A sensor is defined as a receptor (host) that interacts with an analyte (guest) producing a detectable change in a generic signal.[43] The link between **TPMA** molecules and their use as sensors is represented by the dynamic process of helical interconversion of these ligands. This property is exploited by **TPMA** acting as stereodynamic optical probes.

In general, stereodynamic optical probe are characterized by the presence of at least one labile-stereogenic element which can racemize at a specific temperature. The addition of a chiral analyte, which contains one or more stereogenic units, moves this equilibrium toward the formation of one preferential diasteroisomer among the possible ones, then this information is translated in a measurable.[44]

In the context of stereodinamic optical probe, **TPMA** and derivative ligands are finding an ever-increasing interest for their ability to act as molecular sensors for enantiomeric excess (e.e.) determination of chiral compounds. The information provided by**TPMA** sensors is translated in a measurable signal by chiroptical spectroscopy, especially by circular dichroism (CD). This analytical tool is preferred among others due to the widespread availability of sensitive CD instruments (Figure 16).[45]

In order to develop more efficient **TPMA** based chemosensors, many efforts were directed towards the enhancement of the CD absorbance and the synthesis of molecular systems which preferentially form only one diasteroisomer, modulating the supramolecular associations between the probe and the analyte by intermolecular interactions. The continuous improving of these parameters and the possibility to use reversible interactions, rather than the covalent modification of the **TPMA** skeleton, were the key features that implemented these systems as suitable sensors for e.e. determination of asymmetric reaction screening.

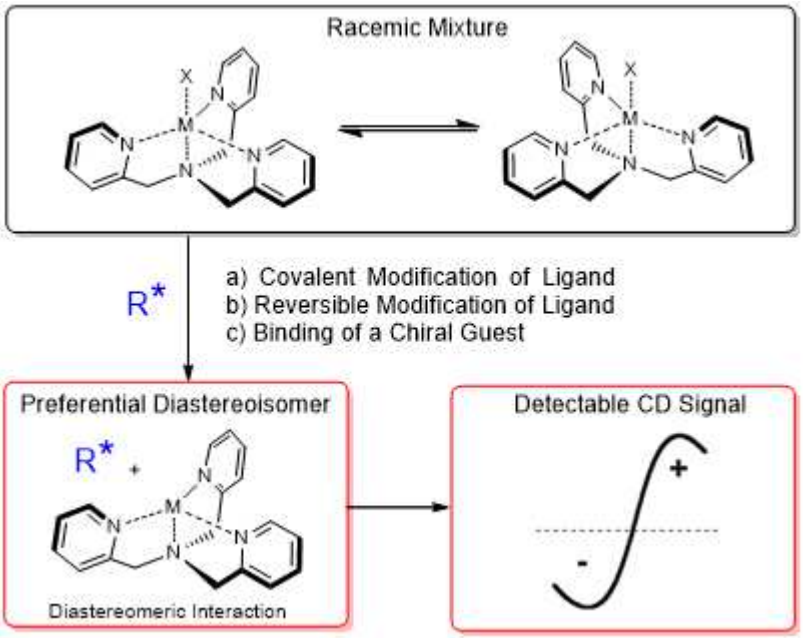

Figure 16 General working of a **TPMA** based stereodinamic probe. The formation of the preferential diasteroisomer could be *via* a) covalent or b) reversible modification of the ligand and c) binding of the chiral molecule to the metal center.

*I.4.3.1 Covalent modification of **TPMA** derivative scaffold with a chiral analyte*

While the general interest is nowadays in reversible modification of the **TPMA** unit, early examples reported by Canary were related to e.e. determination of chiral primary amines and α-amino acids by covalent linkage in a bis(quinolylmethyl)amine **BQPA** scaffold.[46] In these formed system, the amine or the α-amino-acid **18** becomes part of the chelating ligand. After complexation with copper(II), propeller-like structures are obtained, and the direction of the twist is controlled by stereogenic elements of the analytes **20**-**21**. The absolute configuration of the investigated molecules can be interpreted from the couplets of CD spectra of the derivatized complexes (Figure 18).[47] Moreover, it was possible to determine e.e. of chiral primary amines and α-amino acids because it was linearly related to the differential extinction coefficient observed in the CD spectrum for each sample and efficiently

estimated with a standard curve. In these systems, quinolyl arms are chosen over pyridyl ones because of their ability to couple and give rise to strong CD spectra.

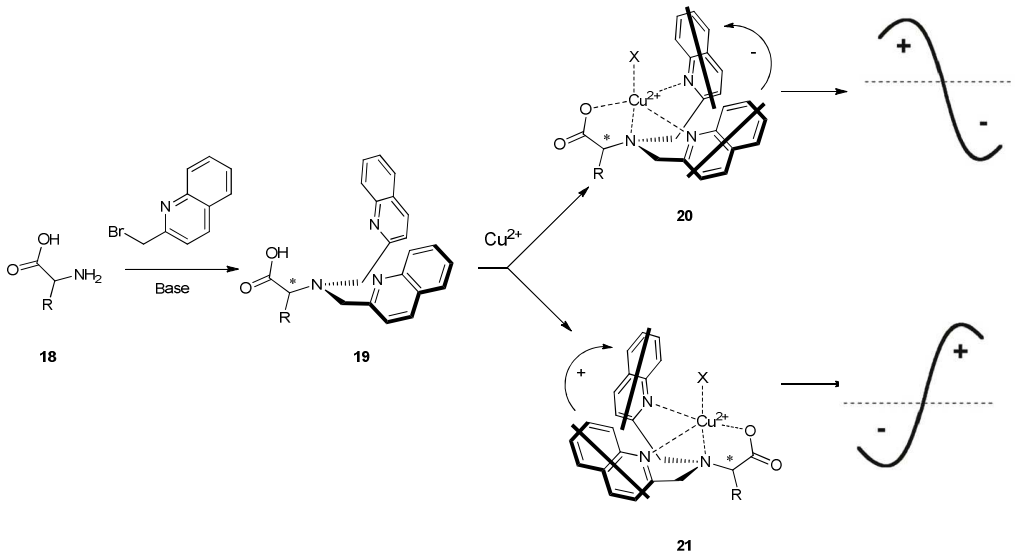

Figure 17 e.e. determination of amino acids embedded in the probe scaffold. Adapted from reference [47].

*I.4.3.2 Reversible modification of **TPMA** and derivative scaffold with the chiral analyte*

A fundamental contribution for the development of new sensors based on reversible modification of **TPMA** scaffold for e.e. determination was provided by Anslyn *et al* in 2011. At the beginning, they discovered a new metal-mediated dynamic multi-component assembly based on the association between 2-picolinaldehyde and di-(2-picolyl)amine assisted by Zn(II). The stability of the resulting metal complex provides the driving force for the assembly with an equilibrium constant for complex formation of $6.6*10^3$ M^{-1}. Moreover, the synthesis of this system is based on the dynamic covalent chemistry (DCC),so the reversibility of the assembly combined with the possibility of exchange the components present in solution paved the way for several applications as library creation and molecular recognition. [48]

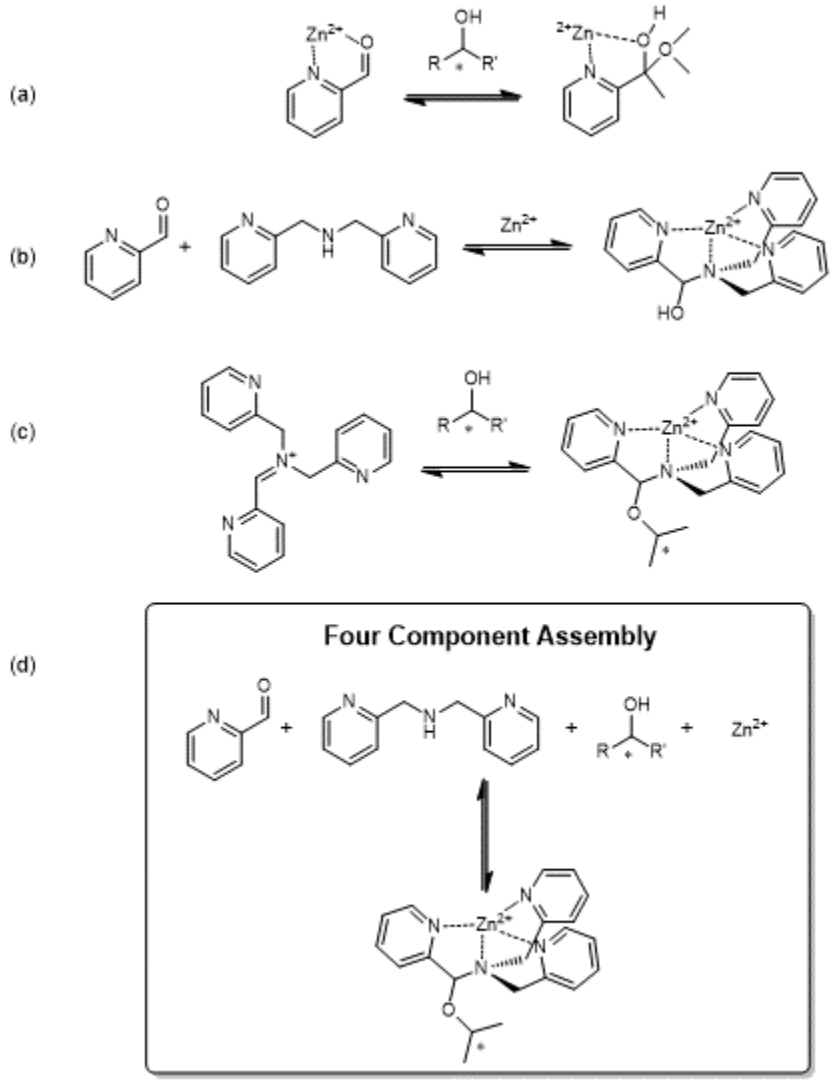

Scheme 2. Illustration of the equilibria for secondary alcohols binding. a) Lewis acid activation of carbonyls via chelation control, and reversible binding of secondary alcohols to give hemiacetals. b) Zinc templated three-component dynamic assembly to create hemiaminal. c) Proposed **TPMA** based iminium ion for alcohol binding and metal complex formation. d) Four-component reversible covalent assembly for secondary alcohol binding, probably through iminum ion as intermediate. Trifluoromethanesulfonate triflate (OTf) is the counterion for all the intermediates. Adapted from reference [48].

This assembly was successfully applied for chirality sensing of secondary alcohols, embedding them directly in the **TPMA** skeleton using DCC. The strategy includes the carbonyl activation and hemiaminal stabilization, leading to a four-component reversible assembly that creates a tetradentate ligand and incorporates secondary alcohols with exceptionally high affinity (Scheme 2).[49] In this process, the intermediate responsible of binding and exchange of alcohols is an iminium ion.

The enantiomeric excess determination of chiral secondary alcohol was possible due to the induced twist of the Zn complex, caused by the new formed stereocenter. It could be a preferential P (clockwise) or M (counterclockwise) twist that depends upon the handedness of the stereocenter formed in the **TPMA** ligand and it is related to which enantiomer of the analyte was embedded. The preferential twist could be observed as a Cotton effect in circular dichroism (CD) spectra resulting from exciton coupled circular dichroism (ECCD). The novelty of this four-component assembly was the large and reproducible signals in the CD spectra for secondary alcohols with respect to other detection systems, CD spectra of the assemblies for six chiral alcohols **22**-**24** are displayed in Figure 18. *S*-stereocenters in the alcohols resulted in a positive Cotton effects at 269 nm, whereas the *R*-stereocenters gave equal intensity negative Cotton effects. Hence, the sign of the signals is indicative of the handedness of the alcohol stereocenter. Moreover, in this work the e.e. of unknown samples was determined after the registration of the CD spectra of 11 samples with known e.e. values which were used to build a calibration curve.

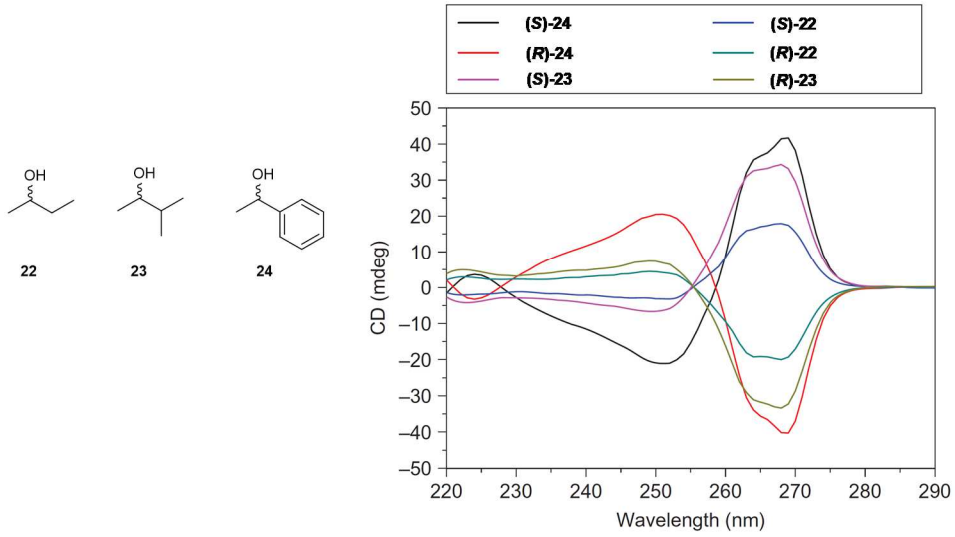

Figure 18. CD spectra of the four component assembly derived from three alcohols **22**-**24**. Adapted from reference [49].

The overall results obtained with this dynamic four-component assembly have opened the way to a new typology of synthetic receptors applicable in supramolecular analytical chemistry.[50] Many efforts were directed in enlarging the variety of chiral chemical species detectable with this system. As example, mono-secondary amines[51] resulted also suitable for e.e sensing.

Beside the versatility of the presented systems, the prediction of spectral properties by using well-established steric parameters for the analytes turned out to be useful for a rapid e.e. screening because the need for calibration curves and enantiomerically enriched samples were avoided.[52] In this context, the dynamic multicomponent covalent assembly incorporating chiral secondary alcohols differing for steric parameters were explored using linear free energy relationship (LFER) based steric parameters.[53] The diastereomeric ratio (d.r.) between the two possible four component assembly (**TPMA** + chiral analyte) was correlated with the magnitude ECCD induced by chiral alcohols. Moreover, Charton steric parameters

were successfully correlated with the d.r. values. Through the combination of these correlations, both the d.r. and CD intensity were predicted for test alcohols. Finally, the hypothesized enantiomeric excess (e.e.) of test samples with various alcohol structures was experimentally confirmed (Figure 19).

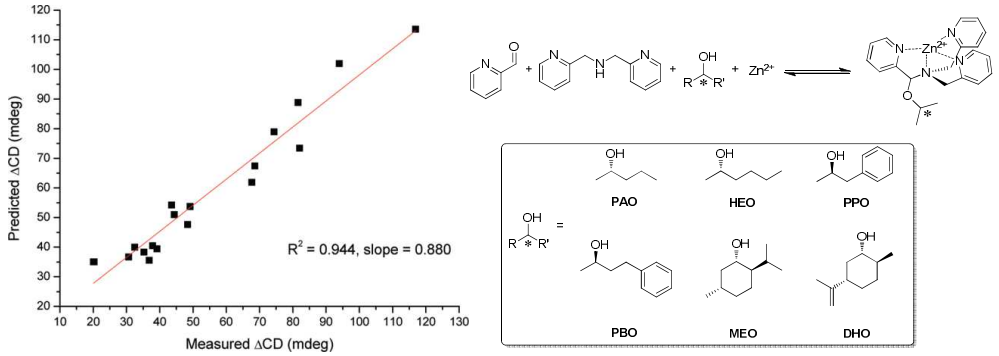

Figure 19. Correlation between ΔCD values predicted from Charton steric parameters for the alchol analyzed at 268 nm and the corresponding experimental values. Adapted from reference [53].

The CD spectra of the dynamic multicomponent covalent assembly were also rationalized by qualitative chemical models and computational studies. In particular, qualitative models were proposed to predict the preferential diastereoisomer and its twist.[54] The analysis of crystal structure of the hemiaminal compound combined with the structure of the chiral secondary alcohol gave a model that correlate the chirality of the analyte with the resulting twist. In fact, *R* and *S* alcohols will preferentially create *S* and *R* hemiaminal ether stereocenters respectively and as a result, *R* alcohols was associated to P twists and *S* alcohols to M twists. This steric-based model took into account only the kinetic of the nucleophilic attack geometries, while in a reversible reaction the outcome is thermodinamically controlled. To test this consideration, computational approaches were employed for complex embedding chiral alcohol **X** to predict diastereomeric ratios and the preferential twist on the basis of the configuration of the newly created stereocenter. The calculations confirmed and supported the predictions made above, concerning a correlation

between the kinetic and thermodynamic preferences at the newly formed stereocenter as well as the dominant helical twists.

The continuous efforts to understand and predict the behavior of this multicomponent covalent assembly, combined with its reliability and efficacy for e.e. determination, allowed its use in a High-Throughput Screening methodology (HTS) for asymmetric synthesis. HTS methods are becoming increasingly essential in discovering chiral catalysts or auxiliaries for asymmetric transformations due to the advent of parallel synthesis and combinatorial chemistry. Both parallel synthesis and combinatorial chemistry can lead to the exploration of a range of structural candidates and reaction conditions in order to obtain the highest enantiomeric excess of a desired transformation. One current bottleneck in these approaches to asymmetric reactions is the determination of e.e., which has led researchers to explore a wide range of HTS techniques.[45]

Chiral HPLC and GC are conventionally used for e.e. determination. However, they are not suitable for HTS of e.e. when hundreds to even thousands of reactions must be analyzed. For this reason, optical assays for e.e. determination using colorimetric, fluorescence, or circular dichroism (CD) spectroscopy, are being developed for the analysis of chiral organic compounds. In this context, as described by Krische, the asymmetric Ir-catalyzed C–C coupling of primary alcohols with allyl-acetates to form chiral secondary homo-allylic alcohols were performed in parallel to optimize the e.e. values of this specific reaction.[55] Approximately 400 examples of this reaction were performed by varying the catalyst, added acids and bases, and starting reactants, to form 4-phenyl-1-butene-4-ol.

Furthermore, a parallel and rapid quantitative TLC method to pre-screen the allylation by measuring the yield of each reaction, revealed in which conditions detectable and reliable e.e. values in the CD-based assay can be obtained. Afterwards, the e.e. values for the transformations were determined in a high-throughput fashion using the 4-component assembly, since the circular dichroism signal generated is indicative of the extent of asymmetric induction. Combining TLC and CD-assay methods to measure yields and e.e. values respectively, it was possible to optimize the reaction conditions to obtain higher e.e. values. The

fundamental highlight of this work is the huge amunt of e.e. data which can be recorded with a supramolecular assembly, in a rapid and reliable fashion, to simultaneously analyze different synthetic routes.

*I.4.3.3 Reversible modification and/or binding of chiral analyte to **TPMA** and derivative scaffolds*

The reversible modification of **TPMA** ligand have demonstrated how the incorporation of a chiral molecule in the **TPMA** skeleton led to a dynamic multicomponent covalent assembly usefull to measure the enantiomeric excess. The same application was envisaged directly binding the chiral analyte to the metal of **TPMA** complex. In this context, one of the first examples of stereodynamic probe consisted in an achiral ligand like **BQPA** and exerted its function in the presence of a chiral guest. This system took advantage of the equilibrium between the two enantiomeric propeller-like complexes present in solution.
Specifically, the dichroic analysis of **BQPA** complexes gave no signals in an achiral environment because their enantiomers were in a fast equilibrium at room temperature and in solution were present as a "racemic" mixture. After the addition of a chiral guest to the system, the most stable diasteromer is favored in solution and gives rise to a dichroic signal in which the sign, given by the chromophores twist around the metal, is directly influenced by the guest handedness (Figure 16).[56] Advancement within this approach were reported by Anslyn and Canary in 2011.[57] In this case, it was demonstrated that copper(II) complexes of **BQPA** could be used as sensors for ee detection of chiral carboxylates. A chiral carboxylate binds to the apical position of the metal center leading to a preferential enantiomeric complex. The novel formed complex produces a CD signal which is characterized by a magnitude and shape for each guest molecule and this feature allowed the determination of the configuration of the guest analyte. In this work,linear discriminant analysis (LDA) was used as statistical analysis technique for pattern recognition protocol. This data analysis allowed the identification of *R* and *S* chiral carboxilic acid (Figure 20).

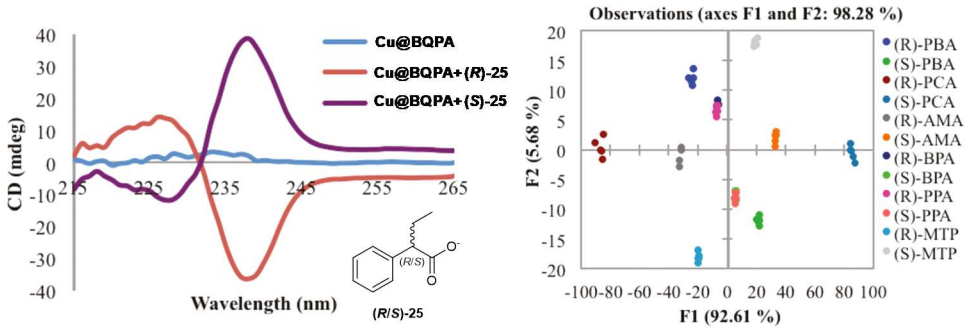

Figure 20. CD spectra of **BQPA** system for the determination of chiral carboxylic acid e.e. Starting complex (blue) and the two opposite diasteromers (red and violet). LDA analysis of the CD signals, *R* and *S* carboxylic acid are distinguished along PC1. Adapted from reference [57].

Therefore, a model was created for the host-guest complex able to predict the sign of the observed CD signal. For a quantitative analysis, calibration curves were built for e.e. calculation, showing an average error of 3% when applied to unknown composition substrates.

Using the same approach, chiral discrimination of α-amino acids and β-homoamino acids was possible due to the association between the copper(II)-containing assembly and the chiral analytes.[58] The observed ECCD signals for the enantiomers of each embedded molecule were equal but opposite, showing different size and shape depending from the individual amino-acid investigated. Also in this work, LDA was applied to differentiate the amino acids, both enantio- and chemo-selectively, giving the absolute configuration and identity of the amino acid. These analyses showed good differentiation of the amino acid guests with the use of only one host molecule.

A system for e.e. determination of chiral α-amino acids that combines the incorporation of the chiral analyte in the sensors scaffold and its coordination to **TPMA** metal center were investigated by the research group where this thesis has been carried out. The reported novel multicomponent assembly was formed by a modified tris(pyridylmethyl)amine complex functionalized with an aldehyde moiety, a series of chiral α-amino acids and a zinc salt.[59] This system exploied the DCC of imine bond, the amino-acid reacts with the aldehyde bringing its carboxylate function

close to the zinc metal ion of the complex. The amino acid handedness influences directly the overall twist of the propeller-shaped **TPMA** based molecule. In this system, the **TPMA** complex, as expected, does not show any circular dichroism spectrum due to the equilibrium of the two propeller-like enantiomers with opposing twist. On the contrary, the amino acid functionalized complex gives rise to a sharp CD spectrum that results from only one diasteroisomer which is favored in solution, and the two different diasteromers show mirror spectra. Intensity and shape of the spectra are different for each different α-amino acid, therefore calibration curves built from solution of known composition of the chiral analyte show a good linear fit and were utilized to obtain the e.e. of unknown samples.

A closer and more recent investigation on the same system revealed that in solution the dimeric dinuclear complex is the main species present.[60] In this supramolecular architecture two amino acid carboxylic ends bind the metal ion of another **TPMA,** bridging them together (Figure 21). In the presence of another equivalent of metal ion the complex becomes trinuclear, with the third metal ion bound to the pocket generated by the condensed amino acids.

Interestingly, the trinuclear complex showed an increase in the intensity of the CD spectrum of one order of magnitude. This behavior could be explained by the extra metal which brings closer in space the two chromophore responsible of the excitation process.

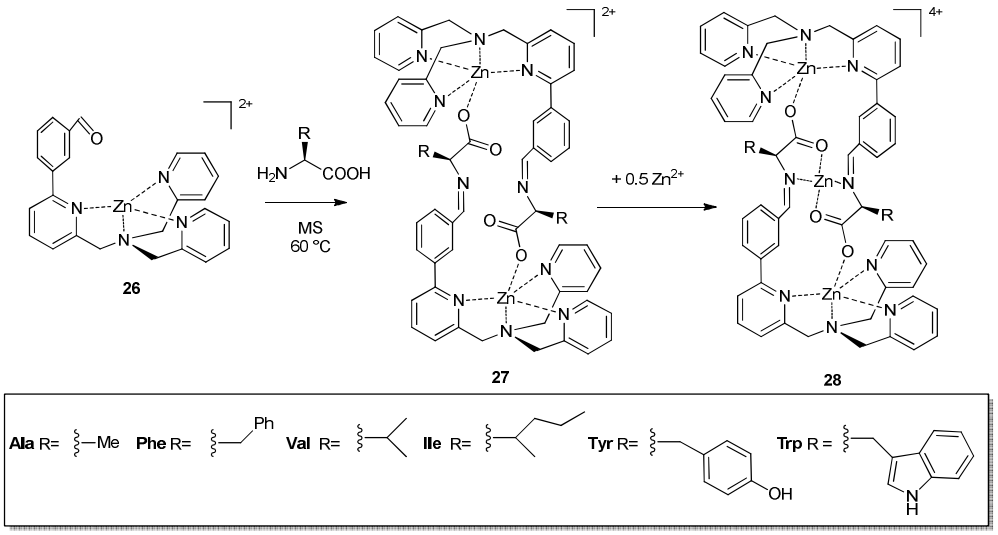

Figure 21. Dinuclear **27** and trinuclear **28** complex with bridging amino-acids. Adapted from reference [60].

An evolution of this system was recently reported by the same group.[61] In this case, the modification of the aldehyde position in the **TPMA** skeleton, led to a dinuclear architecture more stable to water than the previous one. Moreover, a much more intense CD spectrum was obtained as well as a structure which resulted less sensitive to an excess of metal ions. However, beside these advantages they were not effective with every amino acid.

A slightly different approach was followed in 2016 by the same authors, using the **TPMA**-α amino acids architecture previously reported.[62] In this case, the chirality of the analyte was sensed via VCD (vibrational circular dichroism), exploiting the fact that some transition metals such as Co^{2+}, displayed strongly enhanced VCD spectra. As example, increased VCD bands in the assembly **28-Co3** respect to the **28-Zn3** (Figure 22) helped to overtake one of the main back draws of VDC analysis that consists in weak signals, requiring long acquisition time and high substrate concentration. Using this protocol, absolute configuration of amino acids was obtained in shorter time if compared with previous works.

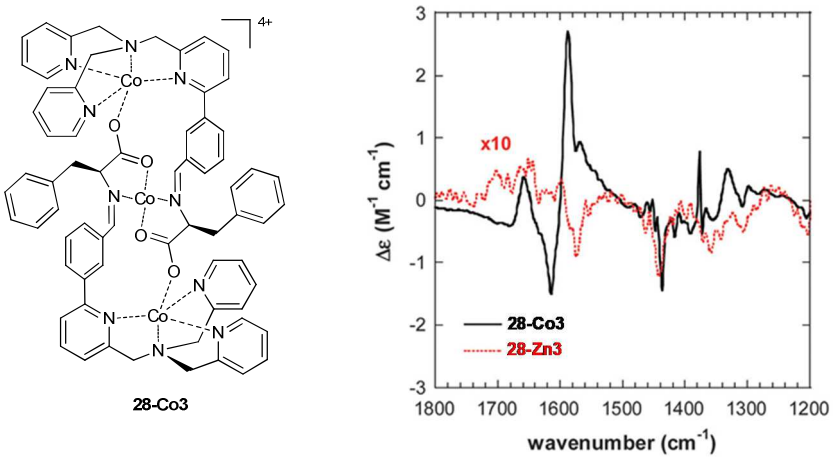

Figure 22. Trinuclear complex **28-Co3** crystal structure and comparison between VCD spectrum of cobalt and zinc complexes. Counterion is perchlorate and it is omitted for clarity. Adapted from reference [62].

A new supramolecular application that involves the stereodinamic probe behavior of a modified **BQPA** ligand was recently reported by J. Clayden *et al*.[63] The molecule mimics a G-protein-coupled receptor (GPCR) and it is made of a binding site outside the bilayer (**BQPA**), an helical foldamer core that inserts into a membrane and a conformationally labile fluorophore (two interacting pyrenes). In this system, upon binding a chiral substrate to **BPQA** a specific conformational change of the propeller-like probe is induced, and this signal is propagated over several nanometers into a phospholipid bilayer by a membrane bound synthetic receptor. The signal transmitted is capable of altering the fluorescence spectrum of the bipyrenes moiety by coupling or uncoupling the responsive fluorophores. (Figure 23)

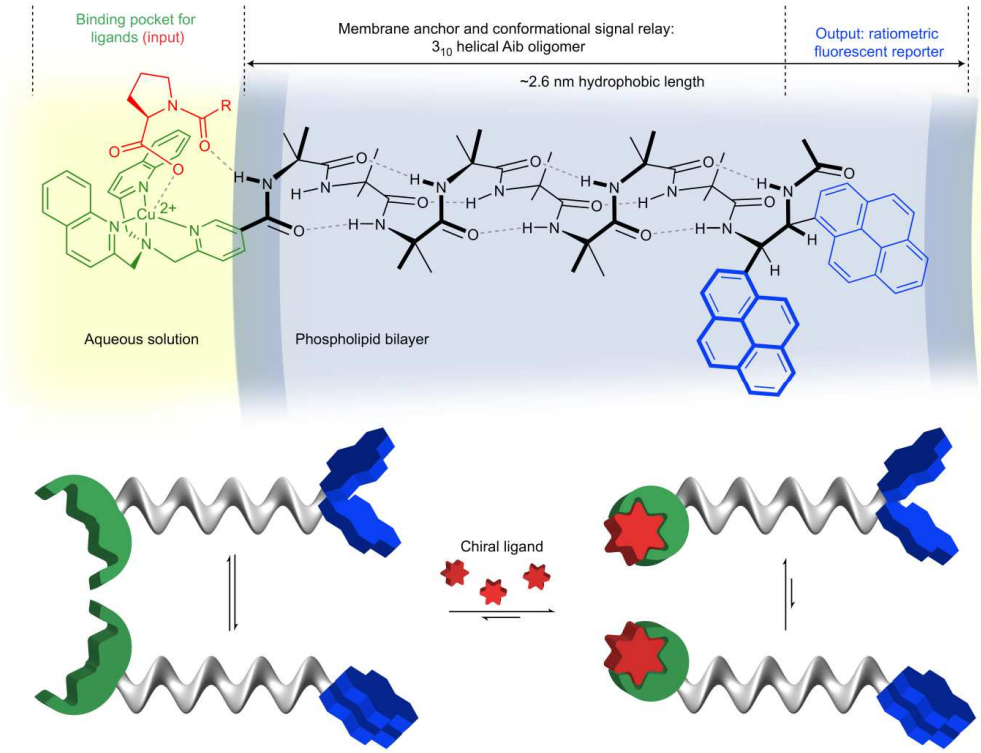

Figure 23. A description of the GPCR mimic receptor and its working mechanism. Adapted from reference [63].

I.4.4 TPMA as Capping unit in Confined spaces

In recent years, the advancement of synthetic supramolecular capsules, cages and confined spaces in general has led to new molecular systems displaying outstanding properties in molecular recognition and catalysis. The applications of these systems are widely treated in exhaustive reviews about molecular containers and confined stimuli-responsive assembly.[64] In this part, we want to highlight the use of **TPMA** complexes as building block for the synthesis of novel confined space, taking advantage of their straightforward functionalization, chemical stability and the capabilities to coordinate several metal ions.

Early reports on the subject date back to 2006 with the work of Reinaud who used **TPMA** as a functional moiety to cap a calixarene skeleton. This new C_3-symmetric host behaves as a single proton sponge, good ammonium ion acceptor and binds strongly sodium ion. In addition, the novel adduct binds neutral guest molecules such as urea, alcohol or amide in a cooperative way. These systems, Calix[6]**TPMA 29** and its sodium and protonated derivatives (**29**-**Na+** and **29-H**+), display conformational features that differ from the properties observed for all the other calix[6]-azacryptands due to the high sterical constrains inferred from the **TPMA** cap (Figure 24).[65]

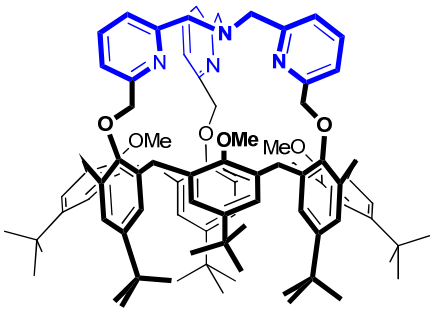

29

Figure 24 Reinaud **TPMA** capped Calix[6]**TPMA** calixarene.

Thus, the covalently attached rigid **TPMA** cap gives rise to a restricted mobility of this host. This property is reflected, as example, into the capability of the system to respond in a different manner to several stimuli. The per-ipso-nitrated **TPMA-**capped calix[6]arene (**30-32)** has showed a particular behavior during guests recognition. The complexation of the **TPMA** cap (by H^+ or Cu^+) associated with the encapsulation of a guests (acetone, acetonitrile or benzonitrile) triggers an induced-fit process leading to the loss of the typical cone conformation **30** of the host in favor of alternate conformations **31** and **32**.[66] This "pivoting" response of one or two walls of the calixarene core, induces a large mechanical motion of the corresponding aromatic units leading correspondingly to the partial cone conformation **31** and to the 1,3 alternate conformation **32** (Scheme 3).

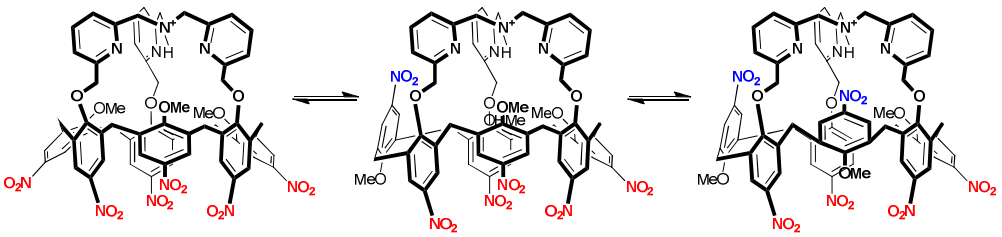

Scheme 3. Different conformers of the per-ipso-nitrated **TPMA-**capped calix[6]arene **30-32**. Adapted from reference [66].

The role of the rigid **TPMA** to pre-organize and influence the conformation of the calix[6]arene strucuture was investigated in a selective demethylation reaction of a series of calix[6]arene.

This reaction relies on two key points: (i) the nucleophilic attack of iodide using TMSI as a reagent and (ii) the correct orientation of the methoxy groups that must be projected away from the cone structure. Only the rigid **TPMA** capped calix[6]azacryptand adopts spontaneously the conformation favorable to the reaction of the methoxy groups and the reaction is fast and selective.[67]

TPMA capability to coordinate metal ions was exploited in these systems providing several metal functionalized Cu(II) funnel complexes that accept not only neutral

guests but also anionic such as a hydroxide[68] and fluoride.[69] The stability of this Calix-**TPMA** Cu based was proved also for Cu(I) oxidation state leading to cuprous complexes based on calix[6]tpma ligand able to promote a reaction in the solid state (Scheme 4).[70]

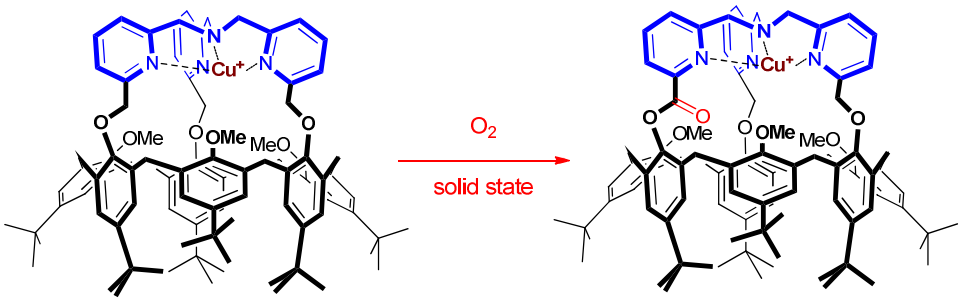

33 34

Scheme 4. Cu-calix[6]TPMA **33** oxidation process in solid state. Adapted from reference [70].

This system represents a unique case of oxygenation in the solid state of an organic moiety (a CH_2 group of **TPMA**) by O_2 mediated by a single Cu(I) center. The reaction is chemo- and regioselective, giving a keto product. This selectivity attests to a metal-centered four-electron oxidation reaction, a process that has been scarcely reported with other model complexes. Interestingly, Cu(I) and Cu(II) calix[6]tpma complexes have been object of a detailed study in which binding and redox properties are controlled by a cavity.[71] Moreover, calix[6]tpma has showed to retain host-guest properties in both Cu(I) and Cu(II) oxidation state and this phenomenon was investigated also in aqueous solvent.[72] The works of Reinaud *et. al.* highlighted the role of **TPMA** ligand as part of a supramolecular structure. The capability to provide a rigid cap for calix[6]azacryptand and to coordinate metal ions led to the above mentioned supramolecular applications.

Recent works involving **TPMA** as part of novel confined spaces were developed by Badjic and Martinez groups.

Badjic reported a nesting structure assembly that reminds a “Russian stacking doll”.[73] This structure is made by a zinc(II) **TPMA** complex opportunely functionalized with amines in order to be complementary to concave molecular

baskets, and having correspondingly gliycine and (*S*)-alanine amino acids at the rim (Figure 25). The assembly formation was confirmed by ^{1}H NMR and ESI-MS analysis, and it was determined that **TPMA** zinc complex could be entrapped into the molecular baskets with a K_b= (2.0 ± 0.2) × 10^3 M^{-1}. A property of this system is related to the C_3-symmetric enantiopure molecular baskets, containing (*S*)-alanine groups at the rim. It was found to transfer its static chirality to the **TPMA** complex, twisting the ligand pyridine rings into a left-handed (*M*) propeller. This phenomenum was promoted *via* intermolecular contacts between the two components and the molecular basket was acting like a second coordination sphere. These findings and this specific assembly extended the catalytic function and chiral discrimination capability of **TPMA**.

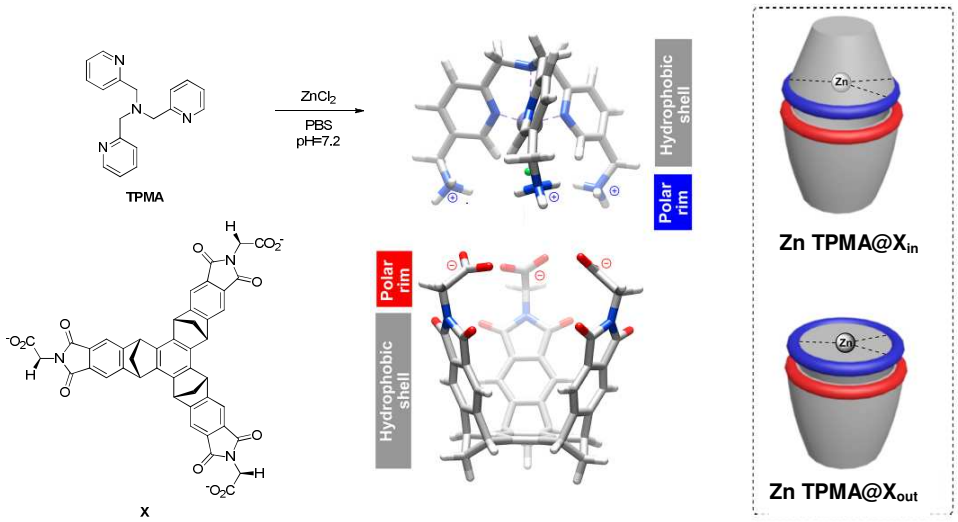

Figure 25. "Russian staking doll" assembly of a **TPMA** and a basket molecule. Adapted from reference [73].

Another example of supramolecular structures incorporating a **TPMA** unit was recently reported by Martinez.[74] These assemblies, namely hemicryptophane cages, was synthesized combining a cyclotriveratrylene unit and a **TPMA** ligand. The straightforward synthesis and successful modification of size and shape of the

cavity, changing the linker between the two units, demonstrated the versatility of these structures.

One remarkable feature of these cages is the chirality provided by the cyclotriveratrylene part. The synthesis of these cages produced a racemic mixture that could be easily resolved using chiral HPLC, giving unprecedented enantiopure cages (Figure 30). After zinc (II) coordination to the **TPMA** unit, it was possible to perform molecular recognition toward a series of zwitterionic guests.

According to the metal binding abilities of the **TPMA**, these cages represents enantiopure hosts available as chemical platforms for recognition and catalysis within a confined space.

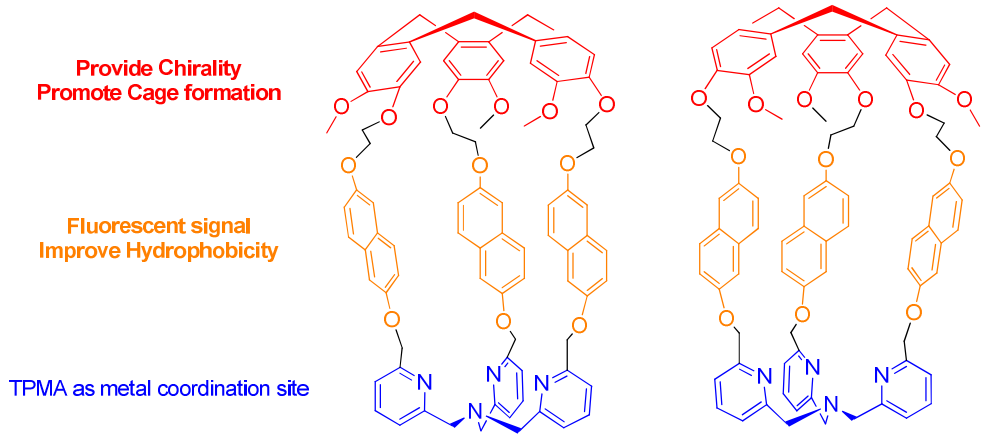

Figure 26 Enantiomers of the hemicryptophane cage. Adapted from reference [74].

I.5 Aim of the thesis

The increasing importance of **TPMA** applications in supramolecular chemistry combined with the above-mentioned features of the ligand led to the scope of this Ph.D. thesis. It deals with the synthesis of molecular cages based on **TPMA** scaffold and characterised by the presence of metals having a non-saturated coordination sphere in the inner part of the system. The new molecular architectures were synthesized taking advantage of Dynamic Covalent Chemistry DCC, in particular imine condensation, on opportunely functionalized tris-(pyridylmethyl)amines **TPMA** metal complexes. The main objective is to control the self-assembly of the **TPMA** metal complexes in order to obtain new functional systems.

In *Chapter 1* is reported the synthesis of a novel supramolecular cage built from the self-assembly of tris(2-pyridylmethyl)amine **TPMA** zinc complexes through imine condensation chemistry. The cage recognition properties over a variety of structurally related dicarboxylic acid guests, together with the kinetic study of the template assembly and disassembly, have been investigated in detail. This knowledge has been used to selectively modulate the rate of both assembly and disassembly processes. In particular, a novel disassembly method induced by strain release of the guest has been developed.

In *Chapter 2* is reported the extension of the cage series varying the structural parameter and the metal ion coordinated to the **TPMA** unit. These cages have been obtained through the self-assembly of modified tris(pyridylmethyl)amine complexes and different diamines have been chosen to vary their size and flexibility. The recognition properties of this cage series were characterized with a novel rapid method based on ESI-MS leading to the systematic study of the binding profiles of a series of linear saturated dicarboxylic. This methodology has allowed to detect the contribution of small structural changes can contribute to the recognition events. Moreover, it was possible to study molecular systems which contains paramagnetic metals that are not suitable for classical binding constant determination by ^{1}H NMR.

In *Chapter 3* the synthesis of a novel chiral supramolecular cage and the capability of this structure to control the helicity of a perfluorinated carbon chain are reported.

The helix configuration of the perfluoroalkyl chain was evaluated with a combination of theoretical calculations of the host-guest complex and the support of Vibrational Circular Dichroism (VCD) experiments

In *Chapter 4* a detailed study on homo and hetero co-encapuslation processes within a supramolecular cage is reported. In particular, the model case under study regards the possibility to have different *p*-substituted benzoic acid, within a supramolecular cage containing two metals. While electron-withdrawing EWG substituents are preferential guests, it has been possible to evaluate the conditions in which hetero co-encapuslation is favoured. This part of the study has been carried out in part at the University of Cambridge (UK) in the group of Prof. C.A. Hunter.

References

[1] T. P. Yoon, E. N. Jacobsen, *Science* **2003**, *299*, 1691.

[2] J.-M. Lehn, *Angew. Chem. Int. Ed.* **1990**, *29*, 1304-1319.

[3] (a) S. H. A. M. Leenders, R. Gramage-Doria, B. de Bruin, J. N. H. Reek, *Chem. Soc. Rev.* **2015**, *44*, 433-448; (b) D. J. Berrisford, C. Bolm, K. B. Sharpless, *Angew. Chem. Int. Ed.* **1995**, *34*, 1059-1070.

[4] (a) J. A. Faiz, V. Heitz, J.-P. Sauvage, *Chem. Soc. Rev.* **2009**, *38*, 422-442; (b) S. Durot, J. Taesch, V. Heitz, *Chem. Rev.* **2014**, *114*, 8542-8578; (c) J. Zhang, Y. Li, W. Yang, S.-W. Lai, C. Zhou, H. Liu, C.-M. Che, Y. Li, *Chem. Comm.* **2012**, *48*, 3602-3604; (d) B. Champin, P. Mobian, J.-P. Sauvage, *Chem. Soc. Rev.* **2007**, *36*, 358-366; (e) M. Gong, Z. Cao, W. Liu, E. M. Nichols, P. T. Smith, J. S. Derrick, Y.-S. Liu, J. Liu, X. Wen, C. J. Chang, *ACS Centr.Sci.* **2017**, *3*, 1032-1040.

[5] (a) T. Kusukawa, M. Fujita, *J. Am. Chem. Soc.* **2002**, *124*, 13576-13582; (b) K. Harris, D. Fujita, M. Fujita, *Chem. Comm.* **2013**, *49*, 6703-6712.

[6] T. Schröder, R. Brodbeck, M. C. Letzel, A. Mix, B. Schnatwinkel, M. Tonigold, D. Volkmer, J. Mattay, *Tetrahedron Lett.* **2008**, *49*, 5939-5942.

[7] Y. Hitomi, A. Ando, H. Matsui, T. Ito, T. Tanaka, S. Ogo, T. Funabiki, *Inorg. Chem.* **2005**, *44*, 3473-3478.

[8] aK. Chen, M. Costas, J. Kim, A. K. Tipton, L. Que, *J. Am. Chem. Soc.* **2002**, *124*, 3026-3035; (b) T. K. Paine, M. Costas, J. Kaizer, L. Que Jr, *JBIC J. Bio. Inorg. Chem.* **2006**, *11*, 272-276; (c) M. Borrell, M. Costas, *J. Am. Chem. Soc.* **2017**, *139*, 12821-12829; (d) E. E. Chufán, B. Mondal, T. Gandhi, E. Kim, N. D. Rubie, P. Moënne-Loccoz, K. D. Karlin, *Inorg. Chem.* **2007**, *46*, 6382-6394.

[9] M. Yamaguchi, H. Kousaka, S. Izawa, Y. Ichii, T. Kumano, D. Masui, T. Yamagishi, *Inorg. Chem.* **2006**, *45*, 8342-8354.

[10] (a) K. D. Karlin, *Science* **1993**, *261*, 701-708; (b) N. Wei, N. N. Murthy, Q. Chen, J. Zubieta, K. D. Karlin, *Inorg. Chem.* **1994**, *33*, 1953-1965; (c) E. Kim, E. E. Chufán, K. Kamaraj, K. D. Karlin, *Chem. Rev.* **2004**, *104*, 1077-1134.

[11] (a) F. Mancin, P. Tecilla, *New J. of Chem.* **2007**, *31*, 800-817; (b) L. Zhu, O. dos Santos, C. W. Koo, M. Rybstein, L. Pape, J. W. Canary, *Inorg. Chem.* **2003**, *42*, 7912-7920; (c) G. Feng, J. C. Mareque-Rivas, R. Torres Martín de Rosales, N. H. Williams, *J. Am. Chem. Soc.* **2005**, *127*, 13470-13471; (d) J. C. Mareque-Rivas, R. Torres Martin de Rosales, S. Parsons, *Chem. Comm.* **2004**, 610-611.

[12] (a) T. Pintauer, K. Matyjaszewski, *Coord. Chem. Rev.* **2005**, *249*, 1155-1184; (b) N. V. Tsarevsky, W. A. Braunecker, A. Vacca, P. Gans, K. Matyjaszewski, *Macromolecular Symposia* **2007**, *248*, 60-70.(c) K. Matyjaszewski, *Macromolecules* **2012**, *45*, 4015-4039.

[13] (a) G. Anderegg, F. Wenk, *Helv. Chim. Acta* **1967**, *50*, 2330-2332; (b) G. Anderegg, E. Hubmann, N. G. Podder, F. Wenk, *Helv.Chim. Acta* **1977**, *60*, 123-140.

[14] (a) A. F. Abdel-Magid, K. G. Carson, B. D. Harris, C. A. Maryanoff, R. D. Shah, *J. Org. Chem.* **1996**, *61*, 3849-3862; bA. G. Blackman, *Eur. J. Inorg. Chem.* **2008**, *2008*, 2633-2647.

[15] M. M. da Mota, J. Rodgers, S. M. Nelson, *J. Chem. Soc. A: Inorg., Phys., Theor.* **1969**, 2036-2044.

[16] (a) S. K. Brownstein, P. Y. Plouffe, C. Bensimon, J. Tse, *Inorg. Chem.* **1994**, *33*, 354-358; (b) Z. He, D. C. Craig, S. B. Colbran, *J. of the Chem. Soc., Dalton Trans.* **2002**, 4224-4235; (c) D. G. Lonnon, D. C. Craig, S. B. Colbran, *Dalton Trans.* **2006**, 3785-3797; (d) R. Wietzke, M. Mazzanti, J.-M. Latour, J. Pécaut, P.-Y. Cordier, C. Madic, *Inorg. Chem.* **1998**, *37*, 6690-6697.

[17] A. Hazell, J. McGinley, H. Toftlund, *J. Chem. Soc., Dalton Trans.* **1999**, 1271-1276.

[18] (a) E. Szajna, P. Dobrowolski, A. L. Fuller, A. M. Arif, L. M. Berreau, *Inorg. Chem.* **2004**, *43*, 3988-3997; (b) A. Diebold, K. S. Hagen, *Inorg. Chem.* **1998**, *37*, 215-223.

[19] Z. Hui Zhang, X. He Bu, Z. Ang Zhu, Y. Ti Chen, *Polyhedron* **1996**, *15*, 2787-2792.

[20] S. Zahn, J. W. Canary, *J. Am. Chem. Soc.* **2002**, *124*, 9204-9211.

[21] (a) T. Zhang, E. V. Anslyn, *Org. Lett.* **2006**, *8*, 1649-1652; (b) S. L. Tobey, E. V. Anslyn, *Org. Lett.* **2003**, *5*, 2029-2031; (c) S. L. Tobey, E. V. Anslyn, *J. Am. Chem. Soc.* **2003**, *125*, 14807-14815; (d) H. Sugimoto, H. Miyake, H. Tsukube, *J. Chem. Soc., Dalton Trans.* **2002**, 4535-4540; (e) M. M. Makowska-Grzyska, E. Szajna, C. Shipley, A. M. Arif, M. H. Mitchell, J. A. Halfen, L. M. Berreau, *Inorg. Chem.* **2003**, *42*, 7472-7488.

[22] (a) D. Parker, *Coordination Chem. Rev.* **2000**, *205*, 109-130; (b) J. I. Bruce, R. S. Dickins, L. J. Govenlock, T. Gunnlaugsson, S. Lopinski, M. P. Lowe, D. Parker, R. D. Peacock, J. J. B. Perry, S. Aime, M. Botta, *J. Am. Chem. Soc.* **2000**, *122*, 9674-9684.
[23] T. Yamada, S. Shinoda, H. Tsukube, *Chem. Comm.* **2002**, 1218-1219.
[24] Y. Kataoka, D. Paul, H. Miyake, S. Shinoda, H. Tsukube, *Dalton Trans.* **2007**, 2784-2791.
[25] M. E. Masaki, D. Paul, R. Nakamura, Y. Kataoka, S. Shinoda, H. Tsukube, *Tetrahedron* **2009**, *65*, 2525-2530.
[26] Y. Mikata, K. Kawata, S. Takeuchi, K. Nakanishi, H. Konno, S. Itami, K. Yasuda, S. Tamotsu, S. C. Burdette, *Dalton Trans.* **2014**, *43*, 10751-10759.
[27] (a) J. W. Canary, *Chem. Soc. Rev.* **2009**, *38*, 747-756; (b) K.-K. Yu, K. Li, J.-T. Hou, X.-Q. Yu, *Tetrahedron Letters* **2013**, *54*, 5771-5774.
[28] M. Royzen, A. Durandin, V. G. Young, N. E. Geacintov, J. W. Canary, *J. Am. Chem. Soc.* **2006**, *128*, 3854-3855.
[29] (a) Y. Mikata, Y. Nodomi, R. Ohnishi, A. Kizu, H. Konno, *Dalton Trans.* **2015**, *44*, 8021-8030; (b) J. M. Castagnetto, J. W. Canary, *Chem. Comm.* **1998**, 203-204.
[30] H.-H. Wang, Q. Gan, X.-J. Wang, L. Xue, S.-H. Liu, H. Jiang, *Org. Letters* **2007**, *9*, 4995-4998.
[31] J. Liang, J. Zhang, L. Zhu, A. Duarandin, V. G. Young, N. Geacintov, J. W. Canary, *Inorg. Chem.* **2009**, *48*, 11196-11208.
[32] (a) S. Sumalekshmy, M. M. Henary, N. Siegel, P. V. Lawson, Wu, K. Schmidt, J.-L. Brédas, J. W. Perry, C. J. Fahrni, *J. Am. Chem. Soc.* **2007**, *129*, 11888-11889; (b) X. Meng, S. Wang, Y. Li, M. Zhu, Q. Guo, *Chem. Comm.* **2012**, *48*, 4196-4198.
[33] (a) C.-l. Chuang, K. Lim, Q. Chen, J. Zubieta, J. W. Canary, *Inorg. Chem.* **1995**, *34*, 2562-2568; (b) C.-L. Chuang, O. dos Santos, X. Xu, J. W. Canary, *Inorg. Chem.* **1997**, *36*, 1967-1972.
[34] K. D. Karlin, Y. Gultneh, in *Progress in Inorg. Chem.*, John Wiley & Sons, Inc., **1987**, pp. 219-327.
[35] J. W. Canary, C. S. Allen, J. M. Castagnetto, Y. Wang, *J. Am. Chem. Soc.* **1995**, *117*, 8484-8485.
[36] J. W. Canary, C. S. Allen, J. M. Castagnetto, Y.-H. Chiu, P. J. Toscano, Y. Wang, *Inorg. Chem.* **1998**, *37*, 6255-6262.
[37] J. M. Castagnetto, X. Xu, N. D. Berova, J. W. Canary, *Chirality* **1997**, *9*, 616-622.
[38] B. L. Feringa, R. A. van Delden, N. Koumura, E. M. Geertsema, *Chem. Rev.* **2000**, *100*, 1789-1816.
[39] J. W. Canary, S. Mortezaei, J. Liang, *Coord. Chem. Rev.* **2010**, *254*, 2249-2266.
[40] S. Zahn, J. W. Canary, *Angew. Chem. Int. Ed.* **1998**, *37*, 305-307.
[41] J. Zhang, J. W. Canary, *Org. Lett.* **2006**, *8*, 3907-3910.
[42] S. Zahn, J. W. Canary, *Science* **2000**, *288*, 1404.
[43] L. You, D. Zha, E. V. Anslyn, *Chem. Rev.* **2015**, *115*, 7840-7892.
[44] C. Wolf, K. W. Bentley, *Chem. Soc. Rev.* **2013**, *42*, 5408-5424.
[45] D. Leung, S. O. Kang, E. V. Anslyn, *Chem. Soc. Rev.* **2012**, *41*, 448-479.
[46] (a) A. E. Holmes, S. Zahn, J. W. Canary, *Chirality* **2002**, *14*, 471-477; (b) J. Zhang, A. E. Holmes, A. Sharma, N. R. Brooks, R. S. Rarig, J. Zubieta, J. W. Canary, *Chirality* **2003**, *15*, 180-189.
[47] Y.-H. Chiu, O. dos Santos, J. W. Canary, *Tetrahedron* **1999**, *55*, 12069-12078.
[48] L. You, S. R. Long, V. M. Lynch, E. V. Anslyn, *Chem. Eur. J.* **2011**, *17*, 11017-11023.
[49] L. You, J. S. Berman, E. V. Anslyn, *Nat. Chem.* **2011**, *3*, 943-948.
[50] E. V. Anslyn, *J. Org. Chem.* **2007**, *72*, 687-699.
[51] Y. Zhou, Y. Ren, L. Zhang, L. You, Y. Yuan, E. V. Anslyn, *Tetrahedron* **2015**, *71*, 3515-3521.
[52] C.-Y. Lin, S. Lim, E. V. Anslyn, *J. Am. Chem. Soc.* **2016**, *138*, 8045-8047.
[53] L. You, J. S. Berman, A. Lucksanawichien, E. V. Anslyn, *J. Am. Chem. Soc.* **2012**, *134*, 7126-7134.
[54] L. You, G. Pescitelli, E. V. Anslyn, L. Di Bari, *J. Am. Chem. Soc.* **2012**, *134*, 7117-7125.
[55] H. H. Jo, X. Gao, L. You, E. V. Anslyn, M. J. Krische, *Chem. Sci.* **2015**, *6*, 6747-6753.
[56] J. W. Canary, A. E. Holmes, J. Liu, *Enantiomer* **2001**, *6*, 181-188.
[57] L. A. Joyce, M. S. Maynor, J. M. Dragna, G. M. da Cruz, V. M. Lynch, J. W. Canary, E. V. Anslyn, *J. Am. Chem. Soc.* **2011**, *133*, 13746-13752.
[58] L. A. Joyce, J. W. Canary, E. V. Anslyn, *Chem. Eur. J.* **2012**, *18*, 8064-8069.
[59] F. A. Scaramuzzo, G. Licini, C. Zonta, *Chem. Eur. J.* **2013**, *19*, 16809-16813.
[60] E. Badetti, K. Wurst, G. Licini, C. Zonta, *Chem. Eur. J.* **2016**, *22*, 6515-6518.
[61] F. A. Scaramuzzo, E. Badetti, G. Licini, C. Zonta, *Eur. J. Org. Chem.* **2017**, *2017*, 1438-1442.

[62] R. Berardozzi, E. Badetti, N. A. Carmo dos Santos, K. Wurst, G. Licini, G. Pescitelli, C. Zonta, L. Di Bari, *Chem. Comm.* **2016**, *52*, 8428-8431.
[63] F. G. A. Lister, B. A. F. Le Bailly, S. J. Webb, J. Clayden, *Nat. Chem.* **2017**, *9*, 420-425.
[64] (a) A. J. McConnell, C. S. Wood, P. P. Neelakandan, J. R. Nitschke, *Chem. Rev.* **2015**, *115*, 7729-7793; (b) S. Zarra, D. M. Wood, D. A. Roberts, J. R. Nitschke, *Chem. Soc. Rev.* **2015**, *44*, 419-432; (c) J.-N. Rebilly, B. Colasson, O. Bistri, D. Over, O. Reinaud, *Chem. Soc. Rev.* **2015**, *44*, 467-489; (d) M. Yoshizawa, J. K. Klosterman, M. Fujita, *Angew. Chem. Int. Ed.* **2009**, *48*, 3418-3438.
[65] X. Zeng, D. Coquière, A. Alenda, E. Garrier, T. Prangé, Y. Li, O. Reinaud, I. Jabin, *Chem. Eur. J.* **2006**, *12*, 6393-6402.
[66] A. Brugnara, L. Fusaro, M. Luhmer, T. Prange, B. Colasson, O. Reinaud, *Org. & Biomolecular Chem.* **2014**, *12*, 2754-2760.
[67] P.-E. Danjou, G. De Leener, D. Cornut, S. Moerkerke, S. Mameri, A. Lascaux, J. Wouters, A. Brugnara, B. Colasson, O. Reinaud, I. Jabin, *J. Org. Chem.* **2015**, *80*, 5084-5091.
[68] G. Izzet, X. Zeng, H. Akdas, J. Marrot, O. Reinaud, *Chem. Comm.* **2007**, 810-812.
[69] A. Brugnara, F. Topic, K. Rissanen, A. d. l. Lande, B. Colasson, O. Reinaud, *Chem. Sci.* **2014**, *5*, 3897-3904.
[70] G. Thiabaud, G. Guillemot, I. Schmitz-Afonso, B. Colasson, O. Reinaud, *Angew. Chem. Int. Ed.* **2009**, *48*, 7383-7386.
[71] N. Le Poul, B. Douziech, J. Zeitouny, G. Thiabaud, H. Colas, F. Conan, N. Cosquer, I. Jabin, C. Lagrost, P. Hapiot, O. Reinaud, Y. Le Mest, *J. Am. Chem. Soc.* **2009**, *131*, 17800-17807.
[72] G. Thiabaud, A. Brugnara, M. Carboni, N. Le Poul, B. Colasson, Y. Le Mest, O. Reinaud, *Org. Lett.* **2012**, *14*, 2500-2503.
[73] L. Zhiquan, S. Polen, C. M. Hadad, T. V. RajanBabu, J. D. Badjić, *J. Am. Chem. Soc.* **2016**, *138*, 8253-8258.
[74] D. Zhang, B. Bousquet, J.-C. Mulatier, D. Pitrat, M. Jean, N. Vanthuyne, L. Guy, J.-P. Dutasta, A. Martinez, *J. Org. Chem.* **2017**, *82*, 6082-6088.

Chapter 1

Triggering Assembly and Disassembly of a Supramolecular Cage

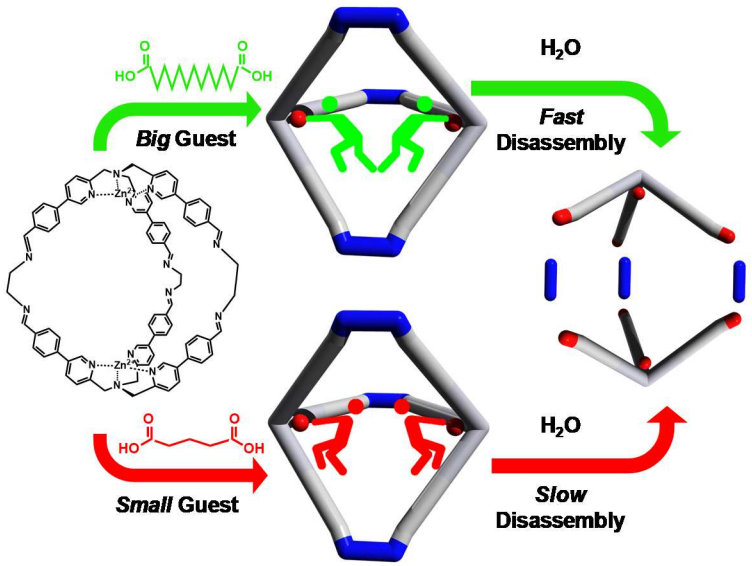

ABSTRACT A novel supramolecular cage built from the self-assembly of tris(2-pyridylmethyl)amine **TPMA** zinc complexes through imine condensation chemistry is reported. The cage recognition properties over a variety of structurally related guests, together with the kinetic study of the template assembly and disassembly, have been investigated in detail. This knowledge has been used to selectively modulate the rate of both assembly and disassembly processes. In particular, a novel disassembly method induced by strain release of the guest has been developed.

1.1 Introduction

Self-assembly of small molecules in complex architectures is becoming the leading strategy for the formation of novel functional systems and materials.[1] Among the different bond-formation synthetic strategies, reversible bond formation involving Dynamic Covalent Chemistry (DCC), in particular imine-condensation combined with coordination chemistry has been extensively used to obtain a large variety of molecular architectures ranging from supramolecular cages to topological structures (Figure 1).[2]

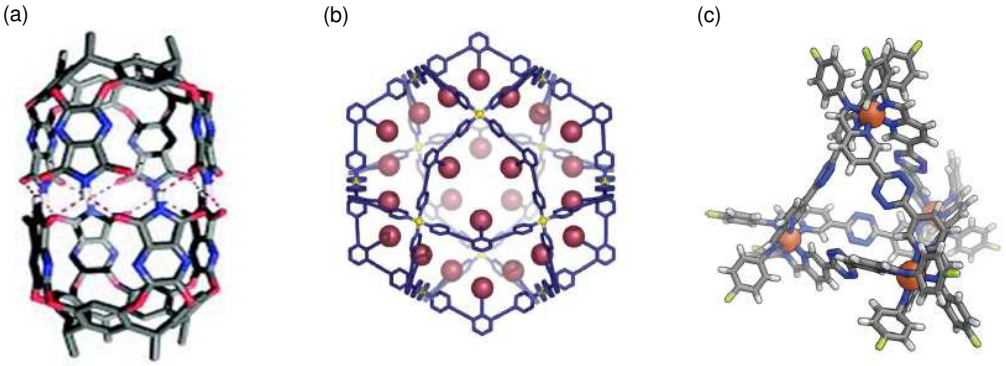

Figure 1. Examples of molecular containers: a) Rebek's nanocapsule driven by hydrogen bonds b) Fujita's cage driven by metal coordination and c) Nitschke' s cage driven by dynamic covalent chemistry (DCC).

Nowadays, the challenge for self-assembled systems is to "time control" their functions and properties which could be modified in response to an external stimulus (pH, light, or the presence of a chemical species).[3] The possibility to time molecular functions (*e.g.* delivery,[4] structural reorganization,[5] stimuli programmed molecular events,[6]…) strongly relies on thermodynamic and kinetic parameters of both assembly and disassembly processes.

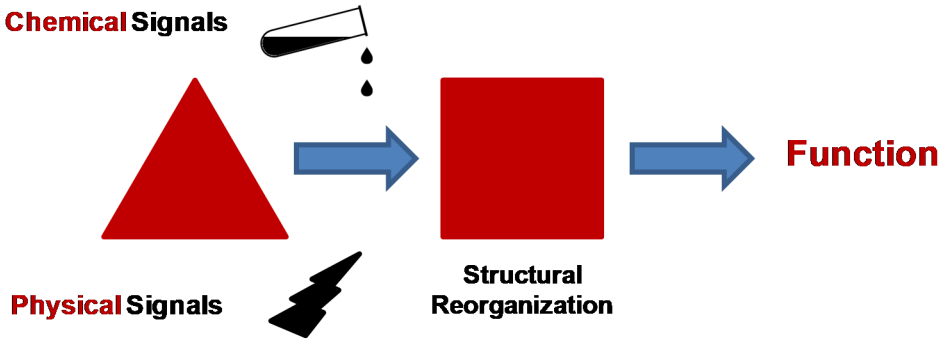

Figure 2. General scheme for a stimuli-responsive system.

However, while the thermodynamic of recognition processes is currently well interpreted, the kinetic aspects of self-assembled molecular architectures remain still unexplored.

In this chapter a novel molecular cage resulting from the self-assembly of two tris(2-pyridylmethyl)amine (**TPMA**) zinc complexes is presented. The molecular recognition properties of the formed cage, together with the experimental kinetic data of assembly and disassembly, reveal interesting and unexpected properties. In particular, a novel method to trigger the disassembly of a supramolecular structure was devised.

1.2 Results ad Discussion

1.2.1 Synthesis of Cage building block Complex 1

Initially, the synthesis of opportunely functionalized T**PMA** complex **1** as building block for supramolecular cage **2** were optimized. The approach adopted for the synthesis of **1** consisted in three step involving a) triple reductive-amination reaction of the commercialy available 5-bromo-2-pyridinecarboxaldehyde **3** b) Suzuki coupling of product **4** with 4-formylphenylboronic acid for the introduction of the

aldehyde moiety and c) complexation of the resulting ligand **5** with $Zn(ClO_4)*6H_2O$ (Scheme 1).

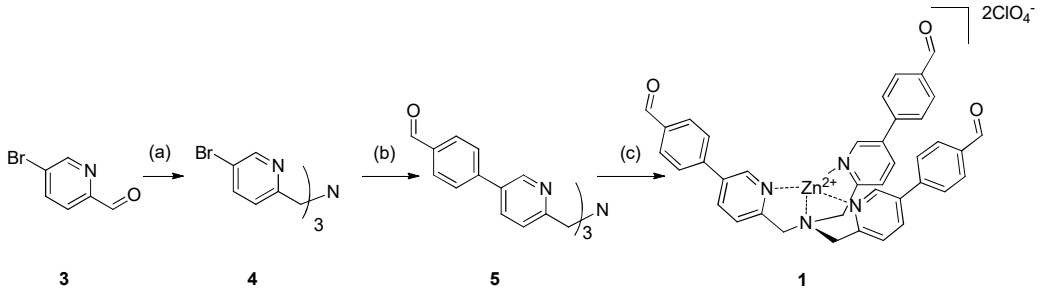

Scheme 1. Synthesis of **1** starting from 5-bromo-2-pyridinecarboxaldehyde. a) NH_4OAc $NaBH(OAc)_3$ CH_2Cl_2 N_2, r.t., 12h (79%); b) 4-formylphenylboronic acid $Pd(PPh_3)_4$, K_2CO_3; Toluene/H_2O/Methanol 1:1:0.5 N_2, 100°C, 48 h (82%) c) $Zn(ClO_4)_2*6H_2O$ CH_3CN, r.t. (90%).

The formation of complex **1** has been confirmed with ESI-MS and ^1H NMR analysis. In the ^1H NMR spectra the CH_2 signals of **TPMA** are shifted downfield respect to the free ligand **5** because of the coordination to the Zn(II) (Figure 2).

2 M has been also identified *via* ESI-MS with the signal at 765.11 m/z. The experimental isotopic pattern overlaps the calculated one (Figure 3).

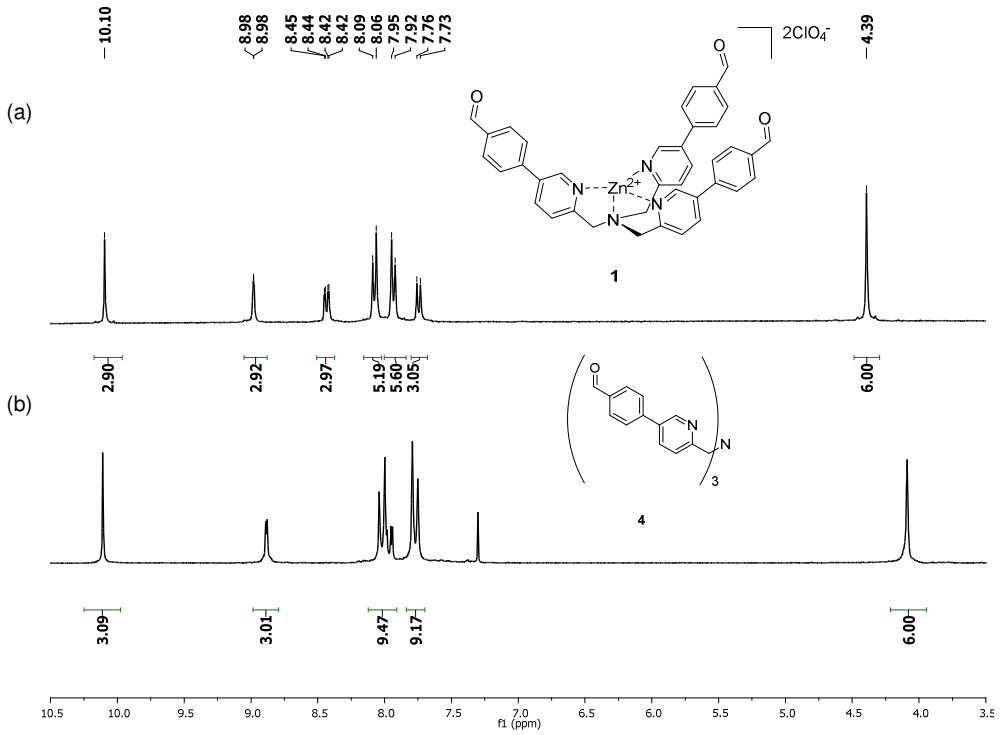

Figure 2. a) ^{1}H-NMR in CD_3CN of complex **1**; b) ^{1}H-NMR in $CDCl_3$ of free ligand **4**.

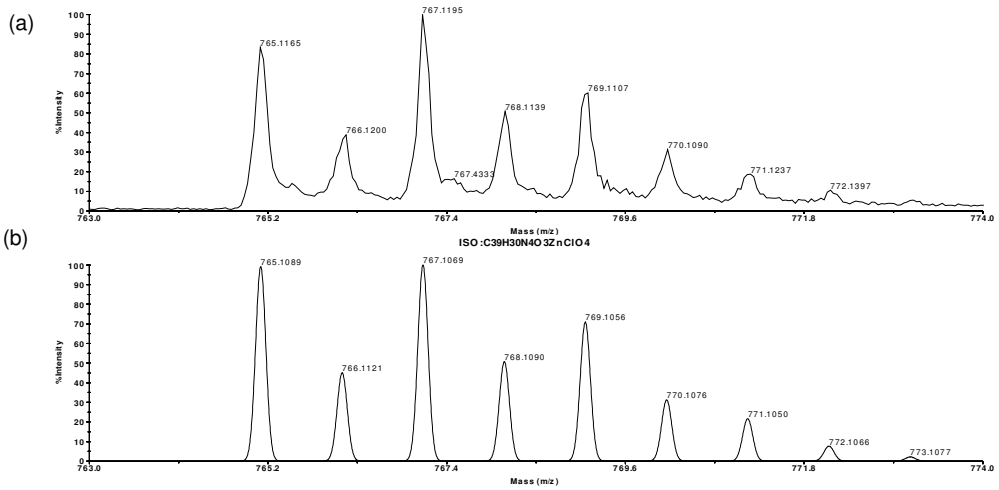

Figure 3. Experimental a) and calculated b) isotopic distribution in the ESI-MS of **1** corresponding to $[C_{39}H_{30}N_4O_3Zn+ClO_4]^+$.

1.2.2 Synthesis of the Novel molecular Cage 2

Taking advantage of dynamic covalent chemistry,[7],[8] a polyimine self-assembled cage based on the opportunely designed **TPMA** zinc complex **1** was synthesized. The reaction of **1** with ethylenediamine **en** in acetonitrile results in the selective formation of the bimetallic molecular cage **2** in 12 hours (Scheme 2).

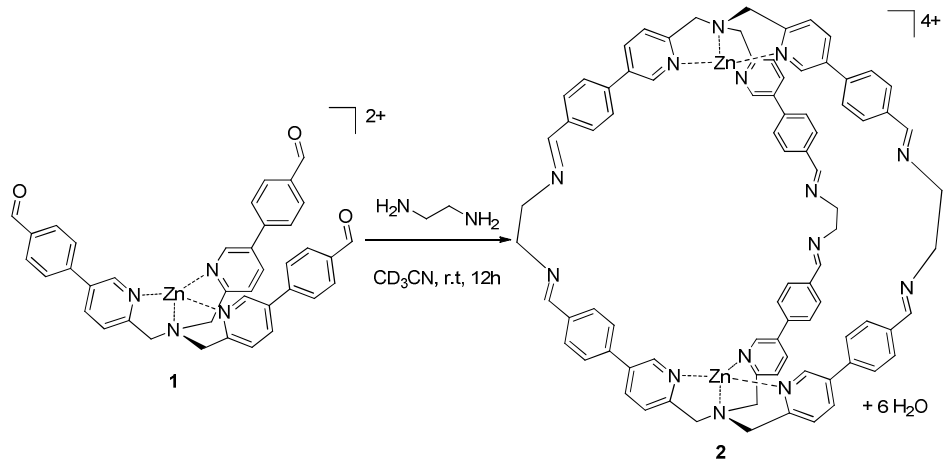

Scheme 2. Synthesis of cage **2** formation from complex **1** and ethylendiamine **en**. $[\mathbf{1}]_0$ = 1.50 mM (1.0 eq.), $[\mathbf{en}]_0$ = 3.75 mM (2.5 eq.). Perchlorate counter anions and embedded **en** have been removed for clarity.

Within this time, the aldehyde protons signal at 10.03 ppm disappears and the formation of the imine signal at 8.82 ppm is observed. ^{1}H NMR reflects the D_3 symmetry of the cage with only two signals in the aliphatic region and six signals in the aromatic region. 2D-NMR and ESI-MS experiments confirm the presence of a single species in solution (See Appendix, Fig. A19-21). Along the improvement of the synthetic method, it has been noticed that in order to obtain high conversion of the cage the reaction needs to be performed in high dilution conditions and employing an excess, up to two equivalents, of ethylenediamine. The diamine, as revealed by DOSY and ROESY experiments, is embedded within the cage.

1.2.3 Recognition properties of cage 2

TPMA metal complexes have already shown their capability to perform molecular recognition.[9],[10] For this reason, dicarboxylic acids inclusion in cage **2** has been explored. Addition of suberic acid $\mathbf{C_8}$ in acetonitrile in sub-stoichiometric amount (from 0.2 to 0.9 equiv.) leads to the formation of a new set of signals that we assigned to the cage filled with the diacid, viz. $\mathbf{C_8@2}$. An excess of $\mathbf{C_8}$ (1.3 equiv.) results in a complete conversion to the filled cage (Figure 4).

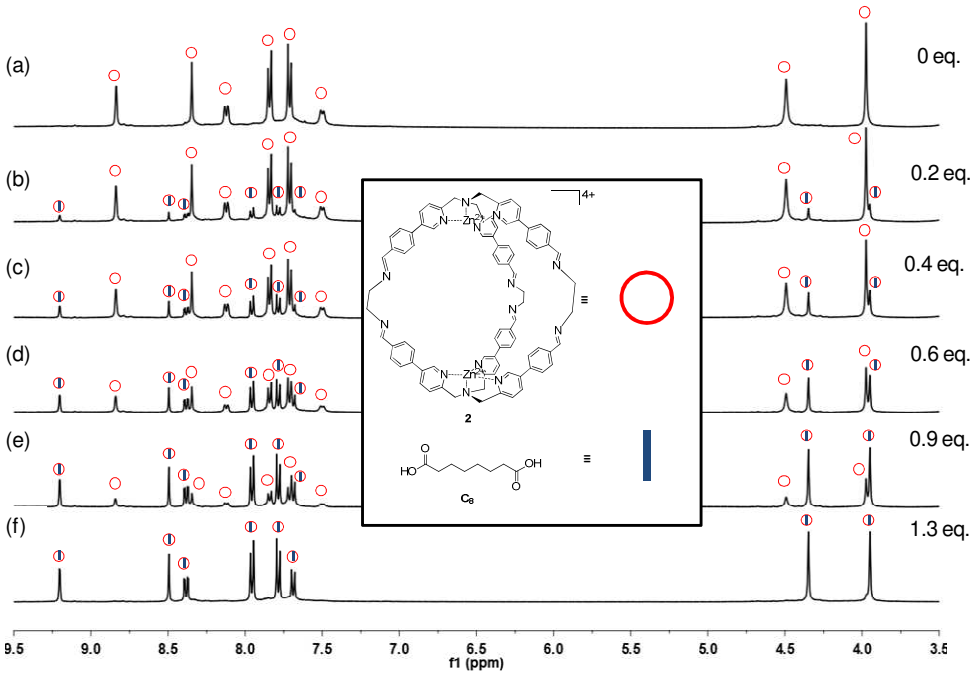

Figure 4. ^{1}H NMR inclusion experiments. Addition of suberic acid $\mathbf{C_8}$ to cage **2** in CD_3CN. (a) Preformed cage **2** (0.001 M cage). The number of peaks is related to the D_3 symmetry of the system. (b)-(e) Addition of sub-stoichiometric amounts (0.2-0.9 equiv) of $\mathbf{C_8}$ results in the formation of a new species that maintains the original symmetry. (f) Addition of 1.3 equiv of suberic acid totally shift the system to the new species $\mathbf{C_8@2}$. Counter anions are perchlorates.

These data allow to establish a 1:1 stoichiometry with a binding constant (K_2) for the association process of 3.6×10^4 M^{-1}. The formation of the inclusion complex $\mathbf{C_8@2}$ is confirmed by two-dimensional NMR spectroscopy (ROESY, DOSY) and ESI-MS experiments (Figure 5 and See Appendix, Fig. A22-26). As revealed by NMR

experiments, addition of diacid results in the protonation of the embedded ethylenediamine and binding of the dicarboxylate anion (See Appendix, Fig. A2-4).
The successful binding of suberic acid **C_8** by cage **2** encouraged us to study the complexation of the diacids ranging from succinic acid **C_4** to tetradecandioic acid **C_{14}** in order to find out the dependence of the free energy of complexation from the aliphatic guest chain length. In other words, the experiment is not designed to find the best binder, but to understand how minimal structural variations affect the encapsulation phenomena.[11] Binding constants for the whole series of diacids have been determined and they are reported in Figure 5.

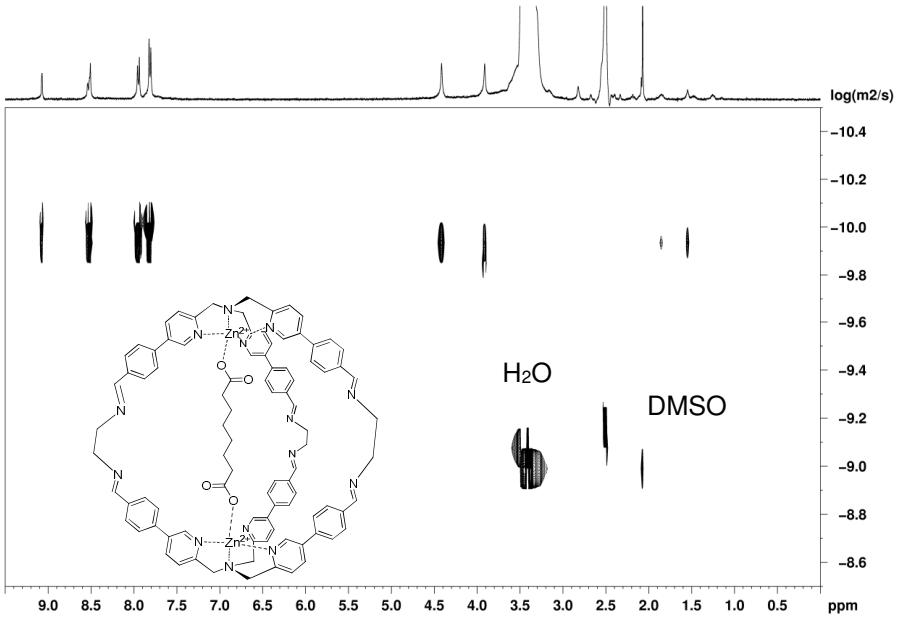

Figure 5.. DOSY spectrum (400 MHz, 301 K, DMSO-d_6) of **C_8@2**.The diffusion coefficient was calculated to be 1.0 x 10^{-10} m^2 s^{-1}, corresponding to a hydrodynamic radius (r_H) of 12.1 Å for **C_8@2**,as calculated by using the Stokes-Einstein equation.[12]

Interestingly, it is possible to highlight a pseudo-Gaussian profile, typical for processes occurring in confined spaces,[13] centered on suberic acid **C_8**. Longer **$C_{9\text{-}14}$** and shorter **$C_{4\text{-}7}$** diacids bind both metal sites simultaneously, but to do so requires a conformational rearrangement of the host and guest which has a higher thermodynamic cost.

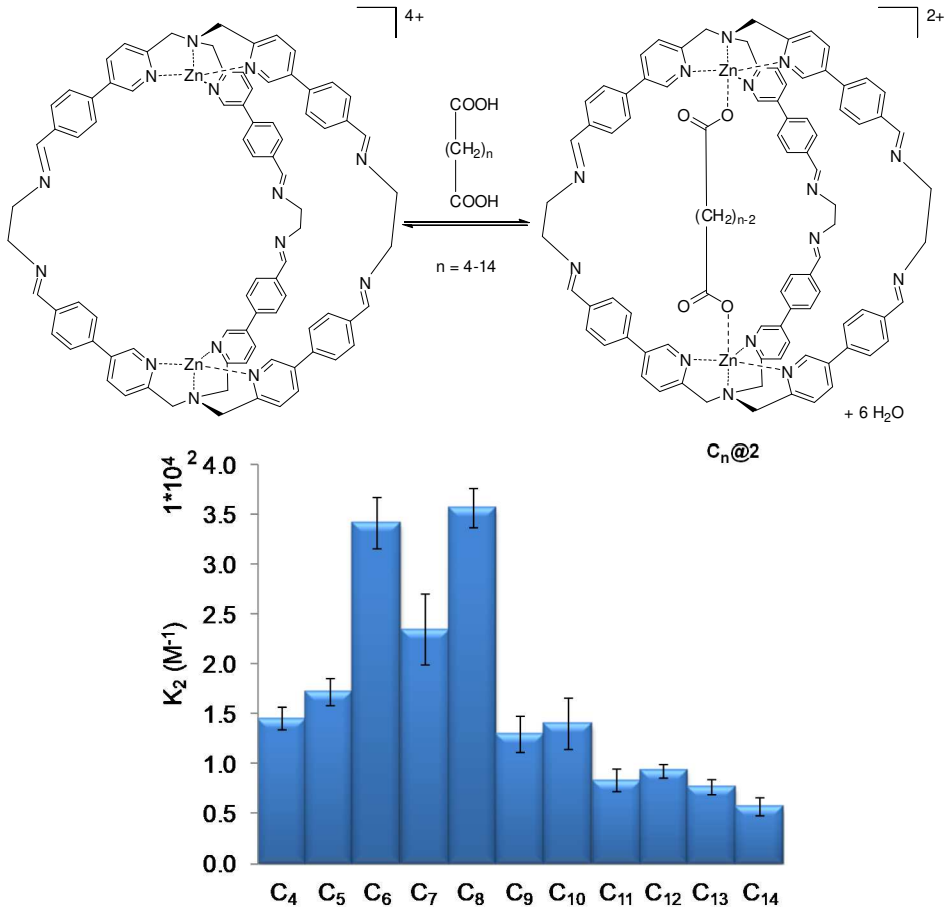

Figure 6. ^{1}H NMR binding constants (K_2) for the inclusion of diacids **C_4-C_{14}** within cage **2** (embedded **en** and perchlorate counter anions are removed for clarity)

In order to gather more information on the formed structures and to explain the cage selectivity, semiempirical PM6 calculations for the inclusion complexes for the whole **$C_{4\text{-}14}$** inclusion series have been performed.[14] As shown in Figure 7a (See Appendix, Fig. A10), the guests are binding at both ends inducing deformation in the cage. This deformation is more evident for shorter diacids as shown by the calculated Zn-Zn distance (Figure 7b). After diacid **C_8** the distance among the two metals is not varying, independently by the guest (Figure 7c) and the dicarboxylic

acid tends to coil within the cage. It is worth to notice that PM6 calculations are able to reproduce the trend of binding energies (Figure 7b).

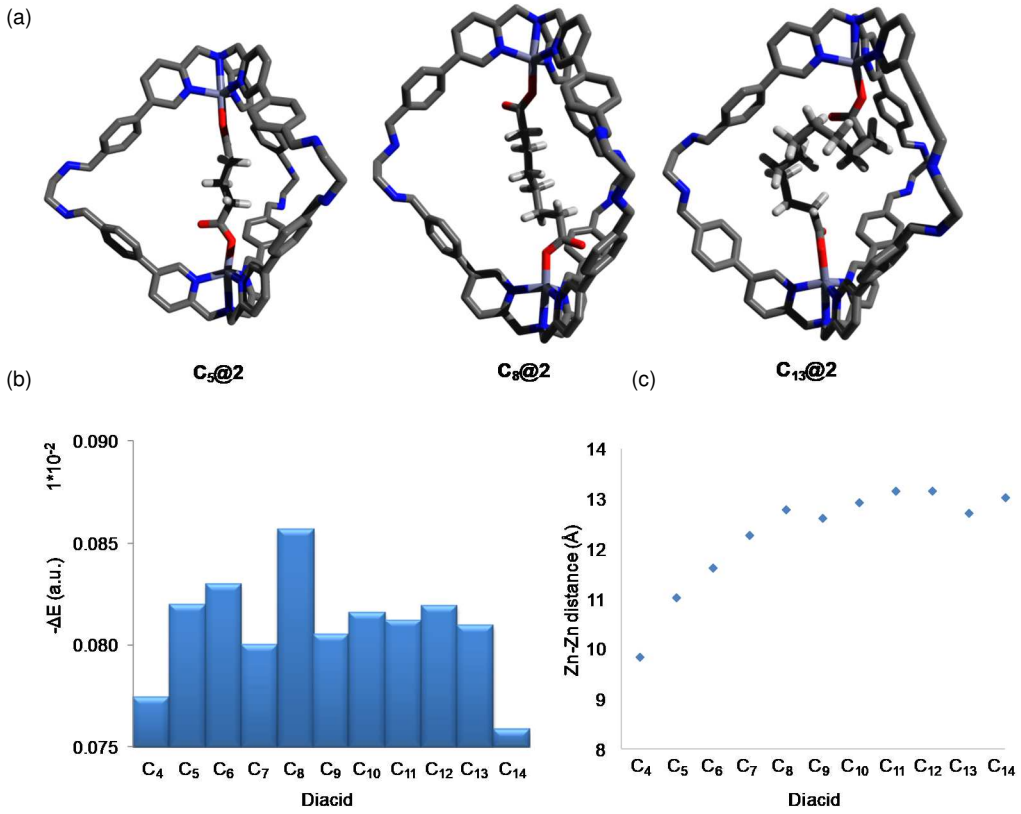

Figure 7. (a) Stick representation of the PM6 minimized structures **C_5@2, C_8@2 C_{11}@2** and **C_{13}@2.** The whole series ranging from **C_4@2** to **C_{14}@2** is in Supplementary Figure S6. (b) PM6 calculated binding energies (a.u) and (c) zinc-zinc distances for the **C_n@2** series..

1.2.4 Assembly and disassembly in the presence of diacids

After the analysis of the binding, rates of cage **2** formation (assembly) and hydrolysis (disassembly) have been measured in the presence of the different diacids. Initial rates for both processes have been determined using ^{1}H NMR without guest and with every single diacid of the **C$_{4-14}$** series. In Figure 8a the initial relative rates have been reported in order to better highlight the effect of the different diacids in the cage formation. As example, synthesis templated by diacid **C$_8$** speeds up cage **2** formation twelve times in comparison with the untemplated process (v_{C8}/v_{blank} = 12).[15] On the other hand, initial rate of cage **2** hydrolysis in the presence of **C$_8$** diacid is comparable to the empty cage (v'_{C8}/v'_{blank} = 1.0 Figure 8b).

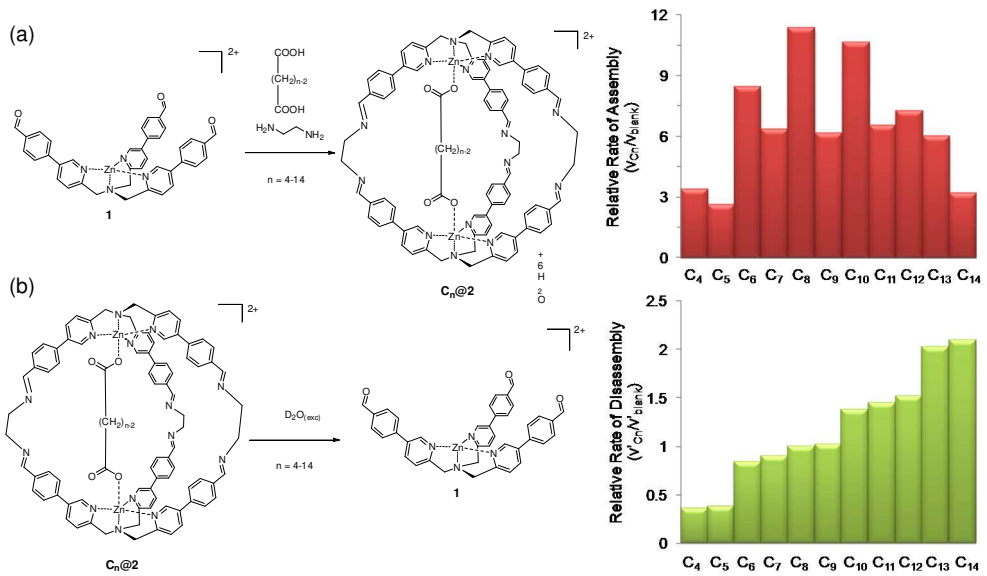

Figure 8. Initial relative rates of assembly (a) and disassembly (b) of cage **2** in the presence of diacids **C$_4$-C$_{14}$**. Initial rates for the formation and hydrolysis of the cages have been measured using ^{1}H NMR and they have been compared with the rates of the empty cage **2**. Initial conditions for: (a) assembly [**1**]$_0$ = 1.50 mM (1.0 eq.), [ethylenediamine]$_0$ = 2.25 mM (1.5 eq.), [**C$_n$**] = 0.75 mM(0.5 eq.) and (b) disassembly [**C$_n$@2**]$_0$ = 0.30 mM, [D_2O]$_0$ = 16 M. In the case of a monocarboxylic acid (hexanoic acid), the rate of formation is 2.5 times faster than the case of the empy cage while the initial relative rate of hydrolysis is 0.7 time slower than the case of the empy cage. In all the structures, the counter anions are perchlorates. The error bars are reported in the Appendix to Chapter 1.

In the whole **C_4-C_{14}** series (Figure 8a), initial relative rates for this templated synthesis highlight a trend which mirrors the binding constant capabilities of cage **2** (Figure 6).This observation suggests that the molecular origin of the rate enhancement can be qualitatively interpreted, besides the capability of the diacids to pre-organize the two **TPMA** complexes **1**, similarly to the abovementioned recognition properties of formed cage **2**.

In other words, while it is not possible to compare binding energies with transition state energies, we can hypothesize that the stabilization of the diacids toward the cage formation has a molecular origin common to those of the formed cage.

On the other hand, an unexpected profile is observed for the initial relative rates of cage hydrolysis (disassembly). In this case, no relationships with the previously measured profiles is present (Figure 8b). The initial relative rate of cage hydrolysis constantly increases with the diacids length. Diacids from **C_4** to **C_6** show hydrolysis rates lower than the empty cage, in particular up to five time slower for the shortest diacid (v'_{C4}/v'_{blank} = 0.4). Shorter diacids tend to keep the two **TPMA** Zn complex units together. In this case, the opening of the cage is associated to a strain gain to keep the interaction of the carboxylates with both metal centers. In between, **C_7** and **C_9** have an influence towards the hydrolytic process similar to those of the solvent molecules within the empty cage (v'_{C8}/v'_{blank} = 1).[16] On the opposite side of the profile, the presence of longer diacids **C_{10}-C_{14}** within the cage is speeding up the hydrolysis, up to almost two times faster for the longest **C_{14}** (v'_{C14}/v'_{free} = 2.0).

A plausible explanation of the diacids active role in the rate of cage hydrolysis can be found in the conformation adopted within the cage by the alkyl chains, which behave as a spring.[17] Therefore, longer diacids are expected to push toward both **TPMA** Zn complex units of the cage in virtue of their coiled conformation. The energy coming from the acids strain release is responsible for the observed acceleration (*viz.* to an opening of the structure a better binding of the longer diacids is expected) (See Appendix, Section 1.3-1.5).

1.2.5 Triggering the assembly and disassembly of cage 2

As proof of principle, an experiment in which the addition of a diacid triggers the assembly of the cage has been devised. The reaction between aldehyde **1** and ethylendiamine results in the slow formation of cage **2** (Figure 9a). However, after the addition of the diacid $\mathbf{C_8}$ (red arrow) an increase of the rate of cage formation is observed leading to a total conversion of the reagents. While this experiment reminds many examples of template synthesis, the triggering method designed for the disassembly is novel. When an excess of water is added to a solution of **2** in which $\mathbf{C_5}$ is present, only 7% of the cage is hydrolyzed after 40 minutes (Figure 9b). Noteworthy, the addition of diacid $\mathbf{C_{13}}$ gives a sharp enhancement of the disassembly rate and allows complete disassembly within 2 hours (See Appendix, Fig. A16-17).[18] In order to exclude general acid catalysis and steric hindrance effect of the guest, in the same conditions monocarboxylic acid and myristic acid, hexanoic acid, have been added in two different experiments instead of a dicarboxylic acid. The addition of hexanoic acid and myristic acid does not results in a change in the rate of hydrolysis. (See Appendix, Fig. A14-15). It has to be noticed that despite $\mathbf{C_5}$ and $\mathbf{C_{13}}$ diacids having a similar binding constant for **2**, they have an opposite behavior in the hydrolysis process. These guests tune the kinetic activity in virtue of their push/pull effects (viz. strain gain/release or pressure/vacuum generation within the cage) within the host.

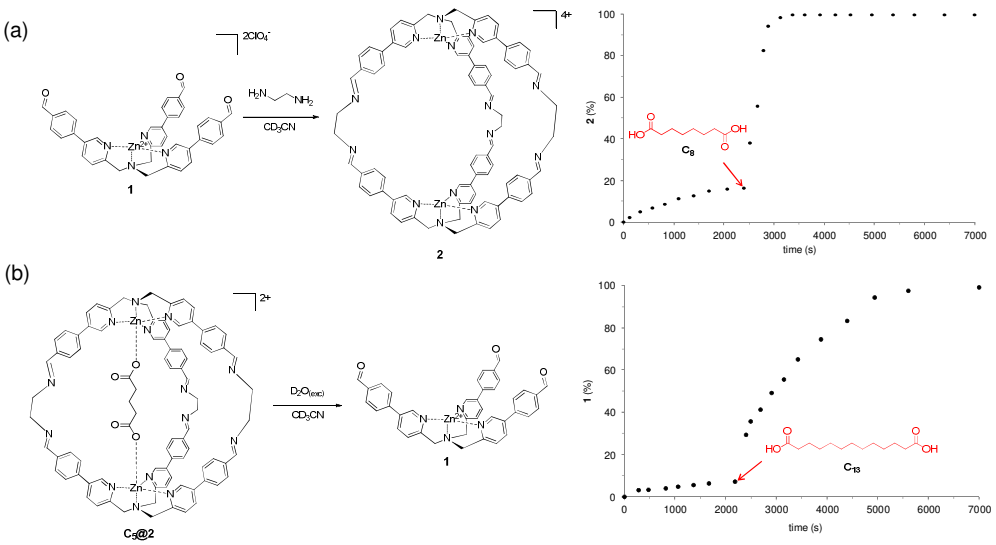

Figure 9. (a) Kinetic profile for the formation of cage **2.** Addition of $\mathbf{C_8}$ increases the assembly rate. (b) Kinetic profile for the hydrolysis of cage **2** in the presence of $\mathbf{C_5}$**.** The addition of $\mathbf{C_{13}}$ increases the disassembly rate. $[\mathbf{C_5@2}]_0$ = 0.30 mM, $[D_2O]_0$ = 16 M, $[\mathbf{C_{13}}]$= 0.30 mM

1.3 Conclusions

In conclusion, we have reported the synthesis of a novel self-assembled imine-based supramolecular cage. The detailed study of the kinetic and thermodynamic parameters guiding the assembly/disassembly processes reveals interesting patterns related to the size of the guest. The possibility to use guests of increasing molecular length has highlighted the link between the thermodynamic of the process formation and the kinetic of the assembly/disassembly. Moreover, two experiments in which the assembly/disassembly is triggered by the presence of a guest have been set up. In particular, the disassembly experiment represents the first example of rate enhancement exerted by strain release of the guest

1.4 Experimental

1.4.1 tris((5-bromopyridin-2-yl)methyl)amine 4

In a 250 ml double neck flask, anhydrous NH_4OAc (1.38 g, 17.9 mmol) and 5-bromo-2-pyridinecarboxaldehyde **3** (10.00 g, 53.7 mmol) were dissolved in dry CH_2Cl_2 (170 mL) under N_2 and left under stirring for 1 hour. Three aliquots of $NaBH(OAc)_3$ (3.80 g, 17.9 mmol) were added waiting one hour between each addition. After that the reaction was stirred for 12 hours at room temperature. The solvent was removed under reduced pressure. The resulting white solid was dissolved in AcOEt and the solution extracted with 0.1 M solution of KOH (3x100 ml). The organic phases were dried on anhydrous $MgSO_4$ and the solvent was removed under reduced pressure. The resulting solid was precipitated by crystallization from THF/hexane to yield a white solid (7.43 g, 79%).

m.p. 95-98 °C ^{1}H NMR (200 MHz, $CDCl_3$) δ (ppm): 8.60 (d, 3H, *J* = 2.0 Hz, ArH), 7.78 (dd, 3H, *J* = 2.0 Hz, *J* = 8.0 Hz, ArH), 7.41 (d, 3H, *J* = 8.0 Hz, ArH), 3.81 (s, 6H, CH_2). ^{13}C NMR (72.5 MHz, $CDCl_3$) δ (ppm): 157.7, 150.5, 139.3, 124.7, 119.4, 59.5. HRMS (ESI-TOF) (*m/z*): $[M+H]^+$ calcd. for $[C_{18}H_{15}Br_3N_4+H]^+$, 524.8920; found 524.8788.FT IR (KBr) ν(cm^{-1}): 1573, 1469, 1365, 1089, 1008. Elemental analysis: C. 40.07; H, 2.92; N, 10.85. Required: C. 41.02; H, 2.87; N, 10.63.

1.4.2 4,4',4''-(6,6',6''-(nitrilotris(methylene))tris(pyridine6,3-diyl)) tribenzaldehyde 5

A mixture of 4 (3.00 g, 5.69 mmol), 4-formylphenylboronic acid (3.84 g, 25.6 mmol), $Pd(PPh_3)_4$ (65 mg, 0,0057 mmol, 1 mol%) and K_2CO_3 (5.51 g, 39.8 mmol) was dissolved in 60 ml of H_2O/toluene/CH_3OH (1:1:0.5). The mixture was stirred under N_2 for 48 hours at 100°C. The solvent was removed under reduced pressure. The resulting yellow oil was dissolved in $CHCl_3$ and the solution extracted with H_2O (3x50 mL). The organic phases were dried on anhydrous $MgSO_4$, filtered on celite and then the solvent was removed under reduced pressure. The resulting solid was

precipitated by crystallization from THF/hexane to yield a pale yellow solid (2.89 g, 82%).

m.p 138 °C
^{1}H NMR (200 MHz, $CDCl_3$) δ (ppm): 10.11 (s, 3H, CHO), 8.89 (d, 3H, *J* = 2.0 Hz, PyrH), 8.02 (dd, 3H, *J* = 8.0 Hz, *J*= 2.0 Hz, PyrH), 7.97 (d, 6H, *J* = 8.25 Hz, ArH), 7.83 (d, 6H, *J* = 8.25 Hz, ArH), 7.72 (d, 3H, *J* = 8.0 Hz, PyrH), 4.09 (s, 6H, CH_2).
^{13}C NMR (75 MHz, $CDCl_3$) δ (ppm): 191.8, 159.4, 147.9, 143.8, 136.0, 135.3, 134.0, 130.7, 127.8, 123.5, 60.1.HRMS (ESI-TOF) *(m/z)*: $[M+H]^+$ calcd. for $[C_{39}H_{30}N_4O_3+H]^+$, 603.2391; found 603.2433. FT-IR (KBr) ν(cm^{-1}): 1700, 1605, 1214, 1174, 825.
Elemental analysis: C. 77.15; H, 5.06; N, 9.25. Required: C. 77.72; H, 5.02; N, 9.30.

1.4.3 Synthesis of complex 1

To a suspension of ligand 4,4',4''-(6,6',6''-(nitrilotris(methylene))tris(pyridine6,3-diyl))tribenzaldehyde **5** (100 mg, 0.17 mmol) in acetonitrile (15 ml) zinc (II) perchlorate hexahydrate was added (40.5 mg, 0.17 mmol) . The solution was stirred at room temperature for 1 hour and the reaction was followed by ^{1}H NMR and ESI-MS. At the end of the reaction diethyl ether (25 ml) was added obtaining quantitatively a crystalline solid then centrifuged and dried. **1** results as a pale yellow solid (128 mg, 90%).
Caution! Perchlorate salts of metal complexes with organic ligands are potentially explosive. They should be handled in small quantity and with caution.

^{1}H NMR (300 MHz, CD_3CN) δ (ppm): 10.09 (s, 3H, CHO), 8.82 (d, 3H, *J*= 2.0 Hz, PyrH), 8.44 (dd, 3H, *J*=8.0 Hz, *J*=2.0 Hz PyrH), 8.07 (d, 6H, *J*=8.0 Hz, ArH), 7.94 (d, 6H, *J*=8.0 Hz, ArH), 7.75 (d, 3H, *J*=8.0 Hz, PyrH), 4.40 (s, 6H,CH_2).
HRMS (ESI-TOF) *(m/z)*: $[M+ClO_4]^+$ calcd. for $[C_{39}H_{30}N_4O_3Zn+ClO_4]^+$, 765.1094; found 765.1165.
Elemental analysis: C. 54.08; H, 4.01; N, 6.85. Required [**1**]$(ClO_4)_2$. C 54.03; H, 3.49; N, 6.46.

1.4.4 Synthesis of cage 2

To 500 µl (1.0 µmol) of a 0.002 M solution of complex **1** in CD_3CN, 125 µl (2.5 µmol) of a 0.02 M solution of ethylendiamine in CD_3CN were added in 6 portions over a period of 6 hours. The mixture was left for 12 hours at room temperature (yield 70% based on internal standard p-xilene).

^1H NMR (400 MHz, CD_3CN) δ (ppm): 8.82 (d, 6H, *J*=2.0 Hz PyrH), 8.36 (s, 6H, NH_{imm}), 8.13 (dd, 6H, *J*=8.0 Hz, *J*=2.0 Hz, PyrH), 7.82 (d, 12H, *J*=8.5 Hz, ArH), 7.68 (d, 12H, *J*=8.5 Hz, ArH), 7.47 (d, 6H, *J*=8.0 Hz, PyrH), 4.46 (s, 12H, CH_2), 3.95 (s, 12H, CH_{2eda}), 2.94 (s, 8H, $CH_{2eda\text{-}embedded}$).
HRMS (ESI-TOF) *(m/z)*: $[M+2ClO_4]^{2+}$ calcd. for $[C_{84}H_{72}N_{14}Zn_2+2ClO_4]^{2+}$, 801.1083; found, 801.1597; $[M+HCOO+ClO_4]^{2+}$ calcd. for $[C_{84}H_{72}N_{14}Zn_2+HCOO+ClO_4]^{2+}$, 774.2049; found, 774.1958; $[M+2HCOO]^{2+}$ calcd. for $[C_{84}H_{72}N_{14}Zn_2+2HCOO]^{2+}$, 747.2295; found, 747.2105; $[M+HCOO+CH_3CN]^{3+}$ calcd. for $[C_{84}H_{72}N_{14}Zn_2+HCOO+CH_3CN]^{3+}$, 496.8291; found, 498.4780; $[M+HCOO+C_2H_8N_2]^{3+}$ calcd. for $[C_{84}H_{72}N_{14}Zn_2+HCOO+C_2H_8N_2]^{3+}$, 503.5124; found, 504.4592; $[M+C_2H_8N_2+CH_3CN]^{4+}$ calcd. for 376.3895 $[C_{84}H_{72}N_{14}Zn_2+C_2H_8N_2+CH_3CN]^{4+}$,found, 376.1180; $[M+2C_2H_8N_2]^{4+}$ calcd. for 381.4019 $[C_{84}H_{72}N_{14}Zn_2+2C_2H_8N_2]^{4+}$,found, 381.8012.

1.4.5 Synthesis of C_8@2

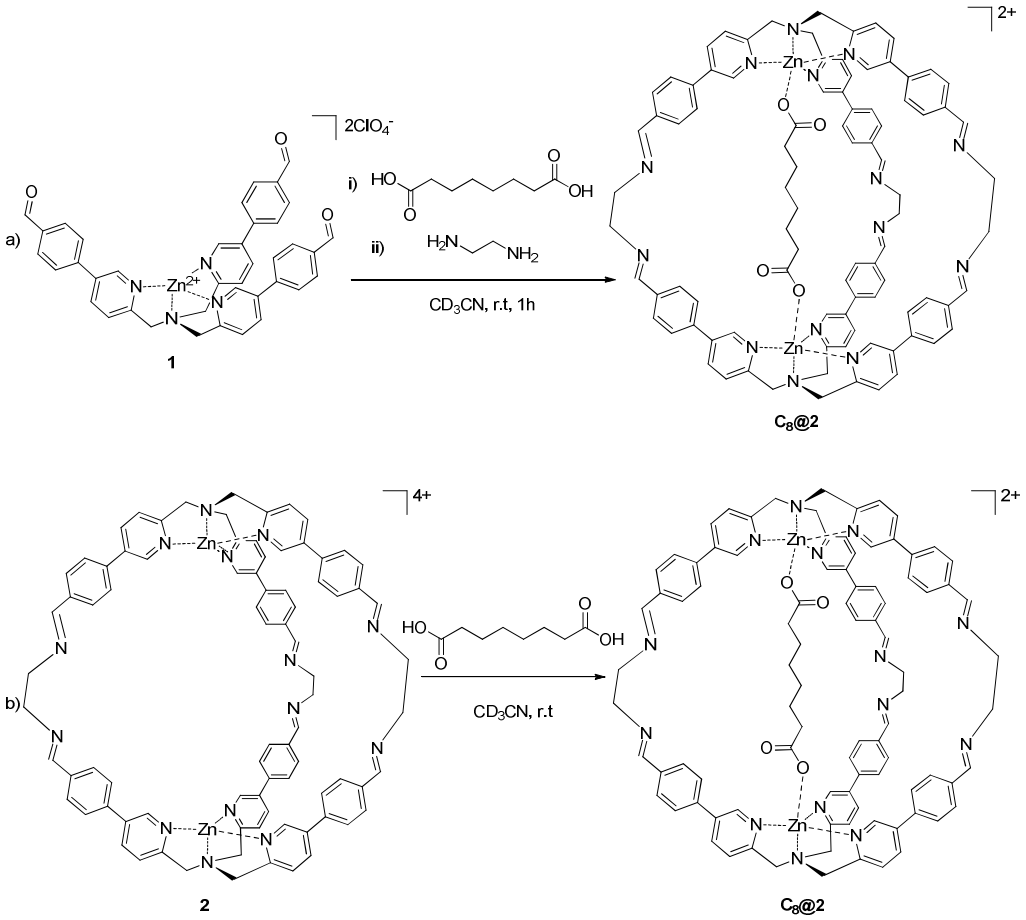

a) To 500 µl (1.0 µmol) of a solution 0.002 M of complex **1** in CD_3CN, 50 µl (0.5 µmol) of a solution 0.01 M in CD_3CN of suberic acid and 125 µl (2.5 µmol) of a solution 0.02 M in CD_3CN of ethylendiamine were added in a NMR tube. The mixture was left for 1 hour at room temperature and checked *via* ^1H NMR (yield 80% based on internal standard p-xilene).

b) To 500 µl (0.5 µmol) of a solution 0.001 M in CD_3CN of cage **2** were added 60 µl (0.6 µmol) of a solution 0.01 M in CD_3CN of suberic acid **C_8** in a NMR tube. The mixture was checked *via* ^1H NMR (yield 95% based on internal standard p-xilene).

^{1}H NMR (400 MHz, CD_3CN) δ (ppm): 9.22 (d, 6H, *J*=2.0 Hz PyrH), 8.51 (s, 6H, NH_{imm}), 8.40 (dd, 6H, *J*=8.0 Hz, *J*=2.0 Hz, PyrH), 7.97 (d, 12H, *J*=8.5 Hz, ArH), 7.80 (d, 12H, *J*=8.5 Hz, ArH), 7.71 (d, 6H, *J*=8.0 Hz, PyrH), 4.37 (s, 12H, CH_2), 3.97 (s, 12H, CH_{2eda}), 2.66 (m, 4H, CH_{2acid}) , 1.66 (m, 4H, CH_{2acid}).

^{1}H NMR (400 MHz, DMSO) δ (ppm): 9.07 (s, 6H, *J*=2.0 Hz PyrH), 8.52 (m, 6H+6H, NH_{imm}, PyrH), 7.94 (d, 12H, *J*=8.0 Hz, ArH), 7.81 (m, 12H+6H, PyrH+ArH), 4.41 (s, 12H, CH_2), 3.91 (s, 12H, CH_{2eda}), 1.84 (m, 4H, CH_{2acid}) , 1.54 (m, 4H, CH_{2acid}).

HRMS (ESI-TOF) *(m/z)*: $[M]^{2+}$ calcd. for $[C_{92}H_{84}N_{14}O_4Zn_2]^{2+}$, 788.2686 found; 788.3544.

References

[1] (a) E. Moulin, G. Cormos, N. Giuseppone, *Chem. Soc. Rev.* **2012**, *41*, 1031-1049; (b) Y. Zhang, M. Barboiu, *Chem. Rev.* **2016**, *116*, 809-834; (c) J.-M. Lehn, *Angew. Chem. Int. Ed.* **2015**, *54*, 3276-3289.

[2] (a) J. Bunzen, J. Iwasa, P. Bonakdarzadeh, E. Numata, K. Rissanen, S. Sato, M. Fujita, *Angew. Chem. Int. Ed.* **2012**, *51*, 3161-3163; (b) Y. Inokuma, S. Yoshioka, J. Ariyoshi, T. Arai, Y. Hitora, K. Takada, S. Matsunaga, K. Rissanen, M. Fujita, *Nature* **2013**, *495*, 461-466; (c) D. A. Leigh, R. G. Pritchard, A. J. Stephens, *Nat. Chem.* **2014**, *6*, 978-982; (d) V. Marcos, A. J. Stephens, J. Jaramillo-Garcia, A. L. Nussbaumer, S. L. Woltering, A. Valero, J.-F. Lemonnier, I. J. Vitorica-Yrezabal, D. A. Leigh, *Science* **2016**, *352*, 1555; (e) K. S. Chichak, S. J. Cantrill, A. R. Pease, S.-H. Chiu, G. W. V. Cave, J. L. Atwood, J. F. Stoddart, *Science* **2004**, *304*, 1308; (f) J.-N. Rebilly, B. Colasson, O. Bistri, D. Over, O. Reinaud, *Chem. Soc. Rev.* **2015**, *44*, 467-489; (g) S. H. A. M. Leenders, R. Gramage-Doria, B. de Bruin, J. N. H. Reek, *Chem. Soc. Rev.* **2015**, *44*, 433-448; (h) S. Durot, J. Taesch, V. Heitz, *Chem. Rev.* **2014**, *114*, 8542-8578; (i) T.-Z. Xie, K. J. Endres, Z. Guo, J. M. Ludlow, C. N. Moorefield, M. J. Saunders, C. Wesdemiotis, G. R. Newkome, *J. Am. Chem. Soc.* **2016**, *138*, 12344-12347.

[3] A. J. McConnell, C. S. Wood, P. P. Neelakandan, J. R. Nitschke, *Chem. Rev.* **2015**, *115*, 7729-7793.

[4] (a) A. M. Castilla, T. K. Ronson, J. R. Nitschke, *J. Am. Chem. Soc.* **2016**, *138*, 2342-2351; (b) R. Haag, *Angew. Chem. Int. Ed.* **2004**, *43*, 278-282; (c) A. B. Grommet, J. L. Bolliger, C. Browne, J. R. Nitschke, *Angew. Chem. Int. Ed.* **2015**, *54*, 15100-15104; (d) A. B. Grommet, J. R. Nitschke, *J. Am. Chem. Soc.* **2017**, *139*, 2176-2179.

[5] (a) M. Baroncini, S. d'Agostino, G. Bergamini, P. Ceroni, A. Comotti, P. Sozzani, I. Bassanetti, F. Grepioni, T. M. Hernandez, S. Silvi, M. Venturi, A. Credi, *Nat. Chem.* **2015**, *7*, 634-640; (b) A. Martinez, L. Guy, J.-P. Dutasta, *J. Am. Chem. Soc.* **2010**, *132*, 16733-16734; (c) S. Chen, M. Yamasaki, S. Polen, J. Gallucci, C. M. Hadad, J. D. Badjić, *J. Am. Chem. Soc.* **2015**, *137*, 12276-12281; (d) F. G. A. Lister, B. A. F. Le Bailly, S. J. Webb, J. Clayden, *Nat. Chem.* **2017**, *9*, 420-425.

[6] (a) C. S. Wood, C. Browne, D. M. Wood, J. R. Nitschke, *ACS Cent. Sci.* **2015**, *1*, 504-509; (b) S. Maiti, I. Fortunati, C. Ferrante, P. Scrimin, L. J. Prins, *Nat. Chem.* **2016**, *8*, 725-731; (c) S. Kassem, A. T. L. Lee, D. A. Leigh, A. Markevicius, J. Solà, *Nat. Chem.* **2016**, *8*, 138-143; (d) E. R. Kay, D. A. Leigh, F. Zerbetto, *Angew. Chem. Int. Ed.* **2007**, *46*, 72-191; (e) L. S. Kaanumalle, C. L. D. Gibb, B. C. Gibb, V. Ramamurthy, *J. Am. Chem. Soc.* **2004**, *126*, 14366-14367; (f) D. M. Dalton, S. R. Ellis, E. M. Nichols, R. A. Mathies, F. D. Toste, R. G. Bergman, K. N. Raymond, *J. Am. Chem. Soc.* **2015**, *137*, 10128-10131; (g) M. J. Langton, F. Keymeulen, M. Ciaccia, N. H. Williams, C. A. Hunter, *Nat. Chem.* **2017**, *9*, 426-430.

[7] (a) J.-M. Lehn, *Chem. Eur. J.* **1999**, *5*, 2455-2463; (b) P. T. Corbett, J. Leclaire, L. Vial, K. R. West, J.-L. Wietor, J. K. M. Sanders, S. Otto, *Chem. Rev.* **2006**, *106*, 3652-3711.

[8] (a) M. Mastalerz, *Angew. Chem. Int. Ed.* **2010**, *49*, 5042-5053; (b) A. Granzhan, C. Schouwey, T. Riis-Johannessen, R. Scopelliti, K. Severin, *J. Am. Chem. Soc.* **2011**, *133*, 7106-7115; (c) T. K. Ronson, C. Giri, N. Kodiah Beyeh, A. Minkkinen, F. Topić, J. J. Holstein, K. Rissanen, J. R. Nitschke, *Chem. Eur. J.* **2013**, *19*, 3374-3382; (d) J. Mosquera, S. Zarra, J. R. Nitschke, *Angew. Chem. Int. Ed.* **2014**, *53*, 1556-1559; (e) G. Zhang, M. Mastalerz, *Chem. Soc. Rev.* **2014**, *43*, 1934-1947; (f) S. Zarra, D. M. Wood, D. A. Roberts, J. R. Nitschke, *Chem. Soc. Rev.* **2015**, *44*, 419-432; (g) T. Mitra, K. E. Jelfs, M. Schmidtmann, A. Ahmed, S. Y. Chong, D. J. Adams, A. I. Cooper, *Nat. Chem.* **2013**, *5*, 276-281; (h) M. Szymański, M. Wierzbicki, M. Gilski, H. Jędrzejewska, M. Sztylko, P. Cmoch, A. Shkurenko, M. Jaskólski, A. Szumna, *Chem. Eur. J.* **2016**, *22*, 3148-3155.

[9] (a) L. A. Joyce, M. S. Maynor, J. M. Dragna, G. M. da Cruz, V. M. Lynch, J. W. Canary, E. V. Anslyn, *J. Am. Chem. Soc.* **2011**, *133*, 13746-13752; (b) L. A. Joyce, J. W. Canary, E. V. Anslyn, *Chem. Eur. J.* **2012**, *18*, 8064-8069; (c) L. You, G. Pescitelli, E. V. Anslyn, L. Di Bari, *J. Am. Chem. Soc.* **2012**, *134*, 7117-7125; (d) L. You, J. S. Berman, E. V. Anslyn, *Nat. Chem.* **2011**, *3*, 943-948.

[10] (a) F. A. Scaramuzzo, G. Licini, C. Zonta, *Chem. Eur. J.* **2013**, *19*, 16809-16813; (b) E. Badetti, K. Wurst, G. Licini, C. Zonta, *Chem. Eur. J.* **2016**, *22*, 6515-6518; (c) R. Berardozzi, E. Badetti,

N. A. Carmo dos Santos, K. Wurst, G. Licini, G. Pescitelli, C. Zonta, L. Di Bari, *Chem. Comm.* **2016**, *52*, 8428-8431; (d) F. A. Scaramuzzo, E. Badetti, G. Licini, C. Zonta, *Eur. J. Org. Chem.* **2017**, *2017*, 1438-1442.

[11] (a) S. Turega, M. Whitehead, B. R. Hall, A. J. H. M. Meijer, C. A. Hunter, M. D. Ward, *Inorg. Chem.* **2013**, *52*, 1122-1132; (b) C. G. P. Taylor, W. Cullen, O. M. Collier, M. D. Ward, *Chem. Eur. J.* **2017**, *23*, 206-213.

[12] R. Evans, Z. Deng, A. K. Rogerson, A. S. McLachlan, J. J. Richards, M. Nilsson, G. A. Morris, *Angew. Chem. Int. Ed.* **2013**, *52*, 3199-3202.

[13] (a) T. Heinz, D. M. Rudkevich, J. Rebek, *Nature* **1998**, *394*, 764-766; (b) L. Trembleau, J. Rebek, *Science* **2003**, *301*, 1219.

[14] See Supporting Information for the methodology of the conformational search.

[15] (a) C. D. Meyer, C. S. Joiner, J. F. Stoddart, *Chem. Soc. Rev.* **2007**, *36*, 1705-1723; (b) M. E. Belowich, J. F. Stoddart, *Chem. Soc. Rev*. **2012**, *41*, 2003-2024.

[16] S. Mecozzi, J. J. Rebek, *Chem. Eur. J.* **1998**, *4*, 1016-1022.

[17] (a) M. Yamanaka, A. Shivanyuk, J. Rebek, *J. Am. Chem. Soc.* **2004**, *126*, 2939-2943; (b) D. Ajami, J. Rebek, *J. Am. Chem. Soc.* **2006**, *128*, 15038-15039; (c) D. Ajami, J. Rebek, *Nat. Chem*. **2009**, *1*, 87-90.

[18] While the rate of exchange between empty to filled cage is slow in the ^{1}H NMR timescale, a fast exchange is observed in the inclusion of two different carboxylic acids in solution.

Chapter 2

Binding Profiles of Self-Assembled Supramolecular Cages from ESI-MS Based Methodology

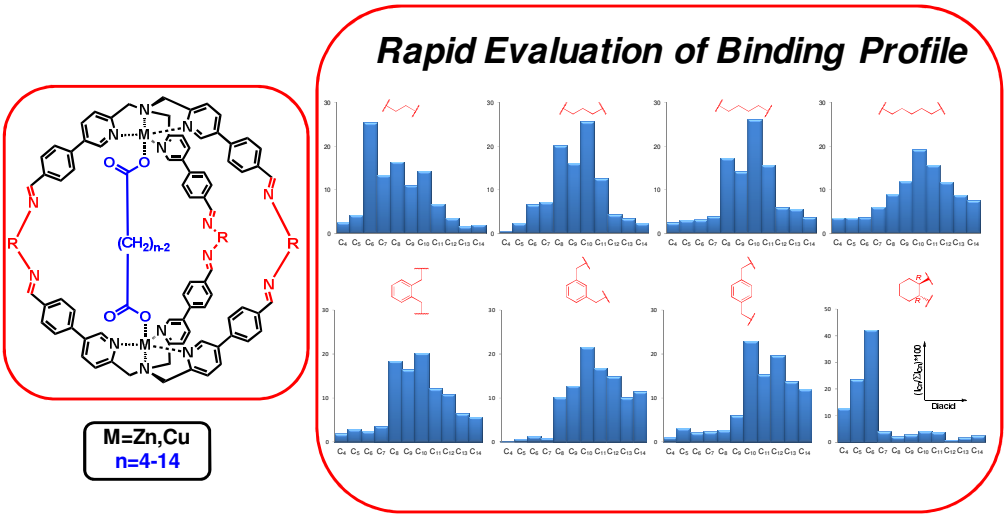

ABSTRACT. A rapid method based on ESI-MS for the determination of binding profiles for linear saturated dicarboxylic acids within a series of different supramolecular cages is reported. These cages have been obtained through the self-assembly of modified tris(pyridylmethyl)amine (**TPMA**) complexes and different diamines have been chosen to vary their size and flexibility. This methodology has allowed to gather how small changes in the structure of the host and guest can contribute to the recognition events. Moreover, it was possible to study molecular systems which contains paramagnetic metals that are not suitable for classical binding constant determination by ^{1}H NMR.

2.1 Introduction

Molecular cages and capsules have been valuable source of knowledge in the understanding of molecular recognition phenomena.[1] The main feature of these structures, is their ability to perform the confinement of guest molecules as molecular host with a well-defined space. Since the early studies by Rebek,[2] it has been accepted that confinement process is ruled by the complementarity and adaptability, in terms of size and shape among host, guest and solvent (Figure 1).[3]

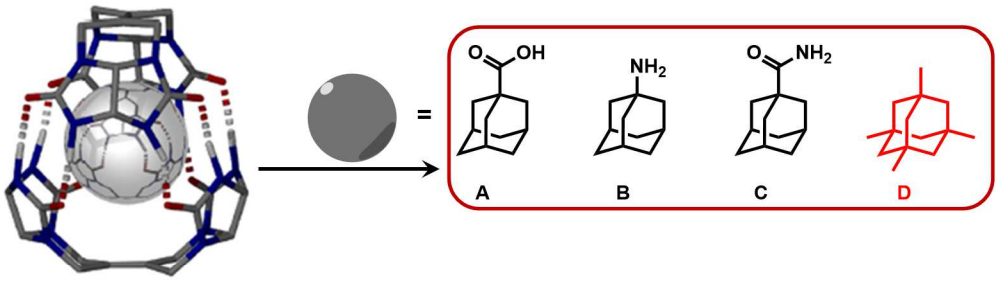

Compound	Binding Constant	Volume [Å]^3	Packing Cofficient
A	780	175	0.56
B	190	157	0.50
C	310	177	0.56
D	6.7	211	0.67

Figure 1. Simplified scheme of the 55% formula of Rebek. With this rule is showed how the binding of guests in self-assembled or covalently linked capsules is related to the occupancy factor or packing coefficient of the guests. Guests **A-C** with packing coefficient about 55% are the most favourable for binding within the capsule, instead **D** (in red) has lower binding constant

Specifically, the interplay of these parameters is determining the thermodynamic and kinetic of the association process. The overall information achieved by these studies has been the foundation for the preparation of supramolecular cages with application in sensing, catalysis, transport and delivery.[4]

More recently, the use of Dynamic Covalent Chemistry (DCC)[5] to obtain confined systems has largely eased the synthesis of supramolecular architectures with an

increasing structural complexity.[6] However, while in principle it is possible to obtain a high number of chemical entities, the fast and reliable determination of the energies involved in binding events still remains a time demanding issue. In other words, most of the time the bottleneck is represented by the binding constant determination using ^{1}H NMR analysis.[7] Beside the large amount of information that can be gathered by this technique,[8] competitive experiments where more than one partner is present in solution are difficult to analyse and, as a consequence, every single guest must be investigated individually. In addition, ^{1}H NMR has several limitations in the presence of paramagnetic metals, therefore related ^{1}H NMR spectra are most of the times difficult to interpret. For these reasons, high throughput screening (HTS) experimental analytical techniques are increasingly used to gather recognition data from DCC experiments.[9]

On this regard, **TPMA** cage system discussed in the previous chapter was extended to other fifteen novel molecular cages which differ for the linker and the metal centres of the two **TPMA** units, together with a study on their recognition properties. However, while taking advantage of DCC chemistry for the extension of the cage series with different linker is straightforward,[10] the determination of the molecular recognition properties of the novel formed systems *via* ^{1}H NMR binding experiments requires a titration for every guest. A fast and reliable method would be preferable for a rapid assessment of the binding capabilities of the newly developed systems.[11]

The latter was gathered with ESI-MS based competition experiments. The methodological approach developed, allowed not only the rapid evaluation of the binding profile of the newly developed Zn(II) cages, but also of other eight corresponding Cu(II) cages, which were completely silent in ^{1}H NMR spectroscopy. Even if the displayed profiles represent relative and not absolute binding energies, deep information on how host and guest small structural variations affect the binding process were retrieved.

2.2 Results ad Discussion

2.2.1 Synthesis of novel supramolecular cages with different linkers

In the initial part of the study, the cages family were extended to diamine linkers different from that used in the previous work, to demonstrate the synthetic versatility of this class of molecular cages and to verify how these linkers were modifying the recognition properties.

Specifically, we envisaged to extend the cages series started with cage **1a•Zn** (*viz.* cage **1** in *Chapter 1*),[12] to four aliphatic diamines differing for length of the spacer (1,3-diaminopropane **3b**; 1,4-diaminobutane **3c**, 1,5-diaminopentane **3d**, (*1R,2R*)-cyclohexyldiamine **3h**) and three xylylenediamines (*ortho*-xylylenediamine **3e,** *meta*-xylylenediamine **3f**, *para*-xylylenediamine **3g**) (Scheme 1). As in our previously reported synthesis, the novel cages were formed by the slow addition of the appropriate diamine linker to a diluted solution of complex **2•Zn** in the presence of a dicarboxylic acid chosen according to the expected length of the cage.[13]

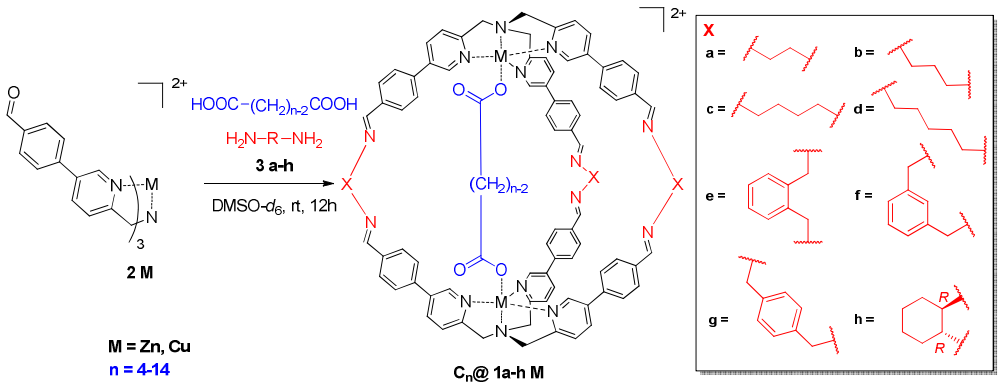

Scheme 1. Synthesis of cages **1a-h•M**. The reaction of **2•M** (1 equiv) with a diamine **3a-h** H_2N-R-NH_2 (2.5 equiv) in the presence of a suitable diacid $\mathbf{C_n}$ in DMSO-d_6 gives the corresponding bimetallic molecular cages $\mathbf{C_n}$**@1a-h•M** in 24 hours. The counteranion is the perchlorate for all the metals.

As example, the addition of **3b** diamine linker (2.5 equiv.) to a solution containing suberic acid **C_8** (0.5 equiv) and complex **2•Zn** (1 equiv) led to the corresponding cage **C_8@1b•Zn** (See Appendix, Fig. A14). Cage formation was confirmed with 2D-NMR (COSY,DOSY) (See Appendix, Fig. A15-16). and MS analysis.

Similarly, the extension of the cages series was undertaken for the other diamine linkers. High yields were obtained for all the different linkers confirming the reliability of the synthetic method. Beside the classic characterisation analysis performed for all the cages(See Appendix, Fig. A10-33). DOSY NMR was also carried out in order to have information on the effect of the diamine linkers length towards the size of the resulting cage. The experimental hydrodynamic radius obtained (See Appendix, Table A1) showed a good correlation with the radius estimated with semiempirical PM6 calculations for each structure (See Appendix, Figure A3). These results confirmed the cage formation in solution and they highlighted the influence of the linker in the modulation of the size of the inner cavity.

2.2.2 ESI-MS Competition Experiment for Cage 1a•Zn

Once the eight molecular cages were synthesised, we started to investigate how the linkers can influence the binding capability of the novel formed systems toward dicarboxylic acids. In this context, classical ^{1}H NMR titrations would result in more than 80 single titration experiments. For this reason, we explored the possibility to use ESI-MS for a qualitative determination of the molecular recognition properties of the new formed systems. ESI-MS represents an ever-growing technique with an increasing capability to interpret molecular recognition events.[14]

At first, we set up a competition experiment where all the eleven dicarboxylic acids, ranging from **C_4** to **C_{14}**, were introduced in a solution containing the components for the formation of cage **1a•Zn** (Scheme 1). In a typical experiment, the dynamic system is allowed to explore all the possible combinations of binding between the cage and the guests, and to equilibrate thermodynamically toward the more stable inclusion cages.

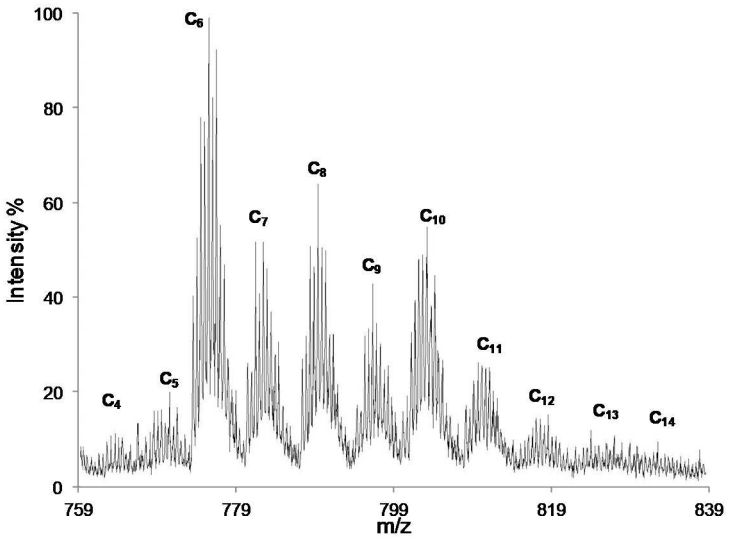

Figure 2.ESI-MS profile for the competition experiment of guests, ranging from C_4 to C_{14} (1 eq. of each guest), in the presence of cage **1a•Zn**. Each isotopic pattern labelled with $\mathbf{C_n}$ represents the inclusion complex $\mathbf{C_n}$**@1a•Zn.**

24 hours after mixing the forming components of cage **1a•Zn** together with the eleven dicarboxylic acids, the reaction mixture, diluted to suitable concentration for MS technique, was injected in the ESI ion source.

The MS spectrometry trace displayed a series of m/z peaks corresponding to the eleven different inclusion cages (Figure 2) $\mathbf{C_n}$**@1a•Zn**. In particular, in the region between 759 to 839 m/z were present the double charged clusters related to the inclusion complexes $\mathbf{C_n}$**@1a•Zn** with their characteristic isotopic pattern.

As it can be seen at first glance, the MS trace of the competition experiment strongly reminds the binding constant profile measured using single ^{1}H NMR experiments. In fact, ^{1}H NMR binding constant experiments revealed a pattern displaying a pseudo-Gaussian profile centred on $\mathbf{C_8}$ (Figure 6, *Chapter 1*). In this case, the highest peak is corresponding to the $\mathbf{C_6}$**@1a•Zn** inclusion complex and it is still possible to observe the characteristic odd-even distribution pattern present also in the ^{1}H NMR titration experiment. This is noteworthy, taking into account that the energetic difference from neighbor guests in the series is small (*e.g.* the energy difference calculates from ^{1}H NMR between $\mathbf{C_9}$**@1a•Zn** and $\mathbf{C_{10}}$**@1a•Zn** is 0.5 kJ/mol).

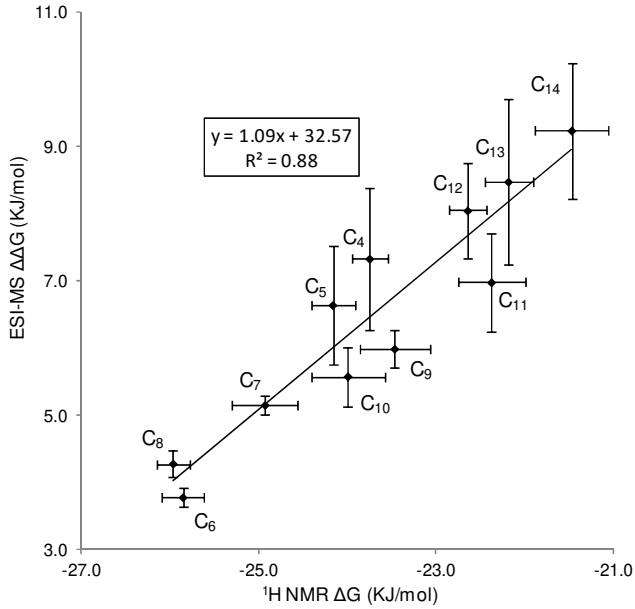

Figure 3 Comparison between the ΔG obtained via 1H-NMR binding constant determination profile (x axis) and the ΔΔG values obtained performing the competition experiment with ESI-MS (y axis).

In order to have a more detailed comparison among the two analyses, the relative intensity of the monoisotopic peaks in the ESI-MS was correlated with the NMR experiments (Figure 3). In particular, the binding constant values obtained *via* ^{1}H NMR and the intensity peaks of ESI-MS were converted into the corresponding ΔG and ΔΔG respectively (See Appendix, Section A 2.3). A good linear correlation confirms the initial visual impression of the ESI-MS trace. The experimental points tend to stay close to the trend line and the slope of the linear correlation is close to unity. As the inclusion complexes **C_n@1a•Zn** are structurally similar, and the correlation expressed between ΔG and ΔΔG obtained respectively from ^{1}H NMR and ESI-MS is linear, we assume that ESI-response factor is similar along the **C_n@1a•Zn** series.[15] However, it is worth of notice that the signals related to inclusion complexes with smaller binding constants (**C_4**, **C_5**, **C_{11}**, **C_{12}**, **C_{14}**) are slightly over estimated and they tend to have high values of standard deviation. This error can arise from a more important contribution of the baseline noise. Nevertheless, the developed methodology can offer in a couple of minutes of acquisition a qualitative

determination of the selected inclusion cage, which open to the possibility to have a good estimation on cage selectivity toward guest of increasing size.

2.2.3 ESI-MS Competition Experiment for Cages 1a-h•Zn

After establishing the reliability of the ESI-MS competition method, we applied this approach to other cages with the same diacids series. The analysis was carried out in a similar fashion to the **1a•Zn** cage. Molecular cages **1b-h•Zn** were prepared in acetonitrile solution performing a competition experiment in which were present all diacids, from succinic $\mathbf{C_4}$ to tetradecandioic $\mathbf{C_{14}}$. The solution was checked after 24 hours by ^{1}H NMR, to evaluate the complete disappearance of the aldehyde signal, and by ESI-MS analysis.

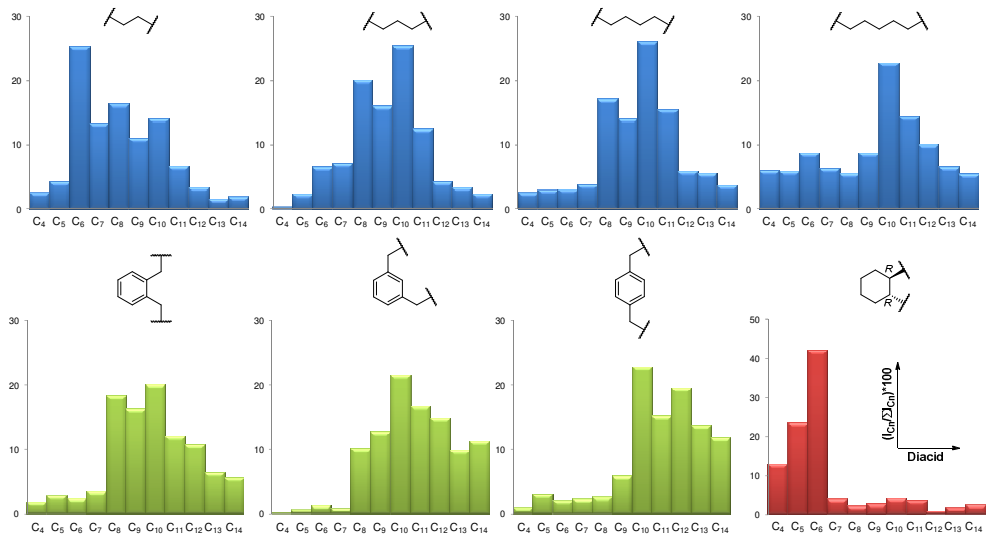

Figure 4. ESI-MS selectivity profiles for $\mathbf{C_n}$**@•1a-h Zn** in the competition experiments. The general observation for all the profile series relies that to an elongation of the diamine linker corresponds a shift to longer diacids as more suitable guests. In the same fashion increasing the flexibility of the linker a wider distribution of the preferential guests is observed. The analysis of the binding profile lead to the following values of weighted arithmetic mean(x_c): **a**=8.05; **b**=9.23; **c**=9.57; **d**=9.67**;** **e**=9.77**;** **f**=10.76; **g**=10.95; **h**=6.39.

The results expressed for each competition experiment as selectivity profiles are reported in Figure 4 (See Appendix, Figure A1).

From the set of experiments, it is possible to notice that the new cages can incorporate all the diacids of the series. Interestingly, there is an evident modulation on the selectivity profile dictated by the characteristics of the diamine linker. As example, in the case of propyl linker **1b** it is possible to observe a widespread pseudo-Gaussian profile centred between suberic acid $\mathbf{C_8}$ and sebacic acid $\mathbf{C_{10}}$. In general, $\mathbf{C_{10}}$ shows the strongest interaction within the cage while shorter diacids $\mathbf{C_{4\text{-}9}}$, as well as longer diacids $\mathbf{C_{11\text{-}14}}$, display a lower intensity. This behaviour is due to the thermodynamic cost for a conformational rearrangement of the host and the guest to perform the recognition process.

In other words, to an elongation of diamine linker, from ethylendiamine **1a** to 1,3-propylendiamine **1b**, the main effect is the shift of the maximum in ESI-MS spectra from $\mathbf{C_6}$ to $\mathbf{C_{10}}$. This observation could be translated in a quantitative data considering the weighted arithmetic mean of each distribution (x_c).

In the case of ethylendiamine **1a** the x_c value is 8.05 and it shifts to 9.23 for the propyl linker **1b**. In the case of longer diamine linkers, namely 1,4-butyldiamine **1c** and 1,5-pentyldiamine **1d**, it is possible to observe a small and continuous shift toward longer dicarboxylic guests. While the preferential guest is still the diacid $\mathbf{C_{10}}$ for both cages formed by the longer linkers (x_c=9.57 for **1c** and 9.67 for **1d**), longer diacids tends to be recognized to a higher extent. Similar considerations explain the ESI-MS traces for the three xylylendiamine linkers (*ortho*-xylylenediamine **1e,** *meta*-xylylenediamine **1f**, *para*-xylylenediamine **1g**). In these systems, to an enlargement of the size cavity due to the presence of xylyl linkers, corresponds a small shift towards longer diacids, though the preferential guest still remains the diacid $\mathbf{C_{10}}$ (x_c=9.77 for **1e**, 10.76 for **1f** and 10.95 for **1g**).

A remarkable change in the shape of the competition curve is observed for the cage formed by *1R,2R*-cyclohexyl linker **1h•Zn**. A narrow selectivity profile centred on adipic acid $\mathbf{C_6}$ (x_c=6.39) is observed for the competition experiment of **1h•Zn** cage. This peculiar selectivity toward shorter diacids with respect to the previous case can be explained by the decreased geometrical distance between the two imine nitrogen

atoms present in the cage. On the other hand, the higher selectivity of **1h•Zn** towards two diacids is a direct consequence of the restriction in the available conformations imposed by the cyclohexyl ring of the **c** linker. While it has been previously observed that tight linkers support cage formation,[16] this is the first example of inclusion complex in which to a tightening of the supramolecular architecture corresponds a higher selectivity.

In summary, **1a-b•Zn** cages are characterized by a recognition profile centred between $\mathbf{C_6}$ and $\mathbf{C_{10}}$. To an increase of the length of the aliphatic diamine linker (from ethyl **1a** to pentyl **1d**), longer diacids get preferentially recognised and the distribution of guests' selectivity becomes slightly wider. In the same fashion, the selectivity of the xylylen series of cages **1e-1f-1g** is modulated by the size of the host and the **1h•Zn** cages selectivity has a profile ruled by the geometry and stiffness of the linker.

2.2.4 Copper cages and X-Ray crystal structure of C_{10}@1b•Cu

A strong limitation of binding constant determination *via* ^{1}H NMR is represented, in the chemistry of self-assembled architectures, by structures containing paramagnetic metals. In fact, paramagnetic metal centres are known to make complicate spectral assignment due to line broadening and large changes in chemical shifts.[17]

In this context, we were interested in the use of a paramagnetic metal, such as Cu(II) coordinated to **TPMA** unit,[18] but these systems are typical examples of structures that are difficult to monitor by ^{1}H NMR. It was also impossible to achieve values of the binding constants by UV titrations because the cage chromophores were only slightly influenced by the binding event and significative variations in the absorption bands, before and after the guest addition, were not detected.

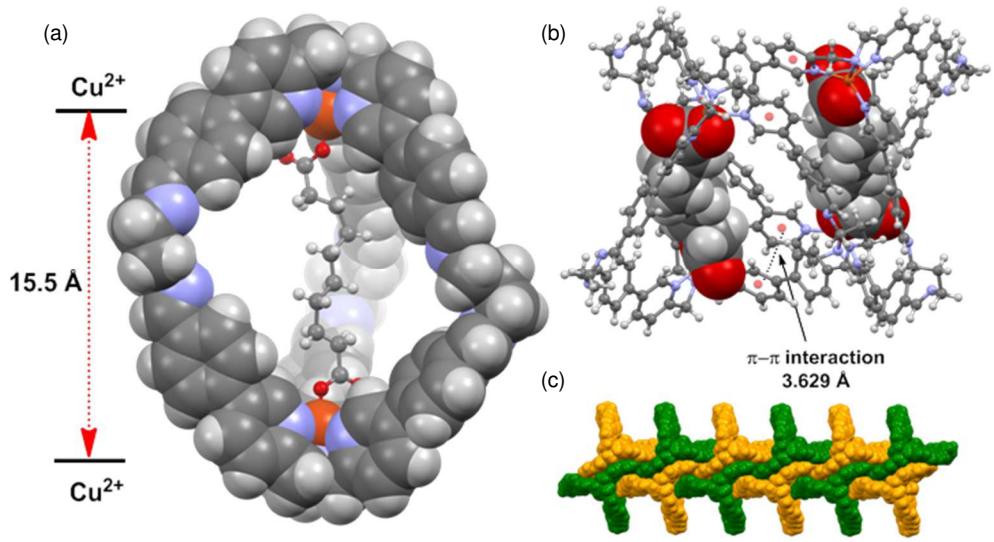

Figure 5. (a) X-ray crystal structure of **C_{10}@2b•Cu** in CPK model displaying the entrapment of sebacic acid **C_{10}** (ball & stick model) inside the cage. (b) Section of 3-D packing to highlight π-π stabilization of **C_{10}@1b•Cu** cage entities. The sebacic acid **C_{10}** is shown in CPK model. (c) 1-D polymer formation.

To evaluate if the ESI-MS methodology was able to support also paramagnetic metals, we synthetised Cu(II) cages starting from the **TPMA** copper complex **2•Cu** (Scheme 2), following the same conditions previously described. As for zinc cages, for each of the eight diamine linkers the corresponding copper cages were obtained, and the recognition properties toward a single dicarboxylic acid were investigated. Among these structures, good quality single crystals suitable for X-ray were obtained for the **C_{10}@1b•Cu** inclusion complex (Figure 4) during a short term mission at Jyväskylä University (FI) in prof. Kari Rissanen group. Cage **C_{10}@1b•Cu** is very compact and has 15.5 Å between the two metal centres (Fig. 4a) to accommodate sebacic acid **C_{10}**.

Because of the flexible cage side arms, and close packing, **C_{10}@1b•Cu** units remarkably displays π-π interactions at centroid-to-centroid distances of 3.629 Å (Figure 5b), subtly responsible for disordered encapsulated **C_{10}**. The π-π interactions are extended one dimensionally (Figure 5c), and the resultant 1-D polymers inter-digitates to promote an efficient and complex 3-D network.

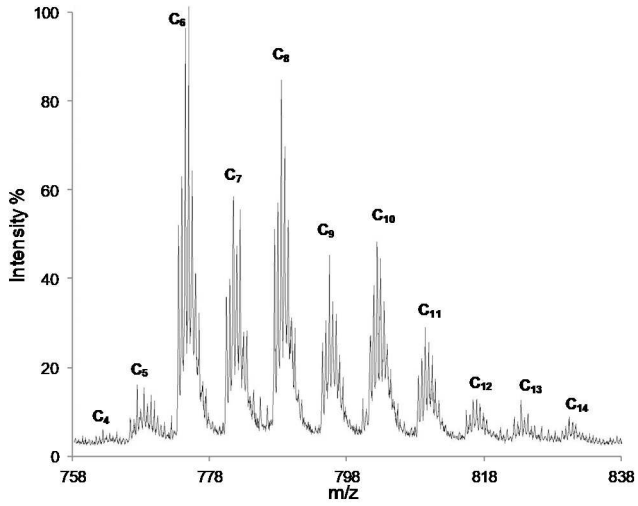

Figure 6. ESI-MS profile for the competition experiment of guests ranging from $\mathbf{C_4}$- to $\mathbf{C_{14}}$ (1 eq. of each guest) in the presence of 1 equivalent of cage **1a•Cu**. Each isotopic pattern labelled with $\mathbf{C_n}$ represents the inclusion complex $\mathbf{C_n}$**@1a•C**

After establishing the recognition properties of copper(II) cages, competition experiments of the diacid $\mathbf{C_4}$-$\mathbf{C_{14}}$ toward the **1a-h•Cu** family were performed as for **1a-h•Zn** cage series. ESI-MS trace (Figure 6) is analogous, beside the difference related to the isotopic pattern of copper, to the profiles reported for the zinc cages (Figure 2). Also in these cases, it is possible to observe selectivity profiles which are similar in shape and intensity to the corresponding **1a-h•Zn** family (Figure 7) and similar considerations on the effect of the linkers can be taken. Interestingly, a closer look to the selectivity profiles reveals a small difference with respect to zinc cages. The selectivity profiles in fact, are always slightly shifted towards longer guests. This variation was expected, and it arises from the shorter distance between the copper and the tertiary amine of the ligand, allowing to accommodate longer guests than the zinc(II) series.[19] The strong correlation between zinc(II) and copper(II) profiles, together with the possibility to accommodate longer diacids for the copper(II) series, corroborate the use of ESI-MS profiles for the analysis of copper(II) cages, which was not possible otherwise.

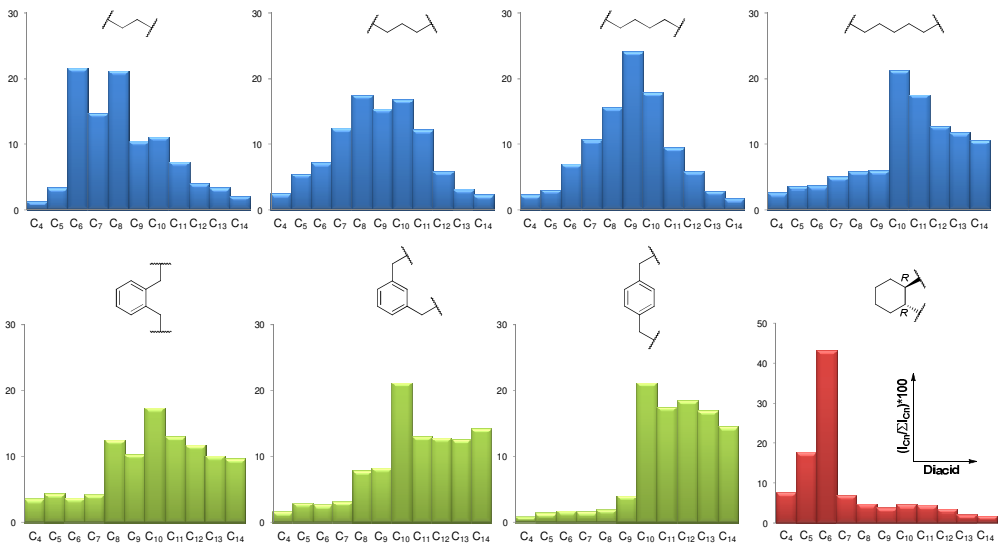

Figure 7. ESI-MS selectivity profiles for **C_n@1a-h•Cu** in the competition experiments. The general observation for all the profile series is similar to that obtained for **2•Zn** complex. A moderate shift of the maximum is observed in the **C_n@1a-h•Cu** cages as expected by the already know shortening of the distance of the metal from the tertiary amine of the ligand. In virtue of this structural variation, longer diacids can accommodate within these cages with respect to the corresponding zinc cages. The analysis of the binding profile lead to the following values of weighted arithmetic mean (x_c) respect to the diacid series: **a**=8.27; **b**=8.85; **c**=8.93; **d**=10.40; **e**=10.00; **f**=10.64; **g**=11.32; **h**=6.84.

2.3 Conclusions

In conclusion, seven zinc(II) and eight copper(II) novel molecular cages differing in size have been synthesized. The selectivity profiles have been investigated using an ESI-MS methodological approach that allows to perform a competition experiment in which all the eleven diacid guests are present in the reaction mixture. This approach has shown to furnish selectivity profiles that are well correlated with NMR titration in the case of **1a•Zn** cage. More importantly, the technique proposed can be used also for copper(II) systems which cannot be investigate either *via* ^{1}H NMR or UV-Vis titrations.

In summary, all molecular cages synthesized in this work are able to bind dicarboxylic acids, and competition experiments have shown trends in molecular recognition properties dictated by the complementarity and adaptability of the

binding partners. These results give interesting knowledge on how different linkers can modulate the flexibility and size of the resulting molecular cages, and their influence in the recognition events. Besides increasing the knowledge on molecular recognition events, the possibility to have high throughput information on the binding capabilities of these systems pave the way for the development of more selective and functional cages.

2.4 Experimental

2.4.1 General procedure for the synthesis of complexes

0.10 mmol of ligand 4,4',4''-(6,6',6''-(nitrilotris(methylene))tris(pyridine6,3-diyl))tribenzaldehyde 1 were dissolved in acetonitrile (15 ml) and 0.10 mmol of the corresponding metal perchlorates hexahydrate were added. The solution was stirred at room temperature for 1 hour and the reaction was followed by ^{1}H NMR and ESI-MS. At the end of the reaction diethyl ether (25 ml) was added obtaining quantitatively a crystalline solid then centrifuged and dried.

2•Zn (pale yellow solid, yield 95%). ^{1}H NMR (300 MHz, CD_3CN) δ (ppm): 10.09 (s, 3H, CHO), 8.82 (d, 3H, J= 2.0 Hz, PyrH), 8.44 (dd, 3H, J=8.0 Hz, J=2.0 Hz PyrH), 8.07 (d, 6H, J=8.0 Hz, ArH), 7.94 (d, 6H, J=8.0 Hz, ArH), 7.75 (d, 3H, J=8.0 Hz, PyrH), 4.40 (s, 6H,CH2). HRMS (ESI-TOF) (m/z): $[M+ClO4]^+$ calcd. for $[C_{39}H_{30}N_4O_3Zn+ClO_4]$+, 765.1094; found 765.1165. Elemental analysis: C. 54.08; H, 4.01; N, 6.85. Required [**2•Zn**]$(ClO_4)_2$. C 54.03; H, 3.49; N, 6.46.
2•Cu (dark green solid, yield 98%).^{1}H NMR (300 MHz, CD_3CN) δ (ppm): 10.11 (s), 8.57 (d), 8.29 (s). HRMS (ESI-TOF) (m/z): $[M+ClO_4]^+$ calcd. for $[C_{39}H_{30}N_4O_3Cu+ClO_4]^+$ 760.1135; found, 760.1202. Elemental analysis: C. 54.23; H, 4.02; N, 5.88. Required: [**2•Cu**]$(ClO_4)_2$ C 54.14; H, 3.50; N, 6.48.

2.4.2 General procedure for the synthesis of molecular cages C_n@1a-h•Zn

To 500 µl (1.0 µmol) of a solution 0.002 M of complex **1** in DMSO-d_6, 50 µl (0.5 µmol) of a solution 0.01 M in DMSO-d_6 of dicarboxylic acid C_n and 125 µl (2.5 µmol) of a solution 0.02 M in DMSO-d_6 of a diamine **4a-h** were added in a NMR tube. The mixture was left for 12 hour at room temperature and checked via ^{1}H NMR and ESI-MS. The yield for all the cages are >90% (Determined via ^{1}H NMR on internal standard *p*-xilene).

C_6@1a•Zn ^{1}H NMR (400 MHz, DMSO-*d_6*) δ (ppm): 9.06 (s, 6H, PyrH), 8.46 (dd, 6H, *J*=8.0 Hz, *J*=2.0 Hz, PyrH), 8.40 (s, 6H, NH_{imm}), 7.93 (d, 12H, *J*=8.0 Hz, ArH), 7.80 (m, 12H+6H, PyrH+ArH), 4.36 (s, 12H, CH_2), 3.94 (m, 12H, $CH_{2\text{-}am}$), 2.55 (m, $CH_{2\text{-}\alpha acid}$), 1.77 (m, 4H, $CH_{2\text{-}\beta acid}$). MS (ESI-MS) *(m/z)*: $[M]^{2+}$ calcd. for $[C_{90}H_{80}N_{14}O_4Zn_2]^{2+}$, 775.3 found; 775.4

C_8@1b•Zn ^{1}H NMR (400 MHz, DMSO-*d_6*) δ (ppm): 9.09 (s, 6H, PyrH), 8.55 (dd, 6H, *J*=8.0 Hz, *J*=2.0 Hz, PyrH), 8.47 (s, 6H, NH_{imm}), 7.98 (d, 12H, *J*=8.0 Hz, ArH), 7.81 (m, 12H+6H, PyrH+ArH), 4.44 (s, 12H, CH_2), 3.69 (m, 12H, $CH_{2\text{-}\alpha am}$), 2.55 (m, 4H, $CH_{2\text{-}\alpha acid}$), 2.04 (m, 6H, $CH_{2\text{-}\beta am}$), 1.88 (m, 4H, $CH_{2\text{-}\beta acid}$), 1.55 (m, 4H, $CH_{2\text{-}\gamma acid}$). MS (ESI-MS) *(m/z)*: $[M]^{2+}$ calcd. for $[C_{95}H_{90}N_{14}O_4Zn_2]^{2+}$, 810.8 found; 810.7

C_{10}@1c•Zn ^{1}H NMR (400 MHz, DMSO-*d_6*) δ (ppm): 9.14 (s, 6H, PyrH), 8.56 (dd, 6H, *J*=8.0 Hz, *J*=2.0 Hz, PyrH), 8.47 (s, 6H, NH_{imm}), 7.90 (d, 12H, *J*=8.0 Hz, ArH), 7.83 (m, 12H+6H, PyrH+ArH), 4.41 (s, 12H, CH_2), 3.67 (m, 12H, $CH_{2\text{-}\alpha am}$), 1.89 (m, 4H, $CH_{2\text{-}\beta acid}$), 1.75 (m, 12H, $CH_{2\text{-}\beta am}$), 1.49 (m, 8H, $CH_{2\text{-}\gamma,\delta acid}$). MS (ESI-MS) *(m/z)*: $[M]^{2+}$ calcd. for $[C_{100}H_{100}N_{14}O_4Zn_2]^{2+}$, 845.9 found; 845.7

C_{10}@1d•Zn ^{1}H NMR (400 MHz, DMSO-*d_6*) δ (ppm): 9.11 (s, 6H, PyrH), 8.52 (dd, 6H, *J*=8.0 Hz, *J*=2.0 Hz, PyrH), 8.45 (s, 6H, NH_{imm}), 7.94 (d, 12H, *J*=8.0 Hz, ArH), 7.80 (m, 12H+6H, PyrH+ArH), 4.43 (s, 12H, CH_2), 3.62 (m, 12H, $CH_{2\text{-}\alpha am}$), 1.85 (m, 4H, $CH_{2\text{-}\beta acid}$), 1.70 (m, 12H, $CH_{2\text{-}\beta am}$), 1.25 (m, 8H, $CH_{2\text{-}\gamma,\delta acid}$). MS (ESI-MS) *(m/z)*: $[M]^{2+}$ calcd. for $[C_{103}H_{106}N_{14}O_4Zn_2]^{2+}$, 866.9 found; 866.9.

C_8@1e•Zn ^{1}H NMR (400 MHz, DMSO-*d_6*) δ (ppm): 9.11 (s, 6H, PyrH), 8.62 (s, 6H, NH_{imm}), 8.54 (dd, 6H, *J*=8.0 Hz, *J*=2.0 Hz, PyrH), 7.99 (d, 12H, *J*=8.0 Hz, ArH), 7.82 (m, 12H+6H, PyrH+ArH), 7.30 (m, 12H, ArH_{am}), 5.01 (s, 12H, $CH_{2\text{-}\alpha am}$), 4.39 (s, 12H, CH_2), 2.58 (m, 4H, $CH_{2\text{-}\alpha acid}$), 1.84 (m, 4H, $CH_{2\text{-}\beta acid}$), 1.51 (m, 4H, $CH_{2\text{-}\gamma acid}$). MS (ESI-MS) *(m/z)*: $[M]^{2+}$ calcd. for $[C_{110}H_{96}N_{14}O_4Zn_2]^{2+}$, 903.8 found; 903.9.

C_{10}@1f•Zn ^{1}H NMR (400 MHz, DMSO-*d_6*) δ (ppm): 9.11 (s, 6H, PyrH), 8.61 (s, 6H, NH_{imm}), 8.53 (dd, 6H, *J*=8.0 Hz, *J*=2.0 Hz, PyrH), 7.96 (d, 12H, *J*=8.0 Hz, ArH), 7.83 (m, 12H+6H, PyrH+ArH), 7.34 (m, 6H, ArH_{am}), 7.23 (m, 6H, ArH_{am}) 4.81 (s, 12H, $CH_{2\text{-}\alpha am}$), 4.41 (s, 12H, CH_2), 1.82 (m, 4H, $CH_{2\text{-}\beta acid}$), 1.42 (m, 4H+4H, $CH_{2\text{-}\gamma,\delta\ acid}$). MS (ESI-MS) *(m/z)*: $[M]^{2+}$ calcd. for $[C_{112}H_{100}N_{14}O_4Zn_2]^{2+}$, 904.4 found; 904.4.

C_{10}@1g•Zn ^{1}H NMR (400 MHz, DMSO-*d_6*) δ (ppm): 9.09 (s, 6H, PyrH), 8.56 (s, 6H, NH_{imm}), 8.51 (dd, 6H, *J*=8.0 Hz, *J*=2.0 Hz, PyrH), 7.95 (d, 12H, *J*=8.0 Hz, ArH), 7.80 (m, 12H+6H, PyrH+ArH), 7.32 (s, 6H, ArH_{am}), 7.32 (s, 12H, ArH_{am}) 4.81 (s, 12H, $CH_{2\text{-}\alpha am}$), 4.38 (s, 12H, CH_2), 1.74 (m, 4H, $CH_{2\text{-}\beta acid}$), 1.34 (m, 4H+4H, $CH_{2\text{-}\gamma,\delta\ acid}$). MS (ESI-MS) *(m/z)*: $[M]^{2+}$ calcd. for $[C_{112}H_{100}N_{14}O_4Zn_2]^{2+}$, 904.4 found; 904.5.
C_6@1h•Zn ^{1}H NMR (400 MHz, DMSO-*d_6*) δ (ppm): 8.88 (s, 6H, PyrH), 8.41 (s, 6H, NH_{imm}), 8.35 (dd, 6H, *J*=8.0 Hz, *J*=2.0 Hz, PyrH), 7.82 (m, 12H+6H, PyrH+ArH), 7.98 (d, 12H, *J*=8.0 Hz, ArH), 4.37 (m, 12H, CH_2), 3.45 (m, 6H, $CH_{\text{-}\alpha am}$), 2.19 (m, 4H, $CH_{2\text{-}\alpha acid}$), 1.67 (m, $CH_{2\text{-}\beta am}$), 1.51 (m, 4H, $CH_{2\text{-}\beta acid}$), 1.18 (m, $CH_{2\text{-}\gamma am}$). MS (ESI-MS) *(m/z)*: $[M]^{2+}$ calcd. for $[C_{102}H_{98}N_{14}O_4Zn_2]^{2+}$, 856.9 found 857.0.

2.4.3 General procedure for the competition experiments

200 µl (1.0 µmol, 1 equiv) of a solution 0.005 M of complex **2•M** in DMSO-d_6, 50 µl (0.5 µmol, 0.5 equiv) of a solution 0.01 M in DMSO-d_6 of dicarboxylic acids **C_4-C_{14}** and 125 µl (2.5 µmol, 2.5 equiv) of a solution 0.02 M in DMSO-d_6 of the desired diamine **3a-h** were added in a NMR tube. The mixture was left for 24 hours at room temperature and checked via ^{1}H NMR and ESI-MS.
In order to override artifacts coming from the ionization method or the MS analysis, the experiments have been carried out using two different instruments (Applied Biosystems ESI-TOF Mariner Biospectrometry Workstation and Agilent Technologies LC/MSD Trap SL AGILENT) which gave comparable results.

References

[1] (a) J. T. A. Jones, T. Hasell, X. Wu, J. Bacsa, K. E. Jelfs, M. Schmidtmann, S. Y. Chong, D. J. Adams, A. Trewin, F. Schiffman, F. Cora, B. Slater, A. Steiner, G. M. Day, A. I. Cooper, *Nature* **2011**, *474*, 367-371; (b) K. Harris, D. Fujita, M. Fujita, *Chem. Comm.* **2013**, *49*, 6703-6712; (c) T. Kusukawa, M. Fujita, *Angew. Chem. Int. Ed.* **1998**, *37*, 3142-3144; (d) J.-N. Rebilly, B. Colasson, O. Bistri, D. Over, O. Reinaud, *Chem. Soc. Rev.* **2015**, *44*, 467-489; (e) S. H. A. M. Leenders, R. Gramage-Doria, B. de Bruin, J. N. H. Reek, *Chem. Soc. Rev.* **2015**, *44*, 433-448; (f) S. Fujii, T. Tada, Y. Komoto, T. Osuga, T. Murase, M. Fujita, M. Kiguchi, *J. Am. Chem. Soc.* **2015**, *137*, 5939-5947; (g) J. R. Romero, G. Aragay, P. Ballester, *Chem. Sci.* **2017**, *8*, 491-498; (h) D. Zhang, J. R. Cochrane, S. Di Pietro, L. Guy, H. Gornitzka, J.-P. Dutasta, A. Martinez, *Chem. Eur. J.* **2017**, *23*, 6495-6498; (i) D. Zhang, B. Bousquet, J.-C. Mulatier, D. Pitrat, M. Jean, N. Vanthuyne, L. Guy, J.-P. Dutasta, A. Martinez, *The J. Org. Chem.* **2017**, *82*, 6082-6088.

[2] (a) T. Heinz, D. M. Rudkevich, J. Rebek, *Nat.ure* **1998**, *394*, 764-766; (b) L. Trembleau, J. Rebek, *Science* **2003**, *301*, 1219; (c) D. Ajami, J. Rebek, *Nat. Chem.* **2009**, *1*, 87-90.

[3] (a) S. Mecozzi, J. J. Rebek, *Chem. Eur. J.* **1998**, *4*, 1016-1022; (b) L. Baldini, P. Ballester, A. Casnati, R. M. Gomila, C. A. Hunter, F. Sansone, R. Ungaro, *J. Am. Chem. Soc.* **2003**, *125*, 14181-14189; (c) W. M. Bloch, Y. Abe, J. J. Holstein, C. M. Wandtke, B. Dittrich, G. H. Clever, *J. Am. Chem. Soc.* **2016**, *138*, 13750-13755.

[4] (a) A. M. Castilla, T. K. Ronson, J. R. Nitschke, *J. Am. Chem. Soc.* **2016**, *138*, 2342-2351; (b) A. B. Grommet, J. L. Bolliger, C. Browne, J. R. Nitschke, *Angew. Chem. Int. Ed.* **2015**, *54*, 15100-15104; (c) A. B. Grommet, J. R. Nitschke, *J. Am. Chem. Soc.* **2017**, *139*, 2176-2179; (d) R. Haag, *Angew. Chem. Int. Ed.* **2004**, *43*, 278-282; (e) T. Sawada, M. Yoshizawa, S. Sato, M. Fujita, *Nat. Chem.* **2009**, *1*, 53-56; (f) V. M. Dong, D. Fiedler, B. Carl, R. G. Bergman, K. N. Raymond, *J. of the Am. Chem. Soc.* **2006**, *128*, 14464-14465; (g) W. Cullen, M. C. Misuraca, C. A. Hunter, N. H. Williams, M. D. Ward, *Nat. Chem.* **2016**, *8*, 231-236; (h) Z. Laughrey, B. C. Gibb, *Chem. Soc. Rev.* **2011**, *40*, 363-386.

[5] (a) J.-M. Lehn, *Chem. Eur. J.* **1999**, *5*, 2455-2463; (b) P. T. Corbett, J. Leclaire, L. Vial, K. R. West, J.-L. Wietor, J. K. M. Sanders, S. Otto, *Chem. Rev.* **2006**, *106*, 3652-3711; (c) S. J. Rowan, S. J. Cantrill, G. R. L. Cousins, J. K. M. Sanders, J. F. Stoddart, *Angew. Chem. Int. Ed.* **2002**, *41*, 898-952.

[6] (a) M. Mastalerz, *Angew. Chem. Int. Ed.* **2010**, *49*, 5042-5053; (b) A. Granzhan, C. Schouwey, T. Riis-Johannessen, R. Scopelliti, K. Severin, *J. Am. Chem. Soc.* **2011**, *133*, 7106-7115; (c) T. Mitra, K. E. Jelfs, M. Schmidtmann, A. Ahmed, S. Y. Chong, D. J. Adams, A. I. Cooper, *Nat. Chem.* **2013**, *5*, 276-281; (d) T. K. Ronson, C. Giri, N. Kodiah Beyeh, A. Minkkinen, F. Topić, J. J. Holstein, K. Rissanen, J. R. Nitschke, *Chem. Eur. J.* **2013**, *19*, 3374-3382; (e) S. Zarra, D. M. Wood, D. A. Roberts, J. R. Nitschke, *Chem. Soc. Rev.* **2015**, *44*, 419-432; (f) M. J. Barrell, A. G. Campaña, M. von Delius, E. M. Geertsema, D. A. Leigh, *Angew. Chem. Int. Ed.* **2011**, *50*, 285-290.

[7] (a) J. Mosquera, S. Zarra, J. R. Nitschke, *Angew. Chem. Int. Ed.* **2014**, *53*, 1556-1559; (b) S. Löffler, J. Lübben, L. Krause, D. Stalke, B. Dittrich, G. H. Clever, *J. Am. Chem. Soc.* **2015**, *137*, 1060-1063; (c) W. Cullen, S. Turega, C. A. Hunter, M. D. Ward, *Chem. Sci.* **2015**, *6*, 625-631; (d) G. Iadevaia, A. E. Stross, A. Neumann, C. A. Hunter, *Chem. Sci.* **2016**, *7*, 1760-1767; (e) D. Nunez-Villanueva, C. A. Hunter, *Chem. Sci.* **2017**, *8*, 206-213.

[8] (a) M. J. Packer, C. Zonta, C. A. Hunter, *J. of Magn.Res.* **2003**, *162*, 102-112; (b) C. A. Hunter, M. C. Misuraca, S. M. Turega, *Chem. Sci.* **2012**, *3*, 2462-2469.

[9] (a) J. Atcher, J. Bujons, I. Alfonso, *Chem. Comm.* **2017**, *53*, 4274-4277; (b) J. Atcher, A. Moure, J. Bujons, I. Alfonso, *Chem. Eur. J.* **2015**, *21*, 6869-6878; (c) A. M. Valdivielso, F. Puig-Castellví, J. Atcher, J. Solà, R. Tauler, I. Alfonso, *Chem. Eur. J.* **2017**, *23*, 10702-10702; (d) M. Ciaccia, I. Tosi, L. Baldini, R. Cacciapaglia, L. Mandolini, S. Di Stefano, C. A. Hunter, *Chem. Sci.* **2015**, *6*, 144-151; (e) L. You, D. Zha, E. V. Anslyn, *Chem. Rev.* **2015**, *115*, 7840-7892; (f) D. Zamora-Olivares, T. S. Kaoud, K. N. Dalby, E. V. Anslyn, *J. Am. Chem. Soc.* **2013**, *135*, 14814-14820; (g) Z. Kostereli, R. Scopelliti, K. Severin, *Chem. Sci.* **2014**, *5*, 2456-2460; (h) T. Takeuchi, S. Matile, *Chem. Comm.* **2013**, *49*, 19-29.

[10] (a) F. A. Scaramuzzo, G. Licini, C. Zonta, *Chem. Eur. J.* **2013**, *19*, 16809-16813; (b) F. A. Scaramuzzo, E. Badetti, G. Licini, C. Zonta, *Eur. J. Org. Chem.* **2017**, *2017*, 1438-1442; (c) R. Berardozzi, E. Badetti, N. A. Carmo dos Santos, K. Wurst, G. Licini, G. Pescitelli, C. Zonta, L. Di Bari, *Chem. Comm.* **2016**, *52*, 8428-8431.
[11] C. Bravin, E. Badetti, F. A. Scaramuzzo, G. Licini, C. Zonta, *J. Am. Chem. Soc.* **2017**, *139*, 6456-6460.
[12] G. Zhang, M. Mastalerz, *Chem. Soc. Rev.* **2014**, *43*, 1934-1947.
[13] (a) S. Turega, W. Cullen, M. Whitehead, C. A. Hunter, M. D. Ward, *J. Am. Chem. Soc.* **2014**, *136*, 8475-8483; (b) C. G. P. Taylor, W. Cullen, O. M. Collier, M. D. Ward, *Chem. Eur. J.* **2017**, *23*, 206-213.
[14] One extra equivalent of diamine has shown to be necessary for cage formation and dicarboxylic acid deprotonation.(See ref. 11)
[15] (a) X. Cheng, R. Chen, J. E. Bruce, B. L. Schwartz, G. A. Anderson, S. A. Hofstadler, D. C. Gale, R. D. Smith, J. Gao, G. B. Sigal, M. Mammen, G. M. Whitesides, *J. Am. Chem. Soc.* **1995**, *117*, 8859-8860; (b) S. R. Wilson, J. Perez, A. Pasternak, *J. Am. Chem. Soc.* **1993**, *115*, 1994-1997; (c) L. Cera, C. A. Schalley, *Chem. Soc. Rev.* **2014**, *43*, 1800-1812; (d) Z. Qi, T. Heinrich, S. Moorthy, C. A. Schalley, *Chem. Soc. Rev.* **2015**, *44*, 515-531; (e) M. Kieffer, B. S. Pilgrim, T. K. Ronson, D. A. Roberts, M. Aleksanyan, J. R. Nitschke, *J. Am. Chem. Soc.* **2016**, *138*, 6813-6821.
[16] (a) S. P. Black, D. M. Wood, F. B. Schwarz, T. K. Ronson, J. J. Holstein, A. R. Stefankiewicz, C. A. Schalley, J. K. M. Sanders, J. R. Nitschke, *Chem. Sci.* **2016**, *7*, 2614-2620; (b) E. Leize, A. Jaffrezic, A. Van Dorsselaer, *J. Mass Spectrometry* **1996**, *31*, 537-544; (c) P. N. W. Baxter, R. G. Khoury, J.-M. Lehn, G. Baum, D. Fenske, *Chem. Eur. J.* **2000**, *6*, 4140-4148.
[17] M. W. Schneider, I. M. Oppel, M. Mastalerz, *Chem. Eur. J.* **2012**, *18*, 4156-4160.
[18] (a) W. C. Isley Iii, S. Zarra, R. K. Carlson, R. A. Bilbeisi, T. K. Ronson, J. R. Nitschke, L. Gagliardi, C. J. Cramer, *Phys. Chem. Chem. Phys.* **2014**, *16*, 10620-10628; (b) S. Turega, M. Whitehead, B. R. Hall, A. J. H. M. Meijer, C. A. Hunter, M. D. Ward, *Inorg. Chem.* **2013**, *52*, 1122-1132.
[19] (a) T. Pintauer, K. Matyjaszewski, *Coord. Chem. Rev.* **2005**, *249*, 1155-1184; (b) N. A. Carmo dos Santos, F. Lorandi, E. Badetti, K. Wurst, A. A. Isse, A. Gennaro, G. Licini, C. Zonta, *Polymer* **2017**, *128*, 169-176.
[20] M. V. Veidis, G. H. Schreiber, T. E. Gough, G. J. Palenik, *J. Am. Chem. Soc.* **1969**, *91*, 1859-1860.

Chapter 3

Helicity Control of a Perfluorinated Carbon Chain within a Supramolecular Cage

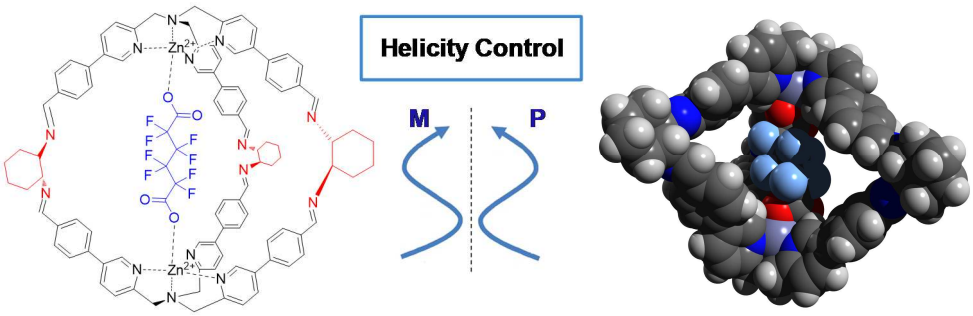

ABSTRACT A novel chiral supramolecular cage and the capability of this structure to control the helicity of a perfluorinated carbon chain are reported. The helix configuration of the perfluoroalkyl chain was evaluated with a combination of theoretical calculations of the host-guest complex and the support of Vibrational Circular Dichroism (VCD) experiments.

3.1 Introduction

Helicity represents a major chiral motif found in nature.[1] It is manifested at the macro- and supramolecular level in a large number of structures, as example α-helix in the secondary structure of proteins, and the double helix formed by two strands of DNA are the most prominent examples. Also perfluorinated-*n*-alkanes with more than four carbon atoms adopt an helical conformations in contrast to the zigzag (all-*anti*) of corresponding perhydroalkanes (Figure 1a-b). [2] [3]

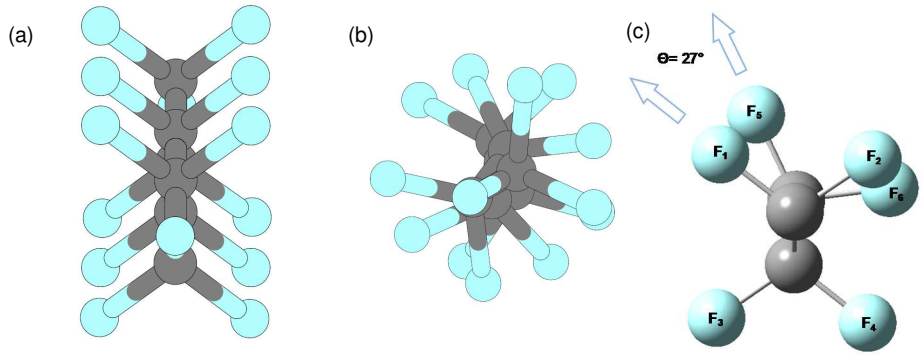

Figure 1. Optimized structure for (a) *n*-hexane and (b) perfluoro-*n*-hexane. (a) The most stable conformation is all-*anti*, (b) the global minima is for the helical structure. (c) . Schematic representation of the projected 1-5 F•••F angle in a perfluorinated carbon chain (θ =27°).

The twisted nature of perfluorinated carbon chain is due to electrosteric repulsions of fluorine atoms in the relative carbon chain 1,3-positions. This particular feature have been observed in solid state [4] and also in solution.[5] In particular, from the solid state analysis, a full 360° twist occurs in 33.6 Å (13 zigzags or 26 chain atoms) and the angle between F_1 and F_5 respectively bound to C_1 and C_3 (projected 1-5 F···F angle) is 27° (Figure 1c). This helical conformation allows to form in principle two enantiomeric helixes which are not superimposable mirror images one of the other (Figure 2).[6]

In recent years, due to the interest in the development of functional materials with defined helicity in the structure, stereo-induction phenomena were investigated.[7] In

particular, it was expoited the covalent attachment of functionality owning a stereogenic centre in order to bias the helicity of a perfluoro-chain.[8]

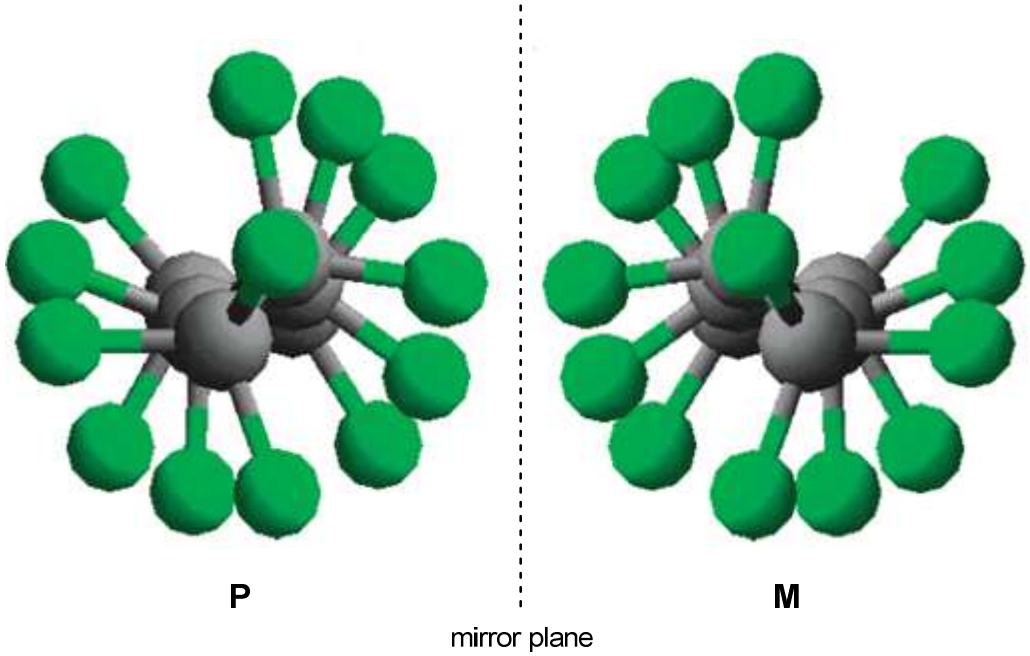

Figure 2. The helical structure of perfluorinated carbon chain compounds. In the case of helix-shaped molecules the P/M or Δ/Λ nomenclatures are used. A right-handed helix is described as P (or plus) and a left-handed as M (or minus).

A relevant example, in which the presence of a stereogenic center induces preferential helical chirality in a perfluorinated chain, was reported by Monde.[9] In particular, the covalent linkage of a chiral benzyl alcohol to a perfluorinated chain resulted in a preferential induction of the handedness of the helical chain. In order to confirm this phenomena, Vibrational Circular Dichroism (VCD) technique was successfully applied to reveal the absolute configuration (AC) of the biased helix of perfluoroalkyl chains in solution. The study was supported with the aid of theoretical calculations and by X-ray crystallography. As expected, inversion of configuration of the benzyl carbon results in an inversion of the helicity of the chain (Figure 3).

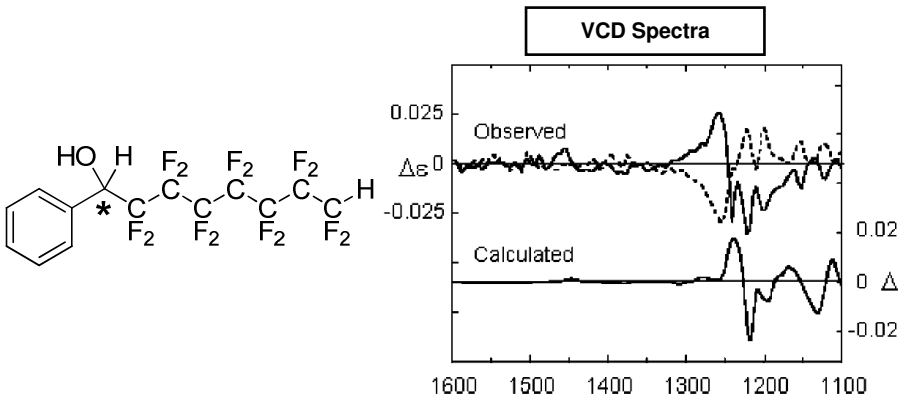

Figure 3. Comparison of experimental VCD spectrum of perfluorinated Monde compound (solid line, upper frame) with the calculated (solid line, lower frame) in the C-F stretching region. The inversion of configuration of the stereoegenic center leads to the mirror image spectrum (dotted line, upper frame).

Inspired by this study, we were wondering if it was possible to induced biased chirality by encapsulation in a chiral confined space. Many supramolecular systems have shown interesting properties in the chirality control,[10] and within this context, supramolecular cages and capsules are of great interest because they help to define the confinement phenomena. In particular, along the recognition process the properties of guest molecule bound within the cavity of these systems are influenced by the structural features of the host.[11] A remarkable example was described by Rebek in the incorporation of an alkyl chain within a supramolecular capsule which led the alkyl chain from the fully extended conformation as its lowest-energy shape to assume a coiled, compressed conformation.[12] While this capsule exerts the ability to "coil" the guest present in the interior cavity, the possibility to control the direction of the twist of the guest chain still represents a challenge for a confined system.

In this chapter is reported initial attempts to induce chirality on a perfluorinated dicarboxylic acid by inclusion on a chiral cage. This has been achieved by the synthesis of two molecular cages similar to those described in the previous chapters.[13] . The helix configuration of the perfluoroalkyl chain was evaluated with a combination of Vibrational Circular Dichroism (VCD) experiments combined with theoretical calculations of the host-guest complex.

3.2 Results ad Discussion

3.2.1 Synthesis of Molecular Cage (*R,R*)-C_{6F}@2

The initial part of the study deals with the synthesis of chiral supramolecular cage **(*R,R*)-C_{6F}@2** based on **TPMA** ligand. The novel structure was formed by slow addition of the chiral diamine linker (1*R*,2*R*)-cyclohexanediamine **(*R,R*)-dach** (2.5 equiv.) to a diluted solution of initial complex **1** (1.0 equiv.) in the presence of a octafluoroadipic acid **C_{6F}** (1.0 equiv.), a perfluorinated dicarboxylic acid chosen according to the expected length of the cage (Scheme 1).

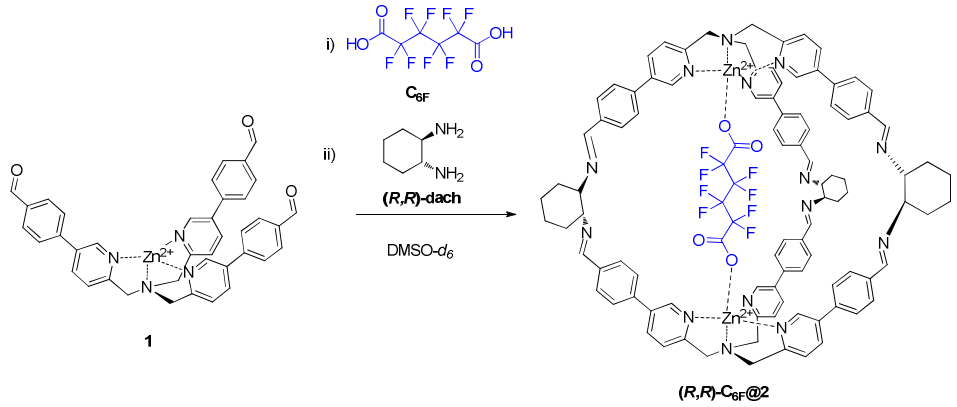

Scheme 1. Imine condensation reaction between metal-complex **1**, **(*R,R*)-dach** and **C_{6F}** acid as templating agent.

Formation of cage **2** was followed by ^{1}H NMR, while the aldehyde proton signal at 10.03 ppm disappears the formation of the imine signal at 8.49 ppm is observed (Figure 4). In addition in the ^{1}H NMR spectra is possible to assign four signals to the aliphatic region belonging to **(*R,R*)-dach** protons and methylene of **TPMA**, and the six signals in the aromatic region to the aromatic systems (See Appendix Fig A1). The presence of the cage in solution was confirmed also by 2D NMR experiments COSY and DOSY (See Appendix Fig A2-4).

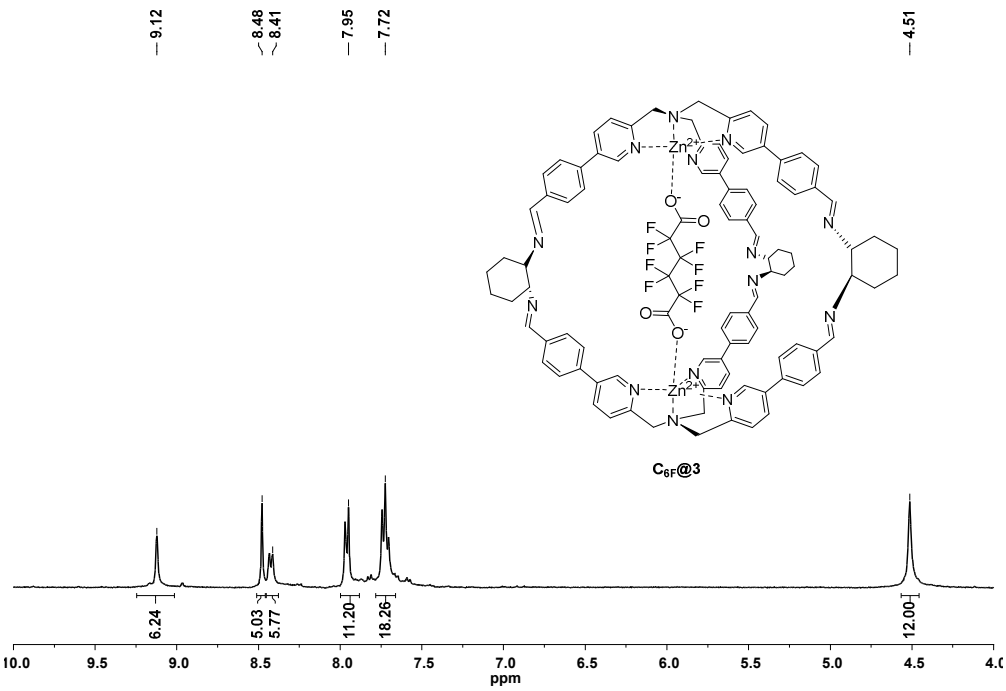

Figure 4. ^{1}H-NMR (400 MHz, 301 K, DMSO-d_6) of cage **C_{6F}@1.**

ESI-MS analysis confirmed the formation of inclusion complex **(*R,R*)-C_{6F}@2** displaying a signal at 929.2 m/z relative to the molecular ion $[C_{102}H_{90}F_8N_{14}O_4Zn_2]^{2+}$ with a perfect agreement between the experimental and calculated isotopic pattern (See Appendix Fig A5).

3.2.2 IR analysis

While the first part of the study was dedicated to the synthesis and characterization of the desired **(*R,R*)-C_{6F}@2** cage**,** in the second part, to get information for the VCD analysis, IR of the host-guest system was performed. It should be noted that VCD approximately 4 to 6 orders of magnitude less sensitive than IR and for this reason the synthesis has to be optimized to have the inclusion cage compound at suitable concentrations.[14]

In the initial attempt, **(*R,R*)-C_{6F}@2** was present at 1 mM concentration revealing the diagnostic signals related to the perfluorinated guest, in particular the C=O stretching (1690 cm^{-1}), C-O stretching (1360 cm^{-1}) and the C-F stretching 1170 cm^{-1}. While these signals were in agreement with the calculated IR spectrum for this cage (See Appendix Fig A6), the intensity were low (~0.2-0.1) to record a VCD spectrum. For this reason, different samples of **(*R,R*)-C_{6F}@2** at increasing cage concentration were prepared only modifying the concentration of all components. The cage samples were synthetized at 5, 10 and 15 mM final concentration and they were monitored *via* ^{1}H NMR (See Appendix Fig A10). Suitable absorbance for the VCD analysis, values between 0.2-0.9 A, were obtained for the sample containing the cage at 10 mM (Figure 5).

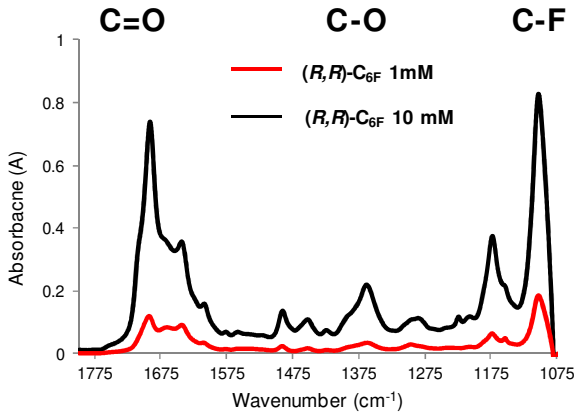

Figure 5. IR spectrum of **(*R,R*)-C_{6F}@2** (red line 1 mM concentration, black line 10 mM concentration, *l*=0.1 mm. DMSO-d_6)

Vibrational Circular Dichroism Experiments for the Determination of Diacid Helicity

Vibrational Circular Dichroism (VCD) is currently a reliable method to assign the absolute configuration (AC) of organic molecules.[15] VCD is generally applicable, because all molecules display a vibrational spectrum, in contrast to Electronic CD

(ECD), which depends on the existence of chromophores and their coupling.[16] Although VCD technique has several limitations, in particular the disadvantage regarding the sensitivity, the main reason that allowed this technique to develop as an essential method for the identification of AC of chiral molecules is to calculate the VCD for each stereoisomer and compare the computed and experimental spectra.[17] In order to calculate the spectra of **(*R,R*)-C_{6F}@2** a conformational analysis, which take of all possible diastereoisomer, was carried out considering the stereochemical elements present in the system. As a consequence of the propeller-like arrangement of the ligand around the metal[17] the cage can be present in three main different diastereoisomers. Two cages with D_3 symmetry in which the two helical arrangements of **TPMA** are the same (*RR*-MM, *RR*-PP) and one in which the two helical arrangements are opposite (*RR*-MP). Within this three cages the perfluorinated carbon chain can adopt two helical forms forming a total of six diasteroisomers (*RR*-MM-M, *RR*-MM-P, *RR*-MP-M, *RR*-MP-P, *RR*-PP-M, *RR*-PP-P Figure 6).

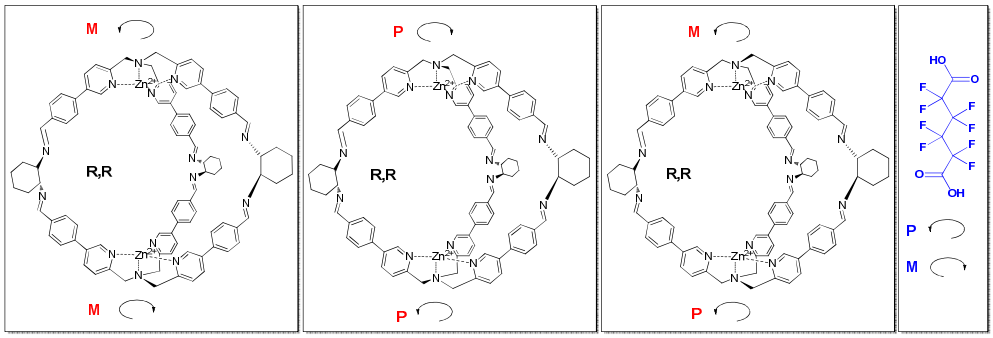

Figure 6. Cage **C_{6F}@2** possible conformational diastereoisomer and the two helix conformation of the perfluorinated dicarboxylic acid. The combination of this elements gives six possible diastereoisomer

Energy and VCD spectra of each diastereoisomer were calculated using Guassian-09 ((See Appendix Table A1).The energy data obtained shows that the most stable diastereoisomer is *RR*-PP-P (Figure 7). According to theoretical calculations the other diasteroisiomers should be present in small concentration in solution, thus we expect to have a VCD spectra which is only coming from the contribution of *RR*-PP-P.

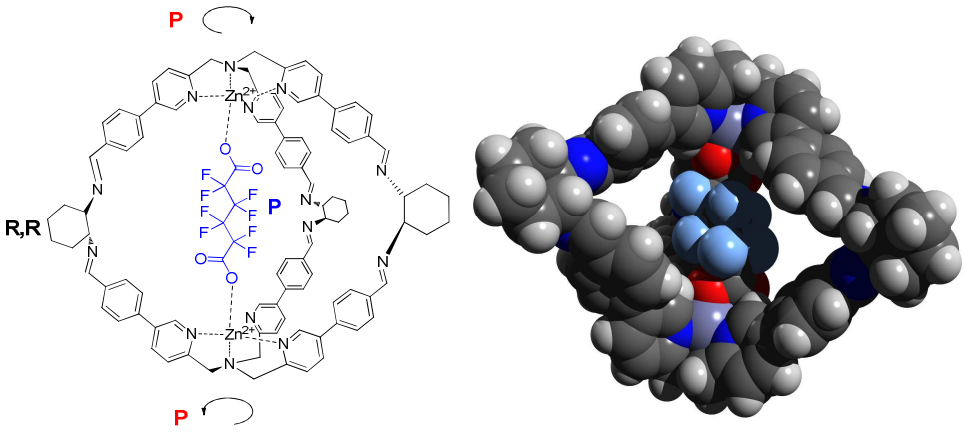

Figure 7. The lower energy diastereoisomer *RR*-PP-P of $\mathbf{C_{6F}@3}$.

VCD spectrum, carried in collaboration with Prof. Abbate (University of Brescia), of (***R,R***)-$\mathbf{C_{6F}@2}$ was recorded at room temperature in DMSO. As reported in Figure 8 a partial overlap between the experimental (red line) and calculated (black line) spectra is present. As example, in the region of C-O an C-F stretching (1370 cm^{-1}, 1150 cm^{-1}) the vibronic absorptions are well reproduced by the computed spectrum. While these results are still preliminary, initial experimental observation are in line with the calculated data on the capability of the cage to induce a preferential helicity of the perfluorinated guest.

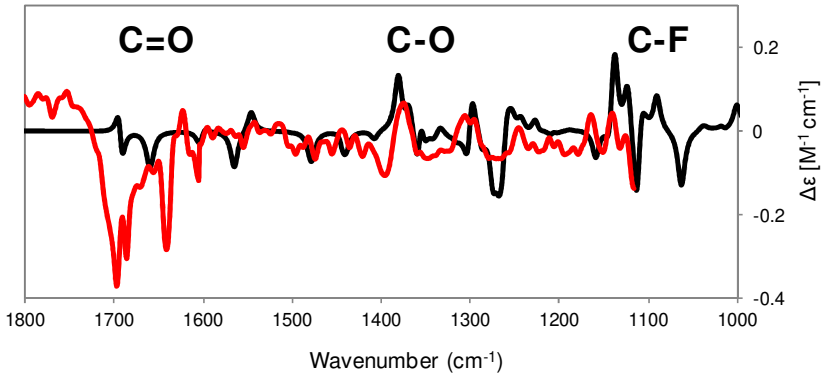

Figure 8. Experimental (red line) and calculated (black line) VCD spectrum of cage **C_{6F}@2-c** (c=10 mM, *l*=50 µm. DMSO-d_6).

Moreover, to have a confirmation of the vibronic feature, the enantiomeric cage **(*S,S*)-C_{6F}@2** was synthesized introducing the opposite chiral moieties (1*S*,2*S*)-cyclohexanediamine **(*S,S*)-dach** (Scheme 1). The characterization of **(*S,S*)-C_{6F}@2** confirmed the presence of the enantiomeric cage respect to **(*R,R*)-C_{6F}@2** (See Appendix Fig A6-9). As expected, VCD spectrum of **(*S,S*)-C_{6F}@2** reports mirror absorptions respect to **(*R,R*)-C_{6F}@2**. In particular, characteristics C-O signal are opposite respect to the previous measure. This experimental data, coupled with the calculated spectra, indicates an inversion of the helix configuration of the guest within the cage (Figure 9).

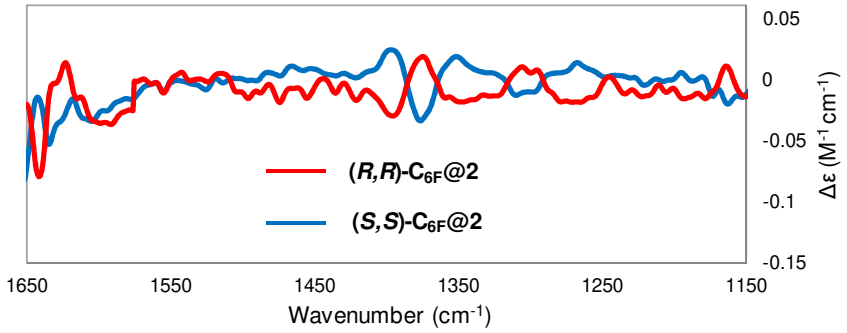

Figure 9. Experimental VCD spectrum for **(*R,R*)-C_{6F}@2** (red line) and **(*S,S*)-C_{6F}@2** (blue line). (c=10 mM, *l*=50 µm. DMSO-d_6).

1.3 Conclusions

In this chapter is reported the synthesis of a chiral molecular cage able to control the helicity of a octafluoroadipic dicarboxylic acid embedded within its cavity. The reaction conditions were optimized to obtain a suitable instrumental response of the VCD analysis, and computational studies were carried to identify the most stable diastereoisomer cage in solution. Initial VCD experiments indicate that the cage is able to induce a preferential helix configuration of the embedded perfluoroalkyl chain.

3.4 Experimental

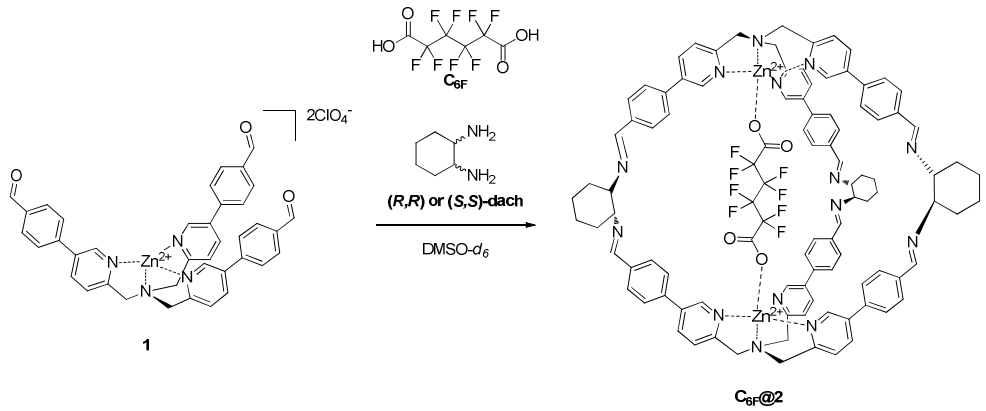

To 500 µl (1.0 µmol) of a solution 0.002 M of complex **1** in DMSO-d_6, 100 µl (1.0 µmol) of a solution 0.01 M in DMSO-d_6 of octafluoroadipic acid **C_{6F}** and 75 µl (1.5 µmol) of a solution 0.02 M in DMSO-d_6 of (1*R*,2*R*)-cyclohexanediamine **(*R,R*)-dach** or (1*S*,2*S*)-cyclohexanediamine **(*S,S*)-dach** were added in a NMR tube. The mixture was left for 12 hour at room temperature and then other 50 µl (1.0 µmol) of chiral diamine solution 0.02 M in DMSO-d_6 of checked *via* ^{1}H NMR (NMR yield>90% determined with internal standard *p*-xylene).

The procedure is the same adopted for the preparation of higher concentration samples. The concentration of complex **1** solution are 0.01, 0.02 and 0.03 mM respectively for cage 5 mM, 10 mM and 15 mM, and the stock solution for the chiral diamine and **C_{6F}** are respectively 0.2 M and 0.1 M.

^{1}H-NMR (400 MHz, (DMSO-d_6) δ (ppm): 9.12 (s, 6H, *J*=2.0 Hz PyrH), 8.48 (s, 6H, NH_{imm}), 8.43 (d, 6H, *J*=8.0 Hz, *J*=2.0 Hz, PyrH), 7.97 (d, 12H, *J*=8.5 Hz, ArH), 7.72 (m, 12H+6H, *J*=8.0 Hz, PyrH), 4.51 (s, 12H, CH_2), 3.18 (s, 6H, CH-dach) 1.76 (m, 12H, CH_2-dach), 1.38 (s, 6H, CH_2-dach). ESI-MS: *m/z*: calcd for $[C_{102}H_{90}F_8N_{14}Zn_2]^{2+}$ 929,7 $[M]^{2+}$ found 929,2 $[M]^{2+}$. FT-IR (optical path: 0,1 mm, DMSO-d_6): 1690 cm^{-1} ($\nu_{C=O}$, *s*), 1360 cm^{-1} (ν_{C-O}, *w*), 1170 cm^{-1} (ν_{C-F}, *m*).VCD (optical path: 0,1 mm, DMSO-d_6): 1700 cm^{-1} ($\nu_{C=O}$, *s*), 1370 cm^{-1} (ν_{C-O}, *w*), 1160 cm^{-1} (ν_{C-F}, *w*).

References

[1] (a) B. L. Feringa, R. A. van Delden, N. Koumura, E. M. Geertsema, *Chem. Rev.* **2000**, *100*, 1789-1816; (b) D. Pijper, B. L. Feringa, *Soft Matter* **2008**, *4*, 1349-1372.

[2] Z. Luo, Q. Zhang, Y. Oderaotoshi, D. P. Curran, *Science* **2001**, *291*, 1766.

[3] Rayne, S.; Forest, K. *Nature Precedings* 2010.

[4] C. W. Bunn, E. R. Howells, *Nature* **1954**, *174*, 549-551.

[5] K. Ute, R. Kinoshita, K.-i. Matsui, N. Miyatake, K. Hatada, *Chem. Lett.* **1992**, *21*, 1337-1340.

[6] S. S. Jang, M. Blanco, W. A. Goddard, G. Caldwell, R. B. Ross, *Macromolecules* **2003**, *36*, 5331-5341.

[7] (a) J. Solà, M. Helliwell, J. Clayden, *J. Am. Chem. Soc.* **2010**, *132*, 4548-4549; (b) L. Byrne, J. Solà, T. Boddaert, T. Marcelli, R. W. Adams, G. A. Morris, J. Clayden, *Angew. Chem. Int. Ed.* **2014**, *126*, 155-159; (c) H. Komori, Y. Inai, *J. Org. Chem.* **2007**, *72*, 4012-4022.

[8] (a) H. Sato, A. Yamagishi, *Int. J. Mol. Sci.* **2013**, *14*; (b) K. Harano, S. Takenaga, S. Okada, Y. Niimi, N. Yoshikai, H. Isobe, K. Suenaga, H. Kataura, M. Koshino, E. Nakamura, *J. Am. Chem. Soc.* **2014**, *136*, 466-473; (c) T. Yajima, E. Tabuchi, E. Nogami, A. Yamagishi, H. Sato, *RSC Adv.* **2015**, *5*, 80542-80547; (d) T. Taniguchi, D. Manai, M. Shibata, Y. Itabashi, K. Monde, *J. Am. Chem. Soc.* **2015**, *137*, 12191-12194.

[9] K. Monde, N. Miura, M. Hashimoto, T. Taniguchi, T. Inabe, *J. Am. Chem. Soc.* **2006**, *128*, 6000-6001.

[10] E. Yashima, N. Ousaka, D. Taura, K. Shimomura, T. Ikai, K. Maeda, *Chem. Rev.* **2016**, *116*, 13752-13990.

[11] (a) S. Mecozzi, J. J. Rebek, *Chem. Eur. J.* **1998**, *4*, 1016-1022; (b) J.-N. Rebilly, B. Colasson, O. Bistri, D. Over, O. Reinaud, *Chem. Soc. Rev.* **2015**, *44*, 467-489; (c) L. Trembleau, J. Rebek, *Science* **2003**, *301*, 1219; (d) D. Ajami, J. Rebek, *J. Am. Chem. Soc.* **2006**, *128*, 15038-15039; (e) T. K. Ronson, C. Giri, N. Kodiah Beyeh, A. Minkkinen, F. Topić, J. J. Holstein, K. Rissanen, J. R. Nitschke, *Chem. Eur. J.* **2013**, *19*, 3374-3382; (f) A. M. Castilla, T. K. Ronson, J. R. Nitschke, *J. Am. Chem. Soc.* **2016**, *138*, 2342-2351; (g) A. B. Grommet, J. R. Nitschke, *J. Am. Chem. Soc.* **2017**, *139*, 2176-2179; (h) J. R. Romero, G. Aragay, P. Ballester, *Chem. Sci.* **2017**, *8*, 491-498; (i) S. Fujii, T. Tada, Y. Komoto, T. Osuga, T. Murase, M. Fujita, M. Kiguchi, *J. Am. Chem. Soc.* **2015**, *137*, 5939-5947; (j) A. Galan, E. C. Escudero-Adan, P. Ballester, *Chem. Sci.* **2017**; (k) B. Chatelet, L. Joucla, D. Padula, L. D. Bari, G. Pilet, V. Robert, V. Dufaud, J.-P. Dutasta, A. Martinez, *Org. Lett.* **2015**, *17*, 500-503; (l) C. Gropp, T. Husch, N. Trapp, M. Reiher, F. Diederich, *J. Am. Chem. Soc.* **2017**, *139*, 12190-12200.

[12] D. Ajami, J. Rebek, *Nat. Chem.* **2009**, *1*, 87-90.

[13] C. Bravin, E. Badetti, F. A. Scaramuzzo, G. Licini, C. Zonta, *J. Am. Chem. Soc.* **2017**, *139*, 6456-6460.

[14] G. Yang, Y. Xu, in *Electronic and Magnetic Properties of Chiral Molecules and Supramolecular Architectures* (Eds.: R. Naaman, D. N. Beratan, D. Waldeck), Springer Berlin Heidelberg, Berlin, Heidelberg, **2011**, pp. 189-236.

[15] (a) L. A. Nafie, T. A. Keiderling, P. J. Stephens, *J. Am. Chem. Soc.* **1976**, *98*, 2715-2723; (b) P. L. Polavarapu, *Chirality* **2012**, *24*, 909-920;

[16] (a) V. P. Nicu, A. Mándi, T. Kurtán, P. L. Polavarapu, *Chirality* **2014**, *26*, 525-531; (b) G. Pescitelli, L. Di Bari, N. Berova, *Chem. Soc. Rev.* **2014**, *43*, 5211-5233.

[17] (a) M. Fuse, G. Mazzeo, G. Longhi, S. Abbate, D. Zerla, I. Rimoldi, A. Contini, E. Cesarotti, *Chem. Comm.* **2015**, *51*, 9385-9387; (b) S. Abbate, G. Mazzeo, S. Meneghini, G. Longhi, S. E. Boiadjiev, D. A. Lightner, *J. Phys. Chem. A* **2015**, *119*, 4261-4267.

Chapter 4

Elements for Mastering Hetero Co-Encapuslation within a Supramolecular Cage

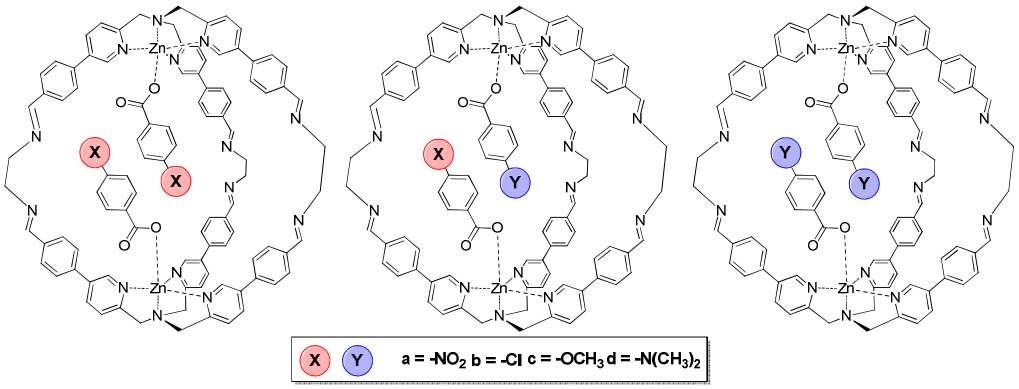

ABSTRACT Beside sensing and delivery, another promising property arising from confinement in discreet molecular hosts comes from the possibility to have in close proximity, and in a defined position molecules. This peculiar feature of confined spaces is opening to novel emerging properties in functional systems and catalysis. The major interest is to have hosts filled with two different molecules, hetero co-encapsulation, which is ruled by steric and electronic properties of the guests. In this chapter, a detailed study on homo and hetero co-encapuslation processes within a supramolecular cage is reported. In particular, the model case under study regards the possibility to have different *p*-substituted benzoic acid, within a supramolecular cage containing two metals. While electron-withdrawing EWG substituents are preferential guests, it has been possible to evaluate the conditions in which hetero co-encapuslation is favoured. This part of the study has been carried out in part at the University of Cambridge (UK) in the group of Prof. C.A. Hunter.

4.1 Introduction

The understanding of molecular recognition processes is fundamental for the development of novel functional assemblies.[1] For this purpose, molecular cages and capsules have been valuable source of information and their capability to act as host for a large variety of guest molecule have been well established.[2] The binding process is generally dictated by the complementarity of the host-guest assembly in terms of shape, size and interactions.[3] This knowledge has constituted the basis for the development of functional containers and their use as molecular reactors.[4], In this particular field, the capability of cages and capsule to accelerate reactions within their cavity is reported for chemical rearrangements of single guests (Figure 1) or reactions involving two different partners.[5] Mastering these processes is crucial for the development of novel functional systems, and the prediction of how two different molecular species could preferentially bind and get in close proximity within a cage, *viz.* hetero co-encapsulation, represents an important task.

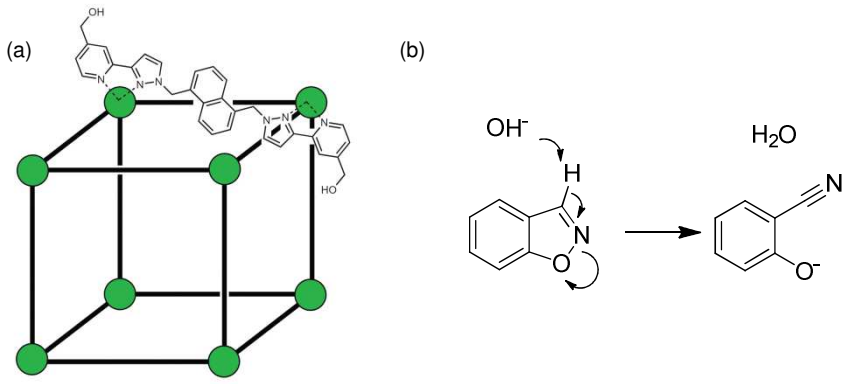

Figure 1. Arrangement of Co(II) ion and the bridging ligand to obtain a $[Co_8L_{12}](BF4)_{16}$ cage and (b) Kemp elimination reaction occurring within the cage.

In this chapter is reported a detailed study on the homo and hetero co-encapuslation of four differently substituted monocarboxylic acid within **TPMA** cage system

discussed in the previous chapters.[6] The study has shown how a delicate interplay of guests parameter tune the possibility to have homo or hetero complexation.

4.2 Results ad Discussion

4.2.1 Recognition Properties of cage 1 towards *p*-substituted benzoic acid series 2a,2d

The initial part has been dedicated to study molecular recognition properties of cage **1** towards four different benzoic acid: 4-Nitrobenzoic acid **2a**, 4-Chlorobenzoicacid **2b**, 4-Methoxybenzoic acid **2c** and 4-(Dimethylamino)benzoic acid **2d.** From these experiments, we expected to understand: *i*) if the system binds mono carboxylic acids, *ii*) the stoichiometry of the binding and *iii*) how variations in the electronic characteristic of the carboxylic acids would influence binding to the metal centre. It should be noted that substituents have been chosen to keep somehow similar the steric hindrance among the guests.

In the first binding experiments, sub-stoichiometric addition of 4-Nitrobenzoic acid **2a** to cage **1** in acetonitrile leads to the formation of a new set of signals that could be assigned to the cage filled with two guest molecules at the same time **(2a-2a)@1**. This observation is confirmed because along the titration points is always observed a 1:2 ratio between the integrals of the host and the guest (8.2 ppm) without any evidence of 1:1 adduct (See Appendix, Fig. A2-3). Moreover, after the addition of more than 2 equivalents of **2a**, the ^{1}H NMR spectrum results in a complete conversion to the filled cage **(2a-2a)@1** (Figure 2). Unexpectedly, the formation of the cage with only one acid is not observed, therefore it is not possible to decompose the contribution of the total process in two constant.

Beside the evidence of a 1:2 stoichiometry and the binding constant determination for the host-guest association process by ^{1}H-NMR titration, the inclusion cage **(2a-2a)@1** was confirmed by two-dimensional NMR spectroscopy (ROESY, DOSY) and ESI-MS experiments (See Appendix, Fig. A15-18).

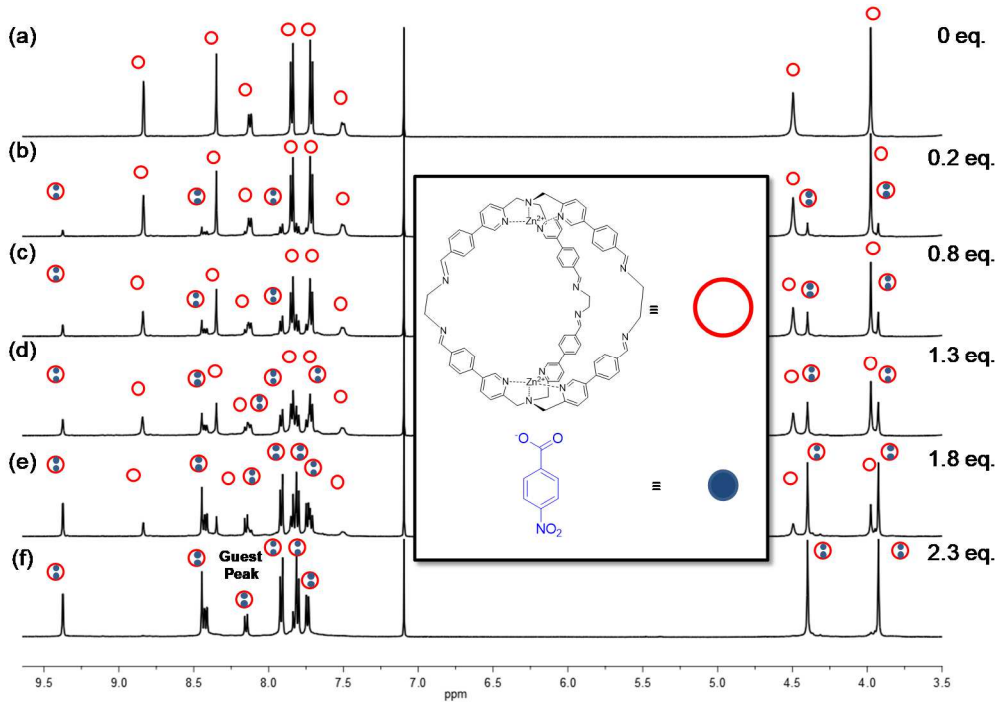

Figure 2. ^{1}H NMR inclusion experiments. Addition of *p*-Nitrobenzoicacid **2a** to cage **1** in CD_3CN. (a) Preformed cage **1** (0.001 M cage).(b)-(F) Addition of sub-stoichiometric amounts (0.2-1.8 equiv) of **2a** results in the formation of a new species that maintains the original symmetry. (f) Addition of 2.3 equiv of **2a** totally shift the system to the new species **(2a-2a)@1**. Counter anions are perchlorates.

Similar considerations can be taken from the titration experiments for the other monocarboxylic acid **2c,2d**, and an Hammet correlation plot was built to correlate the binding constant and the σ parameter for each guest (Figure 3). The results show a linear correlation (R^2=0.938) highlighting that the binding process is favored in the presence of electron withdrawing (EWG) group in the substituted guests. These results indicate that substituents able to stabilize the anionic form of the carboxylate are providing a stronger binding to the metal center. This is in agreement with the ionic bond character between the metal and the carboxylate. More importantly, these results dismiss a relevant contributions coming from the mutual interactions of the π system of the guests in the binding process (See Appendix, Fig. A6).[7]

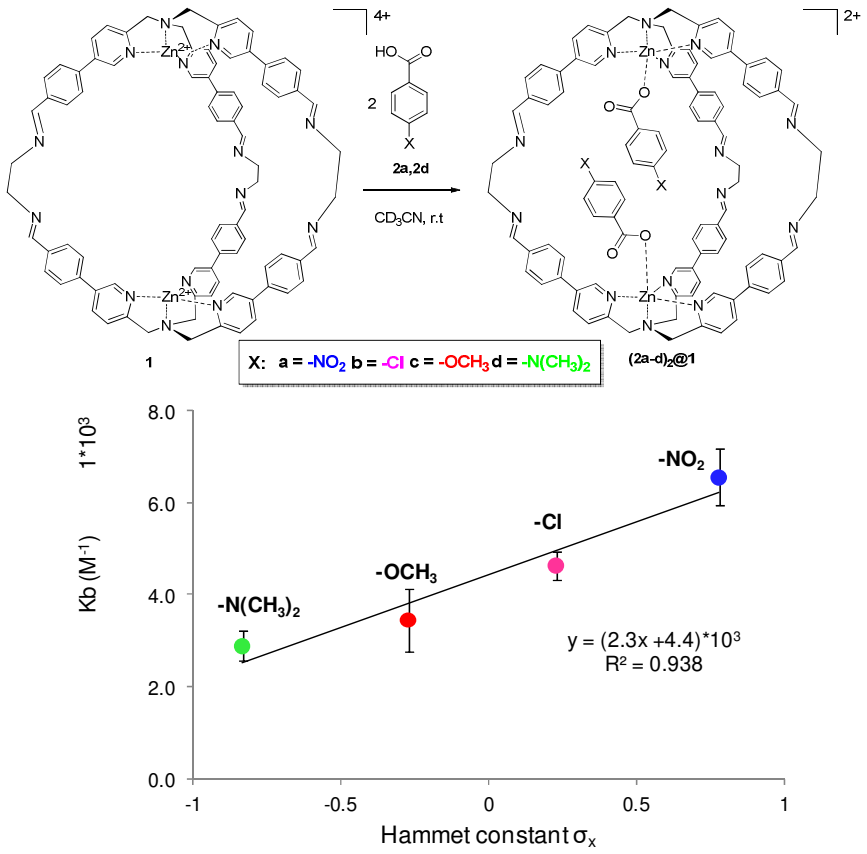

Figure 3. ^{1}H NMR binding constants (K_b) for the inclusion of **2a,2d** within cage **1**in binding stoichiometry 1:2 (embedded **en** and perchlorate counter anions are removed for clarity)

4.2.2 Competition Experiment

The binding constant determination describes a trend in the substituent effect for the guests series **2a,2d**, but to gain preliminary information on hetero co-encapsulation processes a competition experiment between two guests was performed. More in detail, to formed cage **1**, a 1:1 solution of **2a** and **2d** was added in sub-stoichiometric amounts (0.2 equiv.). This experimental setup would offer the possibility to understand how two different guests arrange within cage cavity and the chemical shifts of the formed complexes. Indeed, due to the slow exchange in the NMR timescale for the binding, four different signals in the region of the pyridine ring α proton are observed. With the help of ^{1}H-^{1}H ROESY cross correlations, two signals are attributed to the homo co-encapsulated species, 9.375 ppm for **(2a-2a)@1** and 9.395 ppm for **(2d-2d) @1**. The other two signals corresponds to the non-symmetrical cage containing the hetero co-encapsulated species **(2a-2d)@1** (Figure 4).

Interestingly, ROESY correlations allow to describe a mechanism for the interconversion between the homo and the hetero-species, in which the exchange of a guest between the two **TPMA** units is permitted only if it goes through an homo species (See appendix Scheme A9). After the attribution of all the signals, their integration allowed to determine a ratio between **(2a-2a)@1**, **(2d-2d)@1** and **(2a-2d)@1** are respectively of 1.00:0.52:1.55. This observation agrees with binding constant determination, therefore confirming the substituent effect for the affinity of this guests toward cage **1**.

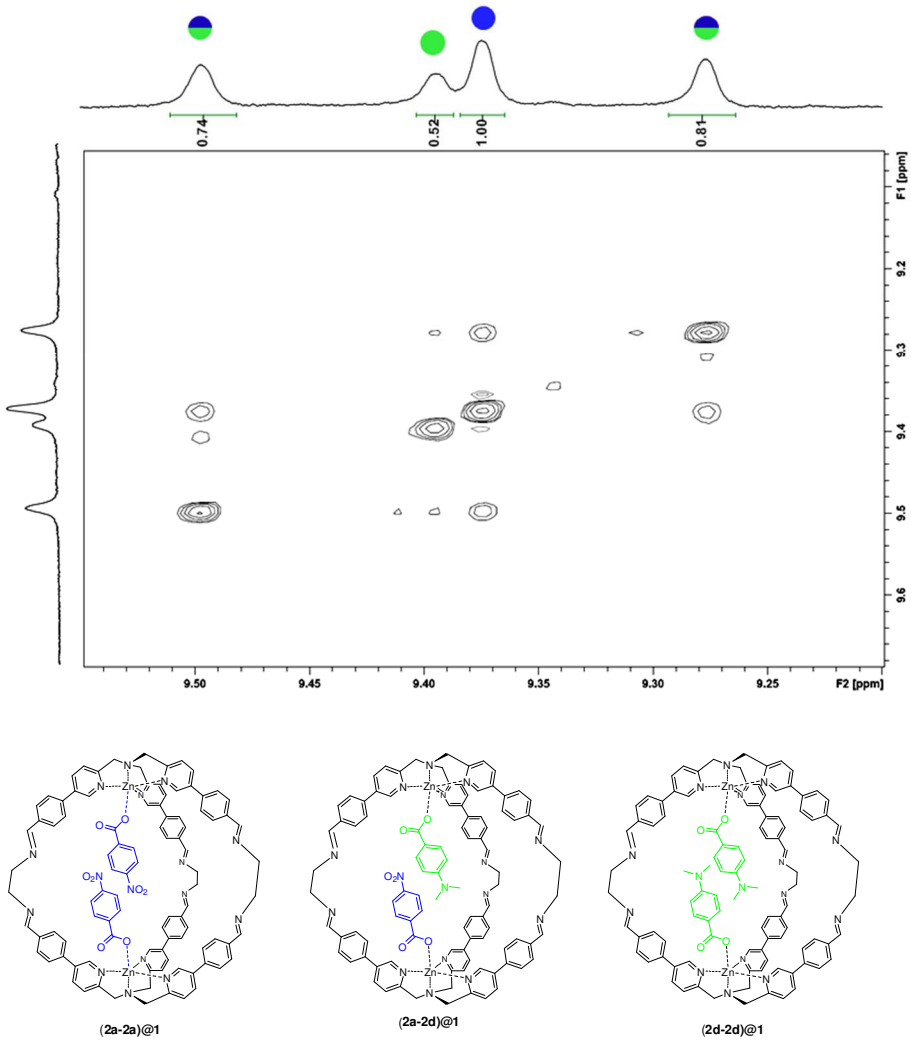

Figure 4. ^{1}H-^{1}H ROESY experiment for the competition experiment between acid **2a** and **2d** in 1:1 ratio. (**(2a-2a)@1** blue dot, **(2a-2d)@1** blue and green dot and **(2d-2d)@1** green dot).

4.2.3 Displacement Experiments

Maximize the hetero co-encapsulation is a main goal for many systems in order to gain new functional properties or for catalytic purposes. However, if one of the two guests has a higher binding constant, its homo co-encapsulation is favored. In our case, **2a** is the strongest binder, therefore it has greater tendency to homo co-

encapsulate. In the last part of the study, our interest was driven to understand how is possible to have the highest concentration of hetero co-encapsulated guests in the presence of two different binders. It should be noted that in our case the differences in binding constants within different partner are small. This is a perfect model to highlight how small variations in the concentration of the different partners influence cage inclusion.

For this purpose, a displacement experiment starting from the strongest binder **2a** toward hetero co-encapsulated species with lower affinity **2b,d** has been performed. This will open the possibility to underline how it is possible, even in the presence of differences in the binding strength, to have hetero partners within the same system. Starting from **(2a-2a)@1**, additions of increasing aliquots of monoacid **2d** to the solution were performed and monitored using ^{1}H NMR (Scheme 1). In this case, only one signal of the pyridine ring α proton is observed for the three possible species. This indicates the interchange between homo and hetero cage is a fast process on NMR timescale.

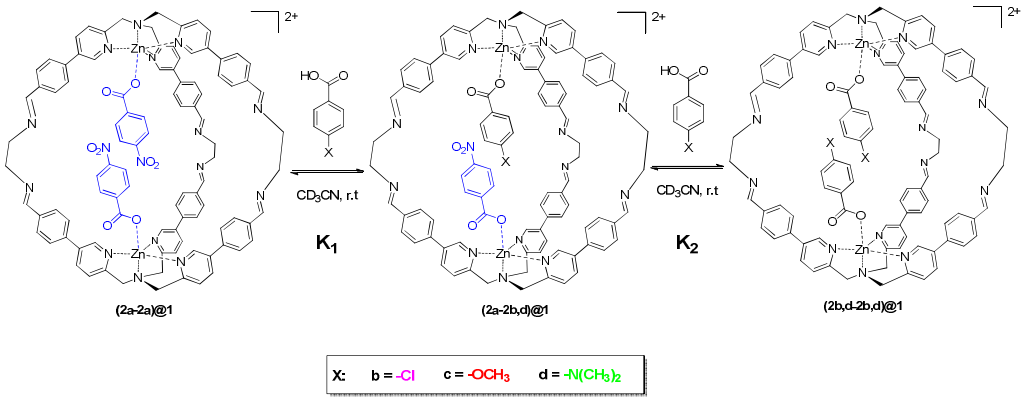

Scheme 1. General displacement experiment starting from cage **(2a)$_2$@1**. In each displacement experiment towards cage **(2a-2a)$_2$@1** the values for K_1 and K_2 are respectively for guest **2b** 0.650 and 0.325; **2c** 0.440 and 0.220; **2d** 0.264 and 0.132

The changes in chemical shift for each signal were recorded and analysed with purpose-written software. This program uses a procedure to fit the data to a displacement isotherm that monitors the sequential formation of **(2a-2d)@1** and **(2d-2d)@1**. The fitting procedure yielded to two displacement constants (K_1 and K_2), taking into account of three chemical shifts that vary during the displacement (See

appendix A11-13). In the case of displacement by **2d** the first and second displacement constants are minor than one (K_1 = 0.529 and K_2 = 0.132) confirming the stronger preference of the cage for the **2a** guest.

As seen in Figure 5, 4-Nitrobenzoic acid **2a** is not totally displaced even at ratio between displacer and initial guests of 8.0 (Addition of more than 16 equivalent of 4-(Dimethylamino)benzoic acid **2d**). Interestingly, from one to three equivalent of **2d** the major species in solution is the hetero cage **(2a-2d)@1**.

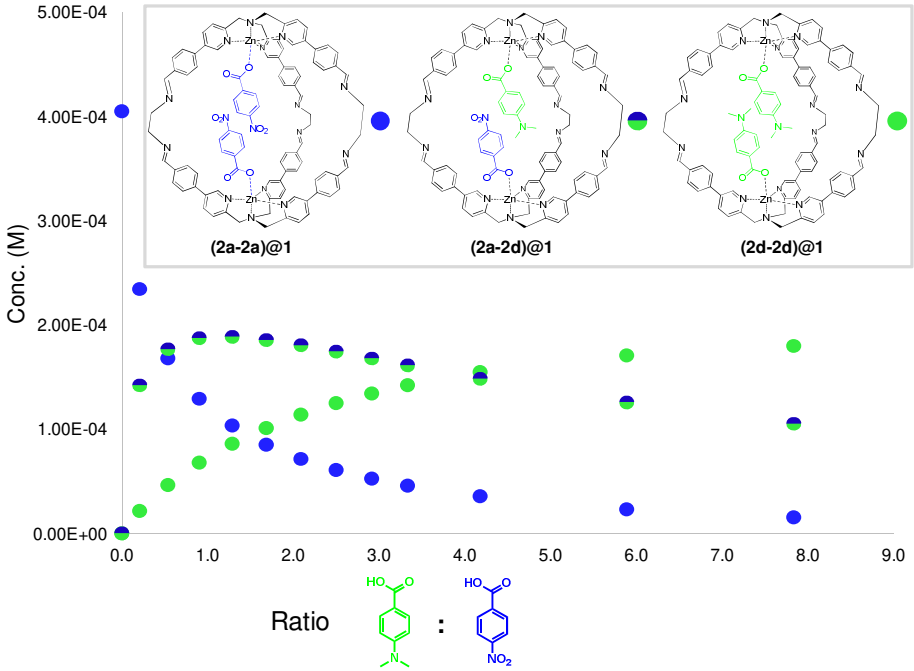

Figure 5. Concentration graph of the displacement experiment of cage **$(2a)_2$@1** with acid **2d.**

In a similar fashion, the displacement experiment has been performed also for the other acids and the displacement constants are reported in Scheme 1. The explanation of the observed trends pair the measurement of the homo cage binding constants.

Particular attention should be given for the concentration of the three hetero cages in the displacement profiles (Figure 6). It could be noticed that the formation of the hetero co-encapsulated species is related to the affinity of each acid to the cage.

As expected, the better displacer **2b** reach the maximum in the concentration of hetero cage at lower concentrations in comparison with worse displacers **2c**,**2d**. However, being a better displacer results in a lower concentration of hetero species at higher displacer concentration. On the other hand, the formation of hetero co-encapsulated species is favoured at higher displacer concentration for the worst binder **2d** (Figure 6). This counterintuitive result describes how the addition of a worse displacer (benzoic acid with ED group) favour the formation of the hetero co-encapsulated species when it is added in increasing quantity, respect to a better displacer (benzoic acid with EWG group).

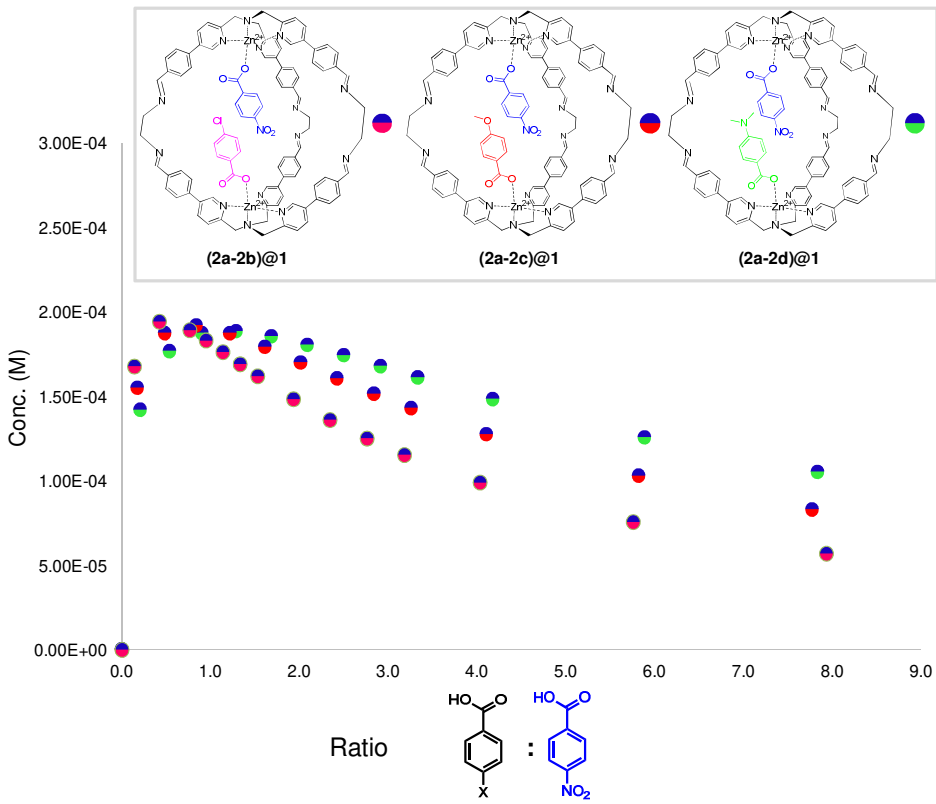

Figure 6. Concentration graph of the hetero co-encapsulated species for the displacement experiment of cage **(2a)$_2$@1** with diacid **2a-d.**

4.3 Conclusions

In this chapter, the co-encapuslation process within a molecular cage of several monocarboxylic acid differing for electronic properties is reported. The binding process is characterized by a host-guest stoichiometry 1:2 and it is favoured if the substituent in the benzoic acid is an electronwithdrawing (EWG) group. Competition and displacement experiments have confirmed this trend in the substituent effect and have contributed to build model to predict the formation of ethero or homo co-encapuslated species. The results showed that the hetero co-encapsulated species is preferred at lower displacer concentration for benzoic acid with more EW group (better displacer), while at higher concentration the hetero species are favoured by benzoic acid with more ED group.

This observation apparently counterintuitive open the possibility to master how two guests can get in close proximity within a confined space with subsequent application in supramolecular catalysis.

4.4 Experimental

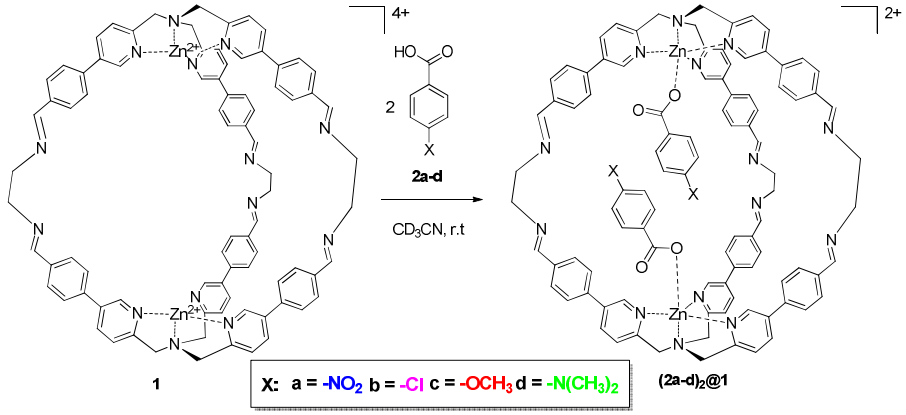

4.4.1 General Procedure for Binding Experiment

To 500 µl (0.5 µmol) of a solution 0.001 M of the cage **1** (based on *p*-xylene standard) in CD_3CN, 20 µl (0.24 µmol) of a solution 0.012 M in CD_3CN of *p*-xylene were added. Small aliquots of guests solution were titrated into this NMR tube. The solution was allowed to equilibrate at room temperature during 30 seconds before acquiring the ^1H NMR spectrum.

(2a-2a)@1 ^1H NMR (500 MHz, CD_3CN) δ (ppm): 9.37 (d, 6H, *J*=2.0 Hz PyrH), 8.45 (s, 6H, NH_{imm}), 8.43 (dd, 6H, *J*=8.0 Hz, *J*=2.0 Hz, PyrH), 8.14 (d, 4H, *J*=8.0 Hz, ArH-NO_2) 7.91 (d, 12H, *J*=8.5 Hz, ArH), 7.80 (m, 12H, ArH+4H ArH-NO_2), 7.73 (dd, 6H, *J*=8.0 Hz, *J*=2.0 Hz, PyrH), 4.40 (s, 12H, CH_2), 3.93 (s, 12H, CH_{2eda}).
ESI-MS *(m/z)*: $[M]^{2+}$ calcd. for $[C_{98}H_{80}N_{16}O_8Zn_2]^{2+}$, 869.7 found; 869.9.
(2b-2b)@1 ^1H NMR (500 MHz, CD_3CN) δ (ppm): 9.33 (d, 6H, *J*=2.0 Hz PyrH), 8.44 (s, 6H, NH_{imm}), 8.38 (dd, 6H, *J*=8.0 Hz, *J*=2.0 Hz, PyrH), 8.06 (m, *J*=8.0 Hz, ArH-Cl) 7.90 (d, 12H, *J*=8.5 Hz, ArH), 7.73 (m, 12H+4H+6H, ArH; ArH-NO_2, Pyr), 4.37 (s, 12H, CH_2), 3.94 (s, 12H, CH_{2eda}).
ESI-MS *(m/z)*: $[M]^{2+}$ calcd. for $[C_{98}H_{80}Cl_2N_{14}O_4Zn_2]^{2+}$, 857.2 found; 857.3.
(2c-2c)@1 ^1H NMR (500 MHz, CD_3CN) δ (ppm): 9.33 (d, 6H, *J*=2.0 Hz PyrH), 8.44 (s, 6H, NH_{imm}), 8.39 (dd, 6H, *J*=8.0 Hz, *J*=2.0 Hz, PyrH), 7.99 (m, 4H, ArH-OCH_3)

7.89 (d, 12H, *J*=8.5 Hz, ArH), 7.68 (m, 12H, ArH+6H PyrH), 6.97 (m, 4H, ArH-OCH_3), 4.37 (s, 12H, CH_2), 3.94 (s, 12H, CH_{2eda}).
ESI-MS *(m/z)*: $[M]^{2+}$ calcd. for $[C_{100}H_{86}N_{14}O_6Zn_2]^{2+}$, 853.3 found; 853.2
(2d-2d)@1 ^{1}H NMR (500 MHz, CD_3CN) δ (ppm): 9.40 (d, 6H, *J*=2.0 Hz PyrH), 8.45 (s, 6H, NH_{imm}), 8.38 (dd, 6H, *J*=8.0 Hz, *J*=2.0 Hz, PyrH), 7.97 (m, 4H, ArH-$N(CH_3)_2$) 7.90 (d, 12H, *J*=8.5 Hz, ArH), 7.71 (m, 12H, ArH+6H PyrH), 6.50 (m, 4H, ArH-$N(CH_3)_2$), 4.39 (s, 12H, CH_2), 3.93 (s, 12H, CH_{2eda}).
ESI-MS *(m/z)*: $[M]^{2+}$ calcd. for $[C_{102}H_{92}N_{16}O_4Zn_2]^{2+}$, 866.3 found; 866.1

4.4.2 General Procedure for Competition Experiment

To 500 µl (0.5 µmol) of a solution 0.001 M of the cage **1** (based on *p*-xylene standard) in CD_3CN, 20 µl (0.24 µmol) of a solution 0.012 M in CD_3CN of *p*-xylene were added. Then 10 µl (0.1 µmol) of a 0.01 M mixed solution of two guests of the series **2a,2d** were introduced. The mixture was monitored with ^{1}H NMR.

4.4.3 General Procedure for Displacement Experiment

To 500 µl (0.5 µmol) of a solution 0.001 M of the cage **(2a)$_2$@1** (based on *p*-xylene standard) in CD_3CN, 20 µl (0.24 µmol) of a solution 0.012 M in CD_3CN of *p*-xylene were added. Small aliquots of **2b,2d** competitors guests solution were titrated into this NMR tube. The displacement was monitored by ^{1}H NMR.

References

[1] (a) E. Moulin, G. Cormos, N. Giuseppone, *Chem. Soc. Rev.* **2012**, *41*, 1031-1049; (b) J.-M. Lehn, *Angew. Chem. Int. Ed.* **1990**, *29*, 1304-1319; (c) V. M. Dong, D. Fiedler, B. Carl, R. G. Bergman, K. N. Raymond, *J. Am. Chem. Soc.* **2006**, *128*, 14464-14465; (d) M. J. Langton, N. H. Williams, C. A. Hunter, *J. Am. Chem. Soc.* **2017**, *139*, 6461-6466; (e) G. Iadevaia, A. E. Stross, A. Neumann, C. A. Hunter, *Chem. Sci.* **2016**, *7*, 1760-1767; (f) D. Nunez-Villanueva, C. A. Hunter, *Chem. Sci.* **2017**, *8*, 206-213; (g) D. Núñez-Villanueva, G. Iadevaia, A. E. Stross, M. A. Jinks, J. A. Swain, C. A. Hunter, *J. Am. Chem. Soc.* **2017**, *139*, 6654-6662; (h) A. E. Stross, G. Iadevaia, D. Núñez-Villanueva, C. A. Hunter, *J. Am. Chem. Soc.* **2017**, *139*, 12655-12663.

[2] (a) J. T. A. Jones, T. Hasell, X. Wu, J. Bacsa, K. E. Jelfs, M. Schmidtmann, S. Y. Chong, D. J. Adams, A. Trewin, F. Schiffman, F. Cora, B. Slater, A. Steiner, G. M. Day, A. I. Cooper, *Nature* **2011**, *474*, 367-371; (b) T. Kusukawa, M. Fujita, *Angew. Chem. Int. Ed.* **1998**, *37*, 3142-3144; (c) T. Kusukawa, M. Fujita, *J. Am. Chem. Soc.* **2002**, *124*, 13576-13582; (d) S. H. A. M. Leenders, R. Gramage-Doria, B. de Bruin, J. N. H. Reek, *Chem. Soc. Rev.* **2015**, *44*, 433-448; (e) J.-N. Rebilly, B. Colasson, O. Bistri, D. Over, O. Reinaud, *Chem. Soc. Rev.* **2015**, *44*, 467-489; (f) L. Baldini, P. Ballester, A. Casnati, R. M. Gomila, C. A. Hunter, F. Sansone, R. Ungaro, *J. Am. Chem. Soc.* **2003**, *125*, 14181-14189;(g) S. H. A. M. Leenders, R. Becker, T. Kumpulainen, B. de Bruin, T. Sawada, T. Kato, M. Fujita, J. N. H. Reek, *Chem. Eur. J.* **2016**, *22*, 15468-15474.

[3] (a) T. Heinz, D. M. Rudkevich, J. Rebek, *Nature* **1998**, *394*, 764-766; (b) S. Mecozzi, J. J. Rebek, *Chem. Eur. J.* **1998**, *4*, 1016-1022; (c) W. M. Bloch, Y. Abe, J. J. Holstein, C. M. Wandtke, B. Dittrich, G. H. Clever, *J. Am. Chem. Soc.* **2016**, *138*, 13750-13755; (d) C. A. Hunter, *Angew. Chem. Int. Ed.* **2004**, *43*, 5310-5324; (e) C. A. Hunter, M. C. Misuraca, S. M. Turega, *Chem. Sci.* **2012**, *3*, 2462-2469; (f) S. Turega, W. Cullen, M. Whitehead, C. A. Hunter, M. D. Ward, *J. Am. Chem. Soc.* **2014**, *136*, 8475-8483.

[4] (a) B. Breiner, J. R. Nitschke, in *Supramolecular Chem.*, John Wiley & Sons, Ltd, **2012**; (b) S. Zarra, D. M. Wood, D. A. Roberts, J. R. Nitschke, *Chem. Soc. Rev.* **2015**, *44*, 419-432; (c) C. S. Wood, C. Browne, D. M. Wood, J. R. Nitschke, *ACS Centr. Sci.* **2015**, *1*, 504-509; (d) L. Catti, Q. Zhang, K. Tiefenbacher, *Chem. Eur. J.* **2016**, *22*, 9060-9066; (e) T.-C. Lee, E. Kalenius, A. I. Lazar, K. I. Assaf, N. Kuhnert, C. H. Grün, J. Jänis, O. A. Scherman, W. M. Nau, *Nat Chem* **2013**, *5*, 376-382; (f) M. Yoshizawa, J. K. Klosterman, M. Fujita, *Angew. Chem. Int. Ed.* **2009**, *48*, 3418-3438; (g) M. Raynal, P. Ballester, A. Vidal-Ferran, P. W. N. M. van Leeuwen, *Chem. Soc. Rev.* **2014**, *43*, 1734-1787.

[5] (a) W. Cullen, M. C. Misuraca, C. A. Hunter, N. H. Williams, M. D. Ward, *Nat Chem* **2016**, *8*, 231-236; (b) M. M. J. Smulders, J. R. Nitschke, *Chem. Sci.* **2012**, *3*, 785-788; (c) P. P. Neelakandan, A. Jiménez, J. D. Thoburn, J. R. Nitschke, *Angew. Chem.* **2015**, *127*, 14586-14590; (d) M. D. Pluth, R. G. Bergman, K. N. Raymond, *J. Org. Chem.* **2009**, *74*, 58-63; (e) C. J. Hastings, M. D. Pluth, R. G. Bergman, K. N. Raymond, *J. Am. Chem. Soc.* **2010**, *132*, 6938-6940; (f) D. M. Dalton, S. R. Ellis, E. M. Nichols, R. A. Mathies, F. D. Toste, R. G. Bergman, K. N. Raymond, *J. Am. Chem. Soc.* **2015**, *137*, 10128-10131; (g) C. J. Brown, F. D. Toste, R. G. Bergman, K. N. Raymond, *Chem. Rev.* **2015**, *115*, 3012-3035; (h) P. F. Kuijpers, M. Otte, M. Dürr, I. Ivanović-Burmazović, J. N. H. Reek, B. de Bruin, *ACS Cat.* **2016**, *6*, 3106-3112; (i) L. Xu, W. Hua, S. Hua, J. Li, S. Li, *J. Org.Chem.* **2013**, *78*, 3577-3582; (j) Q.-T. He, X.-P. Li, L.-F. Chen, L. Zhang, W. Wang, C.-Y. Su, *ACS Cat.* **2013**, *3*, 1-9; (k) N.-W. Wu, J. Rebek, *J. Am. Chem. Soc.* **2016**, *138*, 7512-7515; (l) R. J. Hooley, J. Rebek Jr, *Org. Biomol. Chem.* **2007**, *5*, 3631-3636; (m) J. Kang, J. Rebek, *Nature* **1997**, *385*, 50-52; (n) M. Yoshizawa, M. Tamura, M. Fujita, *Science* **2006**, *312*, 251.

[6] C. Bravin, E. Badetti, F. A. Scaramuzzo, G. Licini, C. Zonta, *J. Am. Chem. Soc.* **2017**, *139*, 6456-6460.

[7] (a) C. A. Hunter, J. K. M. Sanders, *J. Am. Chem. Soc.* **1990**, *112*, 5525-5534; (b) H. Adams, C. A. Hunter, K. R. Lawson, J. Perkins, S. E. Spey, C. J. Urch, J. M. Sanderson, *Chem. Eur. J.* **2001**, *7*, 4863-4877; (c) C. A. Hunter, C. M. R. Low, C. Rotger, J. G. Vinter, C. Zonta, *P.N.A.S.* **2002**, *99*, 4873-4876.

Conclusions

In this Ph.D. thesis, we have reported the synthesis and the supramolecular applications of a novel series of self-assembled imine-based supramolecular cages.
In *Chapter 1*, the molecular recognition properties and a detailed study of the kinetic and thermodynamic parameters guiding the assembly/disassembly processes has revealed interesting patterns related to the size of the guest. The possibility to control the assembly/disassembly of the supramolecular architecture has led to a novel method to induce the disassembly of the cage structure. In this direction we are now studying the detailed mechanism of this process. In *Chapter 2*, we have extended the cage series to seven zinc(II) and eight copper(II) novel molecular cages differing in size. The selectivity profiles have been investigated using a novel ESI-MS methodological approach . This technique has allowed the analysis also for copper(II) systems which cannot be investigate either *via* ^{1}H NMR or UV-Vis titrations. In *Chapter 3* is reported the synthesis of a chiral molecular cage able to control the helicity of a octafluoroadipic dicarboxylic acid embedded within its cavity. A combination of VCD analysis and computational studies were carried out to identify the most stable diastereoisomer cage in solution. Initial VCD experiments indicate that the cage is able to induce a preferential helix configuration of the embedded perfluoroalkyl chain. In *Chapter 4*, the co-encapuslation process within a molecular cage of several monocarboxylic acid differing for electronic properties is reported. We have established a host-guest stoichiometry 1:2 of binding and this process is favoured if the substituent in the benzoic acid is an electronwithdrawing (EWG) group. Competition and displacement experiments have contributed to build model to predict the formation of ethero or homo co-encapuslated species.
The novel molecular cages are now under investigation for catalytic porpoises. The cages capability to undergo a straightforward functionalization and their capability to perform molecular recognition makes this systems eligible for several supramolecular applications.

APPENDIX

Appendix to Chapter 1

A1.1 Binding constant determination to 2 (K_b)

To 500 µl (0.5 µmol) of a solution 0.001 M of the cage **2** (based on *p*-xylene standard) in CD_3CN, 20 µl (0.24 µmol) of a solution 0.012 M in CD_3CN of *p*-xylene were added. Small aliquots of the guest solution were titrated into this NMR tube. The solution was allowed to equilibrate at room temperature during 30 seconds before acquiring the ^1H NMR spectrum. The binding constant values for each dicarboxylic acid (**C_4-C_{14}**) are displayed in Table A1. The error reported for each affinity value is the formal standard error calculated using two characteristic peaks in the ^1H NMR spectra and performing the titrations three times.

In the case of **C_8** no influence in the value of the binding constant has been observed in the presence of $HClO_4$ (up to 5 µmol) or NEt_3 (up to 5 µmol).[1]

Diacid	K_b (M^{-1})	±σ (M^{-1})
C_4	14601	1188
C_5	17267	1399
C_6	34165	2550
C_7	23504	3560
C_8	35721	1988
C_9	13026	1782
C_{10}	14115	2553
C_{11}	8388	1124
C_{12}	9344	674
C_{13}	7763	763
C_{14}	5818	908

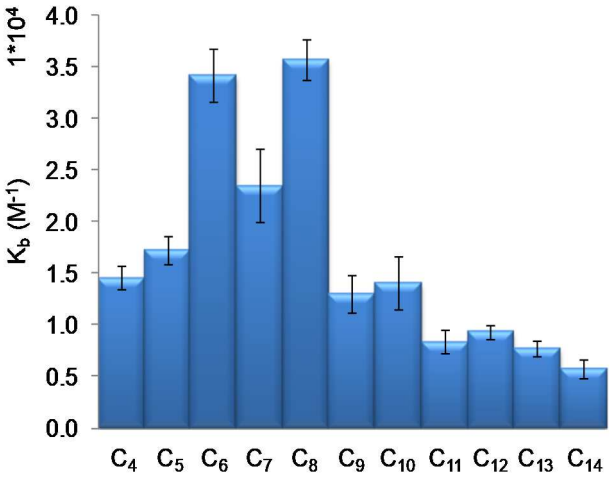

Figure A1. Binding constant values for each dicarboxylic acid [**C_4-C_{14}**].

A1.2 Titration Experiment of Suberic Acid with Molecular Cage 2

The ^{1}H NMR spectrum of the molecular recognition of suberic acid **C_8** is shown in Figure A2. The spectrum is then divided in two regions in order to clarify the NMR signals. The blue region (Figure A3) is related to the proton signals of the molecular cage **2** , while the red (Figure A4) is mainly related to the proton signals of the ethylendiamine embedded in the cage and the aliphatic signals of the protonated diamine in solution. In the red region it is also possible to distinguish the proton related to the dicarboxylic acid within the cage.

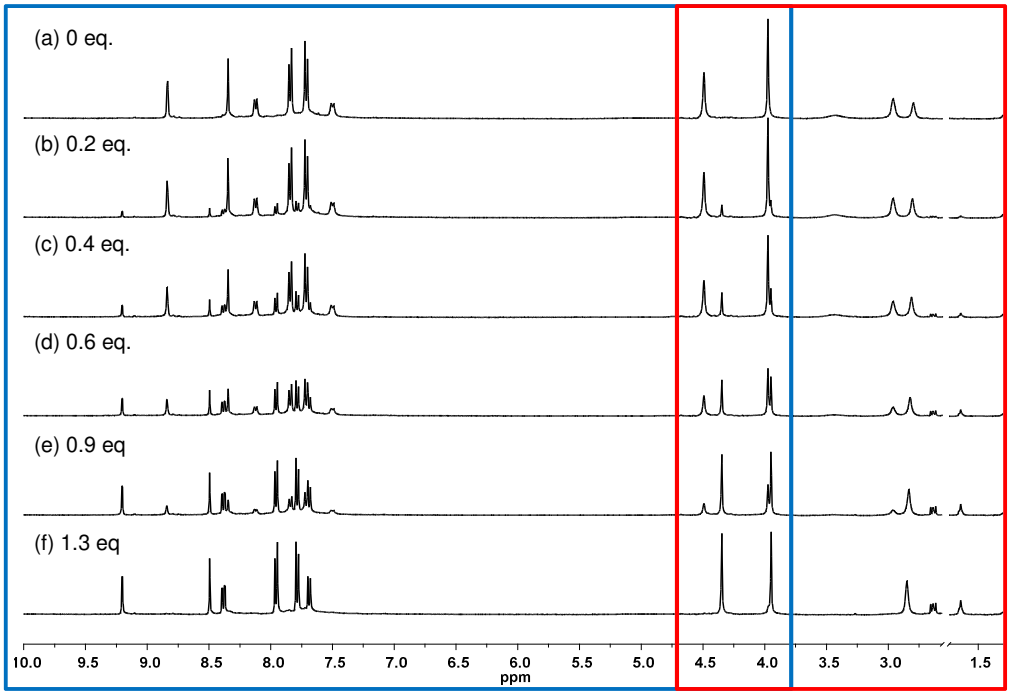

Figure A2. **^{1}H NMR inclusion experiments** Addition of suberic acid **C_8** in the preformed cage **2** in CD_3CN. The blue region of the spectrum is related to molecular cage proton signals . The red region is related to the embedded and the protonated amine in solution and also to the dicarboxylic acid proton signals.

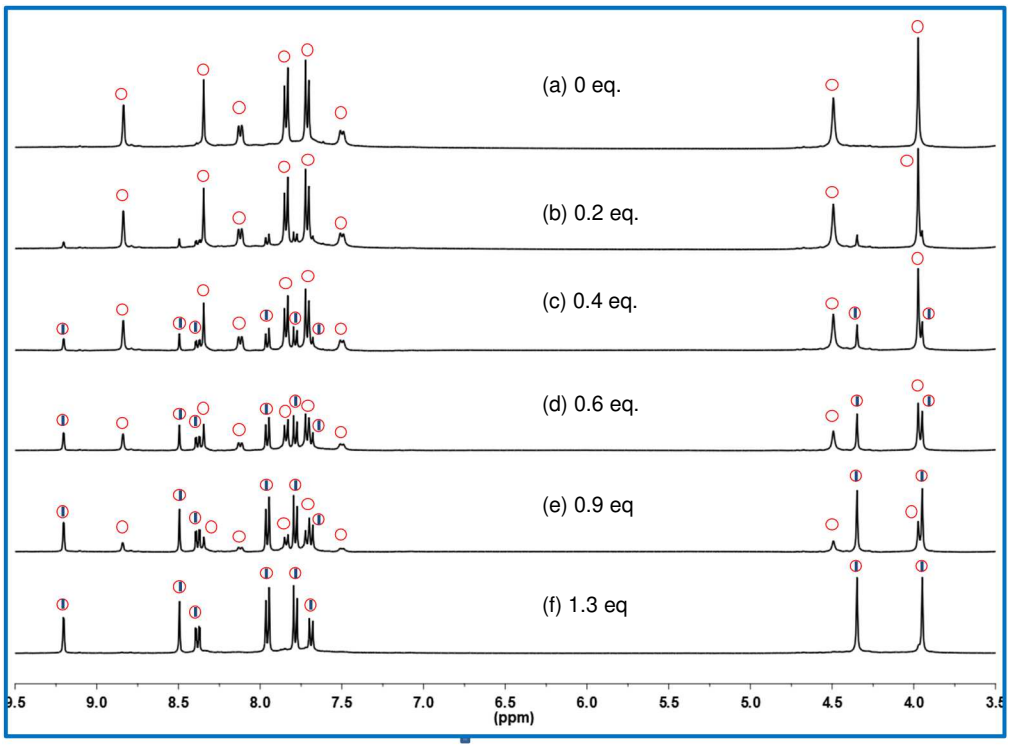

Figure A3. **^{1}H NMR inclusion experiments** Addition of suberic acid **C_8** in the preformed cage **2** in CD_3CN. The red circle indicates cage **2** while the blue stick indicates the dicarboxylic acid **C_8**. a) Preformed cage **2** (0.001 M cage). The number of peaks is related to the D_3 symmetry of the system. b-e) Addition of sub-stoichiometric amounts (0.2-0.9 equiv) of suberic acid results in the formation of a new species that maintains the original symmetry. (f) Addition of 1.3 equiv of suberic acid shifts completely the system to the new species **C_8@2**.

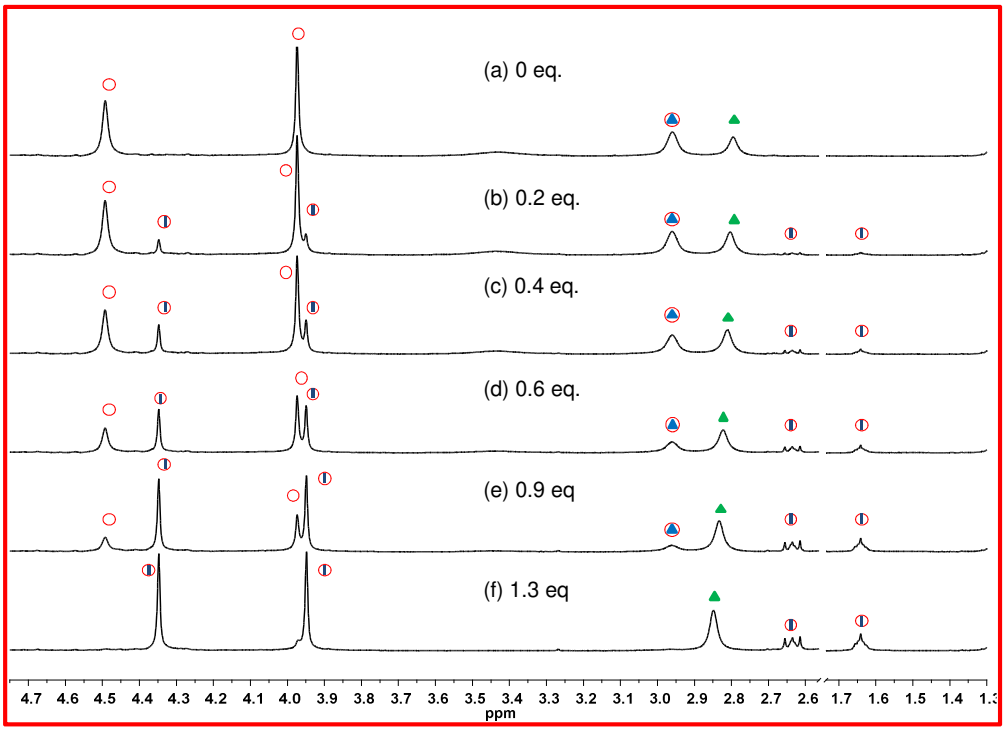

Figure A4. **^{1}H NMR inclusion experiments** Addition of suberic acid **C_8** in the preformed cage **2** in CD_3CN. The red circle indicates cage **2**, blue stick indicates the dicarboxylic acid **C_8**, blue triangle indicates ethylendiamine embedded within the cage and green triangle indicates the ethylendiamine protonated in solution.

In this spectrum the addition of diacid results in the protonation of the embedded ethylenediamine within the cage. The diacid displaces the ehtylendiamine embedded within the cage as it is shown by the decreasing of the integral of relative signal (2.95 ppm). As consequence there is an increase of the integral value of the protonated ethylendiamine in solution (red triangle). The signals at 2.62 and 1.65 ppm correspond to the aliphatic protons of the diacid within the molecular cage. In Figure A5 the trend of the integral values of all the signals is reported, which confirms the displacement of the diamine and the binding of the dicarboxylic acid. In addition the sum of the normalized area of proton signals related the diacid within the cage and the ethylenediamine embedded is constant during the titration experiment.

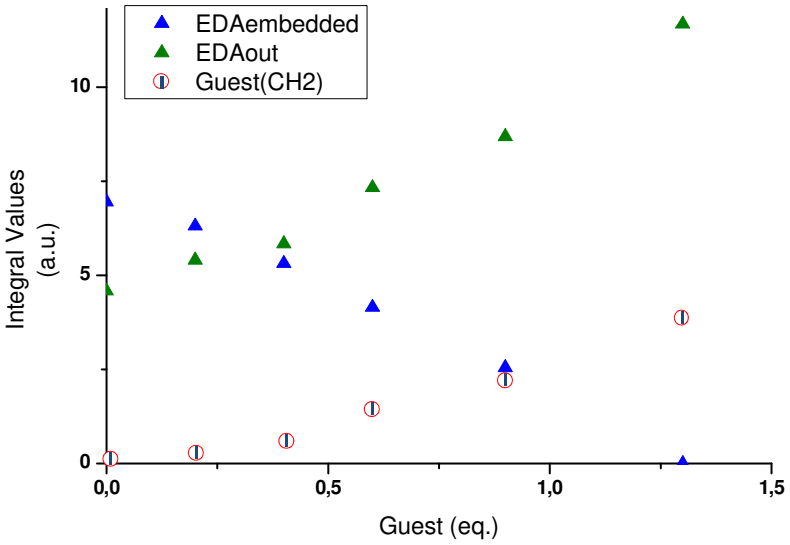

Figure A5. **Integral trend of ^{1}H NMR inclusion experiments.** Addition of suberic acid **C_8** in the preformed cage **2** in CD_3CN. The red circle indicates cage **2**, blue stick indicates the dicarboxylic acid **C_8**, blue triangle indicates ethylendiamine embedded within the cage and green triangle indicates the ethylendiamine protonated in solution.

A1.3 Thermodynamic considerations over the observed effects.

In order to complete the thermodynamic framework for the cage formation/disassembly, the binding constants for the entire dicarboxylic acid series toward **1** (K_1) have been measured (Supporting Information, Figure A8). As expected, all the association constant K_1 are similar. This association process can be regarded as the pre-equilibria for the template formation process and it allows the calculation of the binding constant for the diacid in the transition state (K_{TS}). In particular, for the template formation process K_{TS} is the product of K_1 with initial relative rates of assembly (v_{Cn}/v_{blank}).[2]

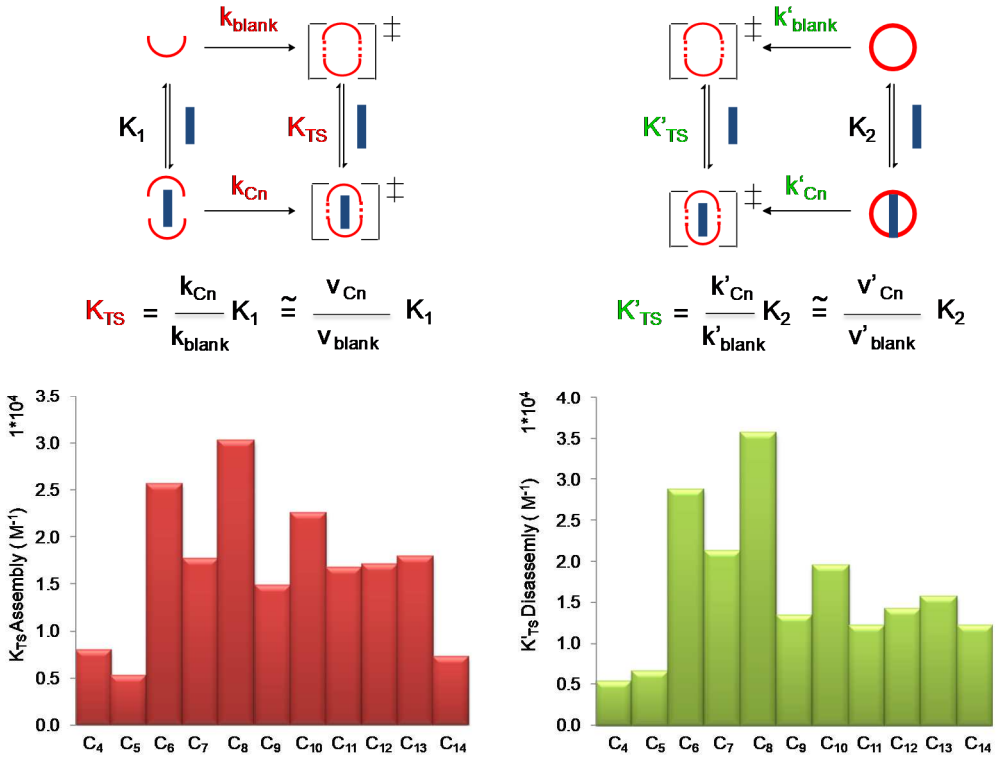

Figure A6. Calculated transition states binding constant K_{TS} from the assembly reaction with the thermodynamic cycle illustrating the relationship between the binding in transistion state (K_{TS}) of the assembly reaction and (K'_{TS}) disassembly reaction (See Supporting information for a full theoretical treatment).

As expected, being the binding constants K_1 similar in value for all the dicarboxilyc acids, the diacids binding constants in the TS of the cage formation process strongly remind the initial relative rate of formation (Figure 8). Similarly, diacids binding constants in the TS of the disassembly reaction (K'_{TS}) can be obtained by the product of the binding of the formed cage K_2 and the initial relative ratio of hydrolysis (v'_{Cn}/v'_{blank}). In this case, being initial relative rates of hydrolysis similar in value, K'_{TS} strongly remind K_2. It can be noticed that a linear correlation of the two calculated binding energies in the transition states is observed (Figure A7).

From these experimental observations the following three general considerations can be taken: *i*) correlation of the calculated K_{TS} suggests a similar transition state for the formation and hydrolysis reactions; *ii*) transition states structures should resemble he formed cage structure being the K_{TS} and K_2 very similar. However, iii) the transition state structure should present a longer Zn-Zn distance in comparison with the formed cage. This is expected as a consequence of the increased binding constant for longer diacids in the TS in respect to the formed cage. The latter observation is in line with the overall result of the hydrolytic process which is the opening of the formed structure. The strain gain/release of the guest from **2** to the transition state is the thermodynamic responsible of the observed effect.

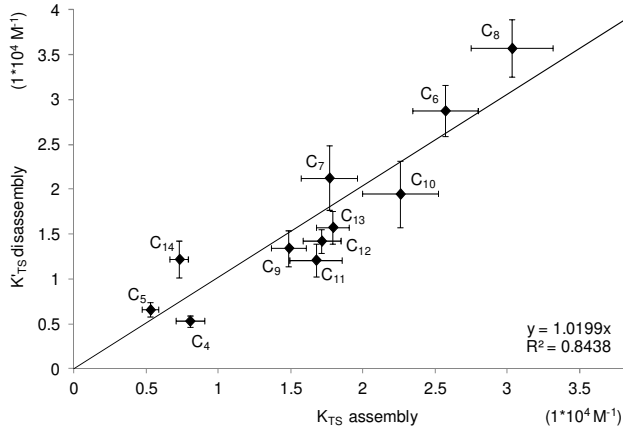

Figure A7. Calculated transition states binding constant from the assembly and disassembly reactions. The values are in good agreement suggesting the same TS for both pathways.

A1.4 Binding Constant Determination K_1

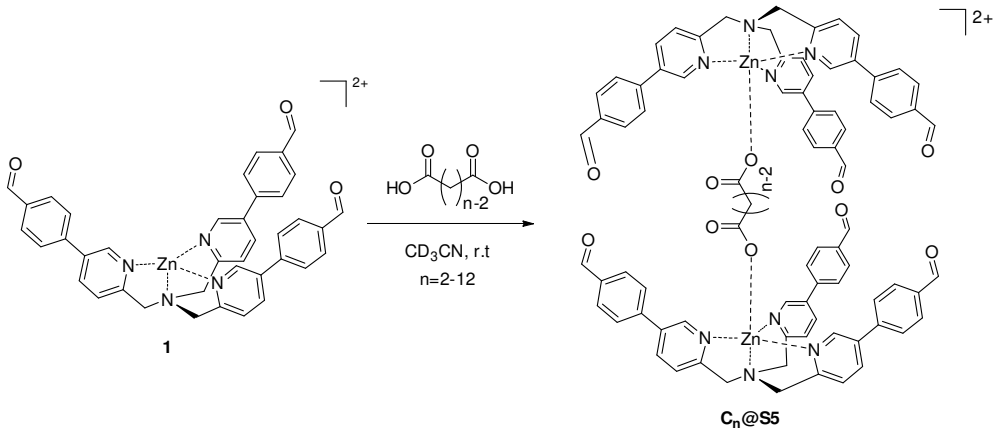

To 500 µl (0.5 µmol) of a solution 0.001 M of complex **1** in CD_3CN, 50 µl (0.25 µmol) of a solution 0.005 M in CD_3CN of *p*-xylene as internal standard were added. Small aliquots of a solution 0.01 M of each dicarboxylic acid ranging from **C_4** to **C_{14}** have been added into this NMR tube. The stock solution of the dicarboxyilic acid contains a stoichiometric quantity of triethylamine to reproduce the formation of the dicarboxylate at the beginning of the reaction. The solution was allowed to equilibrate at room temperature during 30 seconds before acquiring the ^1H NMR spectrum. The binding constant values K_1 for each dicarboxylic acid (**C_4**-**C_{14}**) are displayed in Figure A8. The error reported for each affinity value is the formal standard error calculated using two characteristic peaks in the ^1H NMR spectra and performing the titrations three times.

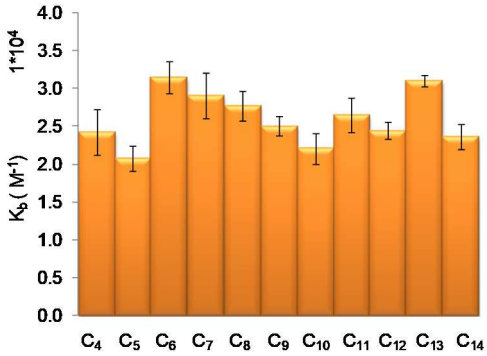

Diacid	K_1 (M^{-1})	±σ (M^{-1})
C_4	2420	600
C_5	2074	330
C_6	3149	415
C_7	2905	600
C_8	2774	401
C_9	2507	262
C_{10}	2206	421
C_{11}	2653	450
C_{12}	2446	234
C_{13}	3103	152
C_{14}	2364	331

Figure A8. Formation rate of each inclusion complex **C_n@2** for the whole series ranging from **C_4@** to **C_{14}@2.**

A1.5 Titration Experiment for determination of binding constant K_1 of Adipate C_6

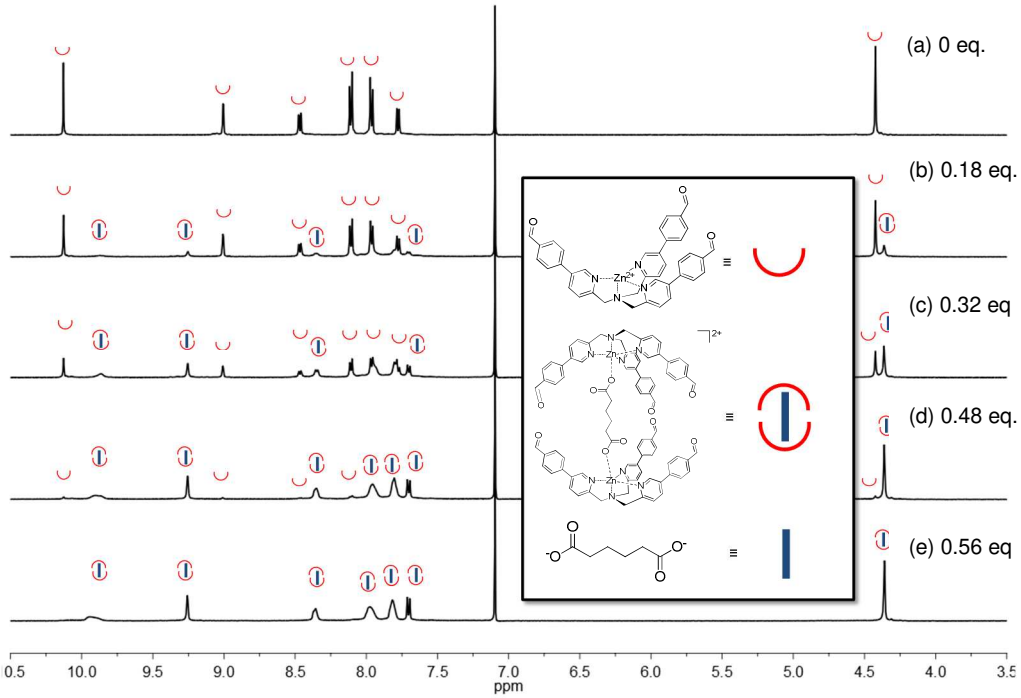

Figure A9. **^{1}H NMR Binding constant determination experiments** Addition of adipate to complex **1** in CD_3CN. The red semicircle indicates complex **1** while the blue stick indicates the dicarboxylate **C_6**. a) Complex **1** (0.001 M). b-d) Addition of sub-stoichiometric amounts (0.1-0.4 equiv) of **adipate** results in the formation of a new species that is corresponding with the two **TPMA** units preorganized by the **adipate**. (e) Addition of 0.56 equiv. of adipate shifts completely the system to the new species **C_6@S_5**. The integration of the final system signals are compatible with the illustrated molecule.The peak at 7.21 ppm corresponds to the internal standard *p*-xylene.

A1.6 Semiempirical PM6 Calculations

Semiempirical PM6 calculations have been performed for the series of the filled cages. Any cage has been initially minimized with the diacid in *all-anti* conformation at the PM6 level using Gaussian 09.[3] The obtained structure has been used as a starting point for a conformer distribution search using Spartan 16.[4] During the search the heavy atoms of the cage were frozen. The best structure from the conformational search has been optimized using semiempirical PM6 calculations using Gaussian 09.

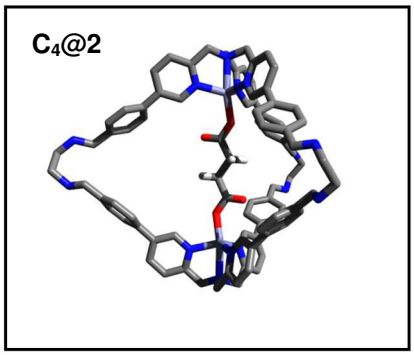

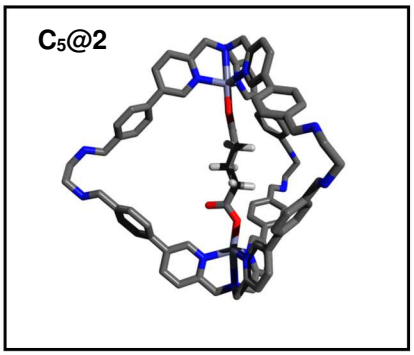

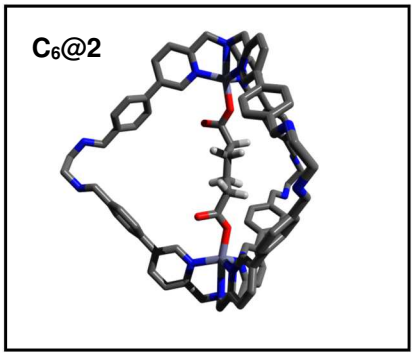

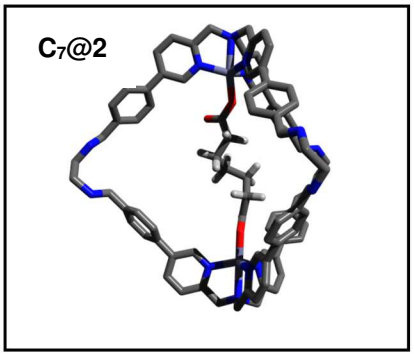

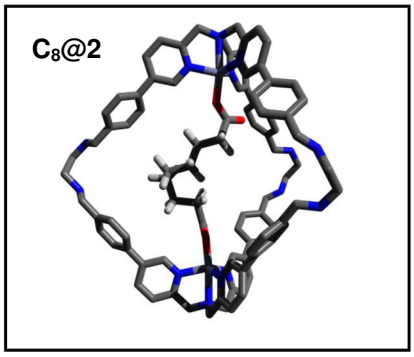

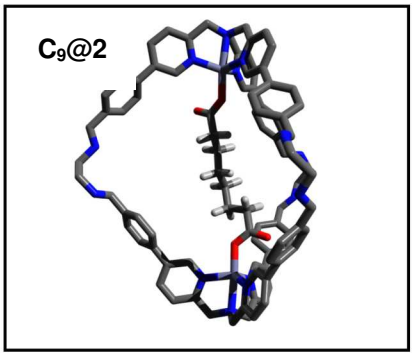

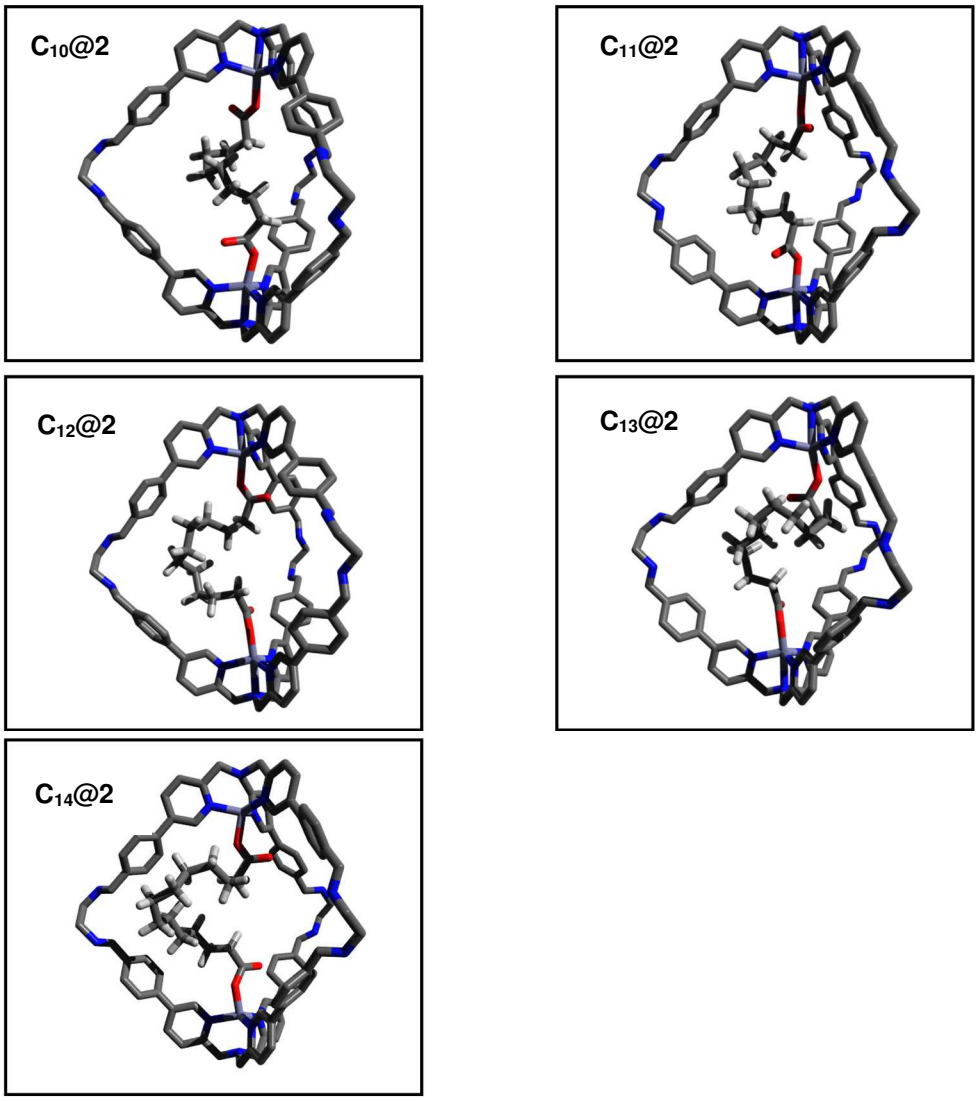

Figure A10. PM6 minimized structures for the inclusion complex **C_n@2** for the whole series ranging from **C_4@2** to **C_{14}@2**.

A1.7 Assembly Experiment

To 500 µl (1.0 µmol) of a solution 0.002 M of complex **1** in CD_3CN, 20 µl (0.24 µmol) of a solution 0.012 M in CD_3CN of *p*-xylene, 50 µl (0.5 µmol) of a solution 0.01 M in CD_3CN of diacid $\mathbf{C_n}$ and 75 µl (1.5 µmol) of a solution 0.02 M in CD_3CN of ethylendiamine were added in a NMR tube. The mixture was monitored at 298 K *via* ^1H NMR. Initial rates have been calculated integrating characteristic signals up to 20% conversion. Blank is the reaction without the acid. In the case of a monocarboxylic acid (hexanoic acid) rate of formation is 2.8 times faster than the case of the empy cage (blank). The kinetic experiments have been carried out at least two times.

Diacid	v ($M*s^{-1}$)	±σ ($M*s^{-1}$)	Relative rate of Assembly (v_{Cn}/v_{blank})
C_4	0.043	0.006	3.4
C_5	0.033	0.005	2.6
C_6	0.106	0.006	8.5
C_7	0.079	0.005	6.3
C_8	0.142	0.011	11.3
C_9	0.077	0.005	6.2
C_{10}	0.133	0.006	10.7
C_{11}	0.082	0.006	6.6
C_{12}	0.091	0.006	7.3
C_{13}	0.075	0.005	6.0
C_{14}	0.040	0.003	3.2
Blank	0.013	0.003	1.0
Hexanoic Acid	0.034	0.004	2.8

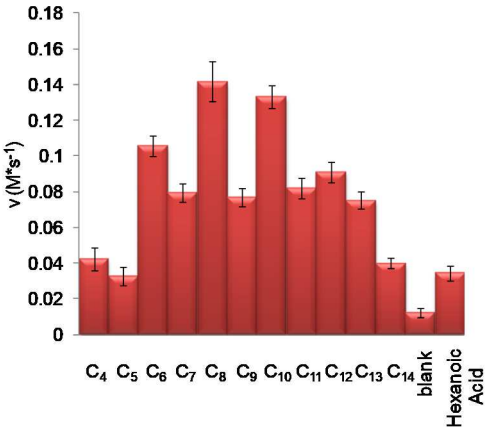

Figure A11. Assembly rate of each inclusion complex $\mathbf{C_n@2}$ for the whole serie ranging from $\mathbf{C_4@2}$ to $\mathbf{C_{14}@2}$.

A1.8 Disassembly Experiment

To 500 µl (0.25 µmol) of a solution 0.5 mM of **C_n@2** in CD_3CN and 20 µl (0.24 µmol) of a solution 0.012 M in CD_3CN of *p*-xylene, 250 µl of D_2O were added in a NMR tube. The mixture was monitored at 298 K *via* ^{1}H-NMR. Initial rate has been calculated integrating characteristic signals up to 20% conversion. In the case of a monocarboxylic acid (hexanoic acid) relative rate of hydrolysis is 0.7 time slower than the case of the empy cage (blank). The kinetic experiments have been carried out at least two times.

Diacid	v' ($M*s^{-1}$)	±σ ($M*s^{-1}$)	Relative rate of Disassembly (v'_{Cn}/v'_{blank})
C_4	0.023	0.002	0.3
C_5	0.024	0.002	0.4
C_6	0.053	0.003	0.8
C_7	0.057	0.004	0.9
C_8	0.063	0.004	1.0
C_9	0.065	0.003	1.0
C_{10}	0.087	0.004	1.4
C_{11}	0.091	0.005	1.4
C_{12}	0.096	0.005	1.5
C_{13}	0.128	0.007	2.0
C_{14}	0.132	0.007	2.1
Blank	0.063	0.002	1.0
Hexanoic Acid	0.047	0.003	0.7

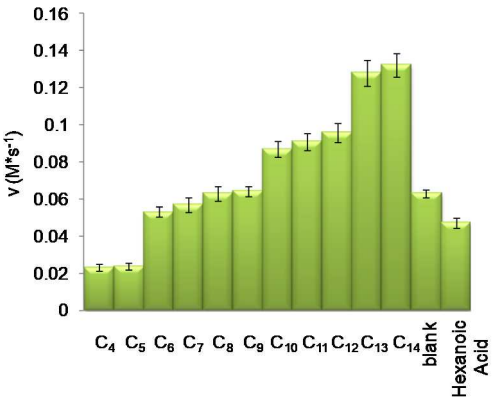

Figure A12. Disassembly rate of each inclusion complex **C_n@2** for the whole serie ranging from **C_4@2** to **C_{14}@2.**

A1.9 Trigger Disassembly Experiment

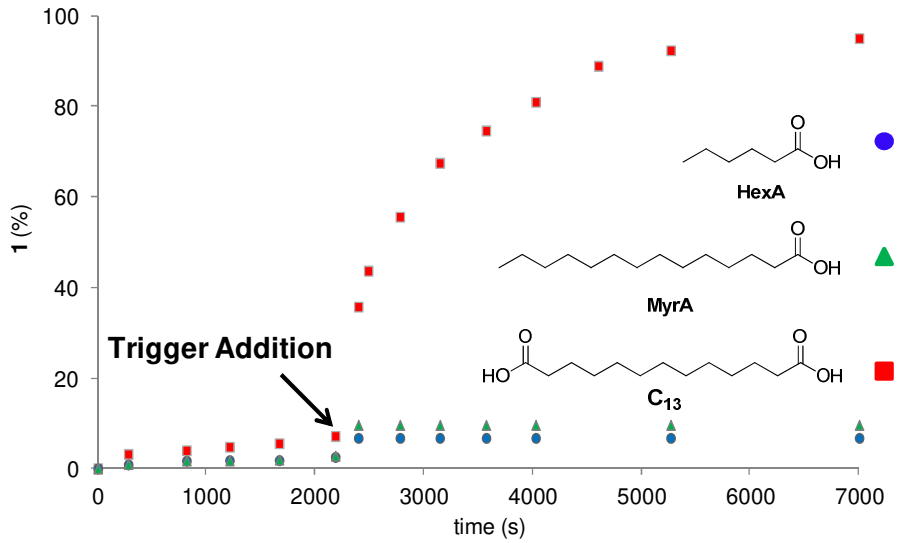

Figure A13. Kinetic profile for the hydrolysis of cage **2** in the presence of $\mathbf{C_5}$. The addition of $\mathbf{C_{13}}$ (red square) increases the dissasembly while addition of hexanoic acid **HexA** (blue circle) and **MyrA** (green triangle) does not increase the disassembly rate. $[\mathbf{C_n@2}]_0$ = 0.30 mM, $[D_2O]_0$ = 16 M. In the case of a monocarboxylic acids $[\mathbf{MirA}]_0$ = 0.60 mM or $[\mathbf{HexA}]_0$ = 0.60 mM. In the case of dicarboxylic acids $[\mathbf{C_{13}}]_0$ = 0.30 mM.

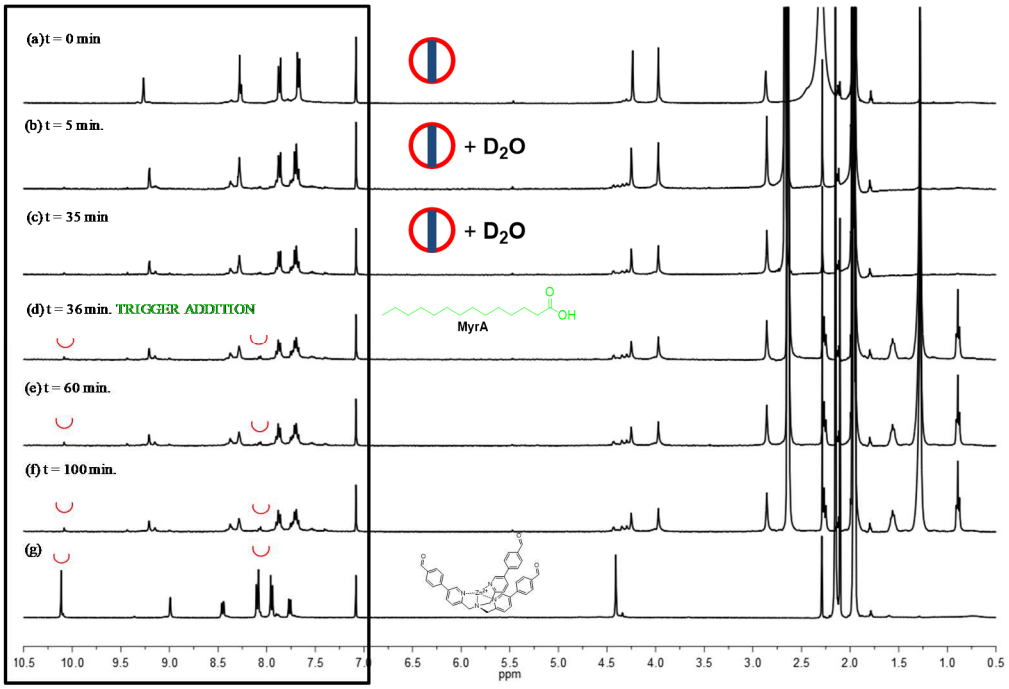

Figure A14. **^{1}H NMR Trigger Disassembly Experiment with Myristic acid (MyrA).** Cage disassembly starting from cage **C_5@2** (red cyrcle filled with blue stick) in CD_3CN. a) Cage **C_5@2** (0.30 mM). b) Addition of D_2O (16 M), c) after 35 minutes the cage is disassasembled less than 10 % NMR yield. d) Addition of the trigger **MyrA** (0.60 mM). e); f) after the trigger addition complex **1** is formed (the signals with the red semicircle are related to the aldheyde protons and the aromatic protons system of the complex) less than 10% NMR yield even after 100 minutes. g) Complex **1** as reference. The peak at 7.21 ppm corresponds to the internal standard *p*-xylene.

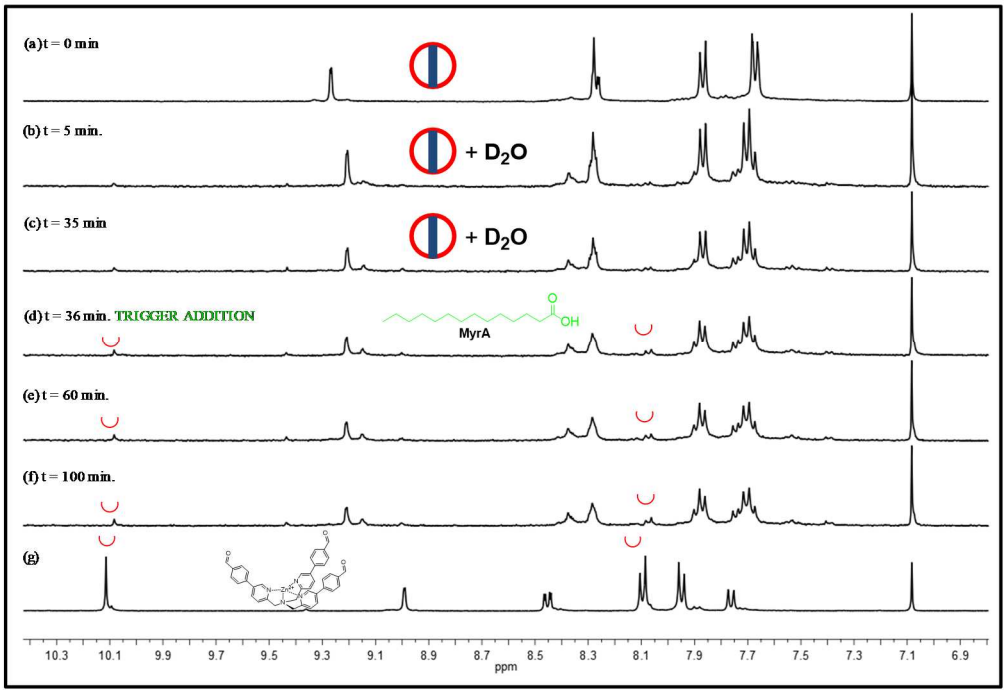

Figure A15. **^{1}H NMR Trigger Disassembly Experiment with Myristic acid (MyrA).** Cage disassembly starting from cage **C_5@2** (red cyrcle filled with blue stick) in CD_3CN. a) Cage **C_5@2** (0.30 mM). b) Addition of D_2O (16 M), c) after 35 minutes the cage is disassasembled less than 10 % NMR yield. d) Addition of the trigger **MyrA** (0.60 mM)**.** e); f) after the trigger addition complex **1** is formed (the signals with the red semicircle are related to the aldheyde protons and the aromatic protons system of the complex) less than 10% NMR yield even after 100 minutes. g) Complex **1** as reference. The peak at 7.21 ppm corresponds to the internal standard *p*-xylene. The moderate shift of the proton of complex **1** in (b-f) are due to the presence of a large amount of D_2O during the reaction.

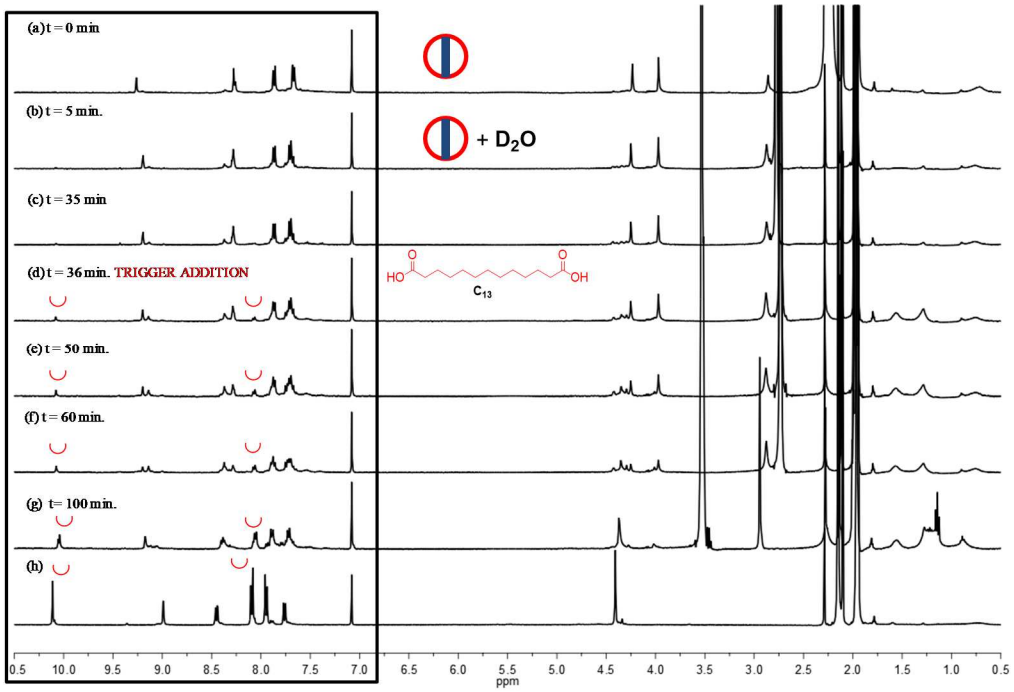

Figure A16. **^{1}H NMR Trigger Disassembly Experiment with C_{13}.** Cage disassembly starting from cage **C_5@2** (red cyrcle filled with blue stick) in CD_3CN. a) Cage **C_5@2** (0.30 mM). b) Addition of D_2O (16 M), c) after 35 minutes the cage is disassasembled less than 10 % NMR yield. d) Addition of the trigger **C_{13}** (0.30 mM) results in the formation of the starting complex **1** (the signals with the red semicircle are related to the aldheyde protons and the aromatic protons system of the complex). e-g) The system is shifted to **1** within one hour after the addition with 95% of NMR yield. h) Complex **1** as reference The peak at 7.21 ppm corresponds to the internal standard *p*-xylene.

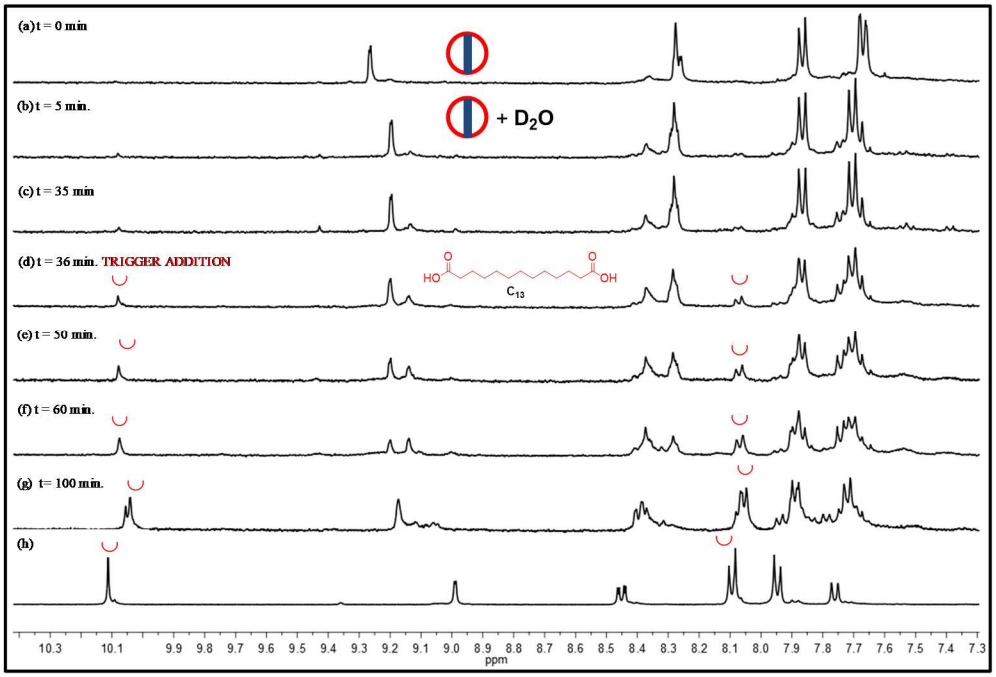

Figure A17. **^{1}H NMR Trigger Disassembly Experiment with C_{13}.** Cage disassembly starting from cage **C_5@2** (red cyrcle filled with blue stick) in CD_3CN. a) Cage **C_5@2** (0.30 mM). b) Addition of D_2O (16 M), c) after 35 minutes the cage is disassasembled less than 10 % NMR yield. d) Addition of the trigger **C_{13}** (0.30 mM) results in the formation of the starting complex **1** (the signals with the red semicircle are related to the aldheyde protons and the aromatic protons system of the complex). e-g) The system is shifted to **1** within one hour after the addition with 95% of NMR yield. h) Complex **1** as reference. The peak at 7.21 ppm corresponds to the internal standard *p*-xylene. The moderate shift of the proton of complex **1** in (b-g) are due to the presence of a large amount of D_2O during the reaction.

A1.10 Cage 2

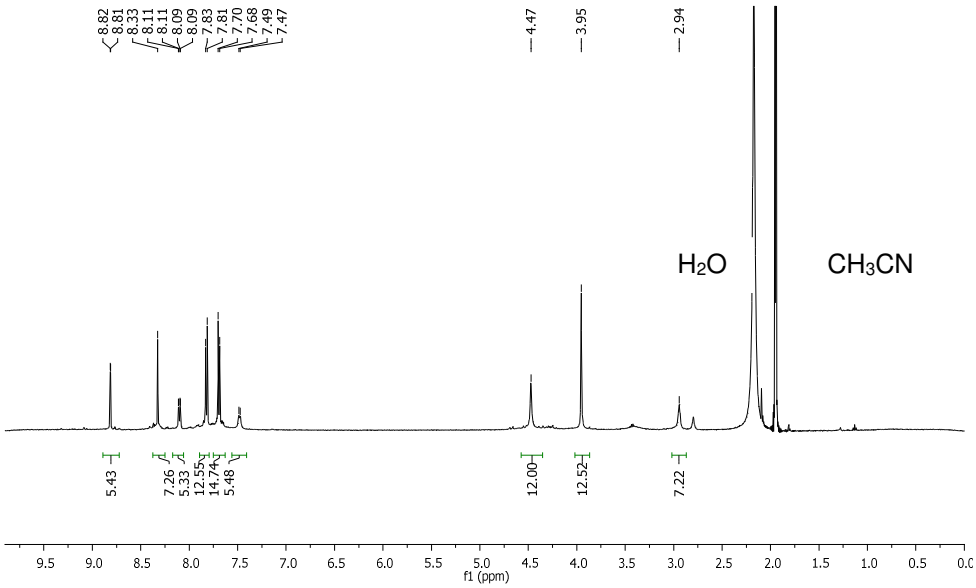

Figure A18. ^{1}H NMR spectrum (400 MHz, 301 K, CD_3CN)of cage **2**.

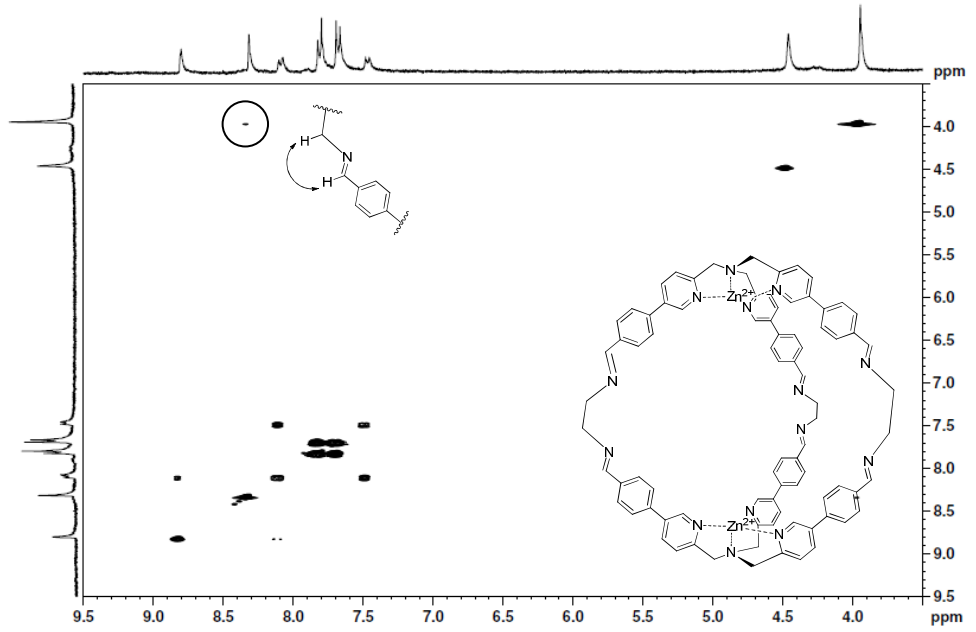

Figure A19. ^{1}H-^{1}H COSY spectrum (400 MHz, 301 K, CD_3CN)of cage **2**.

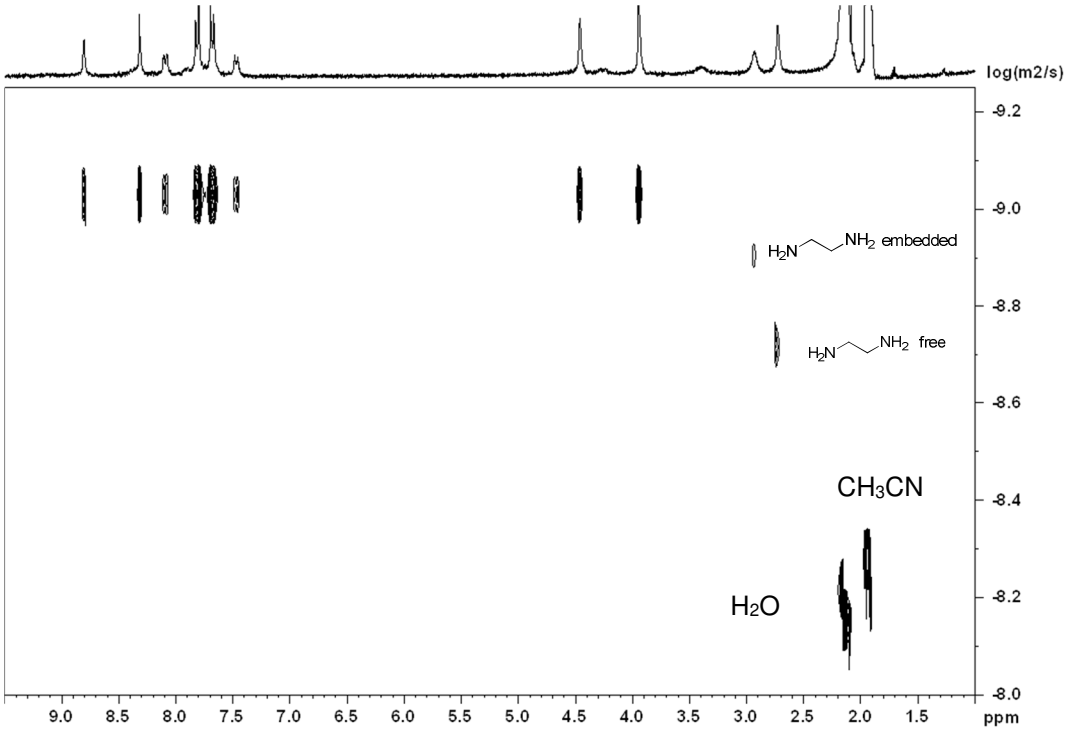

Figure A20. DOSY spectrum (400 MHz, 301 K, CD_3CN) of **2**.The diffusion coefficient for the molecular cage **2** was calculated to be 7.9 x 10^{-10} m^2 s^{-1}, corresponding to a hydrodynamic radius (r_H) of 10.2 Á. The diffusion coefficient for the ehtylendiamine embedded into cage **2** was calculated to be 1.0 x 10^{-9} m^2 s^{-1}, corresponding to a hydrodynamic radius (r_H) of 8.2 Á.The diffusion coefficient for the ehtylendiamine protonated in solution was calculated to be 2.8 x 10^{-10} m^2 s^{-1}, corresponding to a hydrodynamic radius (r_H) of 3.6 Á. All the hydrodynamic radius have been calculated by using the Stokes-Einstein equation.[5]

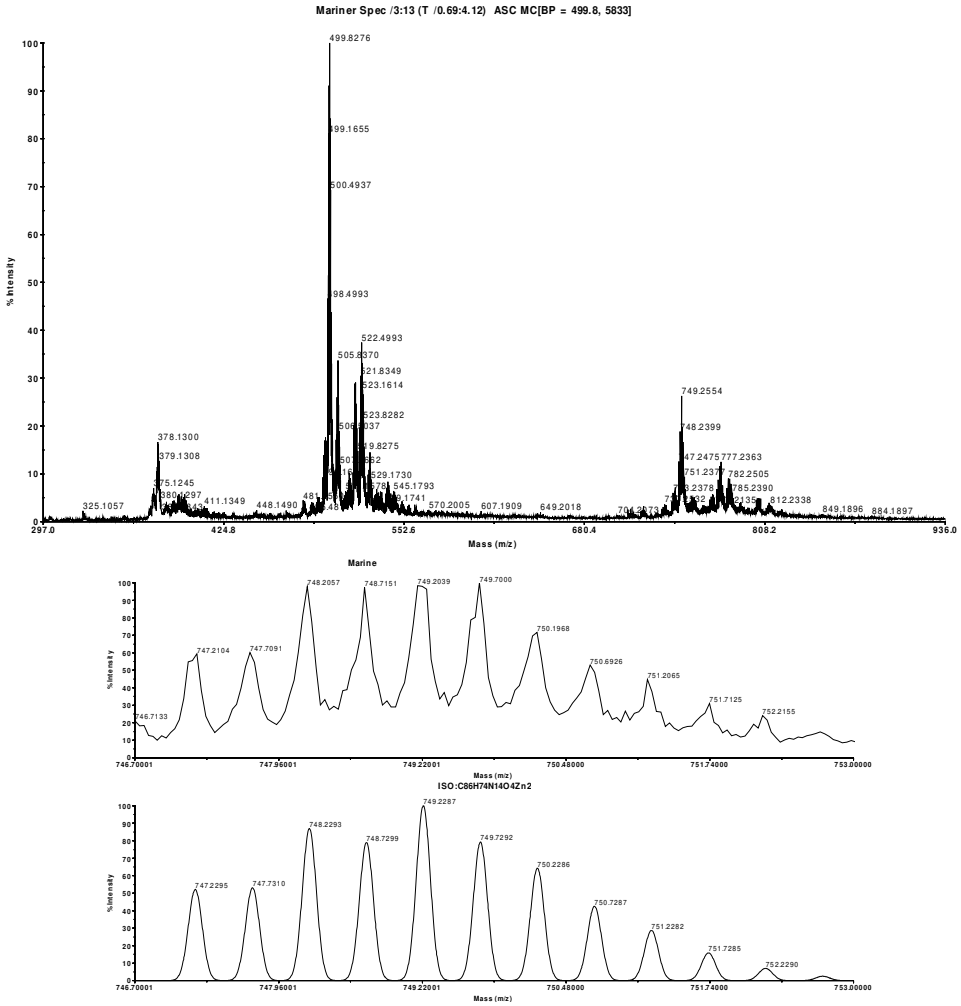

Figure A21. Experimental (top) and calculated (bottom) isotopic distribution in the HRMS (ESI-TOF) of **2** corresponding to $[C_{84}H_{72}N_{14}Zn_2+2HCOO]^{2+}$.

A1.11 C_8@2

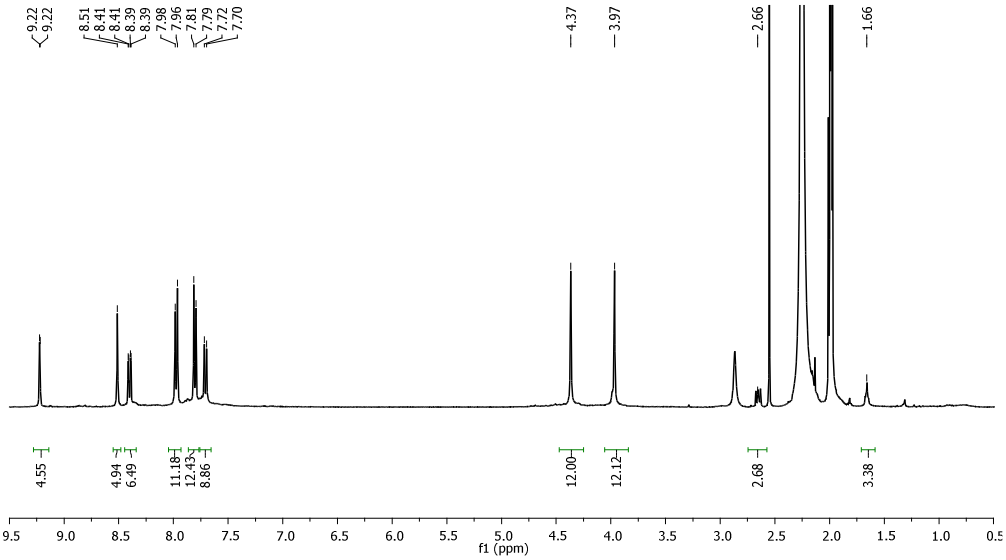

Figure A22. ^{1}H NMR (400 MHz, 301 K, CD_3CN) of inclusion complex **C_8@2**.

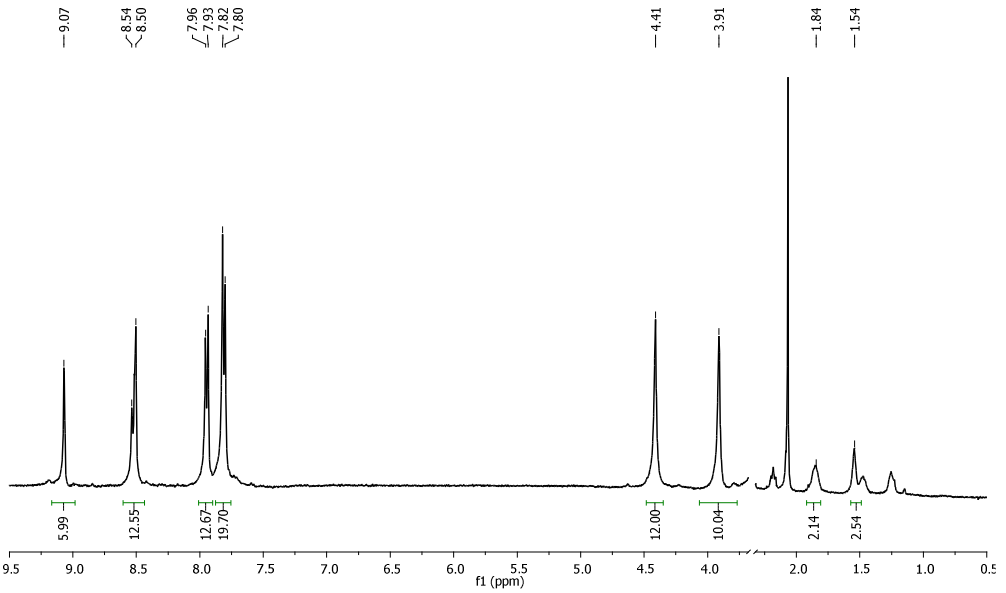

Figure A23. ^{1}H NMR (400 MHz, 301 K, DMSO-d_6) of inclusion complex **C_8@2**.

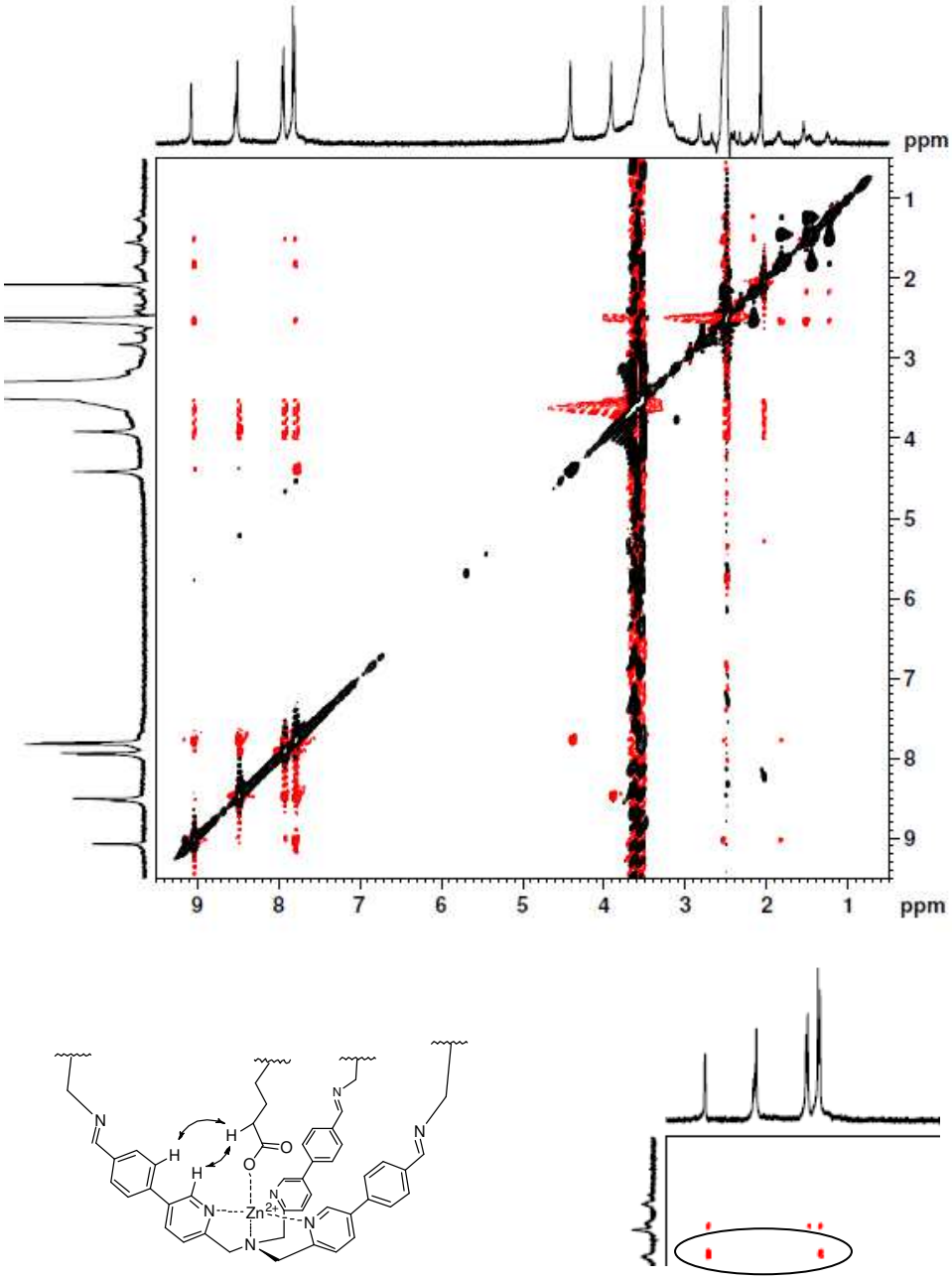

Figure A24.^{1}H-^{1}H ROESY spectrum (400 MHz, 301 K, DMSO-d_6) of inclusion complex **C$_8$@2**.

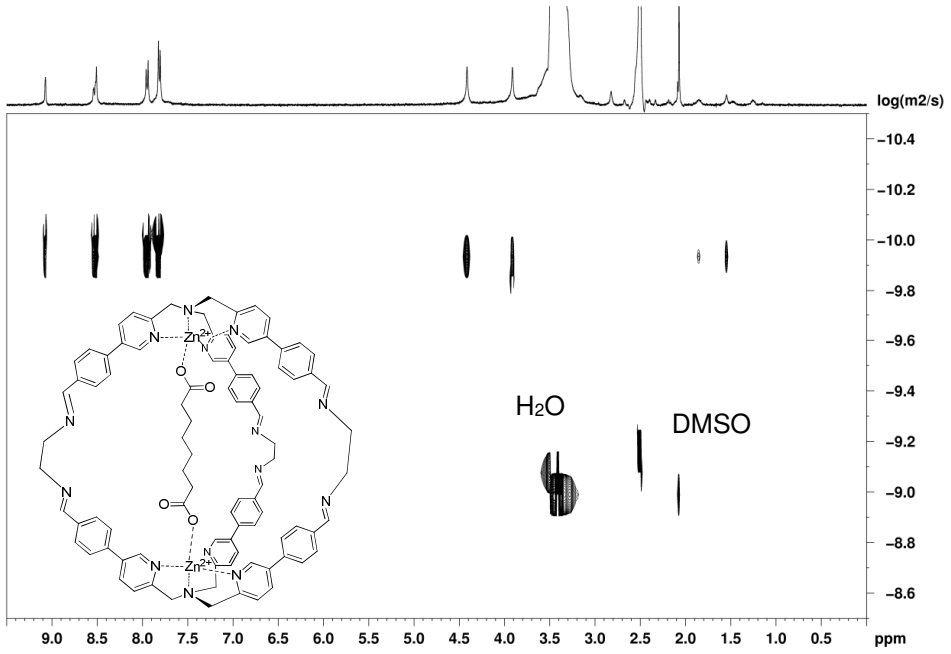

Figure A25. DOSY spectrum (400 MHz, 301 K, DMSO-d_6) of **C_8@2**.The diffusion coefficient was calculated to be 1.0 x 10^{-10} m^2 s^{-1}, corresponding to a hydrodynamic radius (r_H) of 12.1 Å for **C_8@2**,as calculated by using the Stokes-Einstein equation.[5]

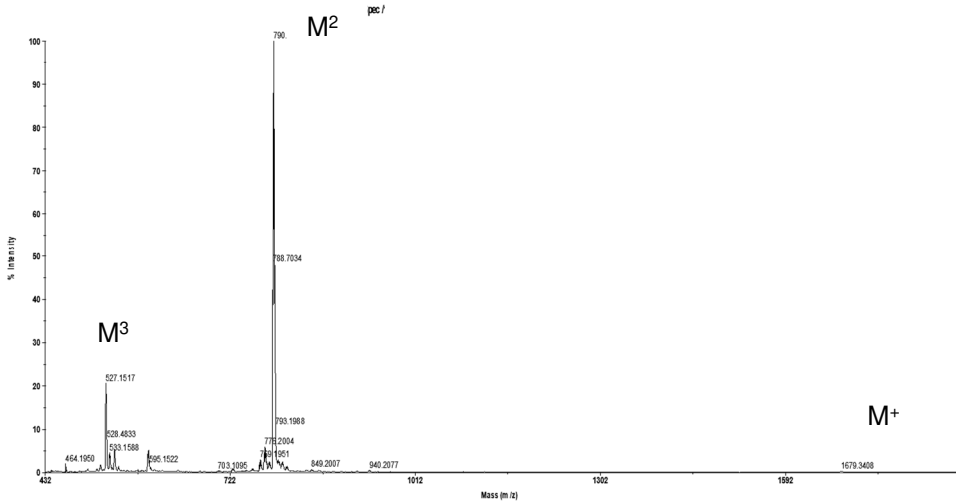

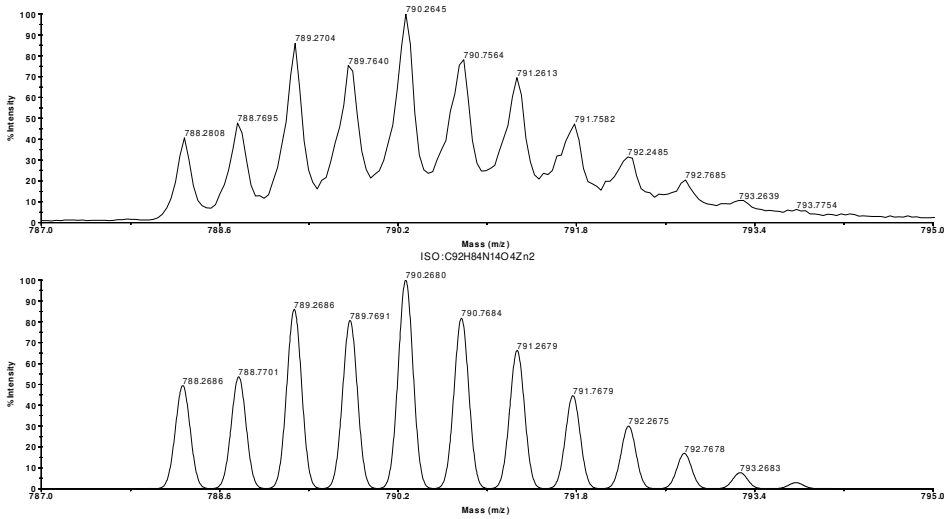

Figure A26. HRMS (ESI-TOF) of inclusion complex **C_8@2**. Experimental (top) and calculated (bottom) isotopic distribution in the HRMS (ESI-TOF) of **C_8@2** corresponding to $[C_{84}H_{72}N_{14}Zn_2+C_8H_{12}O_4]^{2+}$.

5 References

[1] M. K. Chantooni, I. M. Kolthoff, *J. Phys. Chem.* **1975**, *79*, 1176-1182.

[2] M. M. Mader, P. A. Bartlett, *Chem. Rev.* **1997**, *97*, 1281-1302.

[3] [Gaussian 09 Rev. D.01, M. J. Frisch, G. W. Trucks, H. B. Schlegel, G. E. Scuseria, M. A. Robb, J. R.Cheeseman, G. Scalmani, V. Barone, B. Mennucci, G. A. Petersson, H. Nakatsuji, M. Caricato, X. Li, H. P.Hratchian, A. F. Izmaylov, J. Bloino, G. Zheng, J. L. Sonnenberg, M. Hada, M. Ehara, K. Toyota, R. Fukuda, J. Hasegawa, M. Ishida, T. Nakajima, Y. Honda, O. Kitao, H. Nakai, T. Vreven, J. A. Montgomery Jr., J. E. Peralta, F. Ogliaro, M. J. Bearpark, J. Heyd, E. N. Brothers, K. N. Kudin, V. N. Staroverov, R. Kobayashi, J. Normand, K. Raghavachari, A. P. Rendell, J. C. Burant, S. S. Iyengar, J. Tomasi, M. Cossi, N. Rega, N. J. Millam, M. Klene, J. E. Knox, J. B. Cross, V. Bakken, C. Adamo, J. Jaramillo, R. Gomperts, R. E. Stratmann, O. Yazyev, A. J. Austin, R. Cammi, C. Pomelli, J. W. Ochterski, R. L. Martin, K. Morokuma, V. G. Zakrzewski, G. A. Voth, P. Salvador, J. J. Dannenberg, S. Dapprich, A. D. Daniels, Ö. Farkas, J. B. Foresman, J. V. Ortiz, J. Cioslowski, D. J. Fox, Gaussian, Inc., Wallingford, CT, USA, 2009.

[4] Spartan 16, Wavefunction, Inc.

[5] R. Evans, Z. Deng, A. K. Rogerson, A. S. McLachlan, J. J. Richards, M. Nilsson, G. A. Morris, *Angew. Chemie Int. Ed.* **2013**, *52*, 3199-3202.

Appendix to Chapter 2

A 2.1 ESI-MS Competition experiments C_n@1a-h•M

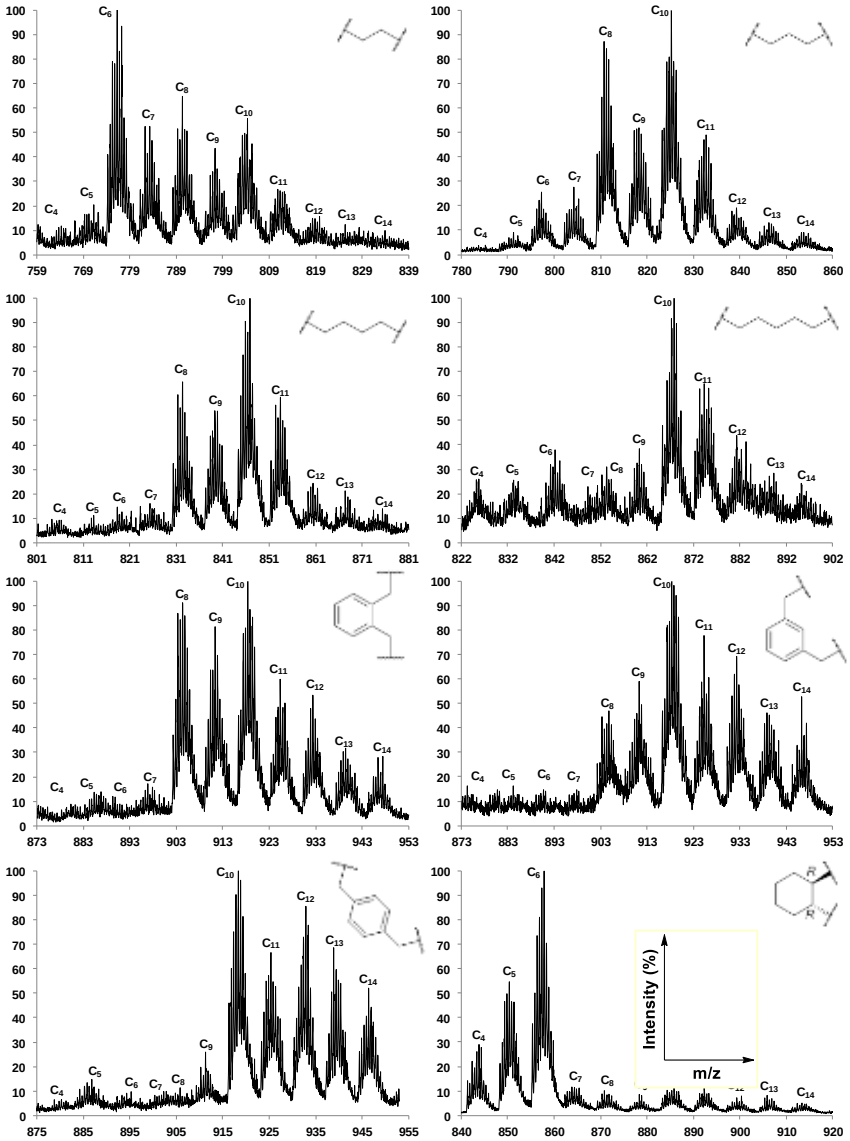

Figure A1 High resolution electrospray ionization mass spectrometry HRMS (ESI-TOF) selectivity profiles of the inclusion competition experiments for **C_n@1a-h•Zn**. **C_n** symbol represent the corresponding inclusion complex **C_n@1a-h•Zn.**

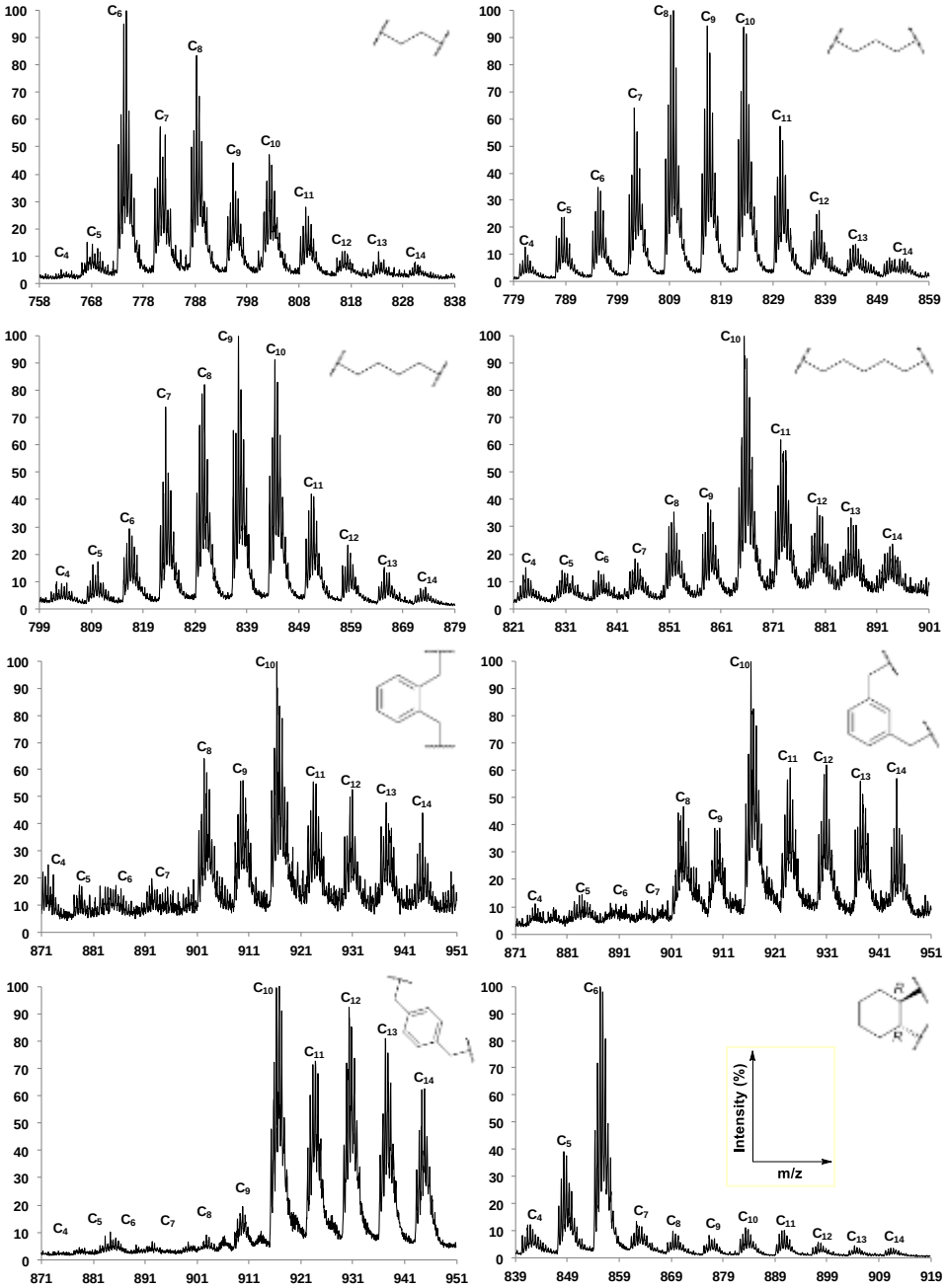

Figure A2 High reolution electrospray ionization mass spectrometry HRMS (ESI-TOF) selectivity profiles of the inclusion competition experiments for **C_n@1a-h•Cu**. **C_n** symbol represent the corresponding inclusion complex **C_n@1a-h•Cu.**

A 2.2 Cage structure analysis. Comparison of experimental hydrodynamic radius obtained *via* DOSY NMR and theoretical values obtained with semiempirical PM6 calculations

Cages **C_n@1a-h•Zn** described in section 2.2 has been characterized with DOSY NMR in order to evaluate how a modification of the diamine linker is reflected into the size of the cages. The diffusion coefficient for each cage and the corresponding hydrodynamic radius (r_H) was calculated by using the Stokes-Einstein equation.[1] This data have been compared with the values obtained by semi-empirical PM6 calculations (Gaussian 09).[2] Theoretical hydrodynamic radius values have been estimated measuring the distance between the two tertiary amine nitrogen atom of the calculated structures (Figure S4). and compared with the experimental hydrodynamic radius obtained *via* DOSY NMR.(Table S1).

Cage	r_H PM6-calc. (Å)	r_H DOSY-exp (Å)
C_6@1a•Zn	9.5	9.0
C_8@1b•Zn	9.6	10.0
C_{10}@1c•Zn	10.6	12.0
C_{10}@1d•Zn	10.6	12.5
C_8@1e•Zn	10.5	10.3
C_{10}@1f•Zn	10.9	10.6
C_{10}@1g•Zn	10.9	11.7
C_6@1h•Zn	8.1	8.6

Table A1 Experimental and theoretical hydrodynamic radius (r_H) of the **C_n@1a-h•Zn** cage series.

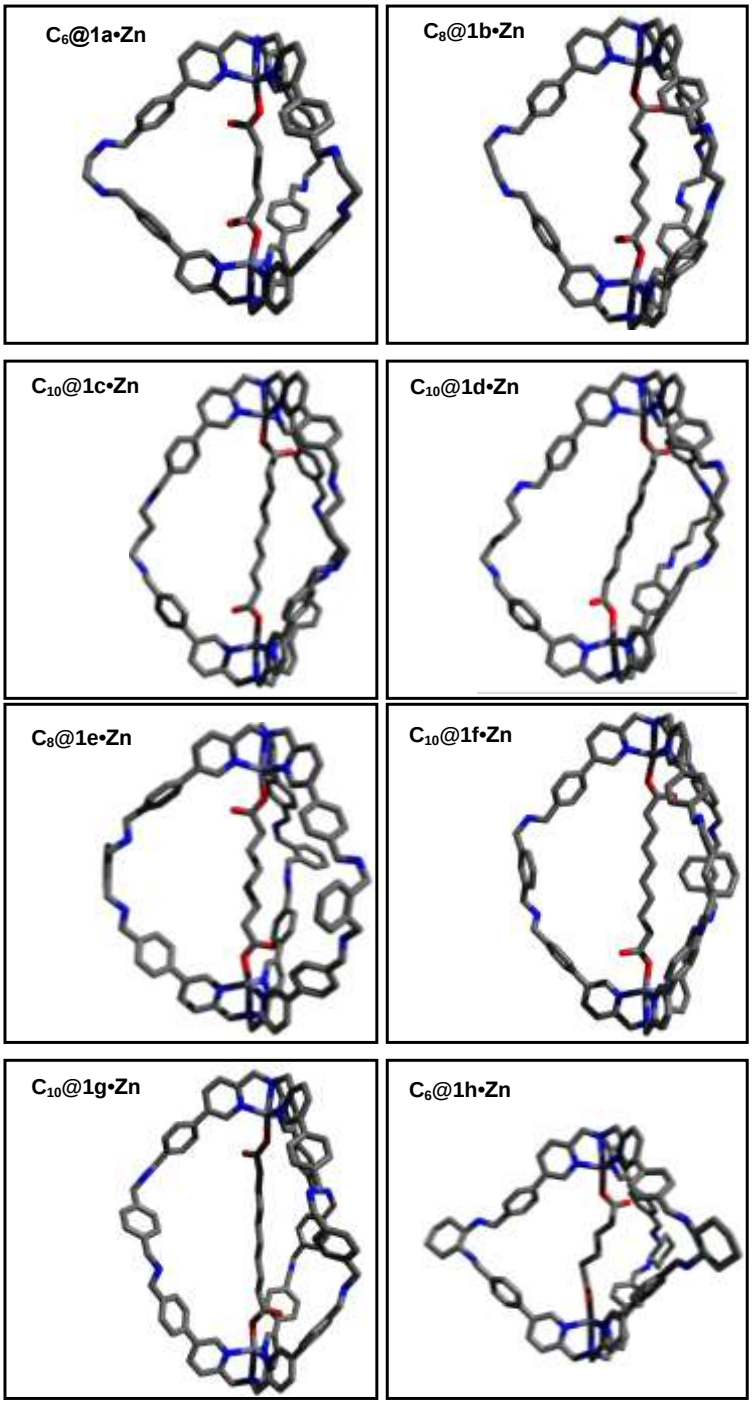

Figure A3 PM6 minimized structures for the cage series **C_n@1a-h•Zn**.

A 2.3 Correlation between ^{1}H NMR and MS experiment for the C_n@1a•Zn series

For each recognition profile, the intensity of the *m/z* monoisotopic peak (I_{Cn}) has been converted to a selectivity factor ($I_{Cn}/\sum I_{Cn}$). We thus correlates these relative values as the probability that a single cage could be occupied by a guest of the series (p_{Cn}). This allows to obtain the relative energy of each structure in solution (ΔΔG) using the Gibbs free energy equation. The error is calculated from the standard deviation values obtained taking three different point in each cluster corresponding to an inclusion complex **C_n@1a•Zn.**

$$\Delta\Delta G = -RT \ln p_{Cn}$$

Cage	^{1}H NMR ΔG (KJ/mol)	ESI-MS ΔΔG (KJ/mol)
C_4@1a•Zn	-23.75±0.20	7.33±1.06
C_5@1a•Zn	-24.16±0.24	6.64±0.87
C_6@1a•Zn	-25.85±0.24	3.78±0.13
C_7@1a•Zn	-24.92±0.37	5.15±0.14
C_8@1a•Zn	-25.96±0.18	4.28±0.21
C_9@1a•Zn	-23.46±0.40	5.99±0.28
C_{10}@1a•Zn	-23.99±0.41	5.58±0.44
C_{11}@1a•Zn	-22.37±0.37	6.98±0.72
C_{12}@1a•Zn	-22.64±0.20	8.05±0.70
C_{13}@1a•Zn	-22.18±0.27	8.48±1.23
C_{14}@1a•Zn	-21.47±0.42	9.94±1.01

Table A2l ΔG values obtained from binding constant determination of diacid series towards cage **1a•Zn**. **C_n@1a-h•Zn** ΔΔG values obtained from the intensity of ESI-MS peaks related to the series **C_n@1a•Zn**.

A 2.4 X-ray analysis

Single crystal X-ray data for **2•Cu, 2•Zn** and **C_{10}@2b•Cu** were collected with Agilent Super-Nova dual source wavelength diffractometer with an Atlas CCD detector using multilayer optics monochromatized Cu- Kα (λ = 1.54184 Å) radiation. The data collection and reduction for **2•Cu, 2•Zn** and **C_{10}@1b•Cu** were performed using the program *CrysAlisPro*,[3] the intensities are corrected for Gaussian face index absorption correction method.[4] All the structures were solved with direct methods (*SHELXS*)[4] and refined by full-matrix least squares on F^2 using the *OLEX2*,[6] which utilizes the *SHELXL*-2013 module.[5] No attempt was made to locate the hydrogens for some solvent molecules, and for some hydrogen atoms involved in hydrogen bonds were introduced from difference Fourier maps. Constraints (EADP) and restraints (DFIX and ISOR) are used where appropriate, and for disordered solvent molecules.

A 2.4.1 Crystal Data for 2•Cu

$C_{53}H_{57}Cl_2CuN_5O_{17}$, Mr = 1170.47gmol^{-1}, Crystal dimensions: 0.20 x 0.15 x 0.11 mm, triclinic, space group *P*-1, *a* = 11.0687(3) Å, *b* = 16.0785(5) Å, *c* = 16.3022(5) Å, α = 101.371(3)º, τ = 91.084(3)º, γ = 109.650(3)°, V = 2667.23(16) Å^3, Z = 2, D_c = 1.457 Mg/m^3, μ= 2.158 mm^{-1}, F000 = 1218, T = 124.44(10) K, θ range for cell measurement: 4.2-73.0°, R_1 = 0.0417 (0.0494), wR = 0.1084 (0.1161), R_{int} = 0.0324, 15416 reflections are measured with 9333 independent reflections of which 8026 are $I_o>2\sigma(I_o)$, 741 parameters, 48 restraints, GooF = 1.029, 0.496<Δρ<-0.372 e/Å^3. CCDC 1424389 contains the supplementary data for this structure.

A 2.4.2 Crystal Data for 2•Zn

$C_{85}H_{77}Cl_4N_9O_{25}SZn_2$, Mr = 1929.15gmol^{-1}, Crystal dimensions: 0.19 x 0.16 x 0.05 mm, triclinic, space group *P*-1, *a* = 13.5765(9) Å, *b* = 13.7524(13) Å, *c* = 27.153(2) Å, α = 77.707(8)º, τ = 78.655(6)º, γ = 71.136(7)°, V = 4642.3(7) Å^3, Z = 2, D_c = 1.380 Mg/m^3, μ= 2.557 mm^{-1}, F000 = 1988, T = 123.00(10) K, θ range for cell measurement: 3.36 - 66.75°, R_1 = 0.1384 (0.2233), wR = 0.3660 (0.4082), R_{int} = 0.1224, 30997 reflections are measured with 26511 independent reflections of which

10506 are $I_o>2\sigma(I_o)$, 1210 parameters, 95 restraints, GooF = 1.096, 1.618<Δρ<-1.110 e/Å^3. CCDC 1424390 contains the supplementary data for this structure.

A 2.4.3. Crystal Data for C_{10}@1b•Cu

$C_{105}H_{106}Cl_2Cu_2N_{18}O_{12}$, Mr = 2010.05gmol^{-1}, Crystal dimensions: 0.20 x 0.15 x 0.11 mm, triclinic, space group *P*-1, *a* = 13.2041(5) Å, *b* = 20.1922(7) Å, *c* = 21.3280(9) Å, α = 73.468(4)º, τ = 74.480(4)º, γ = 78.017(3)°, V = 5199.1(4) Å^3, Z = 2, D_c = 1.284 Mg/m^3, μ= 1.527 mm^{-1}, F000 = 2100, T = 120.00(10) K, θ range for cell measurement: 3.57-66.75°, R_1 = 0.0709 (0.1096), wR = 0.1839 (0.2040), R_{int} = 0.0632, 32997 reflections are measured with 18298 independent reflections of which 11632 are $I_o>2\sigma(I_o)$, 1327 parameters, 53 restraints, GooF = 1.053, 0.783<Δρ<-0.633e/Å^3. The alkyl chains of sebacic acid are disordered, and were modelled in two positions with 40:60% occupancy, and the distances and anisotropic displacement are also restrained for respective disordered carbon atoms. The disordered solvent molecules and some residual electrons are masked during refinement; the mask information is included in the cif file. CCDC 1424391 contains the supplementary data for this structure.

Complexes **2•Cu** and **2•Zn** crystallizes in the triclinic space group *P*-1, as shown in Figure S4a and Figure S4b. Both the complexes were crystallized from CH_3CN/dioxane as solvent conditions, however, in case of **2•Zn**, drop of DMF and DMSO were added to dissolve the precipitates. As a result, the complex **2•Zn** has two crystallographically different entities with metal centers coordinated by DMF and DMSO solvent molecules. Cu(II) has distorted trigonal pyramidal geometry (τ_5 = 0.82)[7] with an N_5 coordination environment. The two Zn(II) metal centers in **2•Zn** complex adopts N_4O coordination spheres, also revealed distorted trigonal pyramidal geometries with tau (τ_5) values of 0.86 and 0.83. All the Cu-N [1.943(2) - 2.092(2) Å][8] and Zn-N [2.036(11) - 2.226(13) Å][9] bond distances are in the typical range and are similar to previous reports. The respective crystal packing is shown in Figure A5 and A6.

C_{10}@1b•Cu system crystallizes in the triclinic P-1, a low degree symmetry space group. The cage built with two copper(II) ions carries four positive charges, counter

balanced with two non-coordinating perchlorate anions outside the cavity and an encapsulated sebacic acid $\mathbf{C_{10}}$ carrying two negative charges.

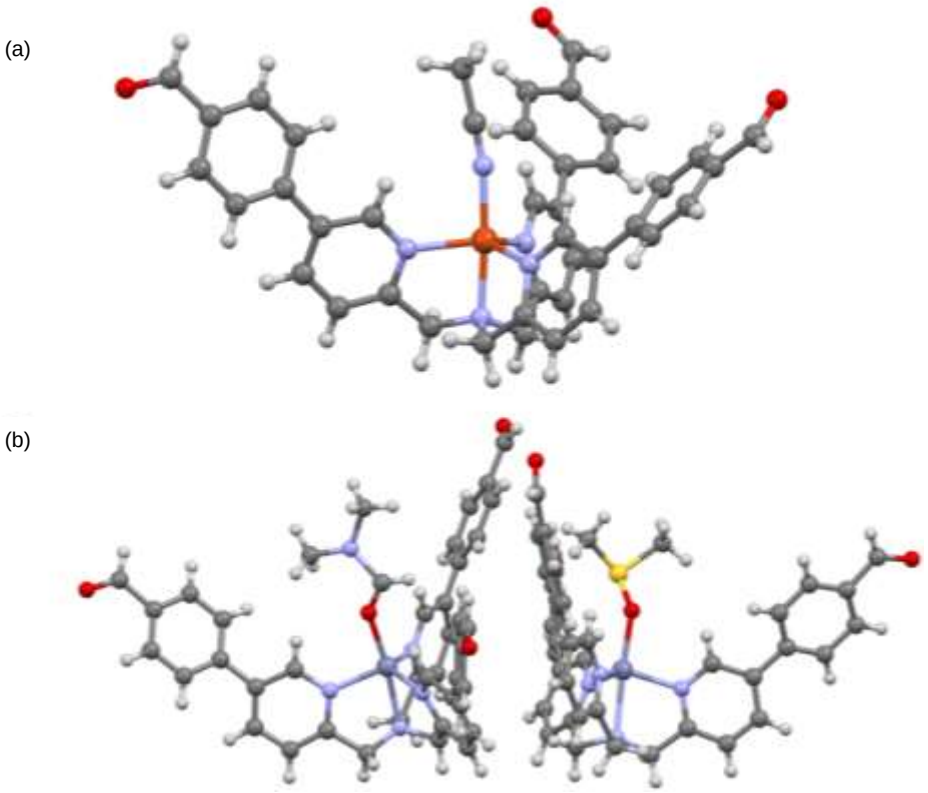

Figure A4 Ball and stick view of complexes (a) **2•Cu**, and (b) **2•Zn**. The non-coordinating perchlorate anions and solvent molecules are omitted for clarity.

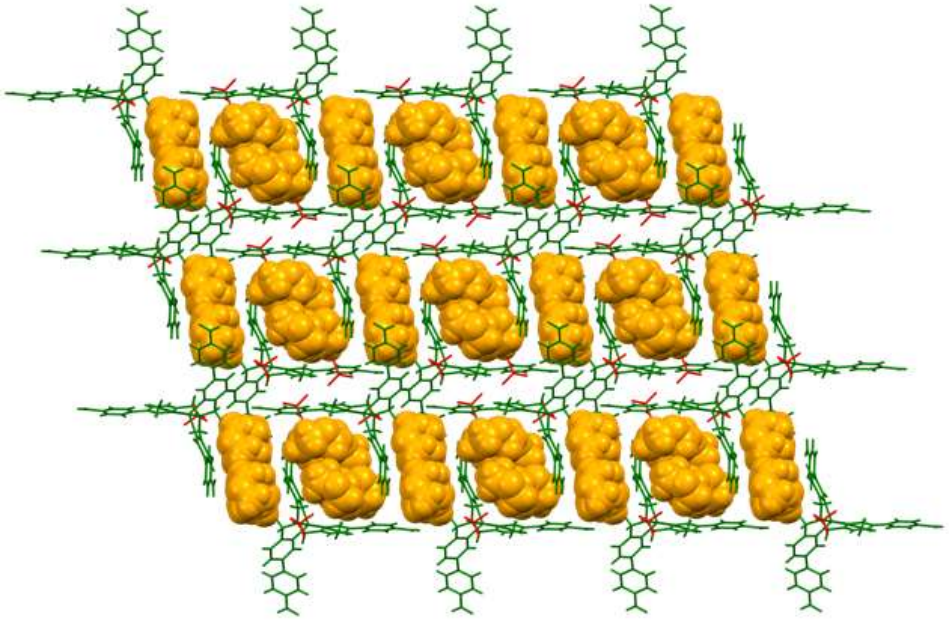

Figure A5 3-D Crystal packing of complex **2•Cu**. Representation: **2•Cu** entities in capped stick model (colored green), non-coordinating perchlorate anions in capped stick model (colored red) and dioxane solvent molecules in CPK model (colored orange).

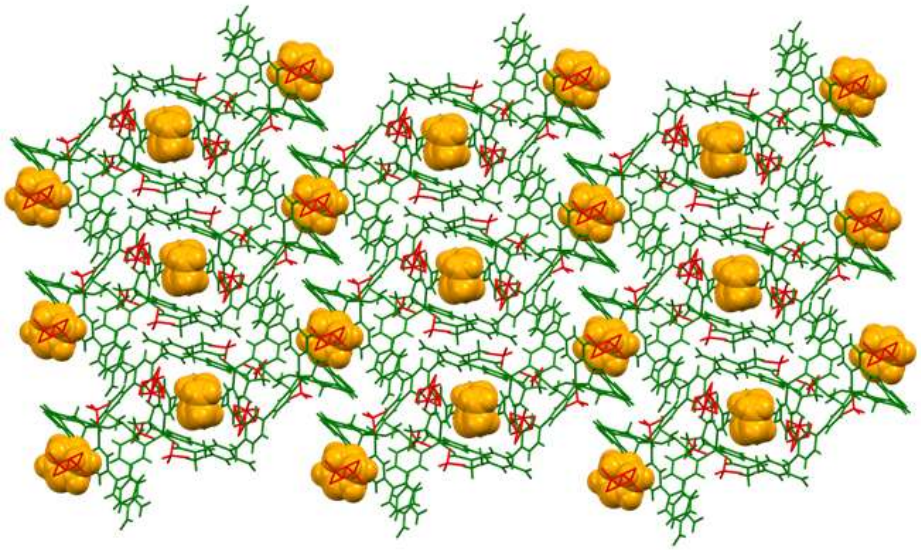

Figure A6 3-D Crystal packing of complex **2•Zn**. Representation: **2•Zn** entities in capped stick model (colored green), non-coordinating perchlorate anions in capped stick model (colored red) and dioxane solvent molecules in CPK model (colored orange).

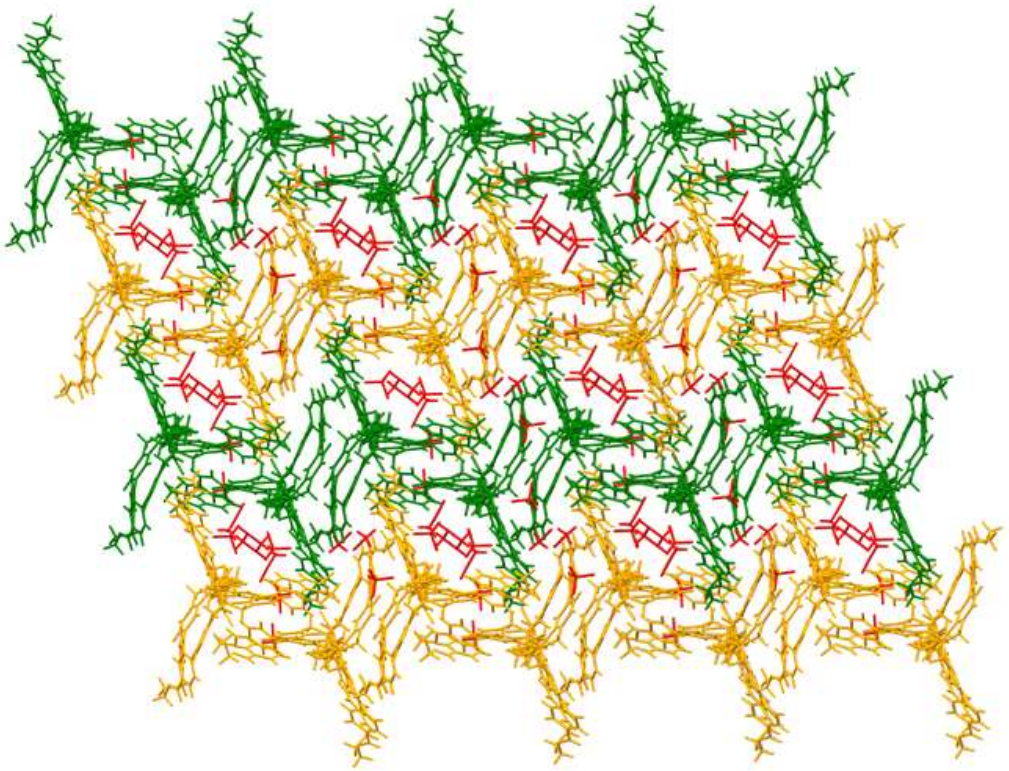

Figure A7 The 3-D Crystal packing of complex **C_{10}@1b•Cu** in capped stick model. Representation: The **C_{10}@1b•Cu** entities in capped stick model (colored green and orange), non-coordinating perchlorate anions and solvent molecules in capped stick model (colored red).

A 2.5 ^{1}H NMR and HRMS characterization

A 2.5.1 Complex 2•Cu

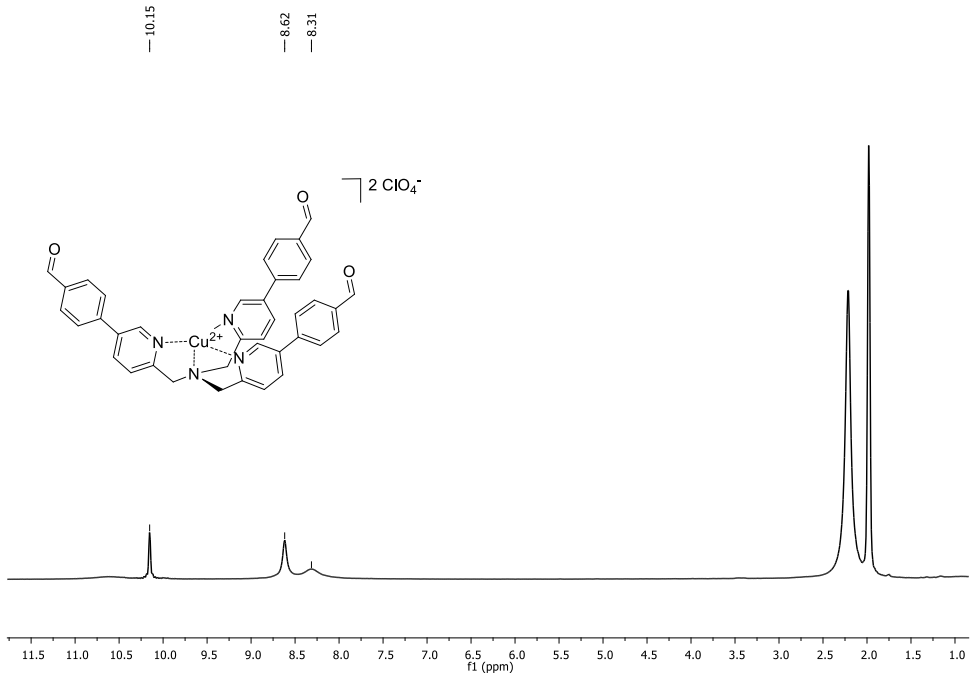

Figure A8 ^{1}H NMR spectrum (400 MHz, 301 K, CD_3CN)of complex **2•Cu.**

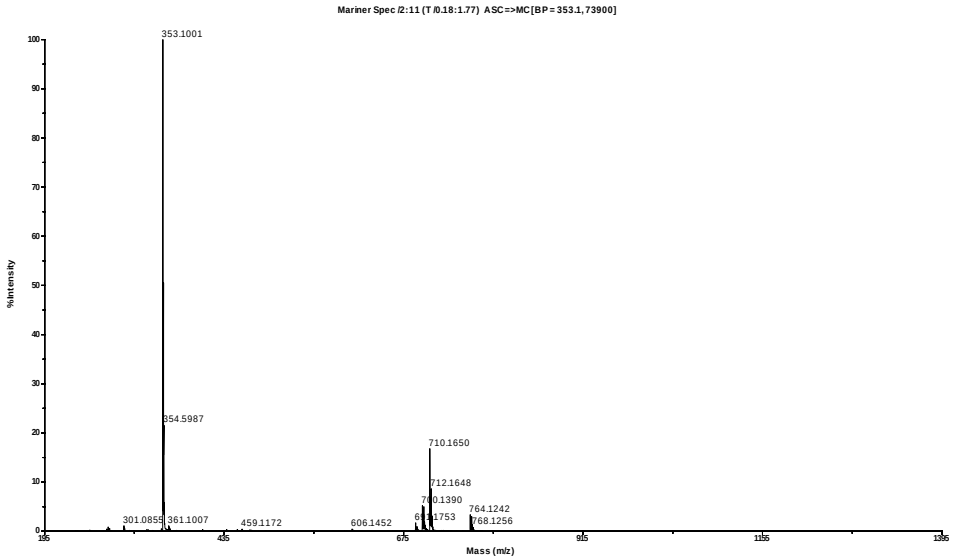

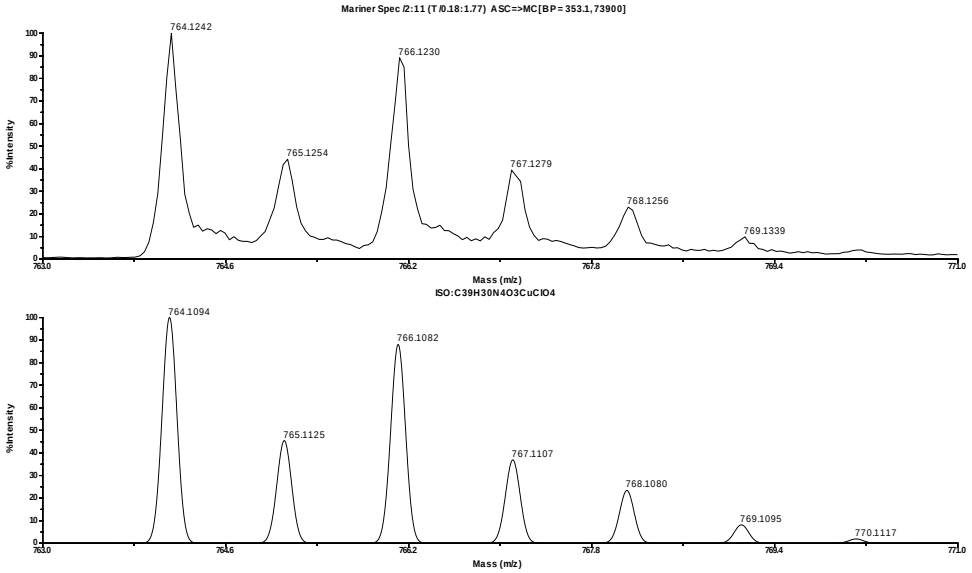

Figure A9 Experimental (top) and calculated (bottom) isotopic distribution in the HRMS (ESI-TOF) of **2•Cu** corresponding to $[C_{39}H_{30}CuN_4O_3{+}ClO_4]^+$.

A 2.5.2 C_6@1a•Zn

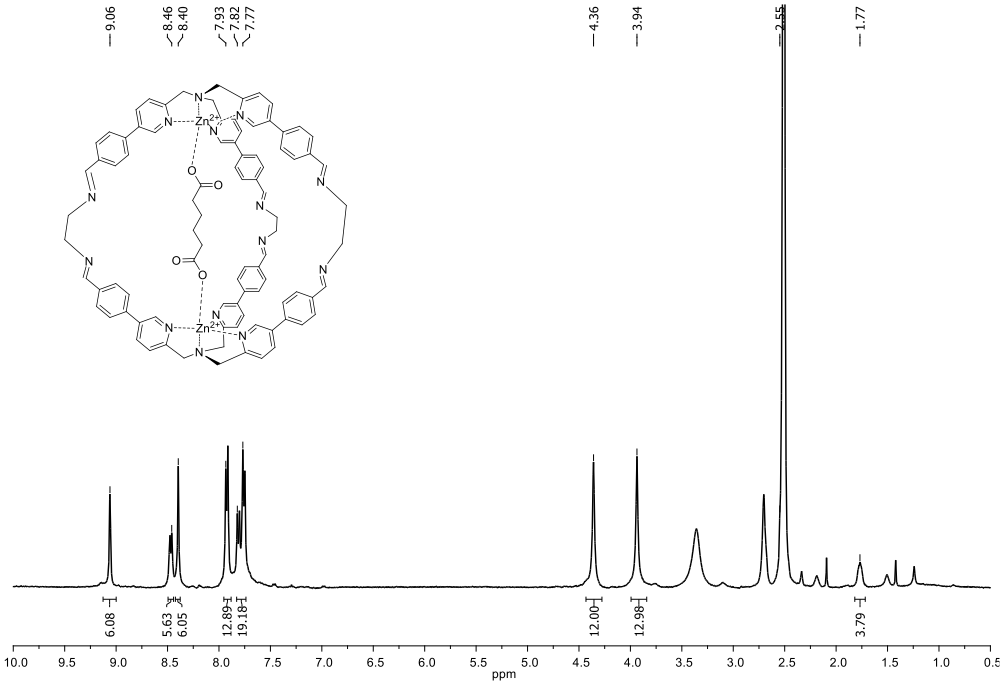

Figure A10. ^{1}H NMR spectrum (400 MHz, 301 K, DMSO-d_6)of cage **C_6@1a•Zn.**

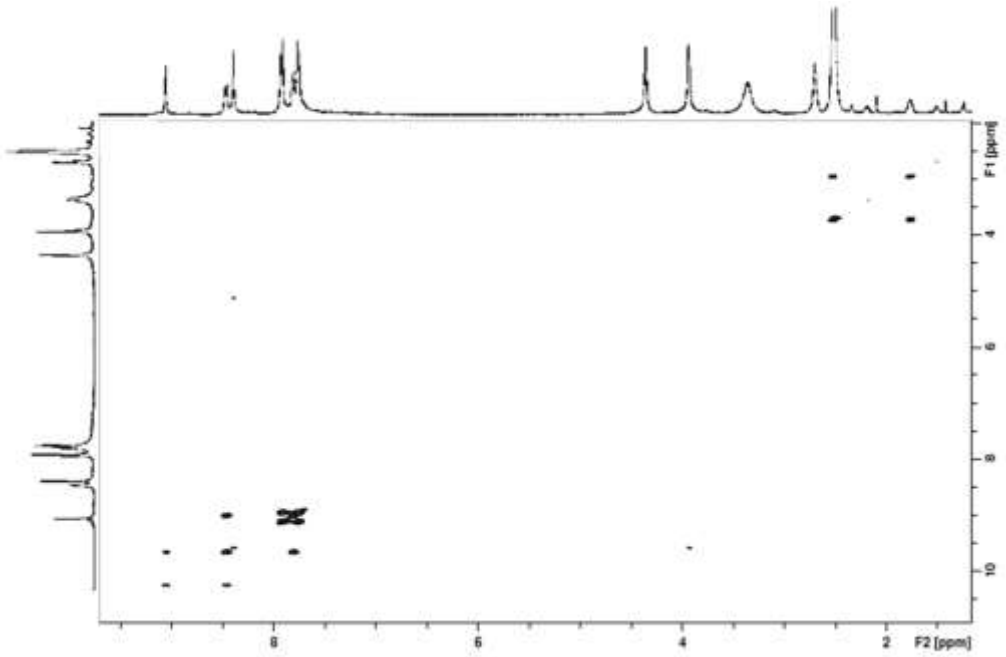

Figure A11. ^{1}H-^{1}H COSY spectrum (400 MHz, 301 K, DMSO-d_6)of cage **C_6@1a•Zn.**

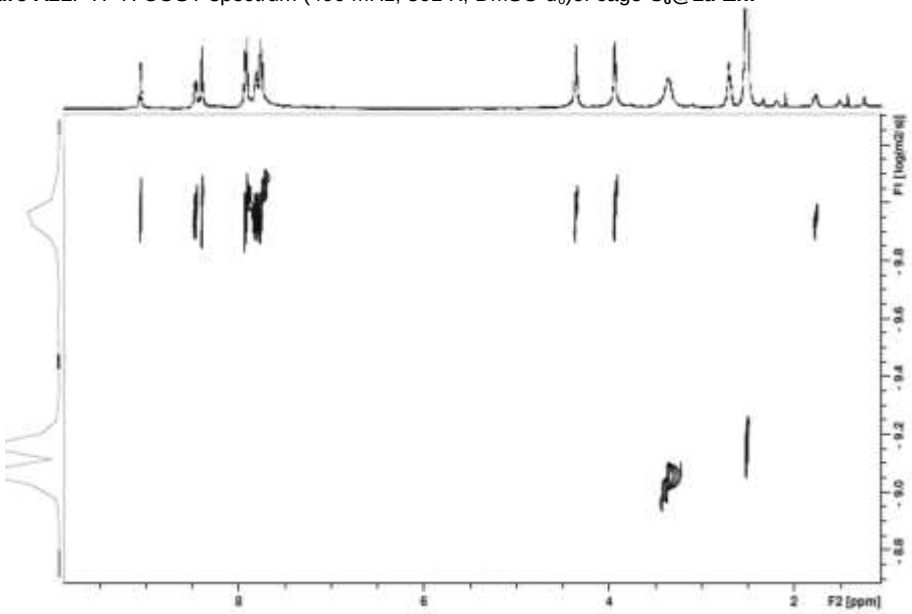

Figure A12 DOSY spectrum (400 MHz, 301 K, DMSO-d_6) of **C_6@1a•Zn.**

A 2.5.3 C_8@1b•Zn

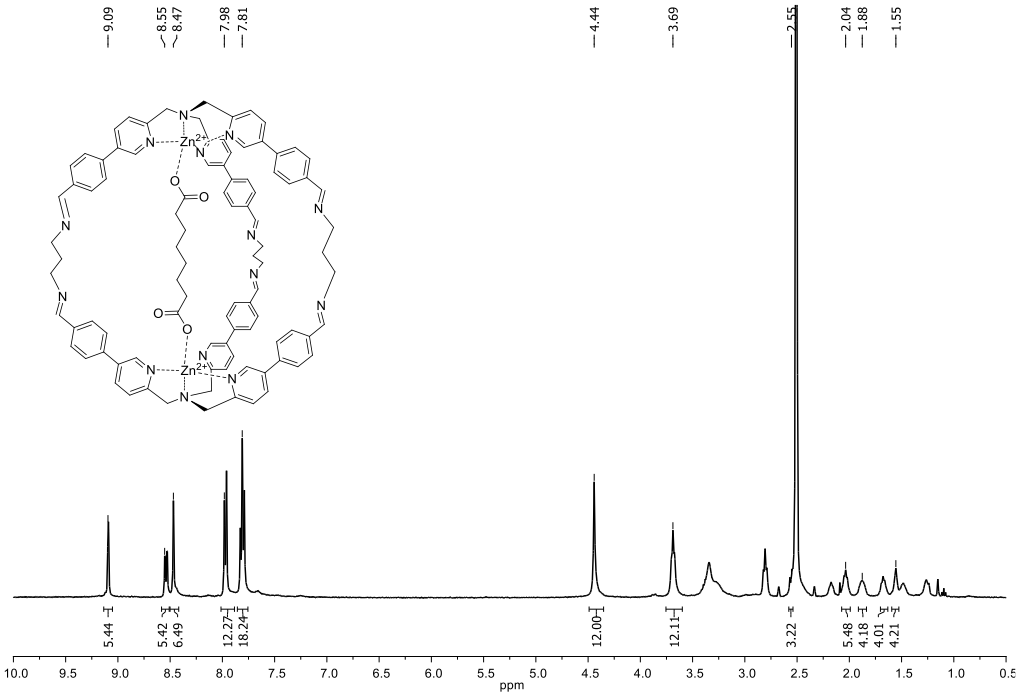

Figure A13 ^{1}H NMR spectrum (400 MHz, 301 K, DMSO-d_6)of cage **C_8@1b•Zn.**

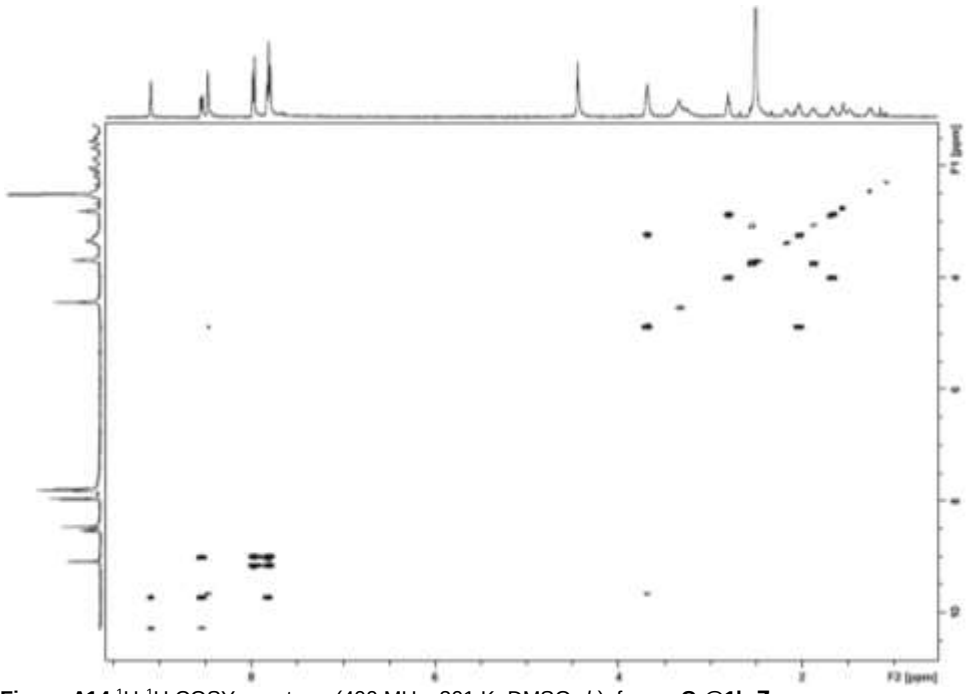

Figure A14 ^{1}H-^{1}H COSY spectrum (400 MHz, 301 K, DMSO-d_6)of cage **C_8@1b•Zn.**

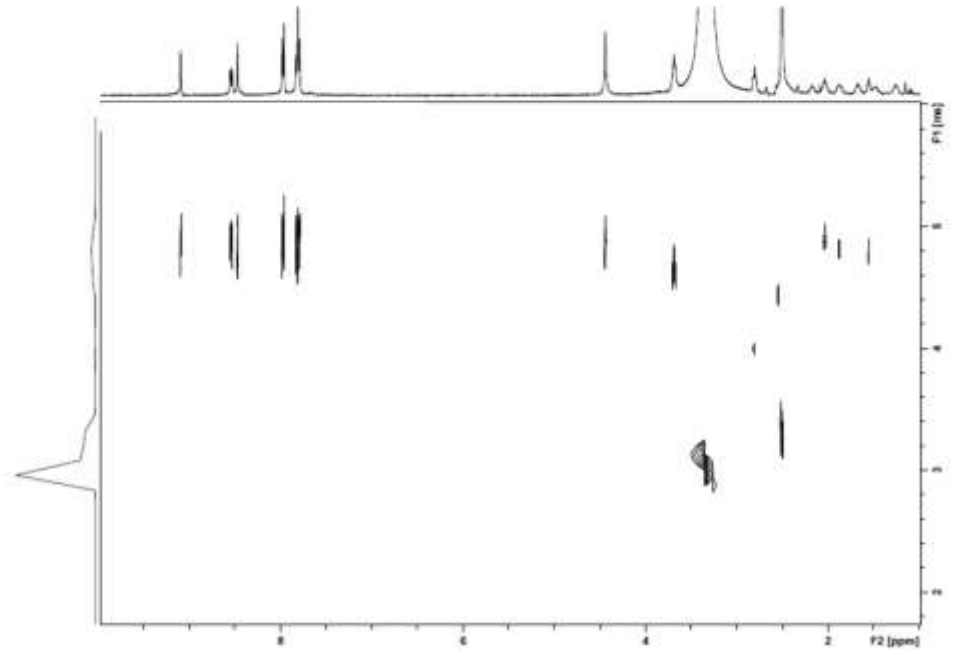

Figure A15 DOSY spectrum (400 MHz, 301 K, DMSO-d_6) of **C_8@1b•Zn.**

A 2.5.4 C_{10}@1c•Zn

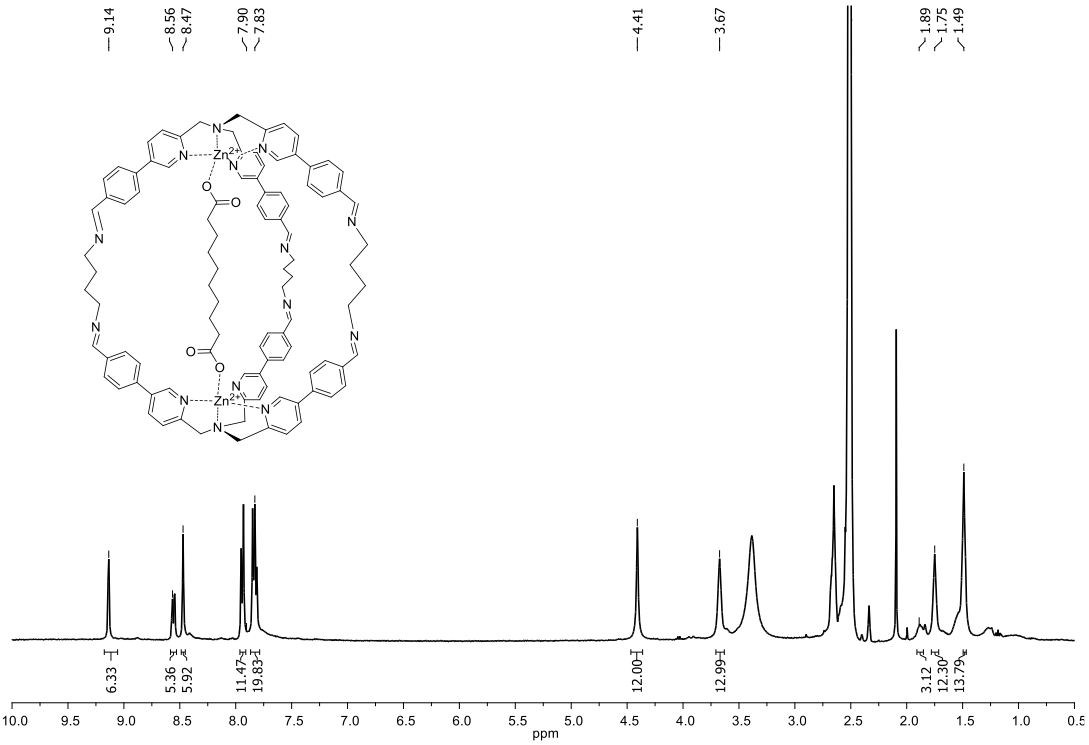

Figure A16 ^{1}H NMR spectrum (400 MHz, 301 K, DMSO-d_6)of cage **C_{10}@1c•Zn.**

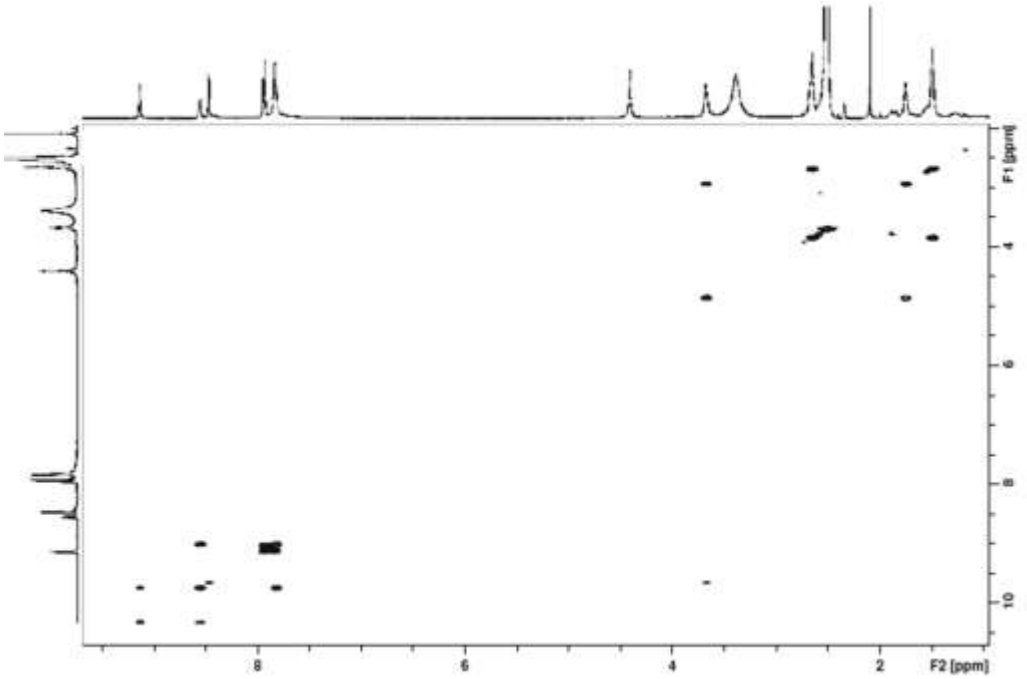

Figure A17 ^{1}H-^{1}H COSY spectrum (400 MHz, 301 K, DMSO-d_6)of cage **C_{10}@1c•Zn.**

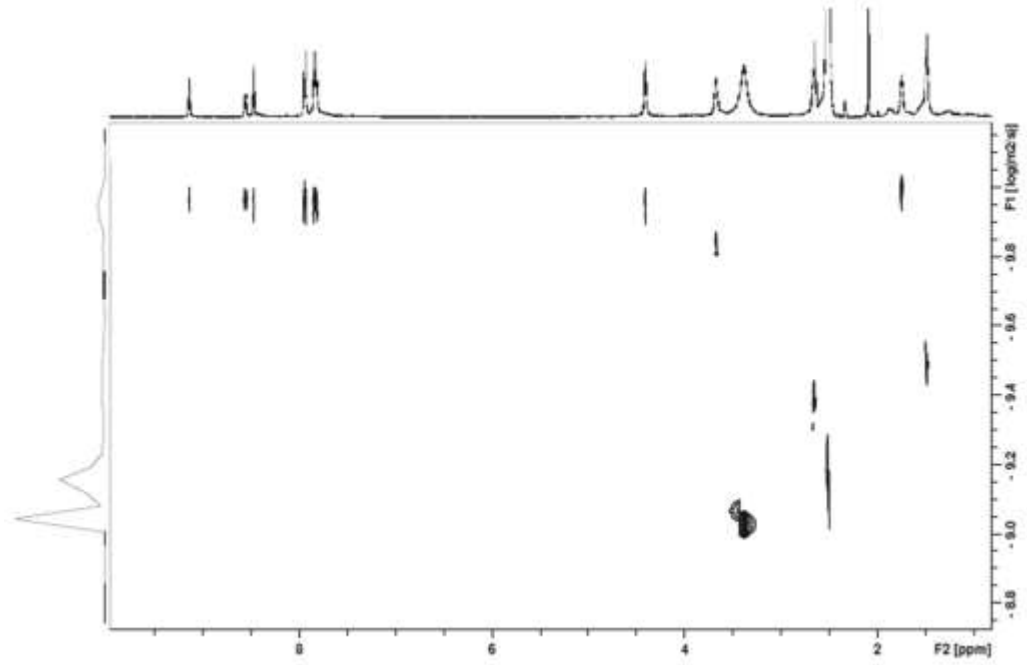

Figure A18 DOSY spectrum (400 MHz, 301 K, DMSO-d_6) of **C_{10}@1c•Zn.**

A 2.5.5 C_{10}@1d•Zn

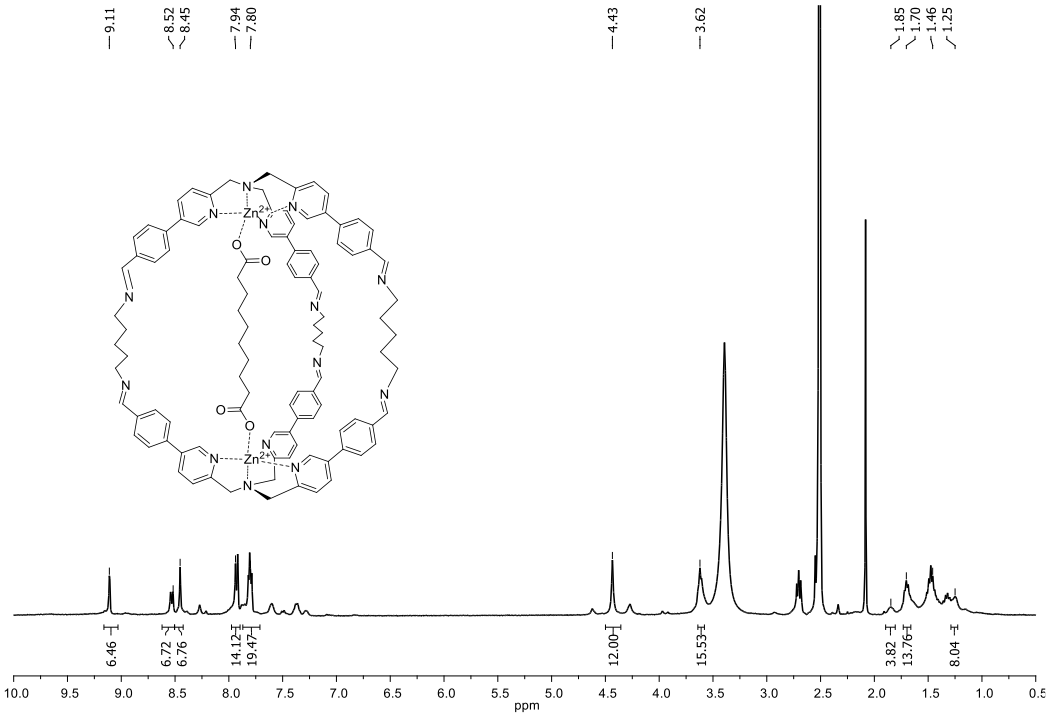

Figure A19 ^{1}H NMR spectrum (400 MHz, 301 K, DMSO-d_6)of cage **C_{10}@1d•Zn.**

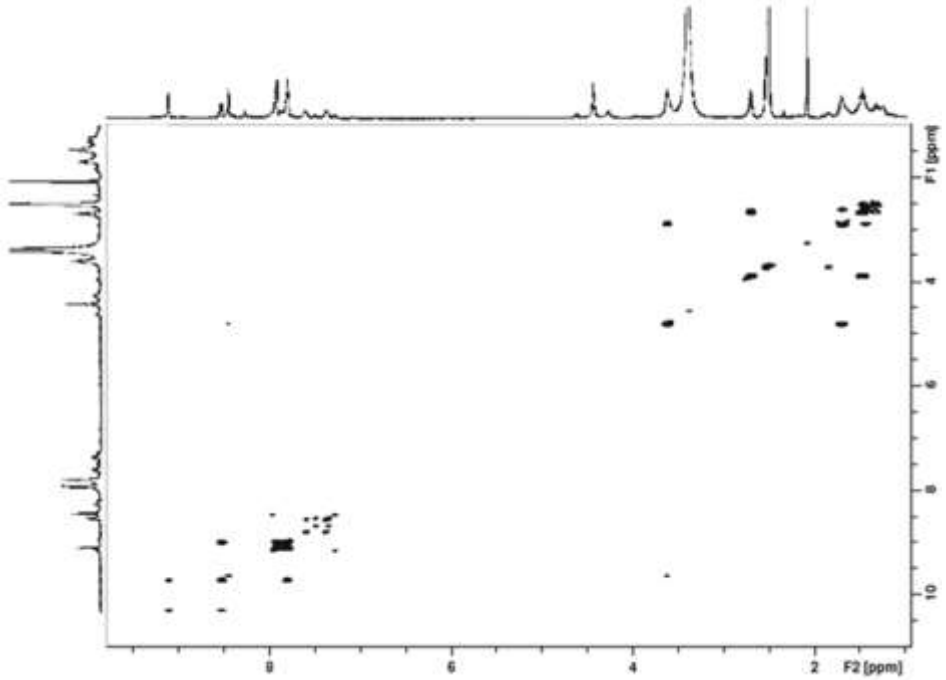

Figure A20 ^{1}H-^{1}H COSY spectrum (400 MHz, 301 K, DMSO-d_6)of cage **C_{10}@1d•Zn.**

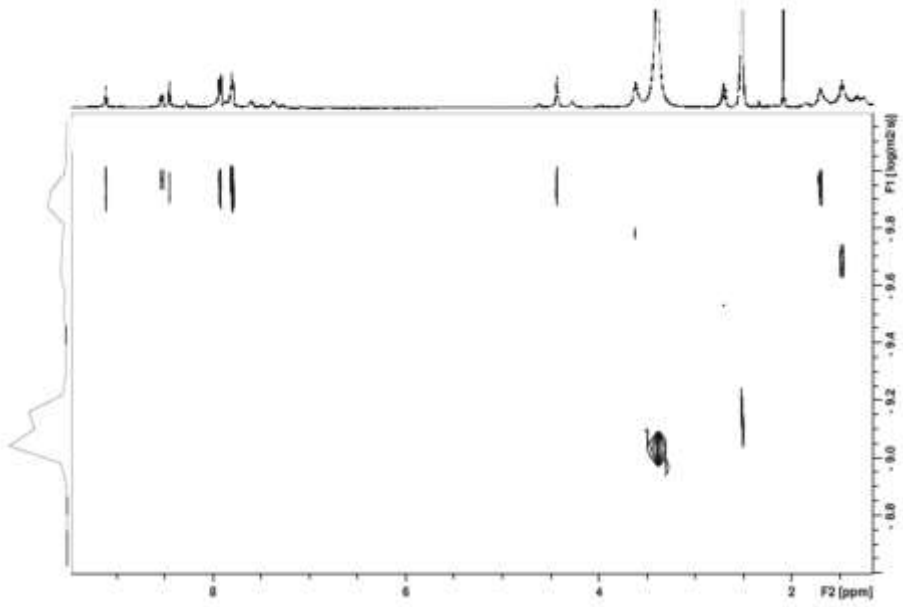

Figure A21 DOSY spectrum (400 MHz, 301 K, DMSO-d_6) of **C_{10}@1d•Zn.**

A 2.5.6 C_8@1e•Zn

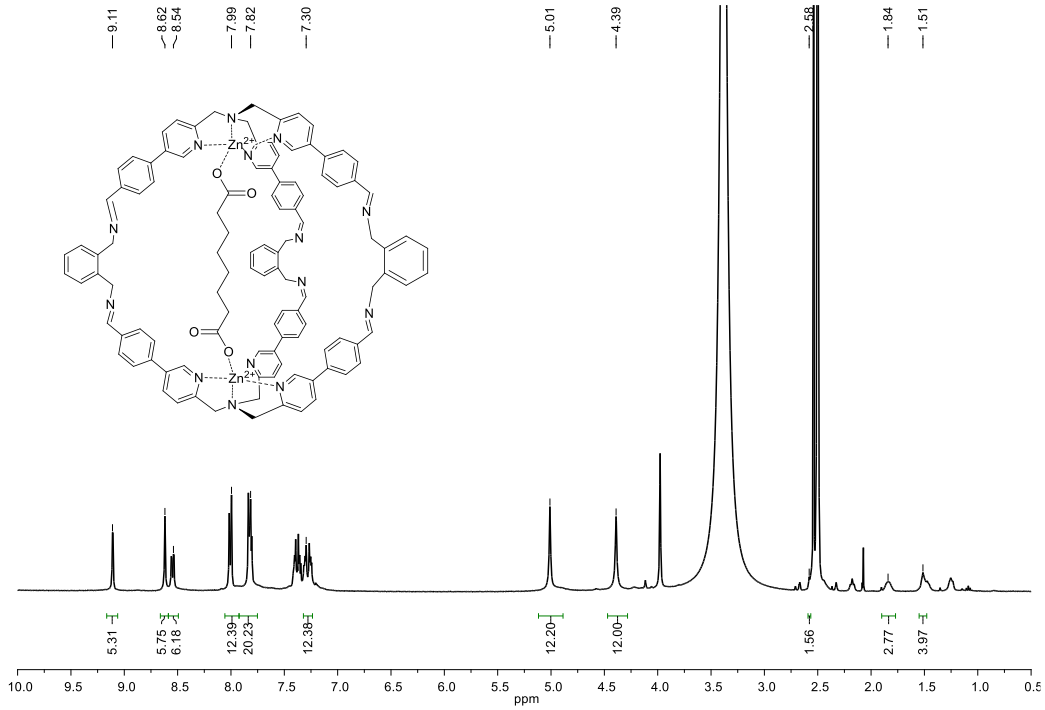

Figure A22 ^{1}H NMR spectrum (400 MHz, 301 K, DMSO-d_6)of cage **C_8@1d•Zn.**

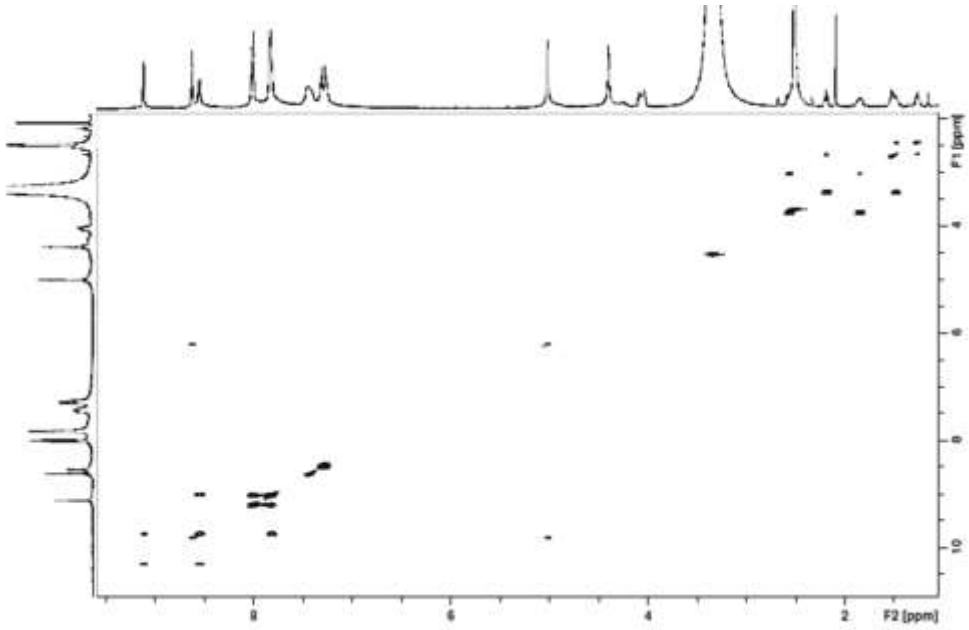

Figure A23 ^{1}H-^{1}H COSY spectrum (400 MHz, 301 K, DMSO-d_6)of cage **C_8@1e•Zn.**

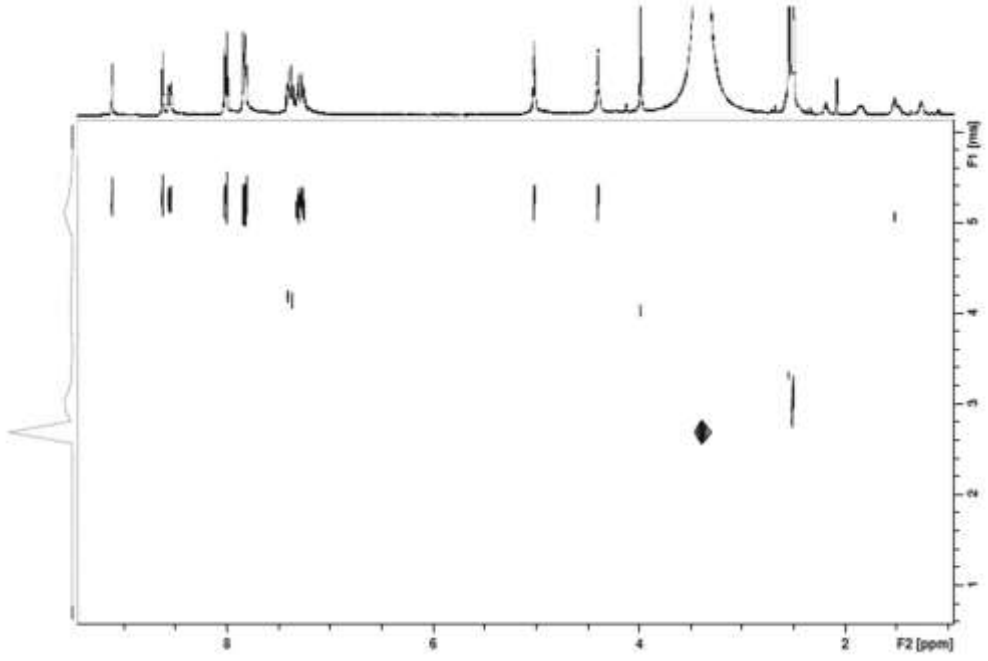

Figure A24 DOSY spectrum (400 MHz, 301 K, DMSO-d_6) of **C8@1e•Zn.**

A 2.5.7 C_{10}@1f•Zn

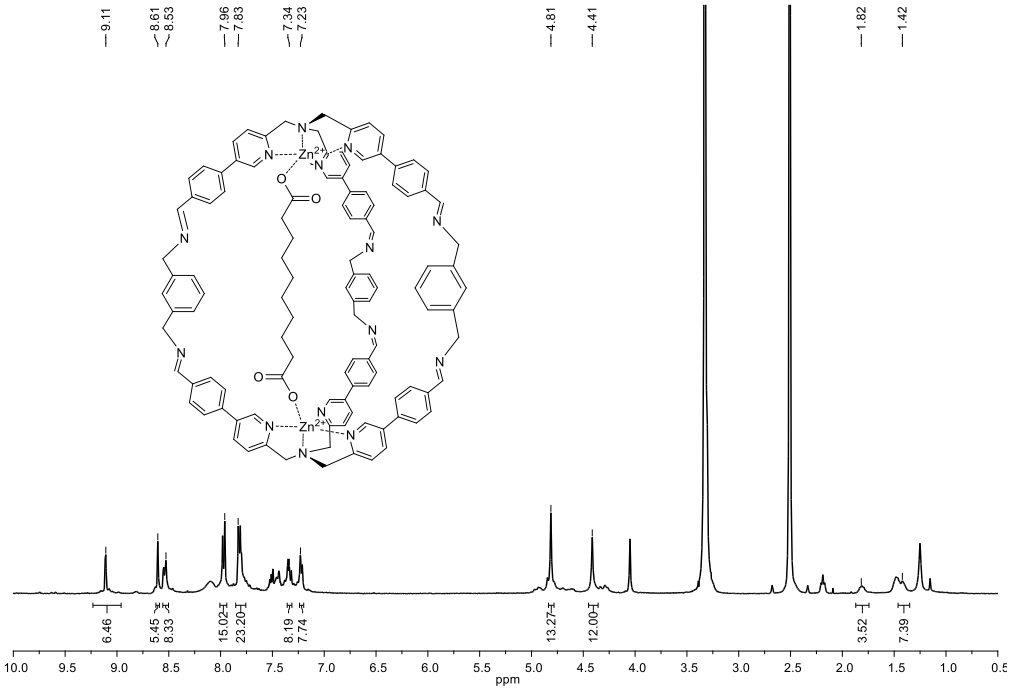

Figure A25 ^{1}H NMR spectrum (400 MHz, 301 K, DMSO-d_6)of cage **C_{10}@1c•Zn.**

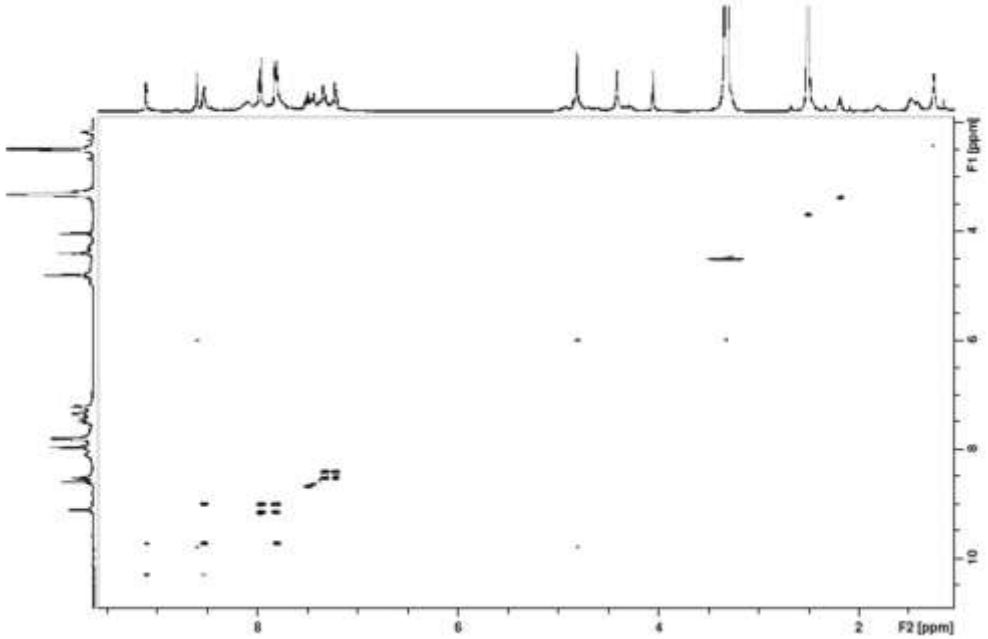

Figure AS26 ^{1}H-^{1}H COSY spectrum (400 MHz, 301 K, DMSO-d_6)of cage **C_{10}@1f•Zn.**

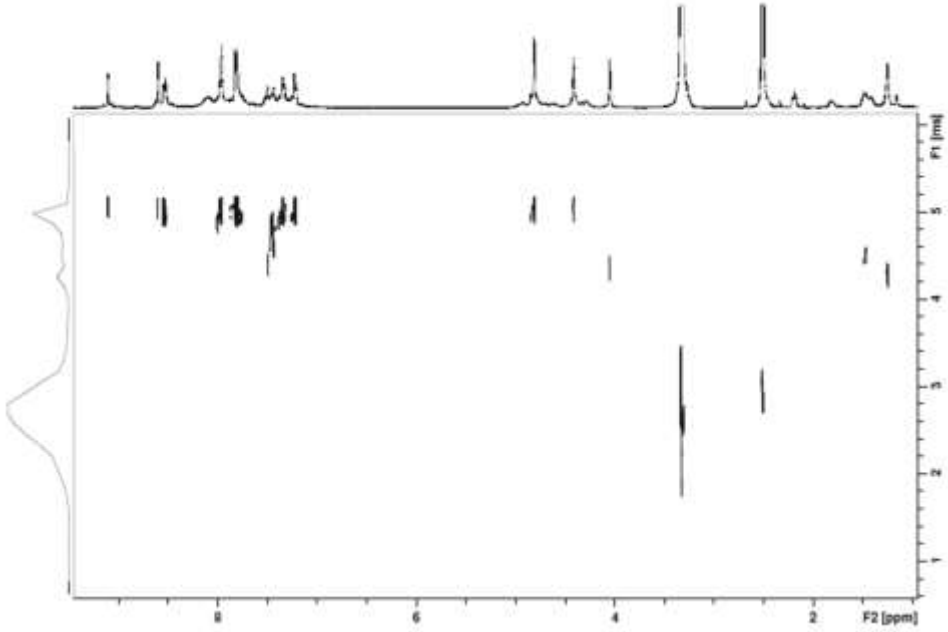

Figure A27 DOSY spectrum (400 MHz, 301 K, DMSO-d_6) of **C_{10}@1f•Zn.**

A 2.5.8 C_{10}@1g•Zn

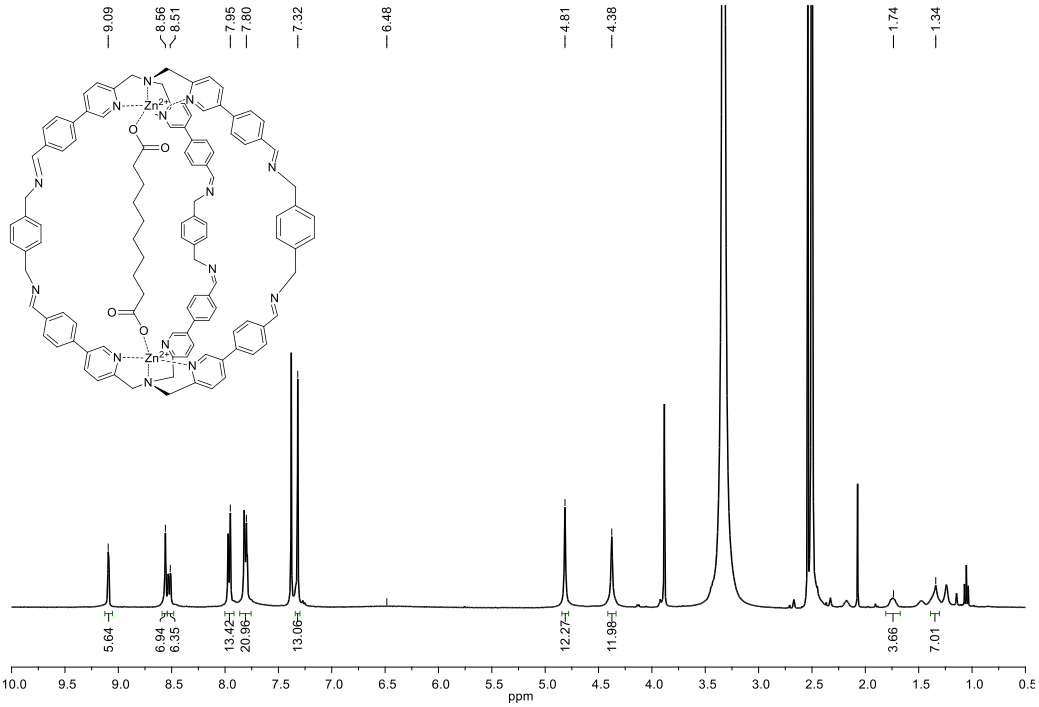

Figure A28 ^{1}H NMR spectrum (400 MHz, 301 K, DMSO-d_6)of cage **C_{10}@1g•Zn.**

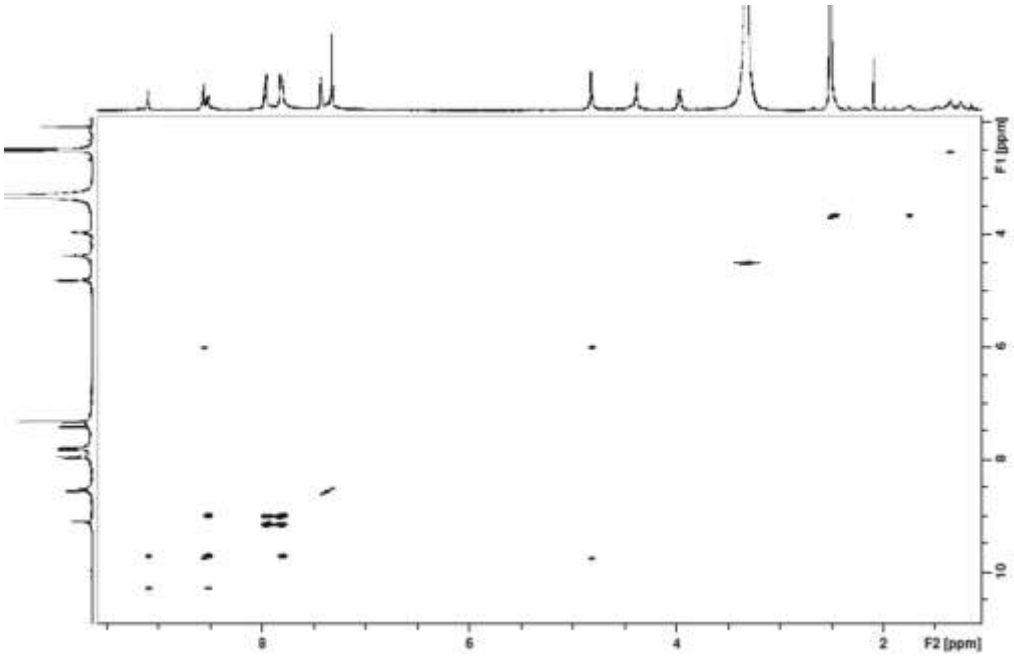

Figure A29 ^{1}H-^{1}H COSY spectrum (400 MHz, 301 K, DMSO-d_6)of cage **C_{10}@1g•Zn.**

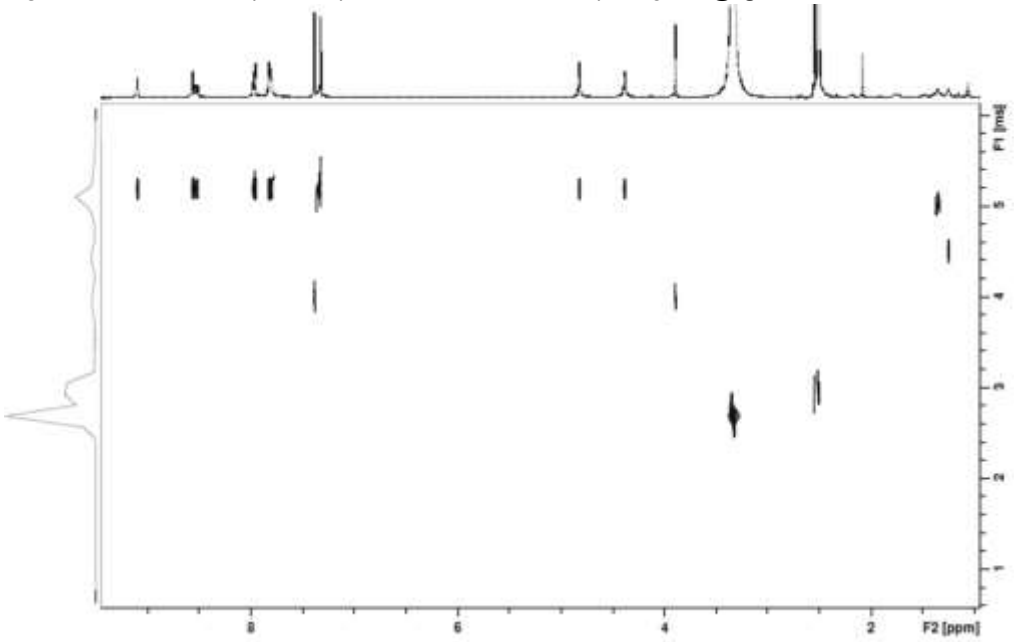

Figure A30 DOSY spectrum (400 MHz, 301 K, DMSO-d_6) of **C_{10}@1g•Zn.**

A 2.5.9 C_6@1h•Zn

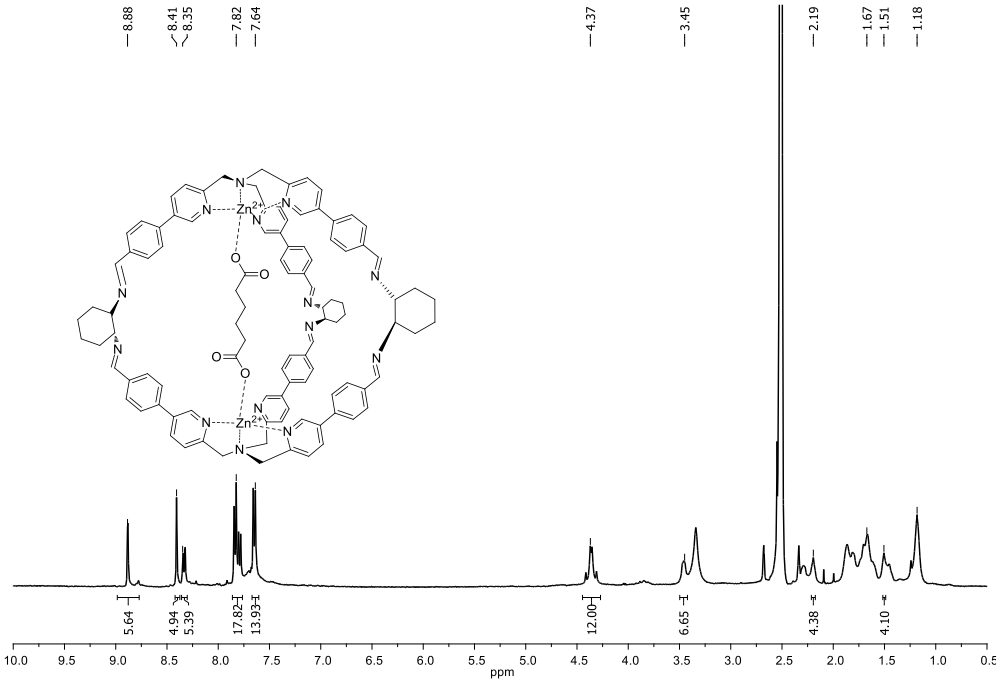

Figure A31 ^{1}H NMR spectrum (400 MHz, 301 K, DMSO-d_6)of cage **C_{10}@1h•Zn.**

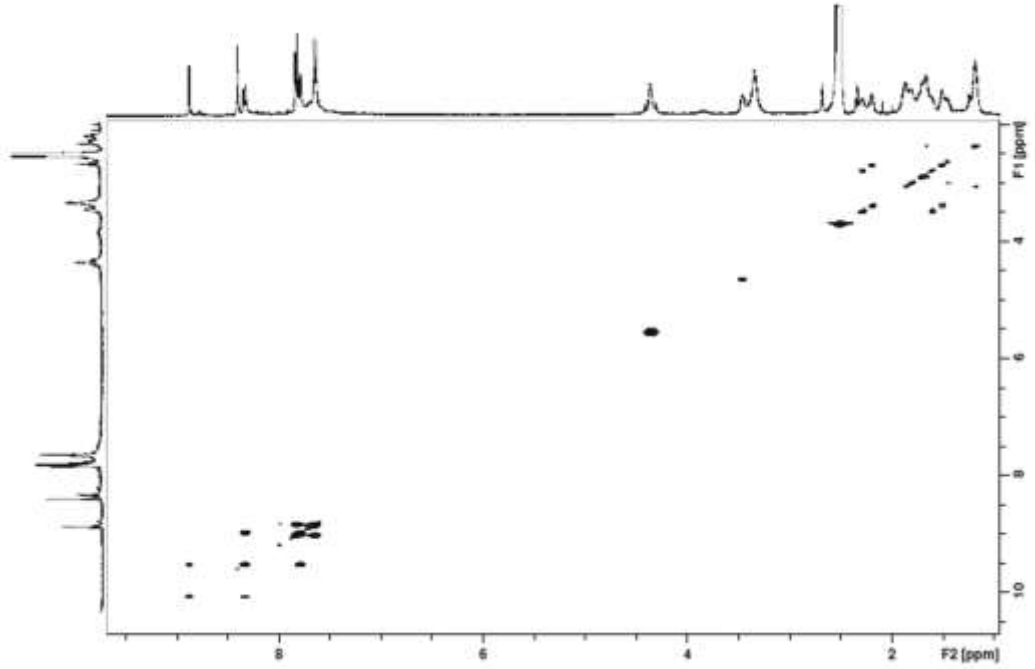

Figure A32 ^{1}H-^{1}H COSY spectrum (400 MHz, 301 K, DMSO-d_6)of cage **C_{10}@1h•Zn.**

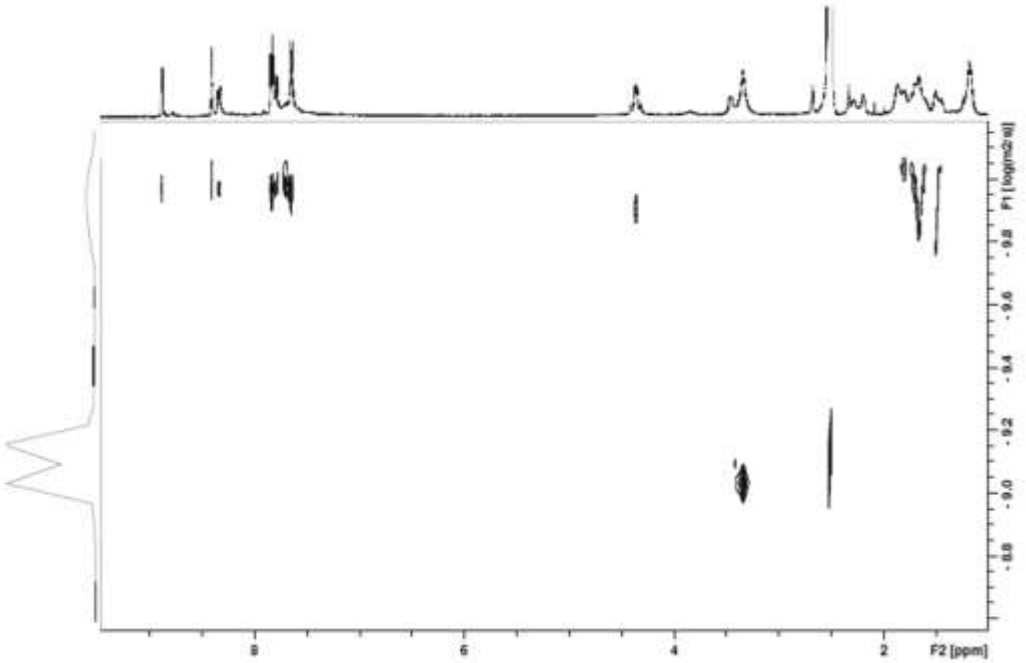

Figure A33 DOSY spectrum (400 MHz, 301 K, DMSO-d_6) of **C_{10}@1h•Zn.**

References

[1] R. Evans, Z. Deng, A. K. Rogerson, A. S. McLachlan, J. J. Richards, M. Nilsson and G. A. Morris, *Angew. Chem. Int. Ed.* **2013**, *52*, 3199-3202.

[2] [Gaussian 09 Rev. D.01, M. J. Frisch, G. W. Trucks, H. B. Schlegel, G. E. Scuseria, M. A. Robb, J. R.Cheeseman, G. Scalmani, V. Barone, B. Mennucci, G. A. Petersson, H. Nakatsuji, M. Caricato, X. Li, H. P.Hratchian, A. F. Izmaylov, J. Bloino, G. Zheng, J. L. Sonnenberg, M. Hada, M. Ehara, K. Toyota, R. Fukuda, J. Hasegawa, M. Ishida, T. Nakajima, Y. Honda, O. Kitao, H. Nakai, T. Vreven, J. A. Montgomery Jr., J. E. Peralta, F. Ogliaro, M. J. Bearpark, J. Heyd, E. N. Brothers, K. N. Kudin, V. N. Staroverov, R. Kobayashi, J. Normand, K. Raghavachari, A. P. Rendell, J. C. Burant, S. S. Iyengar, J. Tomasi, M. Cossi, N. Rega, N. J. Millam, M. Klene, J. E. Knox, J. B. Cross, V. Bakken, C. Adamo, J. Jaramillo, R. Gomperts, R. E. Stratmann, O. Yazyev, A. J. Austin, R. Cammi, C. Pomelli, J. W. Ochterski, R. L. Martin, K. Morokuma, V. G. Zakrzewski, G. A. Voth, P. Salvador, J. J. Dannenberg, S. Dapprich, A. D. Daniels, Ö. Farkas, J. B. Foresman, J. V. Ortiz, J. Cioslowski, D. J. Fox, Gaussian, Inc., Wallingford, CT, USA, 2009.

[3] *CrysAlisPro* (2012), Agilent Technologies. Version 1.171.36.35.

[4] G. M. Sheldrick, A short history of *SHELX Acta Cryst. A* **2008**, *64*, 112-122.

[5] O. V. Dolomanov, L. J. Bourhis, R. J. Gildea, J. A. K. Howard and H. *J.* Puschmann, *Appl. Cryst.* **2009**, *42*, 339-341.

[6] B. S. Lim and R. H. Holm, *Inorg. Chem.*, **2007**, *37*, 4898-4908.

[7] L. Yang, D. R. Powell and R. P. Houser, *Dalt. Trans.* **2007**, *9*, 955-964.

[8] (a) C. Chuang,; K. Lim, Q. Chen, J. Zubieta and J. W. Canary, *Inorg. Chem.*, **1995**, *34*, 2562-2568; (b) E. Szajna-Fuller, G. K. Ingle, R. W. Watkins, A. M. Arif and L. M. Berreau, *Inorg. Chem.*, **2007**, *46*, 2353-2355.

[9] J. C. Mareque-Rivas, R. Torres Martin de Rosales and S. Parsons, *Chem. Commun.* **2004**, *10*, 610-611.

Appendix to Chapter 3

A 3.1 ^{1}H NMR and MS characterization

A 3.1.1 (*R,R*)-C_{6F}@2

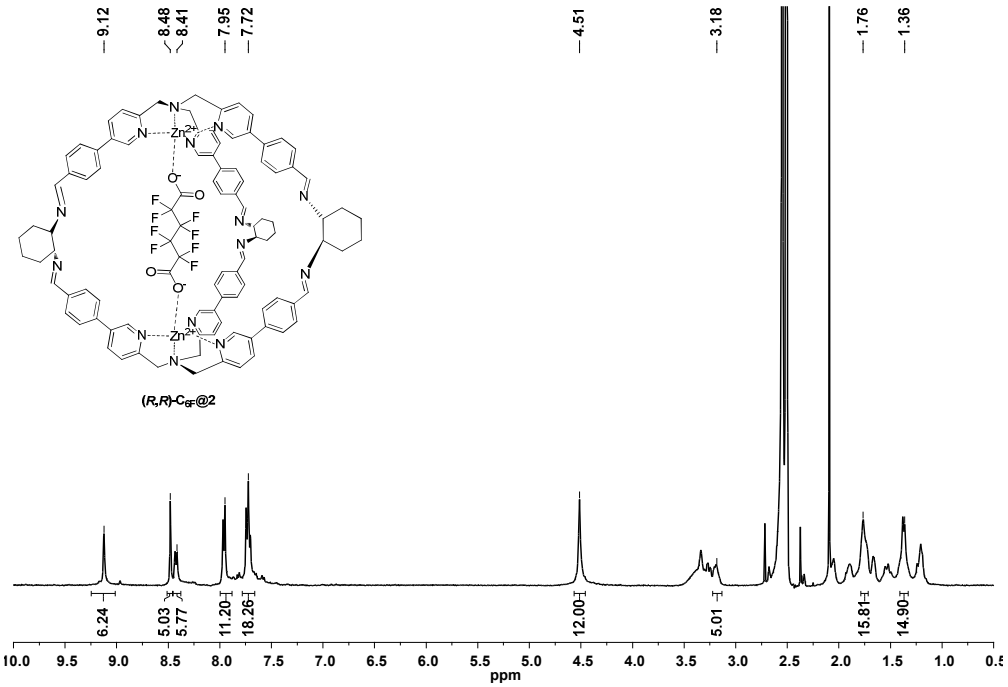

Figure A1. ^{1}H NMR spectrum (400 MHz, 301 K, DMSO-d_6)of cage **(*R,R*)-C_{6F}@2.**

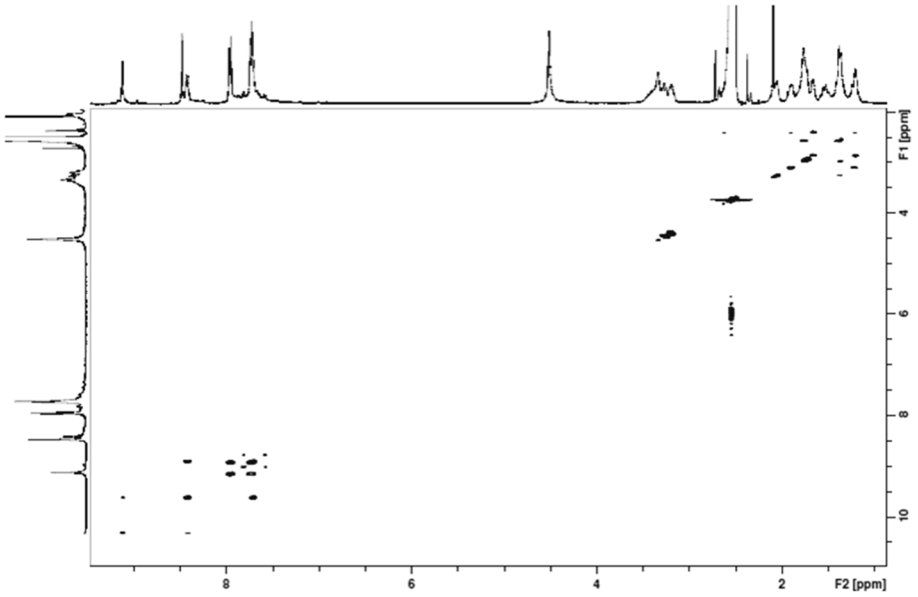

Figure A2. ^{1}H-^{1}H COSY spectrum (400 MHz, 301 K, DMSO-d_6)of cage **(*R,R*)-C_{6F}@2.**

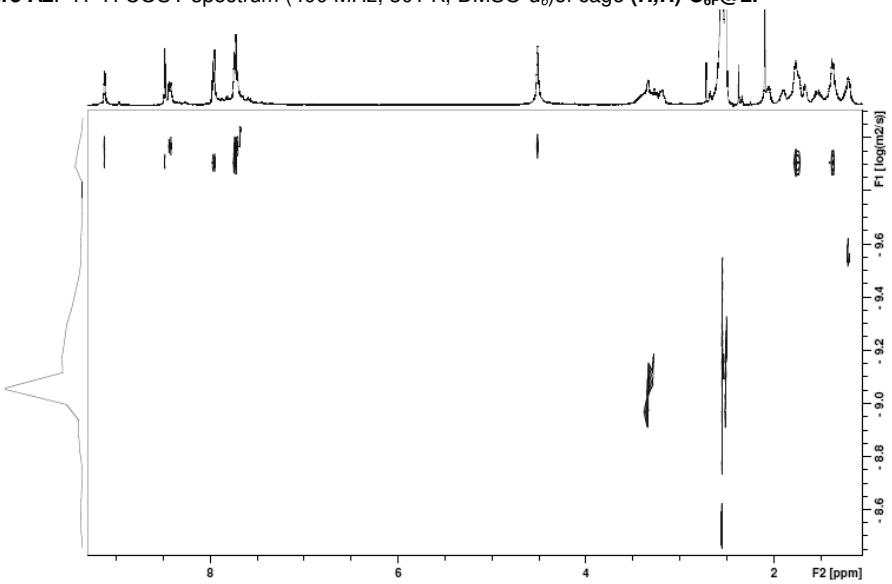

Figure A3 DOSY spectrum (400 MHz, 301 K, DMSO-d_6) of **(*R,R*)-C_{6F}@2.** The diffusion coefficient corresponding hydrodynamic radius (r_H) was calculated to be 9.5±0.4 Å by using the Stokes-Einstein equation.[1]

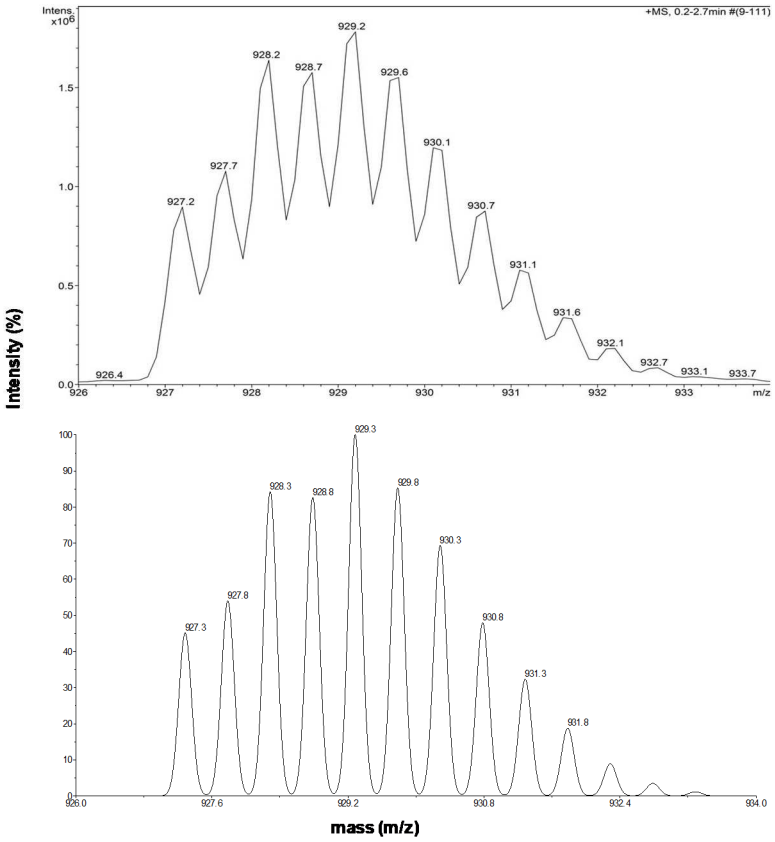

Figure A4. Experimental (top) and calculated (bottom) isotopic distribution in ESI-MS of (***R,R***)-**C_{6F}@2.**corresponding to $[C_{102}H_{90}F_8N_{14}O_4Zn_2]^{2+}$.

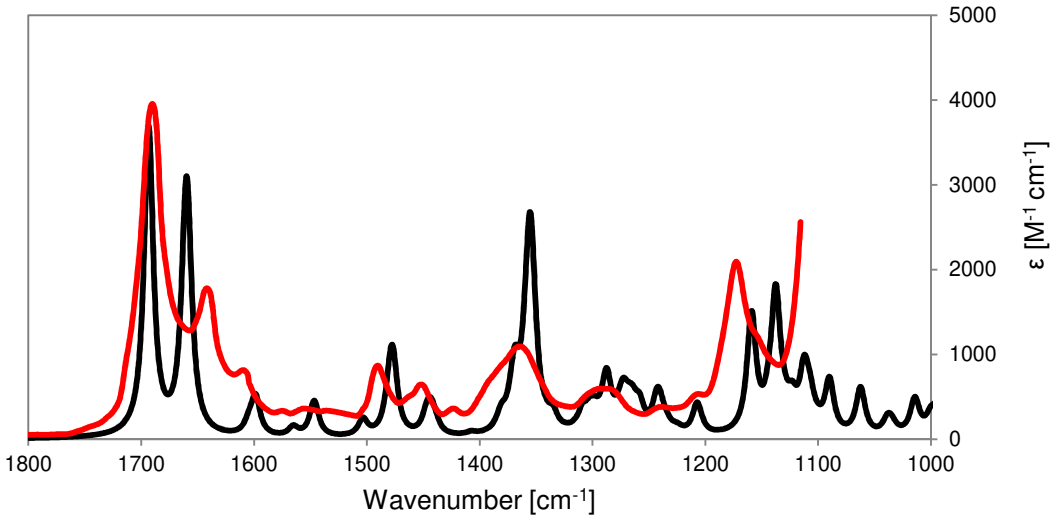

Figure A5. (b) Experimental (red line) and calculated (black line) IR spectrum of the cage **(*R,R*)-C_{6F}@2-c** (c=10 mM, *l*=0.1 mm. DMSO-d_6)

A 3.1.2 (*S,S*)-C_{6F}@2

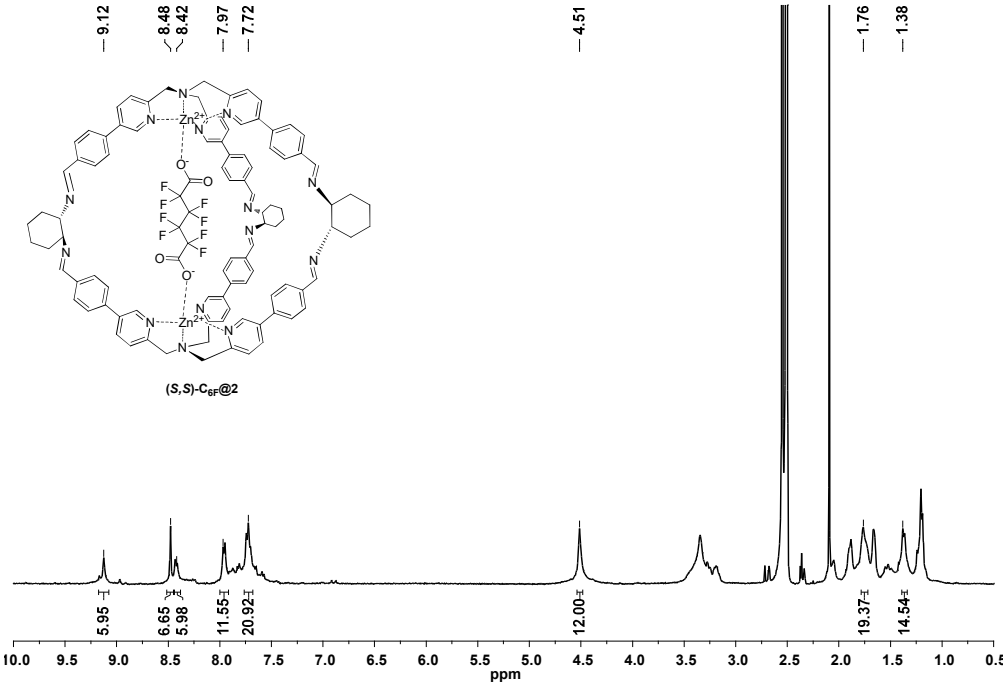

Figure A6. ^{1}H NMR spectrum (400 MHz, 301 K, DMSO-d_6)of cage **(S,*S*)-C_{6F}@2.**

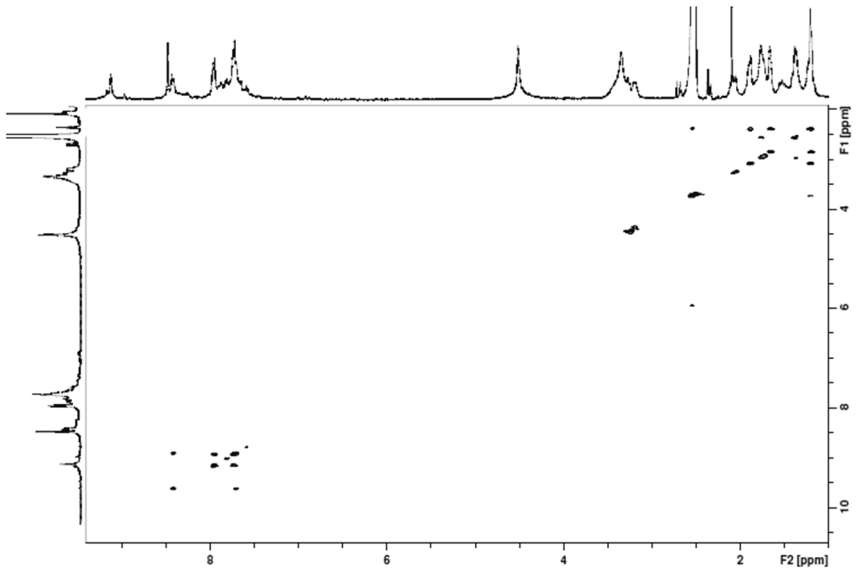

Figure A7. ^{1}H-^{1}H COSY spectrum (400 MHz, 301 K, DMSO-d_6)of cage **(S,*S*)-C_{6F}@2.**

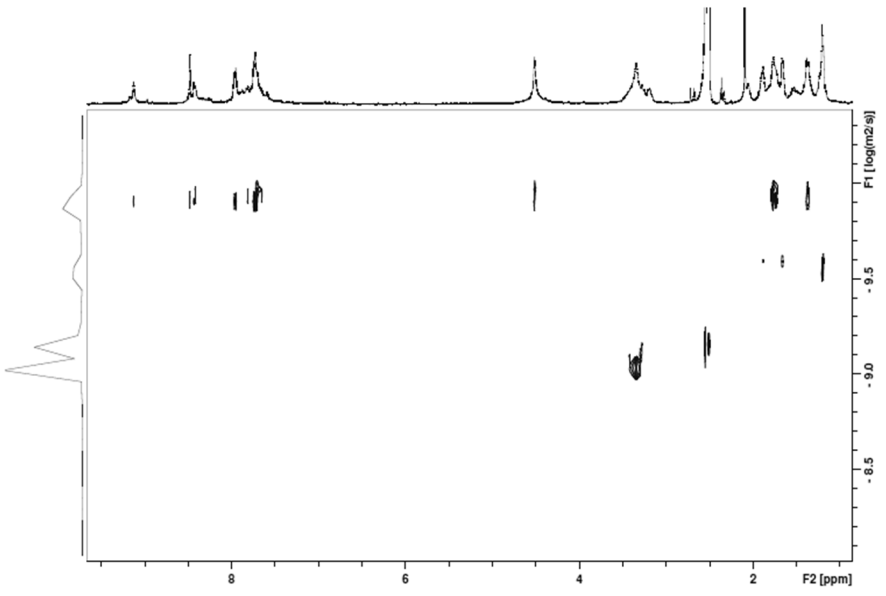

Figure A8 DOSY spectrum (400 MHz, 301 K, DMSO-d_6) of **(S,*S*)-C_{6F}@2.** The diffusion coefficient corresponding hydrodynamic radius (r_H) was calculated to be 9.5±0.2 Å by using the Stokes-Einstein equation.[1]

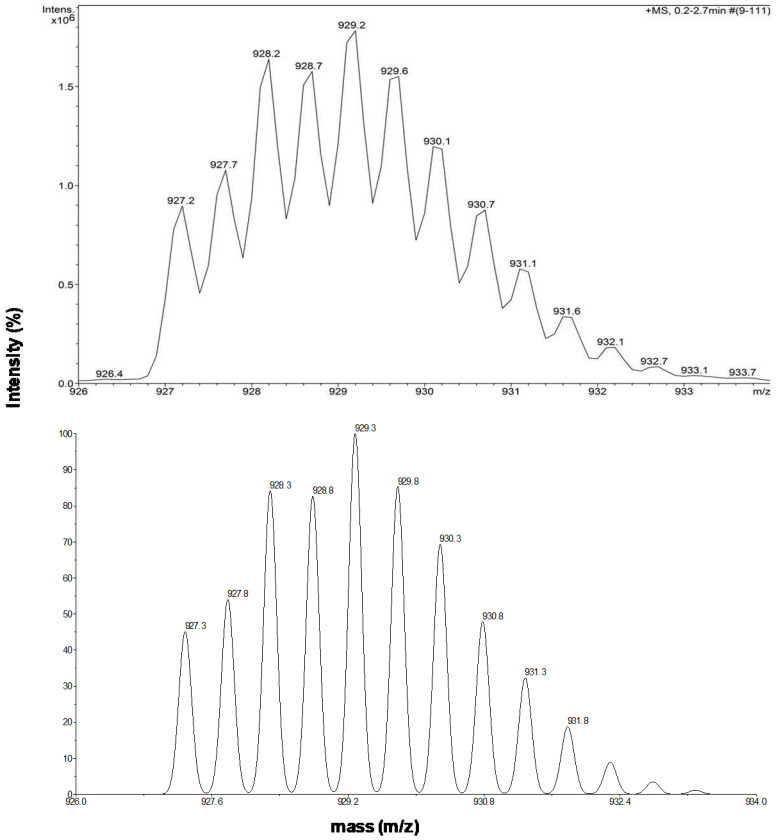

Figure A9. Experimental (top) and calculated (bottom) isotopic distribution in ESI-MS of **(S,*S*)-C_{6F}@2.** corresponding to $[C_{102}H_{90}F_8N_{14}O_4Zn_2]^{2+}$.

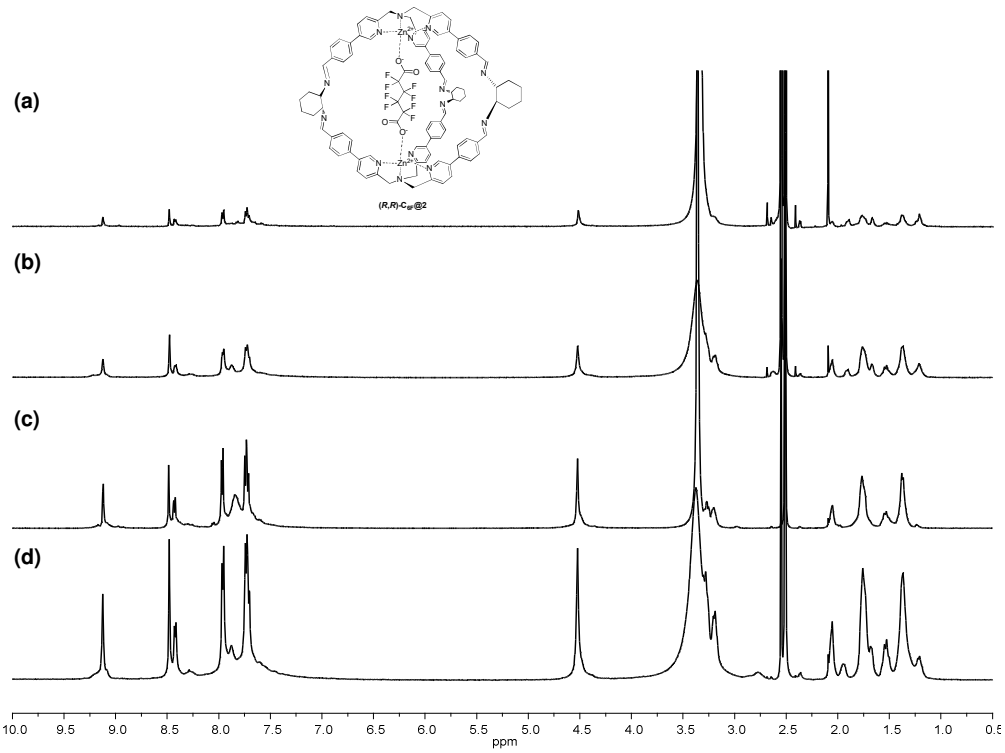

Figure A10 . ^{1}H NMR (400 MHz, 301 K, DMSO-d_6). Cage **(*R,R*)-C_{6F}@2a-d**. The cage was synthesized with different concentration **1** a) 1 mM, b) 5 mM c) 10 mM d) 15 mM. The cage formation and the characteristic peaks are confirmed in each synthesis attempt.

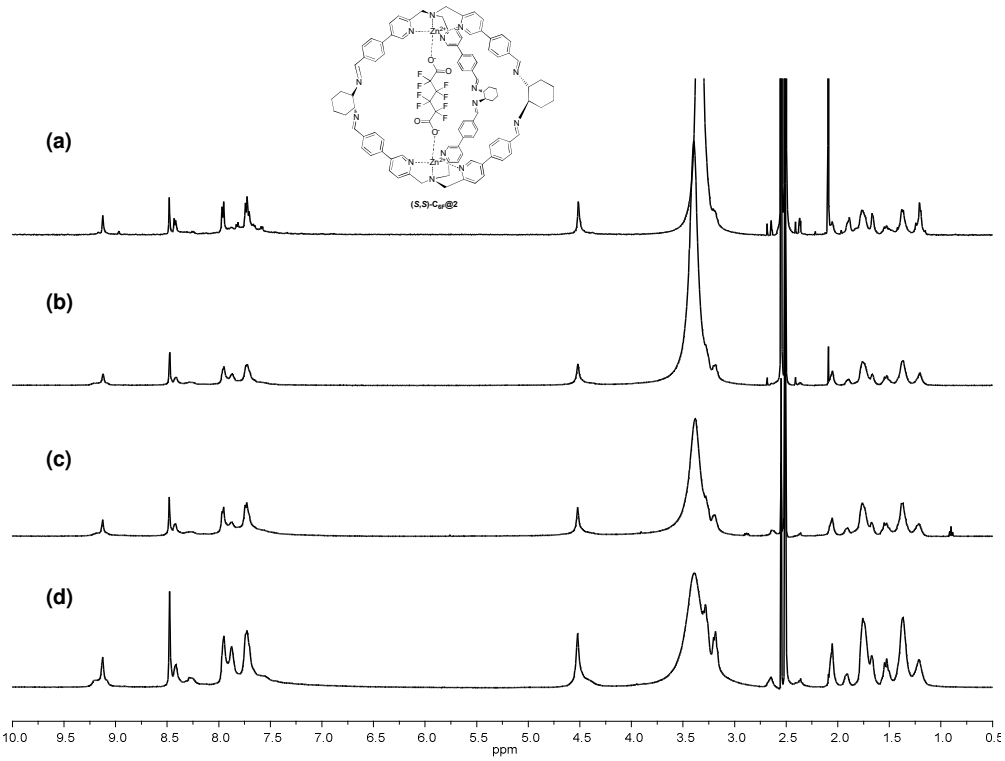

Figure A11 . ^{1}H NMR (400 MHz, 301 K, DMSO-d_6). Cage **(*S,S*)-C_{6F}@2a-d**. The cage was synthesized with different concentration **1** a) 1 mM, b) 5 mM c) 10 mM d) 15 mM. The cage formation and the characteristic peaks are confirmed in each synthesis attempt.

A 3.2 CD measurement of (*R,R*)-C_{6F}@2 (*S,S*)-C_{6F}@2

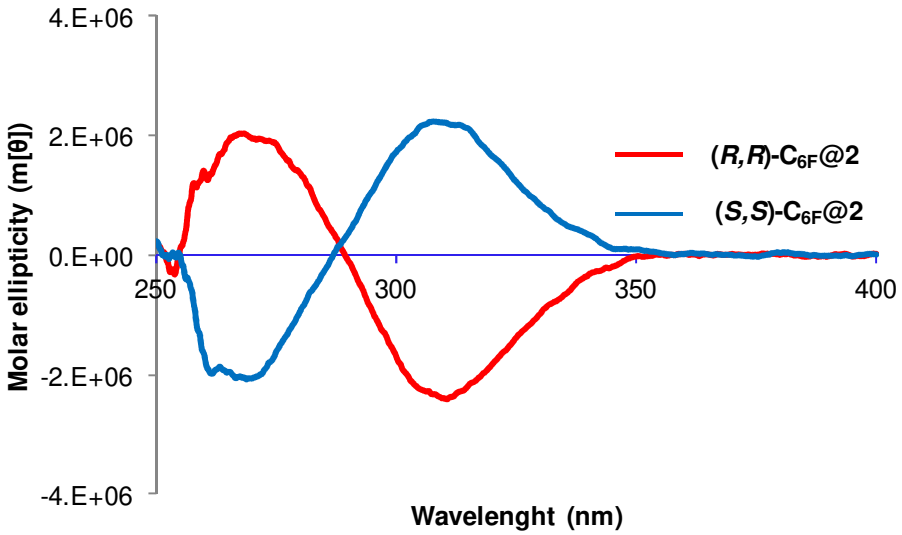

Figure A12 . CD spectra of **(*R,R*)-C_{6F}@2** and **(*S,S*)-C_{6F}@2.** (c=1*10^{-5} mM, *l*=0.1 mm. CD_3CN)

A 3.3 Computational study on cage C_{6F}@2 diasteroisomers

The calculated energy and the corresponding VCD spectra were obtained using Guassian-09.[2] The optimised energy of the six inclusion cages were carried out at B3LYP/6-31g(d,p) level using scrf=(solvent=acetonitrile) and the results are in Table 1. It should be noticed that calculations have been done using acetonitrile as solvent, while the experiment have been carried in DMSO-d_6.

Cage C_{6F}@2 Diastereoisomer	Energy (Hartree)	Relative Energy (Kcal/mol)
RRPP-P	9365,685408	0,0
RRPP-M	9365,676903	5,3
RRMM-P	-9365,67392	7,2
RRMM-M	9365,673465	7,5
RRMP-M	9365,679607	3,6
RRMP-P	9365,683693	1,1

Table a1. Calculated energy for the six possible diastereoisomers. Calculations have been carried out at B3LYP/6-31g(d,p) level using scrf=(solvent=acetonitrile)

References

1. R. Evans, Z. Deng, A. K. Rogerson, A. S. McLachlan, J. J. Richards, M. Nilsson and G. A. Morris, *Angew. Chem. Int. Ed.* **2013**, *52*, 3199-3202.
2. [Gaussian 09 Rev. D.01, M. J. Frisch, G. W. Trucks, H. B. Schlegel, G. E. Scuseria, M. A. Robb, J. R.Cheeseman, G. Scalmani, V. Barone, B. Mennucci, G. A. Petersson, H. Nakatsuji, M. Caricato, X. Li, H. P.Hratchian, A. F. Izmaylov, J. Bloino, G. Zheng, J. L. Sonnenberg, M. Hada, M. Ehara, K. Toyota, R. Fukuda, J. Hasegawa, M. Ishida, T. Nakajima, Y. Honda, O. Kitao, H. Nakai, T. Vreven, J. A. Montgomery Jr., J. E. Peralta, F. Ogliaro, M. J. Bearpark, J. Heyd, E. N. Brothers, K. N. Kudin, V. N. Staroverov, R. Kobayashi, J. Normand, K. Raghavachari, A. P. Rendell, J. C. Burant, S. S. Iyengar, J. Tomasi, M. Cossi, N. Rega, N. J. Millam, M. Klene, J. E. Knox, J. B. Cross, V. Bakken, C. Adamo, J. Jaramillo, R. Gomperts, R. E. Stratmann, O. Yazyev, A. J. Austin, R. Cammi, C. Pomelli, J. W. Ochterski, R. L. Martin, K. Morokuma, V. G. Zakrzewski, G. A. Voth, P. Salvador, J. J. Dannenberg, S. Dapprich, A. D. Daniels, Ö. Farkas, J. B. Foresman, J. V. Ortiz, J. Cioslowski, D. J. Fox, Gaussian, Inc., Wallingford, CT, USA, 2009.

Appendix to Chapter 4

A4.1 Binding constant determination towards cage 1 K_b

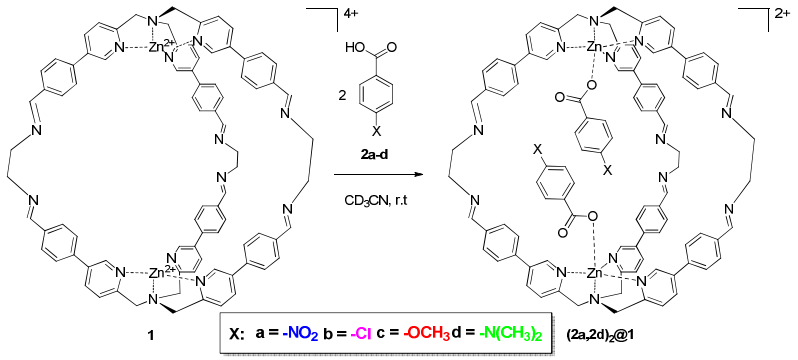

To 500 µl (0.5 µmol) of a solution 0.001 M of the cage **1** (based on *p*-xylene standard) in CD_3CN, 20 µl (0.24 µmol) of a solution 0.012 M in CD_3CN of *p*-xylene were added. Small aliquots of guests solution were titrated into this NMR tube. The solution was allowed to equilibrate at room temperature during 30 seconds before acquiring the ^1H NMR spectrum. The binding constant values for each *p*-substituted benzoic acid **2a,2d** are displayed in Figure A1. The error reported for each affinity value is the formal standard error calculated using two characteristic peaks in the ^1H NMR spectra and performing the titrations three times.

Diacid	K_b (M^{-1})	±σ (M^{-1})
4-(Dimethylamino)benzoic acid **2d**	2889	322
4-Methoxybenzoic Acid **2c**	3441	674
4-Chlorobenzoicacid **2b**	4623	311
4-Nitrobenzoic acid **2a**	6555	623

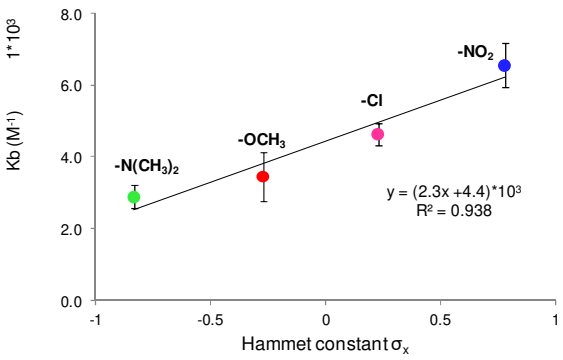

Figure A1. Binding constant values for each *p*-substituted benzoic acid **2a,2d**

A4.2 Determination of Binding Stoichiometry along the titration points for (2a-2a)@1

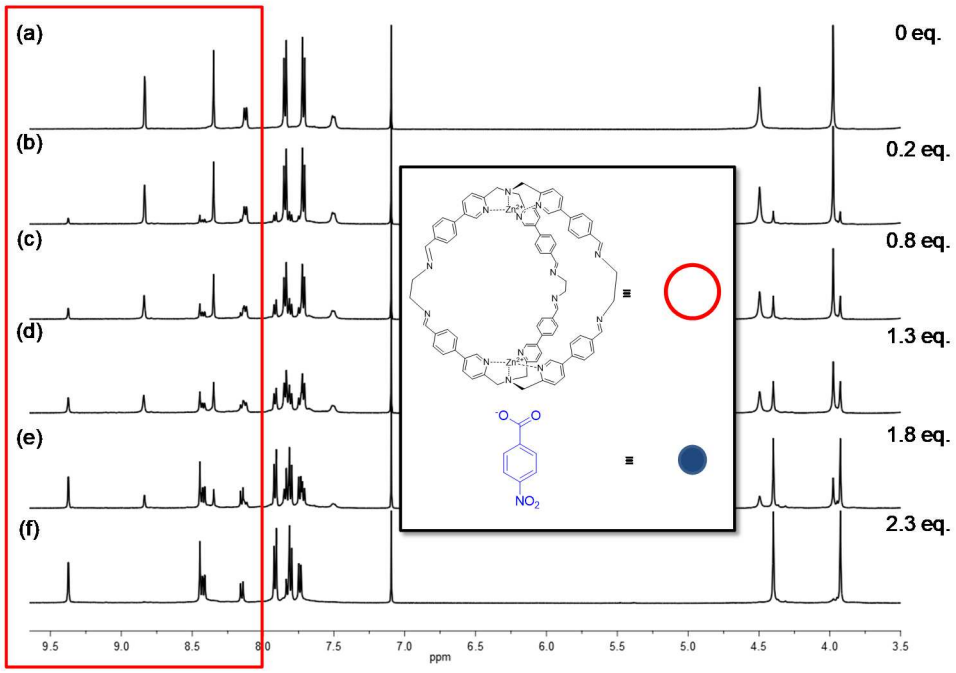

Figure A2. ^{1}H NMR inclusion experiments. Addition of *p*-Nitrobenzoicacid **2a** to cage **1** in CD_3CN. (a) Preformed cage **1** (0.001 M cage).(b)-(F) Addition of sub-stoichiometric amounts (0.2-1.8 equiv) of **2a** results in the formation of a new species that maintains the original symmetry. (f) Addition of 2.3 equiv of **2a** totally shift the system to the new species **(2a-2a)@1**. Counter anions are perchlorates.

The determination of binding stoichiometry was possible thanks to the integration of the signals of the pyridine ring α proton of the filled cage **(2a-2a)@1**, a free host signal and a guest signal.

In the region highlighted it was possible to monitor three diagnostic peaks and in Figure A3 are reported the integrals of the signal at 8.152 ppm which combine a free host signal with a guest signal included in the cage. The experimental values compared with theoretical values calculated in case of 1:1 or 1:2 binding confirm an host-guest stoichiometry 1:2.

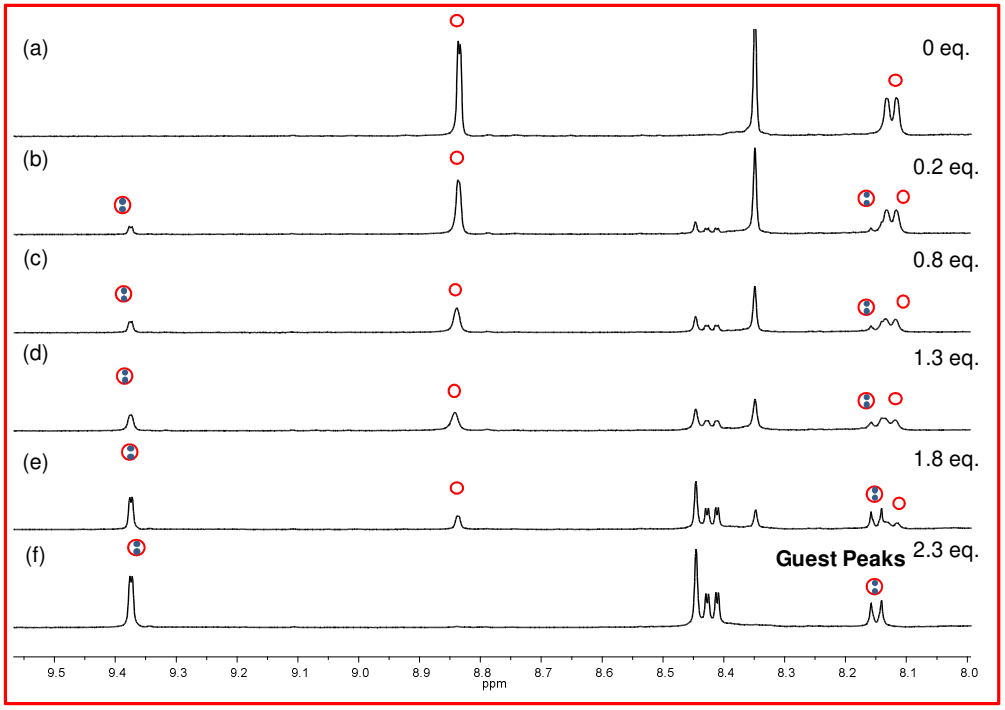

Titration Experiment	Experimental Value	Theoretical Value 2:1 Binding	Theoretical Value 1:1 Binding
(b)	70.20	70.16	68.16
(c)	21.20	20.93	18.93
(d)	14.34	13.27	11.27
(e)	7.15	6.92	4.62
(f)	4.39	4.00	2.00

Figure A3. ^{1}H NMR inclusion experiments. Addition of *p*-Nitrobenzoicacid **2a** to cage **1** in CD_3CN. (a) Preformed cage **1** (0.001 M cage).(b)-(f) Addition of sub-stoichiometric amounts (0.2-1.8 equiv) of **2a** results in the formation of a new species that maintains the original symmetry. (f) Addition of 2.3 equiv of **2a** totally shift the system to the new species **(2a-2a)@1**.

A4.3 Binding constant determination towards starting complex S1

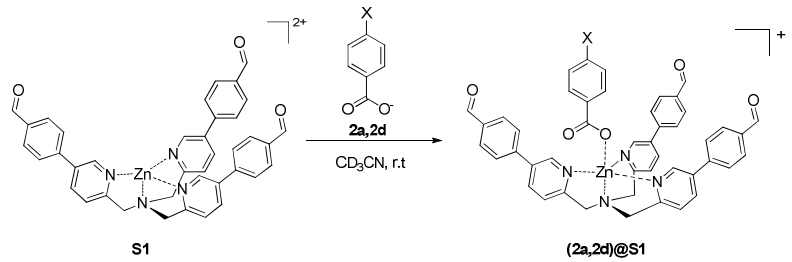

To 500 µl (0.5 µmol) of a solution 0.002 M of the complex **S1** (based on *p*-xylene standard) in CD_3CN, 20 µl (0.24 µmol) of a solution 0.012 M in CD_3CN of *p*-xylene were added. Small aliquots of the triethylammonium salt of each guest solution **2a,2d** were titrated into this NMR tube. The solution was allowed to equilibrate at room temperature during 30 seconds before acquiring the ^1H NMR spectrum. The binding constant values for each *p*-substituted benzoic acid **2a,2d** are displayed in Figure A4 with a stoichiometry of binding 1:1. The error reported for each affinity value is the formal standard error calculated using two characteristic peaks in the ^1H NMR spectra and performing the titrations three times. The ^1H NMR titration experiment for **2a** is displayed in Figure A5

Diacid Salt	K_b (M^{-1})	±σ (M^{-1})
4-(Dimethylamino)benzoic acid **2d**	2493	260
4-Methoxybenzoic Acid **2c**	5537	455
4-Chlorobenzoicacid **2b**	6408	420
4-Nitrobenzoic acid **2a**	7451	125

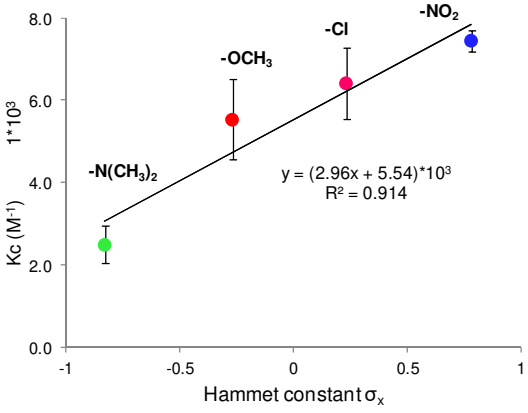

Figure A4. Binding constant values for each *p*-substituted benzoic acid **2a,2d**

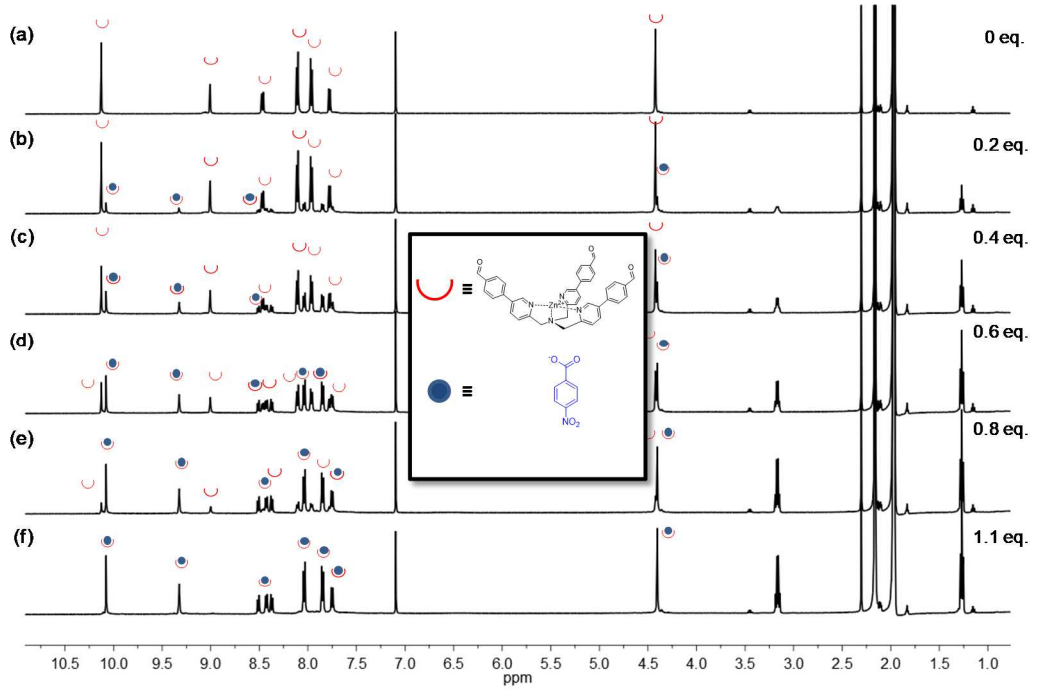

Figure A5. ^{1}H NMR inclusion experiments of *p*-Nitrobenzoic acid **2a** triethylammonium salt towards complex **S1** in CD_3CN. (a) Complex **S1** (0.002 M).(b)-(f) Addition of sub-stoichiometric amounts (0.2-0.8 equiv) of **2a** results in the formation of a new species that maintains the original symmetry. (f) Addition of 1.1 equiv of **2a** totally shift the system to the new species **2a@S1**. Counter anions are perchlorates.

A4.4 Evaluation of π-Stacking between the guests within cage 1

The correlation between the Hammet σ parameter for each guest and the ΔΔG values derived from the binding process of the guests within cage **1** and the binding toward the initial complex confirms non relevant contributions coming from the mutual interactions of the π system of the guests in the binding process (Figure A6).

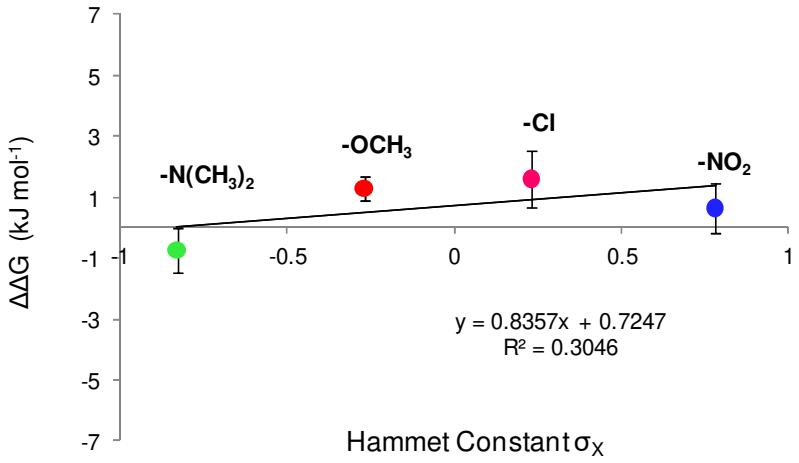

Figure A6. Contribution of π-Stacking of the guests **2a,2d** in the case of homo co-encapsulated species.

A4.5 Competition Experiments

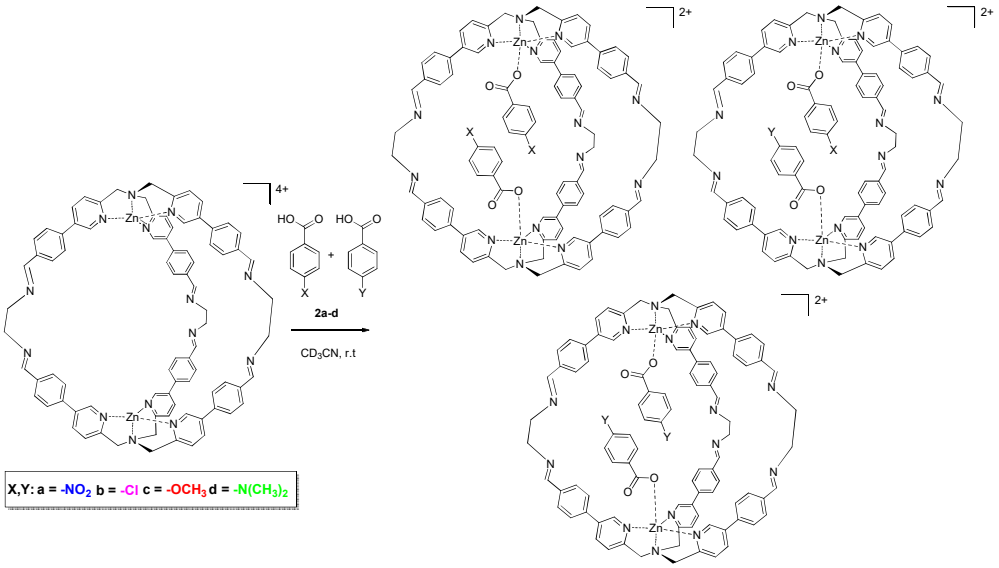

To 500 µl (0.5 µmol) of a solution 0.001 M of the cage **1** (based on *p*-xylene standard) in CD_3CN, 20 µl (0.24 µmol) of a solution 0.012 M in CD_3CN of *p*-xylene were added. Then 10 µl (0.1 µmol) of a 0.01 M mixed solution of two guests of the series **2a,2d** were introduced. The mixture was monitored with ^1H NMR.

The ^1H NMR spectrum of the characteristic region related to the α proton of the pyridine ring of the filled cage at different guests ratio are displayed in Figure A7-8.

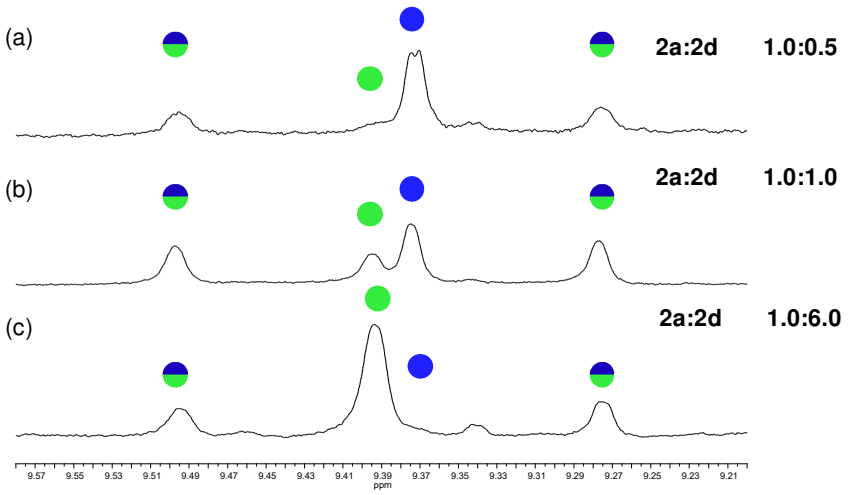

Figure A7. ^{1}H NMR of competition experiments between *p*-Nitrobenzoicacid **2a** and 4-Dimethylaminobenzoic acid **2d** in different guests ratio between **2a:2d** a) 1.0:0.5 b) 1.0:1.0 c) 1.0:6.0

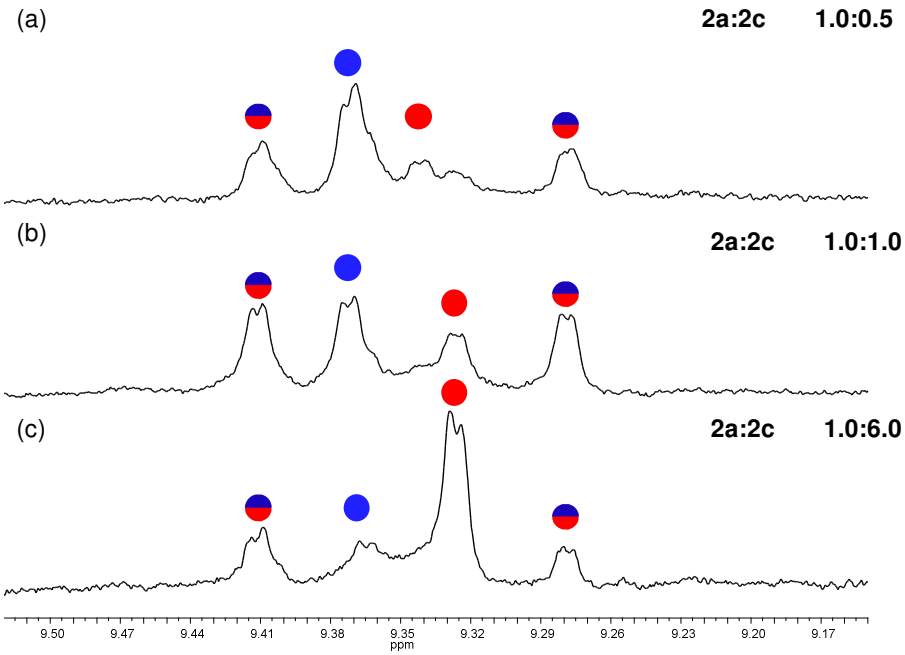

Figure A8. ^{1}H NMR of competition experiments between *p*-Nitrobenzoicacid **2a** and 4-Methoxybenzoic acid **2c** in different guests ratio between **2a:2c** a) 1.0:0.5 b) 1.0:1.0 c) 1.0:6.0

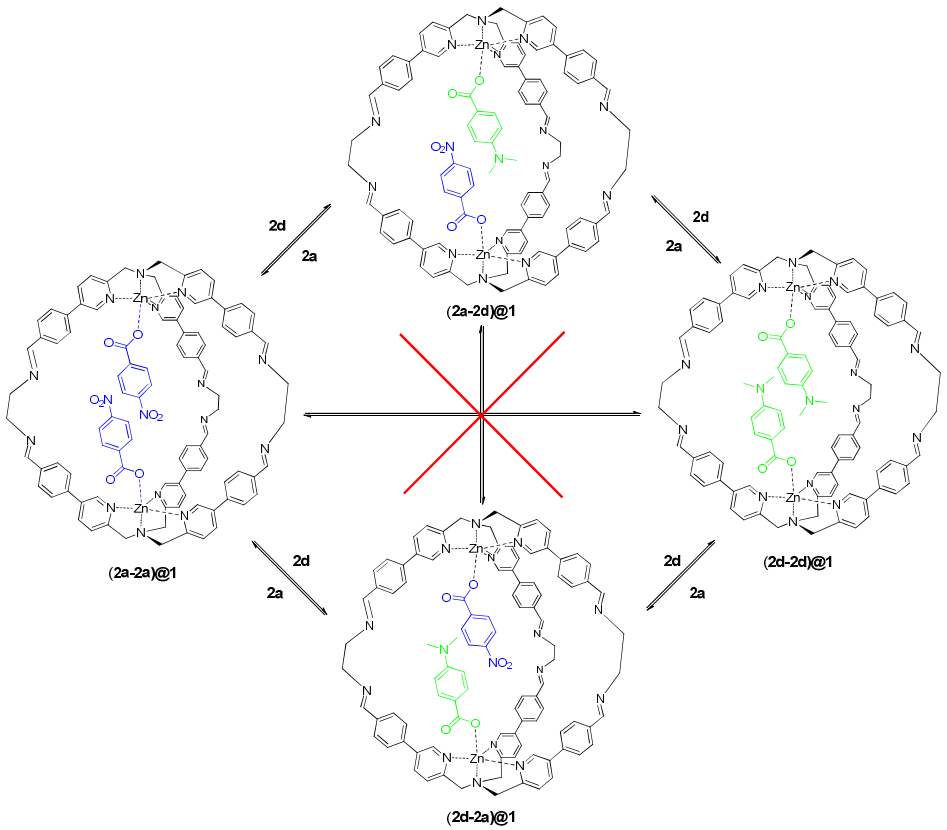

Scheme A9. Mechanism of the proposed equilibria between the homo **(2a)$_2$@1**, **(2d)$_2$@1**and ethero **(2a,d)@1** co-encapsulated species.

A 4.6 Displacement Experiments

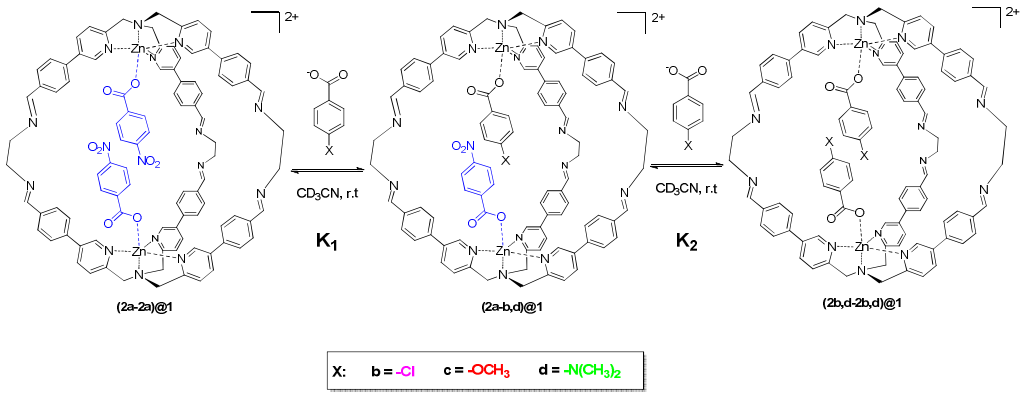

To 500 µl (0.5 µmol) of a solution 0.001 M of the cage **(2a-2a)@1** (based on *p*-xylene standard) in CD_3CN, 20 µl (0.24 µmol) of a solution 0.012 M in CD_3CN of *p*-xylene were added. Small aliquots of **2b,2d** competitors guests solution were titrated into this NMR tube. The displacement was monitored by ^1H NMR and the displacement constants K_1 and K_2 of **(2a-2a)@1** towards guests **2b,2d** were obtained taking into account the relation (explicated in displacement experiment with guest **2d**).

$$\partial_{obs} = X_{(2a-2a)@1} * \partial_{(2a-2a)@1} + X_{(2d-2d)@1} * \partial_{(2d-2d)@1} + X_{(2a-2d)2@1} * \partial_{(2a-2d)2@1}$$

In which the values of the chemical shift (δ) for each species is known and the concentration are obtained through the fitting of the chemical shift variations in each displacement experiment (Figure A8-10). The chemical shifts of the host spectra were monitored as a function of guest concentration and analysed using a purpose written software in Microsoft Excel.

The correlations between K_1 and K_2 with the Hammet constant parameter are reported in Figure A10.

Displacer	K_1	K_2
4-(Dimethylamino)benzoic acid **2d**	0.264	0.132
4-Methoxybenzoic acid **2c**	0.440	0.220
4-Chlorobenzoicacid **2b**	0.650	0.325

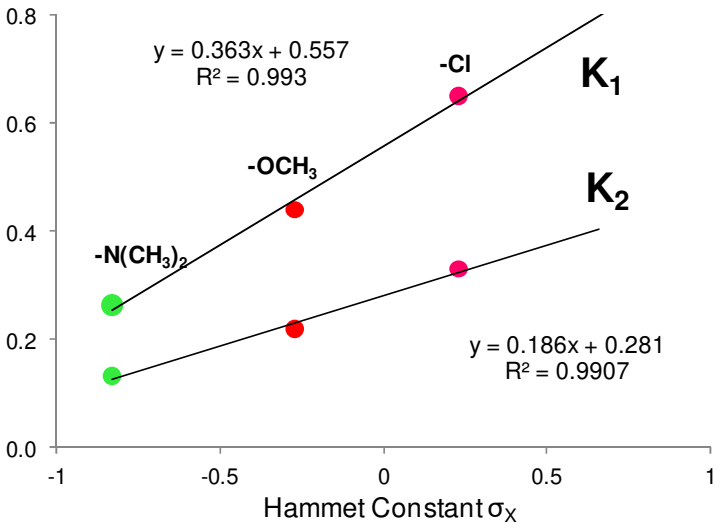

Figure A10. Correlations between K_1 and K_2 with the Hammet constant parameter for each displacement experiment towards cage **(2a-2a)@1.**

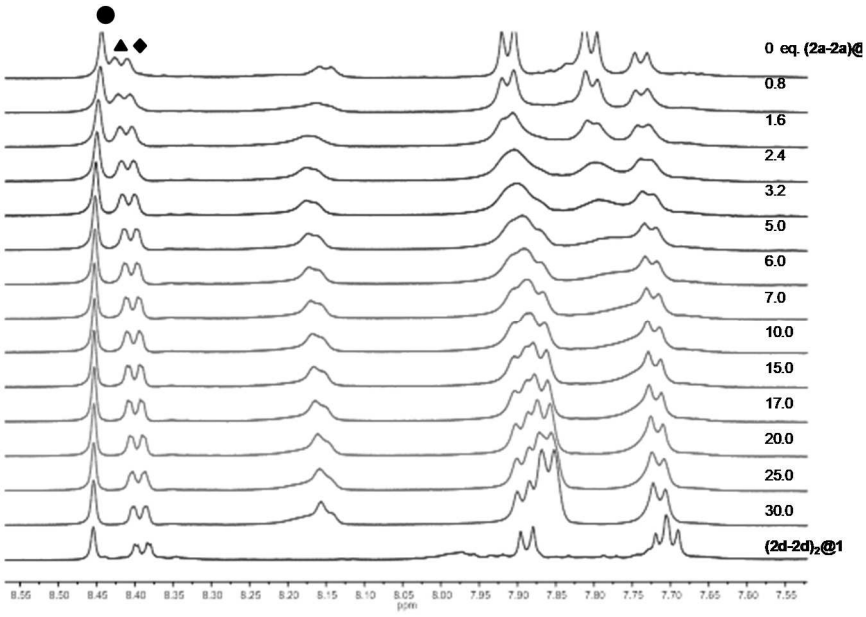

Figure A11. ^{1}H NMR displacement experiment of cage **(2a)$_2$@1** with guest **2d** (Aromatic Region).

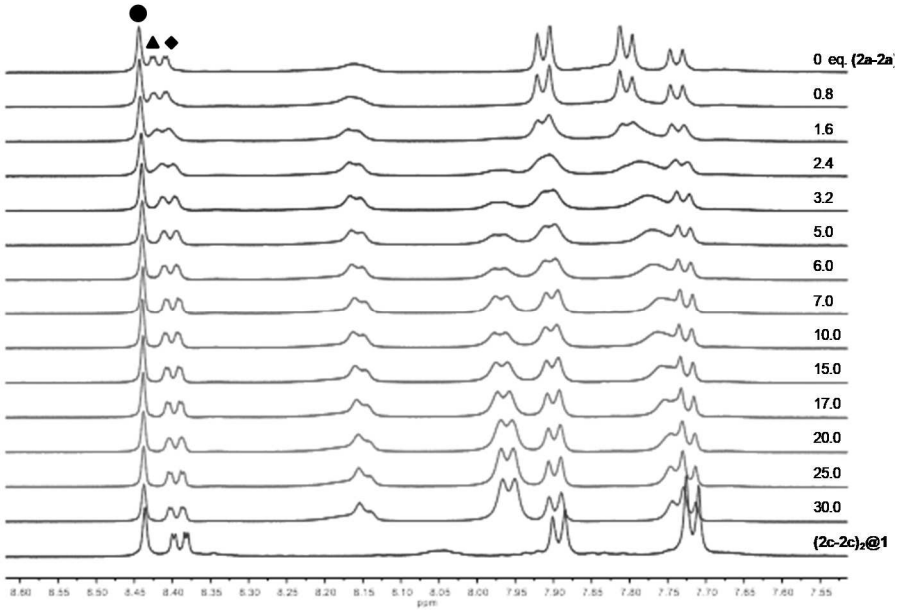

Figure A12. ^{1}H NMR displacement experiment of cage **(2a)$_2$@1** with guest **2c** (Aromatic Region).

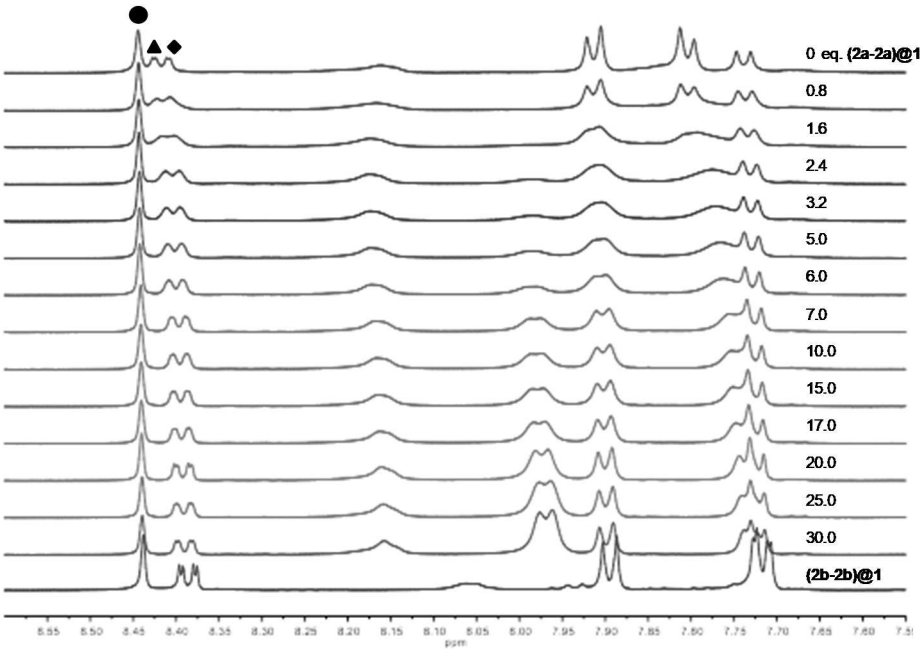

Figure A13. ^{1}H NMR displacement experiment of cage **(2a)$_2$@1** with guest **2b** (Aromatic Region).

A 4.7 ^{1}H NMR and MS characterization

A 4.7.1 (2a-2a)@1

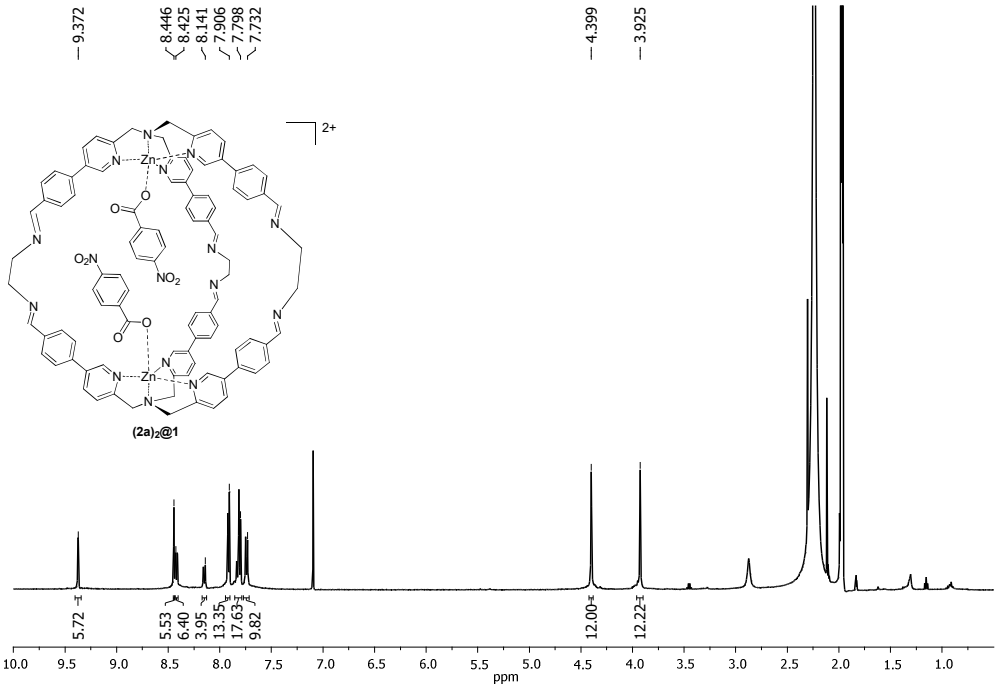

Figure A14. ^{1}H NMR spectrum (500 MHz, 301 K, CD_3CN)of cage **(2a-2a)@1.** (*p*-xylene is used as internal standard 7.095 ppm)

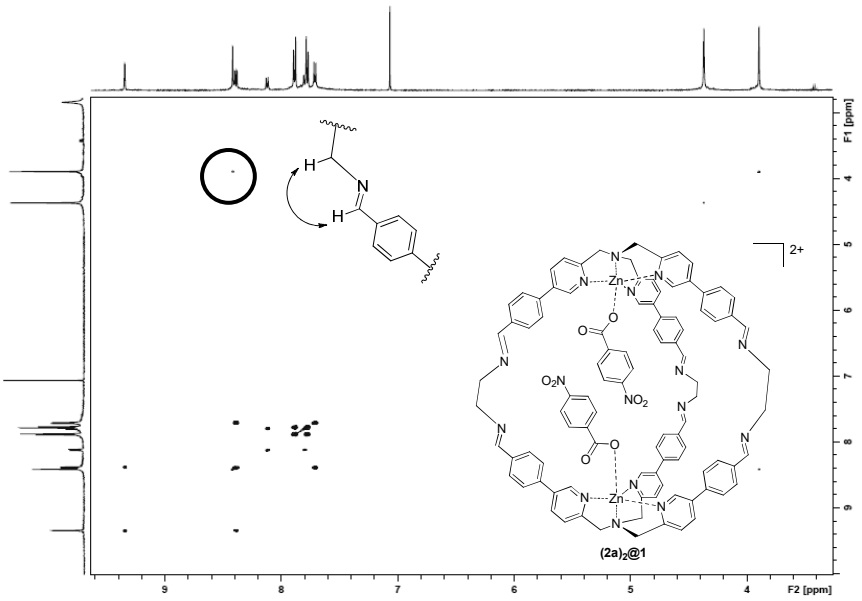

Figure A15. ^{1}H-^{1}H COSY spectrum (500 MHz, 301 K, CD_3CN)of cage **(2a-2a)@1**

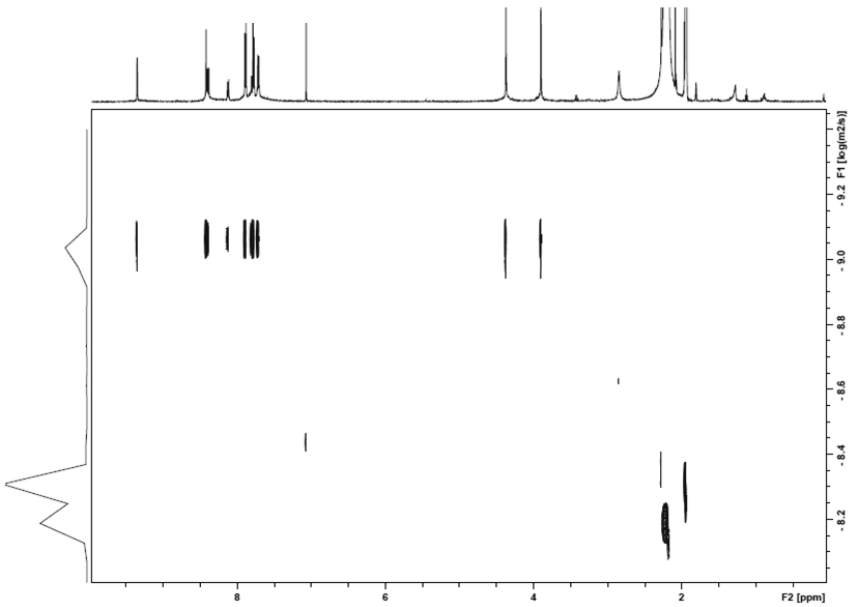

Figure A16 DOSY spectrum (500 MHz, 301 K, CD_3CN) of **(2a-2a)@1**. The diffusion coefficient corresponding hydrodynamic radius (r_H) was calculated to be 12±0.3 Å by using the Stokes-Einstein equation.[1]

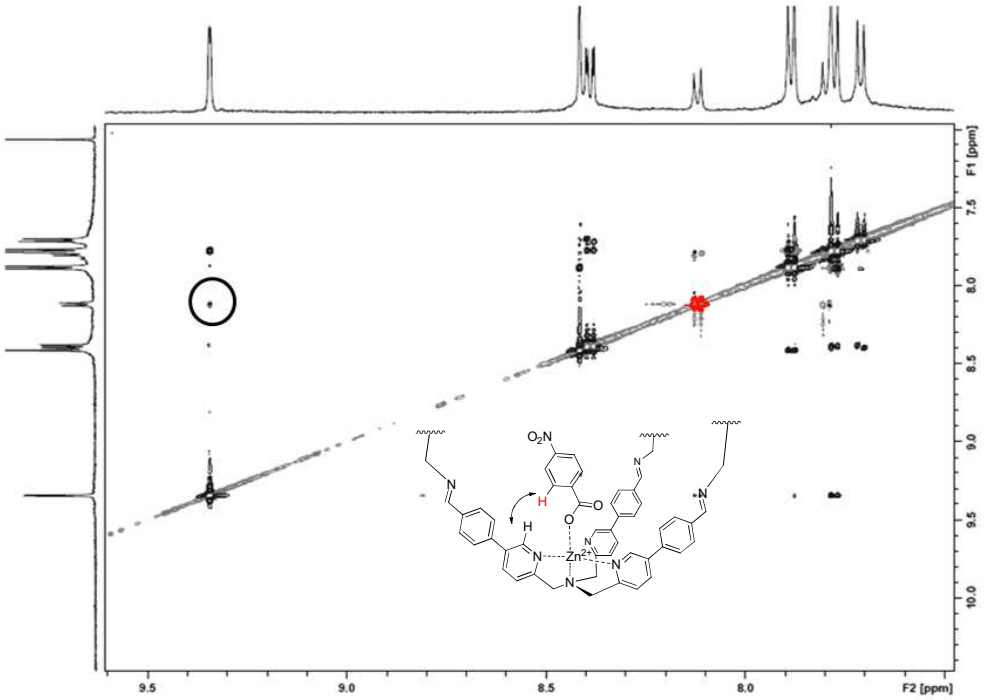

Figure A17. Particular of ^{1}H-^{1}H ROESY spectrum (500 MHz, 301 K, CD_3CN)of cage **(2a-2a)@1**

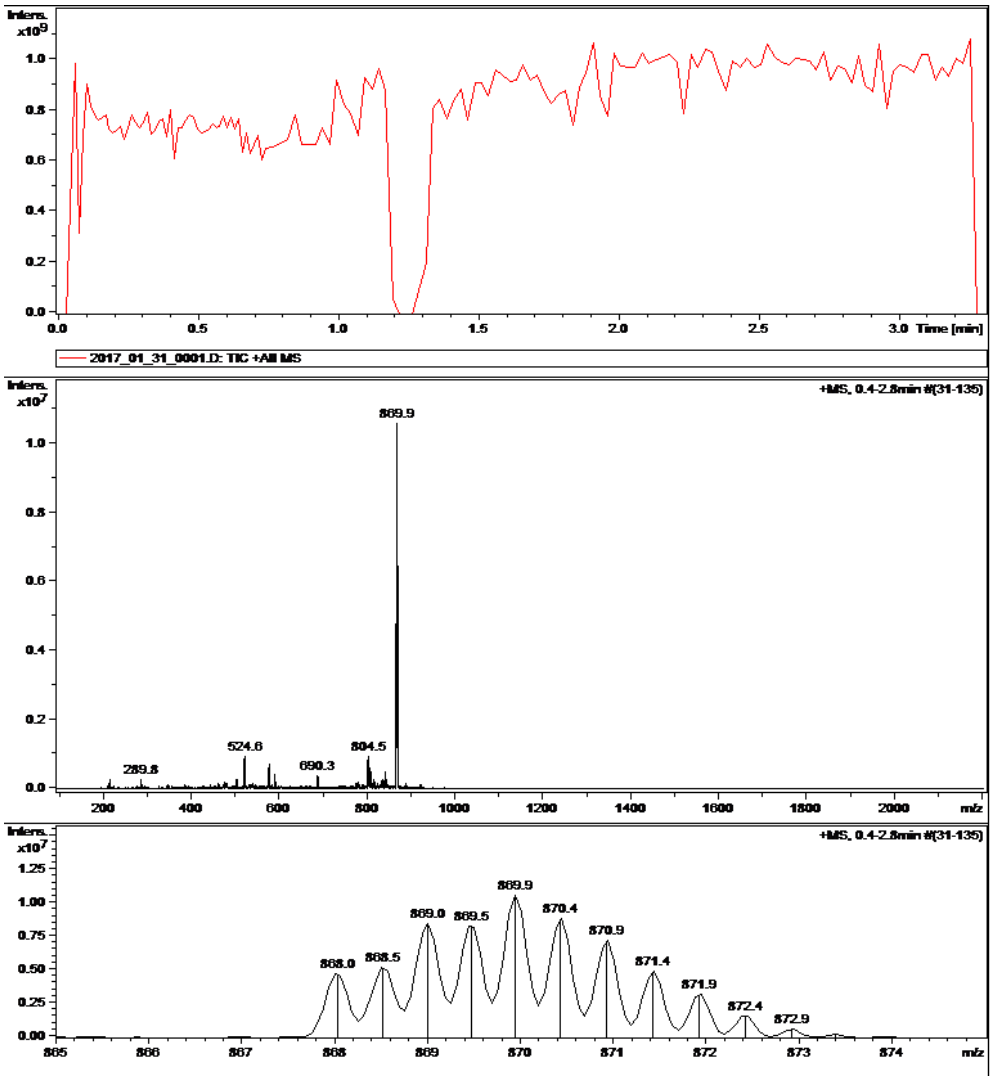

Figure A18. Experimental ESI-MS of **(2a-2a)@1**corresponding to $[C_{98}H_{80}N_{16}O_8Zn_2]^{2+}$.

A 4.7.2 (2b-2b)@1

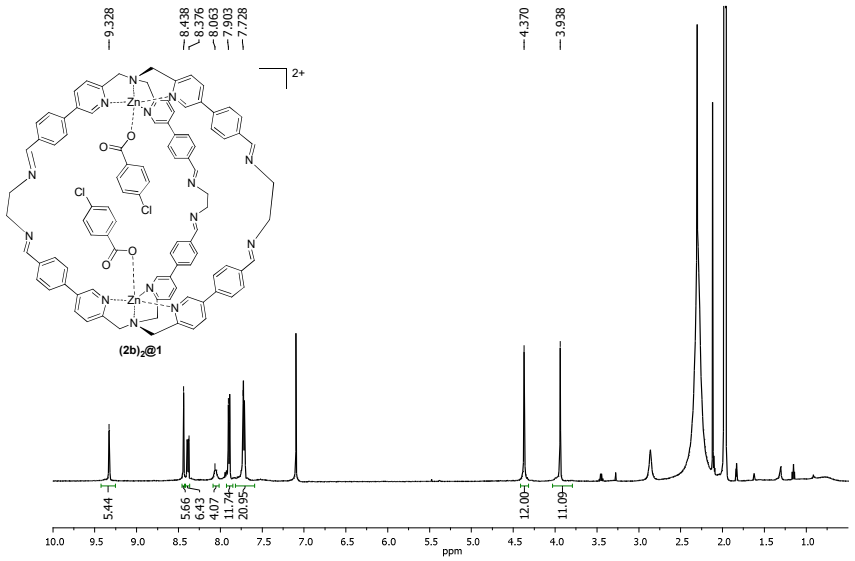

Figure A19. ^{1}H NMR spectrum (500 MHz, 301 K, CD_3CN)of cage **(2b-2b)@1.** (*p*-xylene is used as internal standard 7.095 ppm)

A 4.7.3 $(2c\text{-}2c)_2$@1

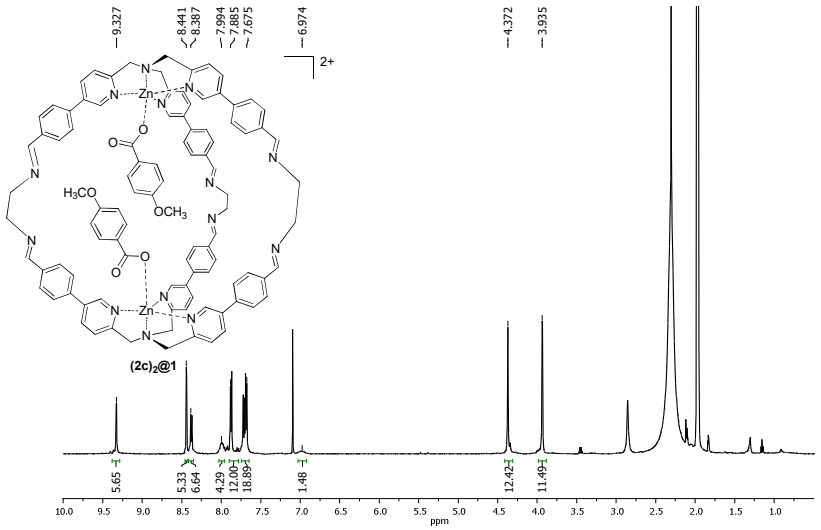

Figure A20. ^{1}H NMR spectrum (500 MHz, 301 K, CD_3CN)of cage **(2c-2c)@1.** (*p*-xylene is used as internal standard 7.095 ppm)

A 4.7.4 (2d-2d)@1

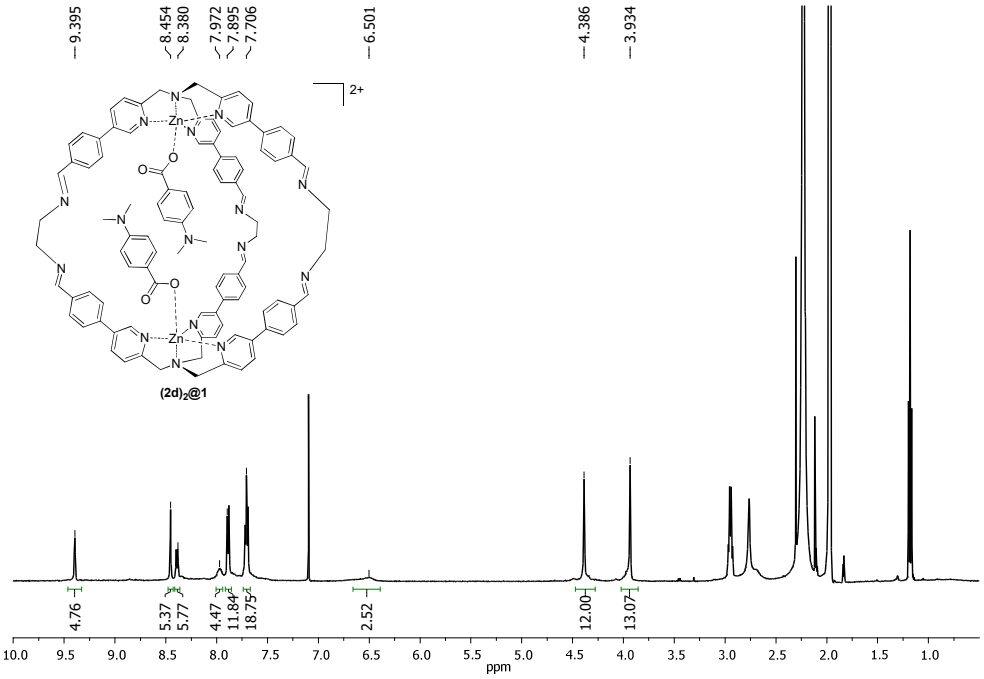

Figure A21. ^{1}H NMR spectrum (500 MHz, 301 K, CD_3CN)of cage **(2d-2d)@1.** (*p*-xylene is used as internal standard 7.095 ppm)

References

1. R. Evans, Z. Deng, A. K. Rogerson, A. S. McLachlan, J. J. Richards, M. Nilsson and G. A. Morris, *Angew. Chem. Int. Ed.* **2013**, *52*, 3199-3202.